A Thesis Submitted for the Degree of PhD at the University of Warwick

Permanent WRAP URL:

http://wrap.warwick.ac.uk/130952

Copyright and reuse:

warwick.ac.uk/lib-publications

Novel Biopolymer Constructs: Physical Properties and Antimicrobial Efficacy

A thesis submitted to the department of Warwick Manufacturing Group of the University of Warwick in the fulfilment of the requirement for the Doctor of Philosophy

Yuen Shan Sandy LEUNG

October 2018

Declaration

I have read and understood the rules on cheating, plagiarism and appropriate referencing as outlined in my handbook and I declare that the work contained in this assignment is my own, unless otherwise acknowledged.
No substantial part of the work submitted here has also been submitted by me in other assessments for this or previous degree courses, and I acknowledge that if this has been done an appropriate reduction in the mark I might otherwise have received will be made.

Signed candidate_____

Abstract

Antimicrobial resistance (AMR) is a life-threatening issue and the situation is deteriorating each year resulting in an increasing number of deaths. The resistance of drugs developed by microbes is a natural process but this can be sped up easily due to unhygienic environments, lack of appropriate guidelines for the use of drugs in certain countries as well as the unclear direction of scientific research into AMR. Some pessimistic experts even believe this problem will never be tackled as it is the result of a long-term human intervention that has affected other biological organisms which inhabit the same ecosystem. Fortunately, such negative comments and predictions have actually accelerated momentum and encouraged and inspired more research activity in this area.

In this project, the main idea involved producing a selection of biopolymer constructs with the specific aim of translating the intrinsic antimicrobial properties of naturally occurring materials (e.g. chitin, lignin, banana leaf) to a biodegradable polymer (PLA) for possible biomedical applications (e.g. would healing). All chitin, lignin and natural products (e.g. banana leaves) have one thing in common which is that they all exhibit intrinsic antimicrobial properties and have great potential for use as non-toxic antimicrobial materials. Versatile engineering tools such as electrospinning, melt-extrusion and injection moulding also allow us to produce additional materials and visualise the possibility of producing the products on an industrial scale. The first interest in this project lied on using ionic liquids (ILs), electrospinning and film casting to produce novel biomaterials. In the later stage of the project, poly(L-lactic acid) as a base polymer matrix, tungsten disulphide and triacetin as a plasticizer were introduced that can be subjected to melt-extrusion and injection moulding along with chitin and lignin.

In this report, the history of antibiotic discovery and key features of antimicrobial resistance are introduced. Previous research conducted is also described in a detailed literature review with supporting evidence focused on chitin, lignin, banana leaves, poly(L-lactic acid), tungsten disulphide as well as techniques used in this project such as electrospinning and melt-extrusion. The detail of the initial scoping experiments electrospinning of biopolymer/ionic liquid solutions is then described as is the introduction of co-solvents and other polymers to assist the electrospinning process. The characteristics of the composites produced using melt-extrusion and injection moulding are also fully discussed. More importantly, bioassays of the composites will be shown which to provide crucial ideas for the key elements required for biomedical applications.

Acknowledgement

Firstly, I would like to thank Professor Andrew Dove who offered me a full scholarship to do a master's degree in polymer chemistry. This is always a major turning point in my life and a great momentum for me to continue to pursue the dream to become a scientist. Secondly, I would also like to thank Professor Tony McNally who supervise my research project during this PhD degree. I always know being my mentor is not easy especially when I had doubts, frustration and negative emotions about myself and the research project. I do greatly appreciate the fact that he is always willing to provide support to make me gain confidence in life.

During the past few years, I met a lot of people who played various important roles in my research project. I would like to thank Dr Chrystala Constantinidou and her students in Warwick Medical School. It was never easy to teach a clumsy chemist/engineer to act like a biologist for conducting bacterial studies. I would also like to thank Dr George Burke and his students from Ulster University to provide crucial information with regards to the experiments about cell viability on some of my samples.

During August – September 2017, I had the opportunity to go to Caltech as visiting summer researcher. I truly had a wonderful time during my stay in California and I would like to thank all the people in the Kornfield's group especially Dr Tiziana De Luccio and Karthik would make me feel welcomed and always ensured that I was happy and provided a lot of things I needed inside or outside the lab. I also feel grateful that Dr Tara Schiller and Dr Daniel Keddie who were also in Caltech during that time and accompanied me to explore California. They have always provided great supports during my up and down and keen to give me advice, encouragement to overcome obstacles. It is indeed a wonderful feeling to have people who can always truly understand me.

Since March 2018, I became an employee at Medherant Ltd and I have met a lot of wonderful colleagues who always make me laugh out loud. I am very lucky to be part of the production team and assigned to do important tasks that allow me to apply the skills I learned and become more confident.

Finally, I would like to thank my parents who always love, care, protect and support me selflessly. I am never good at expressing my true feeling in front of them but I do always feel thankful sincerely. Thank you

List of abbreviation

[AMIM]Cl: 1-Allyl-3-methylimidazolium chloride

BC: Before Christ

BL: Banana leaf/ leaves

[BMIM]Cl: 1-Butyl-3-methylimidazolium chloride

C: Carbon

Cu: Copper

CIM: Conventional injection moulding

CO_2: Carbon dioxide

DMTA: Dynamic mechanical thermal analysis

DP: Dispersity

DSC: Differential scanning calorimetry

EB: Elongation at break

E. coli: *Escherichia coli*

EDS: Energy-dispersive x-ray spectroscopy

EHEC: Enterohemorrhagic

[EMIM]Cl: 1-Ethyl-3-methylimidazolium chloride

FTT: Fourier transform

FTIR: Fourier-transform infrared spectroscopy

G': Storage/elastic modulus

G": Loss/viscous modulus

GPC: Gel permeation chromatography

HA: Hyaluronic acid

HUVEC: Human umbilical vein endothelial cells

H_2O: Water

H_2S: Hydrogen sulphide

IL: Ionic liquid

LA: Lactic acid

L/D: Ratio of flight length of the screw

Li: Lithium

L-LDH: L-lactate dehydrogenase

M-H: Muller-Hinton

M_n: Number-average molecular weight

M.p.: Melting point

MRSA: Methicillin-resistant *Staphylococcus aureus*

MSSA: Methicillin-sensitive *Staphylococcus aureus*

M_w: Weight-average molecular weight

$(NH_4)_2WS_4$: Ammonium thiotungstate

O: Oxygen

OCT: Optimal cutting temperature

OD: Optical density

PBS: Phosphate-buffered saline

PCL: Poly(ε-caprolactone)

PEG: Poly(ethylene glycol)

PET: Poly(ethylene terephthalate)

PEU: Poly(ester-urethane)

PHA: Poly(hydroxyalkanoate)

PLA: Poly(lactic acid)

PLDA: Poly(D-lactic acid)

PLGA: Poly(lactic-co-glycolic)

PLLA: Poly(L-lactic acid)

PLM: Polarised light microscopy

PMMA: Poly(methyl methacrylate)

PP: Poly(propylene)

PPF: Poly(propylene fumarate)

PS: Polystyrene

PVC: Poly(vinyl chloride)

PVOH: Poly(vinyl alcohol)

ROP: Ring-opening polymerisation

S: Sulphur

SAXS: Small angle X-ray scattering

SCORIM: Shear controlled orientation in injection moulding

SEM: Scanning electron microscopy

T_{cc}: Cold crystallisation temperature

TEM: Transmission electron microscopy

T_g: Glass transition temperature

TGA: Thermogravimetric analysis

THF: Tetrahydrofuran

T_m: Melting temperature

UTS: Ultimate tensile strength

W: Tungsten

WAXS: Wide angle X-ray scattering

WO_3: Tungsten trioxide

WS_2: Tungsten disulphide

X_c: Crystallinity

XPS: X-ray photoelectron spectroscopy

XRD: X-ray diffraction

YM: Young's modulus

Table of Contents

Chapter 1.

Introduction

1. Introduction

1.1 Research Proposal

This research provides examples of unique antimicrobials and shown how they can be applied in various applications such as in medical devices targeting the prevention of infectious diseases. There are naturally occurring materials that can act as antimicrobials on a certain level but the imperfections of these materials can be used as a reminder about their limitations which need to be addressed when designing further antimicrobials. Silver can cause side-effects and its non-biodegradable nature can have a negative impact on the environment; effective antimicrobial-ILs might not be suitable to be used as medical devices due to their potential cytotoxicity. More importantly, AMR is always one of the most vital features that should be considered for any antimicrobial.

In comparison to natural products, synthetic products tend to have a higher degree of uncertainty when predicting their toxicity and side effects. In contrast, there are natural products that do not suffer these drawbacks. The phenolic compounds that were discussed can be found in nature and have therapeutic properties. Further examples include honey that was used as medicine in ancient times[1] and it has in fact proven to be effective when treating leg ulcers and provides protection against MRSA;[2] tea tree oil exhibited high anti-biofilm activity towards MRSA and *E. coli*;[3] and collagen extracted from fish can be used for dermal reconstruction and showed significant wound healing effects.[4] Mammals such as the Tasmanian Devil can produce milk that can kill several deadly superbugs which are known to exhibit resistance to existing antibiotics[5] and last year, a new class of antimicrobial compounds were discovered in human breast milk.[6] There are indeed uncountable natural products that can be explored continuously in order to produce more novel antimicrobial materials.

The focus of this project is to develop a selection of biopolymer constructs with the specific aim of translating the intrinsic antimicrobial properties of naturally occurring materials, such as chitin, lignin and banana leaf to a biodegradable polymer (poly(lactic acid)) for possible biomedical applications such as in wound dressings. Techniques such as electrospinning, film-casting, melt-extrusion and injection moulding have been applied and studied to produce the biopolymer constructs, i.e. film and fibre. The physical properties are characterised in detail and more importantly, the antimicrobial properties of the constructs investigated extensively. In addition, it is also a key aspect to understand the major element or component required when designing an antimicrobial biopolymer construct.

Overall, the major proposal of this project is to produce novel composite materials that could possibly exhibit antimicrobial properties. The concept of applying natural materials, non-toxic as well as biodegradable is the general objective of the whole project. All procedures including composite production, characterisation and application with different microbes will be discussed and investigated.

1.2 Aim of the project

It is aim of this project to use natural materials to produce different biopolymer constructs that can exhibit antimicrobial properties and potentially can be incorporated into medical devices. The materials selected include chitin, lignin, banana leaf (BL), ILs, poly(lactic acid) (PLA), tungsten disulphide (WS_2) and triacetin. The techniques include electrospinning, film casting and melt extrusion combined with injection moulding.

The objectives, elements and their relative features involved in this project are summarised schematically in Figure 1.1. The blue text boxes represent the topics covered during 1st year and the first half of 2nd year of the project. During the first half of this project, chitin, lignin and BL were studied and the ILs were used as powerful solvents to process the materials for use with electrospinning and film casting. On the other hand, the orange text boxes represent the topics covered during the second half of 2nd year as well as the 3rd year of the project. During the second half of this project, PLA, WS_2 and triacetin as a plasticizer were introduced and the interest of the project expanded to the use of a common engineering tool, melt-extrusion along with injection moulding to produce biopolymer constructs.

Chitin

Lignin

Banana leaves

- Non-toxic
- Biocompatible
- Biodegradable
- Antimicrobial

Ionic liquids

- Powerful solvents
- High thermal stability
- Green/ re-usuable solvents

Electrospinning/ film casting

- Versatile technique
- Production of polymer membranes
- Used in biomedicine

Antimicrobial agents, medical devices

PLA
- Biocompatible
- Biodegradeble
- Growing studies in biomedicine

Tungsten disulphide (WS$_2$)
- Natural mineral
- Non-toxic

Triacetin
- Plasticization
- Non-toxic
- Edible

Melt-extrusion, injection moulding
- Common processing/ engineering tools
- Volatile solvents not required
- Production of composites in different shapes

Figure 1.1 Overall topics covered in this project

Part 1: (Months 1 to 18)

1. Dissolution of biopolymers using ILs

2. Electrospinning of biopolymer/IL solutions

3. Modification of polymer solutions (introduction of co-solvents, polymer-binder) to enhance the electrospinning process

4. Investigation of the entanglement of ionic liquids and biopolymers influenced by their relative interactions

5. Production of banana leaves membranes using ILs and film casting

Part 2: Months (19 to 36)

1. Production of non-plasticised and plasticised PLA/lignin composites using melt-extrusion and injection moulding

2. Production of non-plasticised and plasticised PLA/chitin composites using melt-extrusion and injection moulding

3. Production of non-plasticised PLAWS$_2$ composites using melt-extrusion and injection moulding

4. Characterisations of the chemical and physical properties of all composites. Investigation of antimicrobial activity of the composite materials.

1.3 The Discovery of Antibiotics

Antimicrobial resistance, AMR is an on-going issue of international importance and if the predicted worst outcome is realised this could lead to approximately 300 million deaths by 2050.[7] Therefore, AMR must be tackled and various approaches have been proposed for avoiding such a crisis. In order to solve this issue effectively, it is vital to understand the origin of AMR starting with the invention of antibiotics and their relevant developments and impacts on our daily life.

Antibiotics are compounds that are able to kill and inhibit the growth of microbial species. They can be produced by bacteria, fungi and commonly applied as medicines to treat or prevent bacterial infection.[8] Although Scottish scientist Sir Alexander Fleming was extremely well-known in discovering the antibiotic, penicillin in 1928 and later awarded a share in the Nobel Prize in Physiology or Medicine in 1945,[9] there are neglected stories about the uses and discovery of antibiotics in the past which merit brief discussion. In ancient Egypt, surgeons during that era applied sour or mouldy bread on patients' wounds to achieve a healing effect.[1] When more formal scientific research began which was published formally, two relevant research studies were reported around the late 1800's in this field.[10-11] In 1877, Louis Pasteur and Robert Koch discovered that the growth of Bacillus anthracis can be inhibited by other airborne bacillus.[10] In a small village named Arzano in Italy, people drank water from a well and Vincenzo Tiberio noticed that they suffered intestinal disorders when the well was cleaned and cleared of mould until a new mould appeared. He then conducted research based on this phenomenon and published a paper in 1895.[12] Two years later, French student Ernest Duchesne submitted a thesis and presented that Penicillium patulum/expansum could kill pathogenic bacteria such as Salmonella typhi and Escherichia coli.[13,11] Unfortunately, he died aged 37 and his finding was not confirmed and rediscovered until the 1940s.[14,15] The most famous event around antibiotics happened in 1928, when A. Fleming discovered that a *Staphylococcus* culture was contaminated by mould which caused the inhibition of its growth. He continued to conduct experiments to identify and confirm the antibacterial compound was penicillin (Figure 1.2).[9,16] In the 1930s, Gerhard Domagk and his team developed an antibacterial

drug, Prontosil[17] and Rene Dubos discovered the first naturally derived antibiotic from soil, Tyrothricin.[18] Unlike penicillin that displays high antibacterial activity against a broad range of bacteria but low toxicity towards human,[9] the former is not effective against enterobacteria and the latter was too toxic to be used systemically. Ernst Chain and Howard Flory tested penicillin on mice and humans who were infected with *Streptococcus pyogenes* and *Staphylococcus aureus* which had proven the effectiveness and safeness of penicillin.[19] Hence, penicillin is still the most important antibiotic in history especially when it can show two of the most vital features of a drug, i.e. active towards a wide range of bacteria but low toxicity on the host.
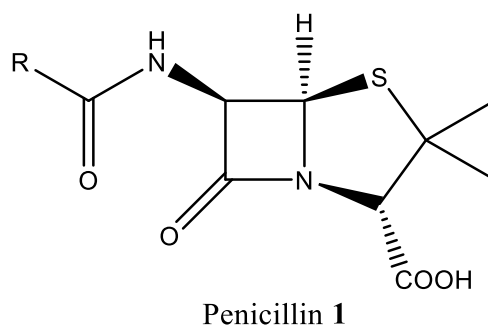
Penicillin **1**

Figure 1.2. Core structure of Penicillin (**1**) (R is a variable group)

During World War II, antibiotics especially penicillin (**1**) was widely used to treat wounded soldiers to prevent infection.[20] This opened the door to new research based on developing antibiotics as well as antibacterial/antimicrobial products.[21] However, bacteria has the ability to evolve and adapt to diverse environments.[22] When E. Chain conducted clinical trials of penicillin (**1**), he had already noticed the consequence of an under-dose of penicillin (**1**) can lead to death and raised the importance of applying a sufficient dose until treatment was completed.[23] In the Nobel Lecture given by A. Fleming in 1945, he stated his concern, "It is not difficult to make microbes resistant to penicillin (**1**) in the laboratory by exposing them to concentrations not sufficient to kill them, and the same thing has occasionally happened in the body."[24] He highlighted the fact that it was not a short, easy journey to discover, develop and test an antibiotic but it could be an easy journey for the microbes to build up a resistance to the drug. As well as trying various strategies to develop new drugs or antibacterial products, antimicrobial resistance, AMR has become another major concern.

1.4 Definition of Antimicrobial Resistance and Current Research Trends

The World Health Organisation, WHO has defined AMR as the resistance of microorganisms towards antimicrobial drugs which were initially effective for treatment of infections caused by them. AMR is in fact a broad term as it applies to microbes that are resistant to drugs not only to antibiotics, but also antifungals, antivirals and antimalarials. In Biology, evolution of resistant strains is a natural process that exists when microorganisms replicate themselves incorrectly or when resistant traits, genes are exchanged between them. Such natural phenomena can be sped up and spread out due to the misuse of antimicrobial drugs, poor infection control practises, inadequate hygiene conditions as well as inappropriate food-handling. As a result, standard treatments eventually become ineffective and infections persist, increasing the risk of spread to others.[25]

The WHO urged control of AMR by doing simple things such as maintaining good hygiene levels by washing hands, minimising contact with sick people, only use prescribed antimicrobials drugs and complete the full treatment at the same time. On the other hand, it is encouraging new innovation, development of new treatments and effective tools in the fight against bacteria.[25] However, the most useful scientific method to tackle AMR still cannot be clearly defined. Scientific research on AMR has increased especially when researchers are always very keen on producing more powerful drugs, especially antibiotics when dealing with infections.[26] Since microbes have the ability to evolve, it is a major concern that creating more powerful drugs will also end up creating multidrug-resistant pathogens known as "superbugs".[27] Albeit controversial, there is indeed a trend to predict what kind of treatment or method should be developed.

As stated earlier before, AMR does not only apply to antibiotics but its development is a great example to describe how future trends can be predicted. There are several ways to categorise antibiotics and one of the common ways is to divide them into natural, natural product derived/semi-synthetic and synthetic. For example, ferrocenyl penicillin (**2**) that was derived from penicillin (**1**)[28] is semi-synthetic and isoniazid (**3**) (Figure 1.3), a synthetic antibiotic that can be used for treating tuberculosis.[29]

Ferrocenyl penicillin **2**   Isoniazid **3**
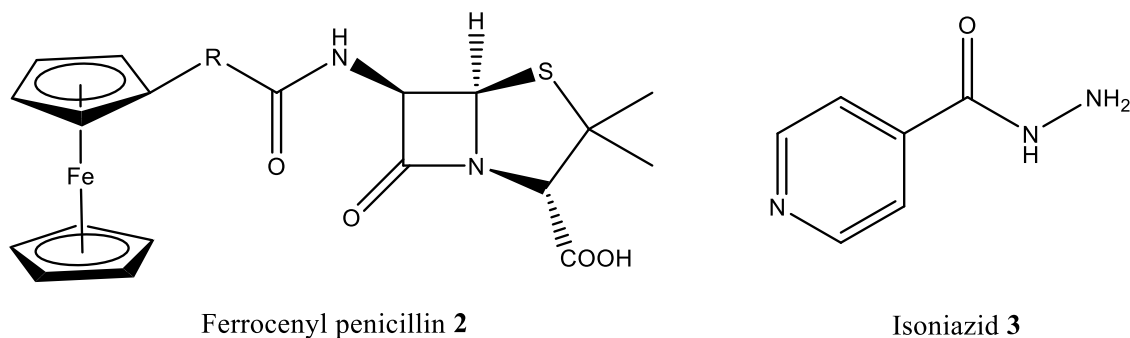
Figure 1.3. Structures of ferrocenyl penicillin (**2**) and isoniazid (**3**)

In general, natural products tend to involve diverse and complex structures, multiple chiral centres, high potency selectivity and multiple modes of action which often provide functional diversity and selectivity for more than one target.[30] However, some natural products do have un-favourable properties such as poor solubility, stability and separation, purification and scaling up of these products has proven to be difficult and a major disadvantage to their development.[31] Hence, some natural products were modified to become semi-synthetic antibiotics and the successful candidates were more potent, less susceptible to inactivating enzymes which induce resistance or they can bind tighter to bacterial targets.[32] To further overcome the difficulties that exist when developing natural or semi-synthetic products, synthetic products were developed especially with a view to obtaining some functional groups and ring systems (aromatic, hetero-aromatic rings, stereo-genic centres) that are lacking in nature. In contrast, they tend to have low molecular weights and are easier purified and can be produced on a large scale.[33] The risks associated with developing these products include toxicity, uptake, dosage, access to target and potential side-effects on hosts.[34]

Unfortunately, it can be an endless and controversial debate about what kind of drug is more advantageous or whether it is reasonable to focus on developing one certain type of drug for tackling AMR. However, nature is still the best, sophisticated and the most inspirational chemist in history to date. As discussed above, A. Fleming and R. Dubos demonstrated the origin of antibiotic efficacy from nature. With technology improving continuously, barriers to developing natural based products should be minimised, and overcome in the future. There are many scientists suggesting that inspiration from nature is still the key to tackling AMR.[35,36] Moreover, nature has also given the ability for the immune/defence systems to evolve in plants, animals and even humans to battle and

protect themselves from their environments.[37] Nature is still a very good source of antimicrobial substances.

1.5 Feature Characteristics of Bacteria

Infections have become one of the top three causes of death worldwide. Common infectious diseases such as septicaemia and pneumonia are often caused by bacteria.[38] Hence, the many features of bacteria are being studied in order to understand how they can be killed effectively.

Amongst all kinds of bacteria, their cell wall plays the most important role. The cell wall can expand or contract with changes in ionic strength or pH of the external environment to provide very good protection. Bacteria can be classified into Gram-positive or Gram-negative bacteria according to their outer structure. The name Gram originated from the Danish scientist Hans Christian Gram whom in 1884 invented a staining method to differentiate the class of bacteria. In this Gram-staining test, bacteria that can retain the crystal violet dye due to its thick layer of peptidoglycan are regarded as Gram-positive bacteria. Conversely, bacteria that do not retain the violet dye and coloured in red or pink are defined as Gram-negative bacteria.[39]

In comparison, Gram-positive bacteria have a simpler structure which make them fragile and susceptible to most drugs. Although their cell wall can differ in various species, major features often include; i) a cytoplasmic membrane which has a thickness of 15-50 nm; ii) peptidoglycan that makes up 50% of the wall by mass and is a covalently cross-linked structure to give a tough, fibrous structure for strength that helps maintain its shape under high internal osmotic pressure and iii) teichoic acid or lipoteichoic acid, a negatively charged polymer to ensure a strongly polar cell surface (Figure 1.4). Examples of Gram-positive bacteria include *Bacilli*, *Staphylococcus* (include superbugs that causes deadly infections, Methicillin-resistant *Staphylococcus aureus* commonly known as MRSA) and *Streptomyces*. They tend to be weaker and can easily be destroyed simply by shaking with glass beads, washing and differential centrifugation.[40]
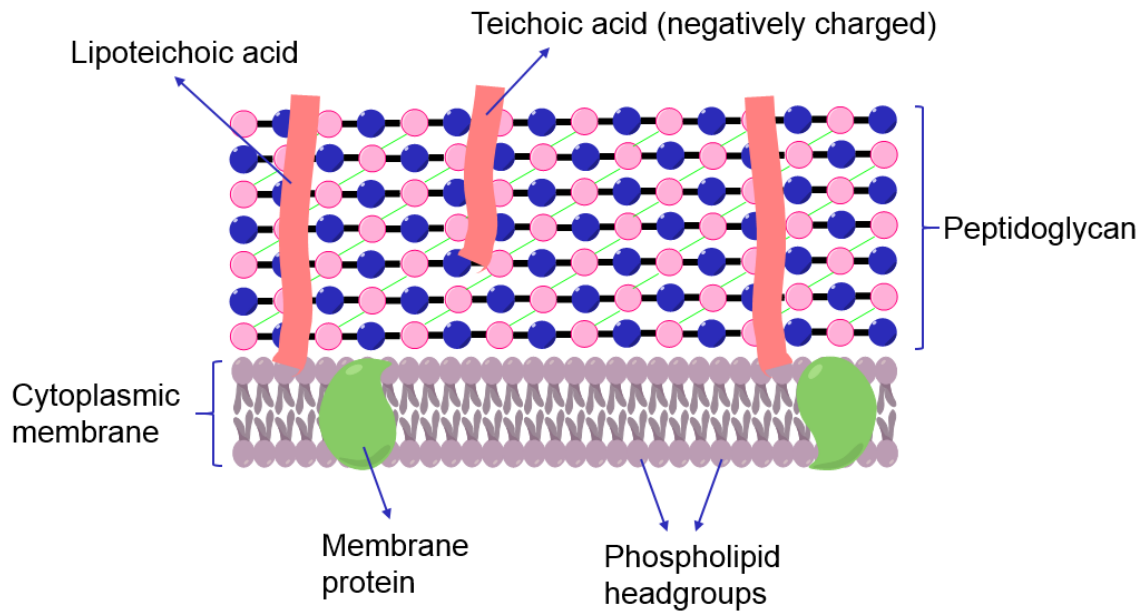
Figure 1.4. Schematic representation of Gram-positive bacterial cell wall[40]

In contrast, Gram-negative bacteria have a more complex structure but some details can vary in different species. The major difference and important features in Gram-negative bacteria is that they have an extra membrane, an outer membrane, an electron-dense layer, and a periplasmic space which can contribute further to wall strength. The porin present in the outer membrane are pores that selectively allow passage of hydrophilic molecules with molecular weight up to 600-700 Da and, such function can highly interfere as to whether antibacterial products can penetrate to the cell (Figure 1.5). As a result, Gram-negative bacteria are stronger, less susceptible to most antibiotics and can build up resistance to drugs more easily. Well-known Gram negative bacteria include Chlamydia, Escherichia coli (E. coli) and Salmonella etc.[40]
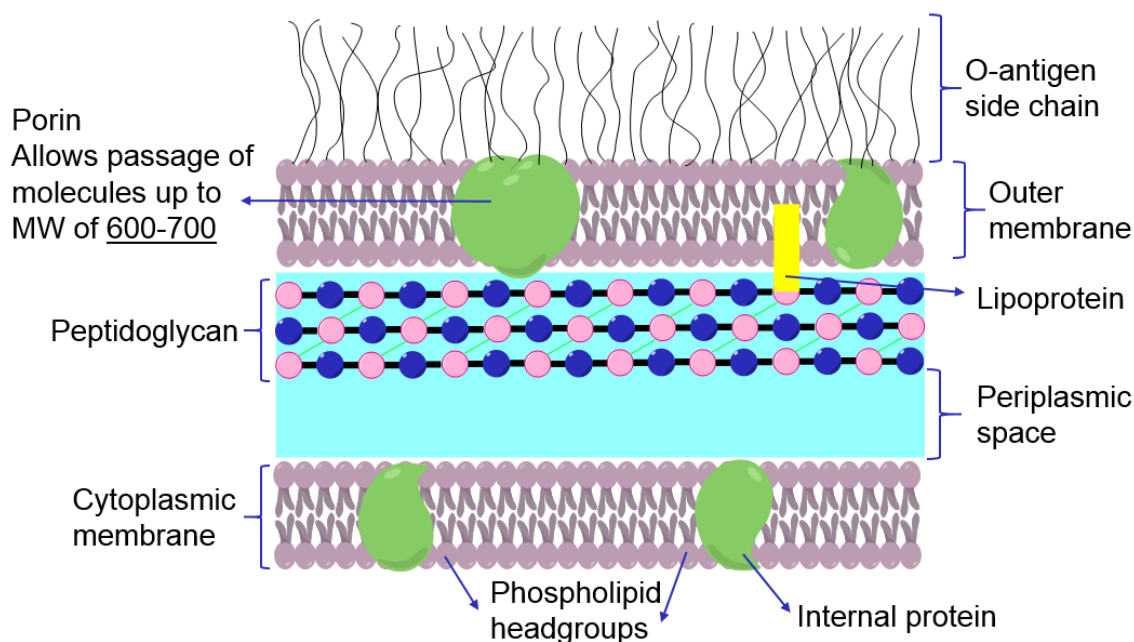
Figure 1.5. Schematic representation of Gram-negative bacterial cell wall[40]

Research on antimicrobial agents has mainly targeted destroying Gram-negative bacteria but this has always proven to be very difficult. In many experiments, they cannot be killed easily or they develop resistance quickly, even in a short period of time. Previous research cannot fully tackle AMR effectively but it can still provide vital information, helpful research focus and inspiration.

1.6 Previous research and recent antimicrobial products

Currently, research on antimicrobial products is becoming more diverse as drug discovery is not always the major topic. More unique strategies have been proposed to prepare antiseptic products that can be used in our daily lives to improve our hygiene, and public health.

1.6.1 Silver as an antimicrobial

One of the most well-known methodologies is to use silver and silver nanoparticles in healthcare, food industry and in domiciliary applications. With regards medical applications, silver and its compounds also has a long history. One of the well-known research breakthroughs in this area was discovered by Carl Moyer who showed that silver nitrate can be used for treating burns.[41] Upon confirmation of silver having a broad spectrum of antimicrobial activity towards planktonic and sessile bacteria,[42] it has been used to produce silver-coated urinary catheters, silver-based dressings[43] to achieve a wound healing effect[44] as well as in eye drops.[45]

However, these silver containing products do have some drawbacks and whether they should continue to be used is somewhat controversial. Albeit not permanent, ingestion of silver can lead to Argyria.[46] Ionic silver and silver derivatives as topical treatments can cause side effects such as methemoglobinemia, electrolyte disturbance, long slough separation time and inactivation of enzyme debriding agents.[47] Another concern with using silver is associated with environmental issues, particularly when silver-containing products are disposed. Since silver ions are regarded as one of the most toxic forms of heavy metal, it has been assigned to the highest toxicity class. Silver and its salts are not biodegradable and so, its wastes will remain in soil or wastewater sludge forever.[48] Finally, the major concern using silver is due to the increasing number of reports showing silver cannot be used to tackle AMR effectively. When silver was applied in endotracheal tubing, formation of biofilm can be prevented for a few days only[49] and it is not suitable for long-term use.[50] Experiments have also been conducted which have shown E. coli being able to build up high resistance to silver.[51]

1.6.2 Ionic Liquids (ILs) as antimicrobial agents

ILs are salts with melting points below the boiling point of water and each molecule is composed of a positive and negative charged ion. Therefore, the functionality and physical properties of ionic liquids can be tuned by combining or altering different ions.[52] The properties of ionic liquids will be discussed in details in chapter 3. ILs as antimicrobials is a relatively recent area of interest as such properties were not reported until 2003 by Pernak *et al*.[53]

There are some outstanding, inspiring studies such as the synthesis of hexadecylimidazolium or pyridinium based *β*-lactam antibiotic, ampicillin (Amp) IL by Cole *et al*. (Figure 1.6).[54] Such ILs can be obtained using anion metathesis and suggest these IL-compounds can become new *β*-lactamase-resistant antibiotics.[55] In this research, the compounds were tested against MRSA (Gram +), Enterococcus faecium (Gram +), E. coli (Gram −) and Klebsiella pneumoniae (Gram −). In 83% of experiments, the Amp-ILs had improved antibacterial efficacy compared with bromide-ILs. In 92% of experiments, it was observed that Amp-ILs had 43 times better antibacterial efficacy compared to the commercially available sodium ampicillin salt. Overall, pyridinium based Amp-IL **5**

slightly outperformed imidazolium based Amp-IL **4** but both types of Amp-ILs achieved a minimum inhibitory concentration as low as 0.4 μM[54] which can be defined as the lowest concentration of an antimicrobial that can inhibit the visible growth of a microorganism after overnight incubation.[56]
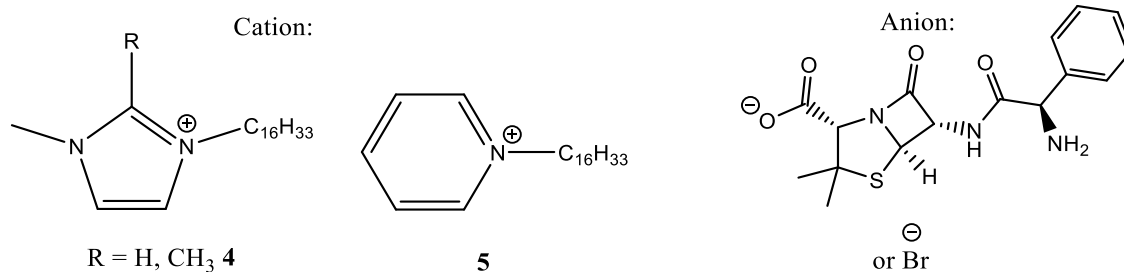
Figure 1.6. General structure of hexadecylimidazolium **4** or pyridinium **5** based IL paired up with ampicillin or bromide ion.

Choi *et al.* designed two ionic liquids based on 1-ethylpyridinium **6** and tributyl(2-hydroxyethyl)phosphonium **7** that also consisted of bis(2-ethylhexyl)-sulfosuccinate, a docusate anion (Figure 1.7). Docusate itself is a synthetic anionic detergent which is marketed among many applications as a laxative for treating constipation.[57] By combining the docusate anion with two different cations to yield a pyridinium-based IL **6** and phosphonium-based IL **7**, the authors showed these ILs to be an efficient plasticizer for medical grade poly(vinyl chloride), PVC. Both ILs are liquid at room temperature, have molecular weight greater than 300 g mol^{-1}, possess good thermal stability and contain polar functional groups on either cation or anion.[58] Apart from acting as plasticizers, the authors proposed that ILs **6** and **7** could also be applied as antimicrobials so that the resultant plasticized PVC can be used in flexible medical devices, such as catheters, and simultaneously be protect against bacteria, and biofilm formation. The authors showed that both ILs **6** and **7** were effective against mainly Gram + bacteria such as MRSA and *Enterococcus* but ineffective towards Gram– bacteria such as *Pseudomonas*, *Klebsiella* and *E. coli*.[58,59]

Cation:

Tributyl(2-hydroxyethyl)phosphonium **7**

1-Ethylpyridinium **6**

Anion:

Bis(2-ethylhexyl)sulfosuccinate (docusate)
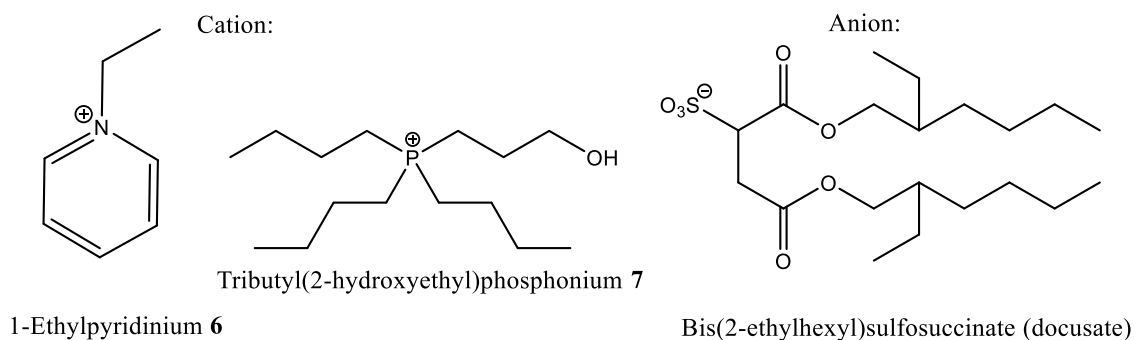
Figure 1.7. General structure of 1-ethylpyridinium **6** and tributyl(2-hydroxyethyl)phosphonium **7** based ILs paired with a docusate anion.

Both the research conducted by M. Cole and S. Choi *et al*. demonstrated how the novel ionic liquids (ILs) synthesized had involved improved antibacterial properties and dual functionality, respectively.

However, there are some uncertainties with regard these ILs. For instance, will bacteria eventually become resistant to the Amp-ILs as analogous to ampicillin?[60] Furthermore, research has shown that many commonly used synthetic plasticizers such as phthalate esters have negative health effects such as inducing infertility[61] and early menopause in females.[62] Although ampicillin (antibiotic) and docusate (antiseptic) alone can be consumed by humans, the cytotoxicity of their relative ILs has not been reported yet. Thus, confirmation of synthetic ILs that can be used as plasticizers without introducing negative effects are required. Generally, ILs with longer alkyl chain length can be better antimicrobial agents due to the increased hydrophobicity that leads to higher lipophilicity[53] and the same trend was observed when the toxicity of ILs was tested with *Daphnia magna*,[63] human HeLa cell[64] and the enzyme, acetylcholinesterase–AChE.[65] Therefore, those ILs that can act as effective antimicrobials are very likely to be toxic to human, although this requires further significant study. In addition, the risk of developing AMR with regard ILs has not been reported to date.

1.6.3 Natural Products as Antimicrobials

In parallel to developing an effective drug or antibiotic to fight against AMR, application of natural products as antimicrobial agents is also a vital topic that cannot be ignored. In fact, the use of antimicrobial and drugs derived from plants (the biomass) is becoming more acceptable in current mainstream medicine. In addition to the ineffectiveness of traditional antibiotics towards new viral deseases,[66] plants have on-going ability to synthesize aromatic components such as phenols or oxygen-substituted derivatives.[67]

These substances can provide defence mechanisms in plants against predation by microorganisms, insects and herbivores and more importantly, some of them were identified as medicinal compounds.[68] Excellent examples of these bioactive compounds include caffeic acid, catechol and eugenol (Figure 1.8).

Caffeic acid **8**   Catechol **9**   Eugenol **10**
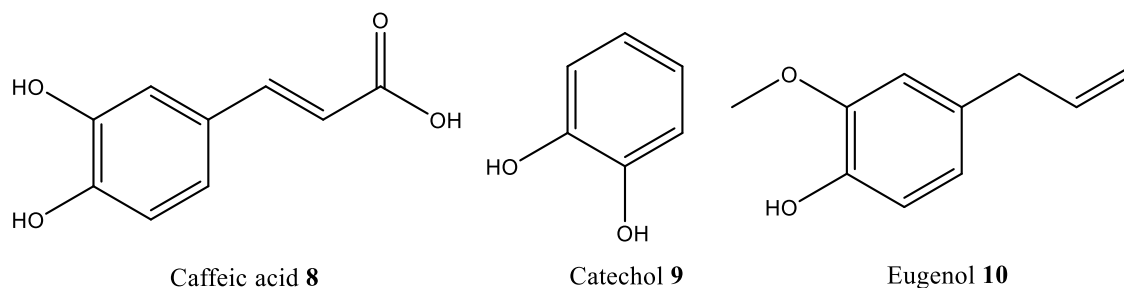
Figure 1.8. Chemical structures of caffeic acid (**8**), catechol (**9**) and eugenol (**10**)

Caffeic acid (**8**) is one common representative of phenylpropane-derived compounds in the highest oxidation state that can be found in all plants and is a vital precursor to the significant building blocks for the biosynthesis of lignin.[69] It also exists in common herbs such as thyme, sage, spearmint[70] and is effective against bacteria.[70] Catechol (**9**) naturally occurs in fruits such as apples and upon exposure to oxygen, it oxidises to reddish-brown melanoid pigments,[71] derivatives of benzoquinone which also exhibit antibacterial activities.[72] Catechol (**9**) also exists in the cuticle of arthropods such as the grasshopper where the cuticle composed of chitin is bounded by catechol (**9**) moiety to protein to form intermolecular crosslinks to give extra strength.[73] Eugenol (**10**) is another naturally occurring phenol that can be extracted from clove oil[74] and cinnamon leaf oil.[75] It was reported that it exhibits bactericidal efficacy towards bacteria such as *Listeria moncytogenes* and *Lactobacillus sakei*.[76] These phenolic compounds all have things in common in that they naturally exist in plants and more importantly they all possess antimicrobial properties. The detailed mechanisms of bacteria growth inhibition by some phenolic compounds are still unclear.[77] In most cases, it is known that the hydrophobic phenolic groups play a key role in disrupting the lipid-protein interaction of bacterial cell membrane and gradually cause extensive leakage of intracellular constituents to ultimately destroy the membrane integrity.[78] In recent years, a very commonly used spice used in cooking such as curry, Turmeric has gained attention in medicine and has been even mentioned by Cancer Research UK.[79] The main ingredient in turmeric is curcumin which is a tautomeric compound that exists as a enol form in organic solvents but keto form in water (Figure 1.9).

Curcumin (**11**, enol form)   Curcumin (**11**, keto form)
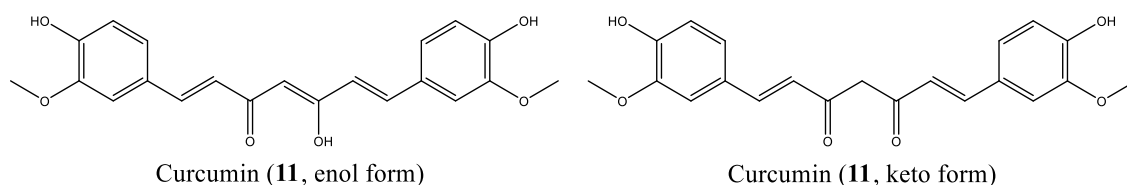
Figure 1.9. Chemical structures of curcumin (**11**) in enol and in keto form

Although there was some research that had doubted the medicinal uses of curcumin (**11**)[80] and even false research published,[81] there is still an interest in gaining a deeper understanding of its biological application. In 2017, the British Medical Journal published a one-off case report that featured a 67-year-old pensioner who cured her myeloma, a form of blood cancer by consuming 8g of curcumin (**11**) daily without additional antimyeloma treatment.[82] Apart from the anticancer property that caused attention to this phenolic compound **11**, it is also known that it exhibits anti-inflammatory,[83] antioxidant,[84] and even antibacterial properties. Curcumin (**11**) can exhibit a bactericidal effect as it can lead to cell membrane permeabilization of both Gram-(+) such as *Staphylococcus aureus* and *Enterococcus faecalis* and Gram-(–) bacteria such as *E. coli* and *Pseudomonas aeruginosa.*[85,86] This compound **11** is indeed a great example to demonstrate the possibility of using a naturally occurring, edible product that has the potential to be used in medicine.

In summary, these naturally occurring materials have provided the inspiration to develop blends of a biopolymer with various medicinal benefits. With the aid of different methods such as electrospinning, film casting, melt-extrusion and injection moulding, novel materials can be produced with antimicrobial efficacy. This research can show the likelihood of translating the intrinsic antimicrobial properties of natural materials (e.g. chitin, lignin, banana leaf) to a biodegradable polymer (PLA) for potential medicinal purposes as well as providing crucial ideas for the key elements required for biomedical applications.

Chapter 2.

Literature Review

2. Literature review

2.1 The Origin of Biopolymers

The term "polymer" is derived from the Greek word πολύς (polus means many/much) and μέρος (meros means parts).[87] A polymer is defined as a large molecule, a macromolecule that is composed of numerous repeating units or a natural macromolecular substance composed of a cross-linked system.[88] Although the term "polymer" first appeared in the literature in 1833 by a Swiss chemist Jöns Jacob Berzelius, its actual definition and concept were proposed by the German organic chemist Hermann Staudinger in 1920[89] and who was later awarded the Nobel Prize in Chemistry in 1953.[90] Staudinger's study in the field of polymers indeed had a very major impact on materials science and industrial plastics development.

Starting from the mid-1970s, polymer production increased by a factor of 10 times and by 2015, polymer production had exceeded 300 million tonnes per year.[91] Polymers are widely processed and used in various application areas and the highest demands include packing materials,[92] in building and construction[93] and automotive.[94] Although these versatile light weight polymeric materials can bring convenience to daily life,[95] they also have a negative impact on the environment. In 2015, only 9% of polymeric waste was recycled, 12% was incinerated and the rest was disposed in landfills or natural environments.[96] Conventional polymers such as poly(ethylene), poly(propylene), poly(styrene) and poly(vinyl chloride)(PVC) that are obtained from fossil hydrocarbons or crude oil are often the major source of plastics waste that end up in landfills. More concerning is the rise of plastic debris entering the oceans which cause negative health concerns to the marine system.[97] Ironically, humans will suffer the most because our freshwater systems are also contaminated somewhat by the same polymeric waste.[96,98] In addition, additives such as plasticizers are often added to alter the thermal and mechanical properties of polymers[99] but most of these additives such as bisphenol-A are identified as mutagenic and/or carcinogenic.[100] All these environmental and health concerns have motivated more research undertaken with the specific target of replacing conventional polymers with biopolymers due to their biodegradable, non-toxic, renewable properties, of which some are even edible and, biocompatible for medical applications.[101]

Biopolymers can be categorised into naturally occurring or those produced synthetically. The former naturally exists in biological systems which can act as structural support, energy or carbon storage.[102] Latex or natural rubber is one of the most well-known and

earliest biopolymer that was developed. This can be traced back to the early Olmec culture (*ca.* 1000 BC) in which latex was used for making balls in Mesoamerican ballgame and the Maya also use latex to make water-proof materials such as for rain-proofing for capes.[103] Nowadays, common biopolymers include polysaccharides such as cellulose which is commonly used for producing paper[104] and its derivatives are also widely developed as plastic films,[105] and the potential of starch-based plastic materials are being recognised and their products generated via injection moulding are available in industry.[106]

In medicine, another naturally occurring biodegradable polymer, hyaluronic acid (HA) was proven that it can be used in tissue engineering/scaffolding and drug delivery.[107] On the other hand, synthetic biopolymers are those that can be produced via chemical syntheses from biologically derived monomers. These monomers are firstly generated using fermentation which then are purified prior to polymerisation.[102] In recent years, some synthetic biopolymers have actively being developed and are gaining technical acceptance over synthetic non-biopolymers. For example, poly(hydroxyalkanoate) (PHA) has received great attention because of its recognised potential as a bioplastic.[108] This material can be produced via bacterial fermentation of sugar or lipids[109] and upon disposal, it can be degraded to CO_2 and H_2O by microorganisms.[110] Another exciting example and increasingly developed biopolymer is poly(lactide) (PLA) that can be obtained by fermentation of carbohydrates from corn, potato and cassava.[111] Degradation of PLA is generally via a hydrolytic process[112] and it was also reported that PLA can be degraded in the presence of enzymes.[113] Currently, this material is applied in making disposable drinking cups, sundae/salad cups, lamination films and blister packages.[114]

The future of biopolymers is still expanding due to their advantages and they could make a key contribution towards the development of a more eco-friendly environment. Biopolymer products can indeed be more commonly seen in daily life. From the examples mentioned above, some of them are safe and non-toxic which are suitable for use in biomedical applications. In the current world where antimicrobial resistance is also a major issue that must be tackled, some reports have shown that with the aid of antimicrobial agents, biopolymers can be developed as antimicrobial food packaging to preserve the freshness and even extend the shelf-life of food.[115] However, there is concern with regard the toxicity of some antimicrobial agents. Their thermal stability during extrusion has limited their use in such applications.[116] Herein, biopolymers that can

potentially be developed into products which display non-toxic, biocompatible and even antimicrobial efficacy will be discussed.

2.2 Production of PLA, PLDA and PLLA

Starting from the late 1970s, the biocompatible nature of PLA and it copolymers have allowed them to be developed for many biomedical applications which include drug delivery[117] and tissue engineering.[118] Although not very well-known, the PLA monomer, lactic acid was first isolated by the Swedish chemist Carl Wilhelm Scheele from sour milk in 1780 and became commercially available in 1881.[119] In France, two scientists, Joseph Louis Gay-Lussac and his student Théophile-Jules Pelouze produced PLA via fermentation of "sugarbeet juice" in 1833. Upon distillation, they produced sublimate lactide which is believed to have been PLA by 1845.[120] More well-known research was done by the American chemist, Wallace Carothers who could only produce low molecular weight PLA from lactic acid (LA). Ultimately, he turned lactic acid to lactide and succeeded the ring-opening polymerisation of lactide to produce high molecular weight PLA (Figure 2.1).[121] At this point, production of PLA was mostly focused on achieving higher molecular PLA. The chirality of lactic acid, lactide and PLA were barely mentioned and the importance of it was not disclosed.
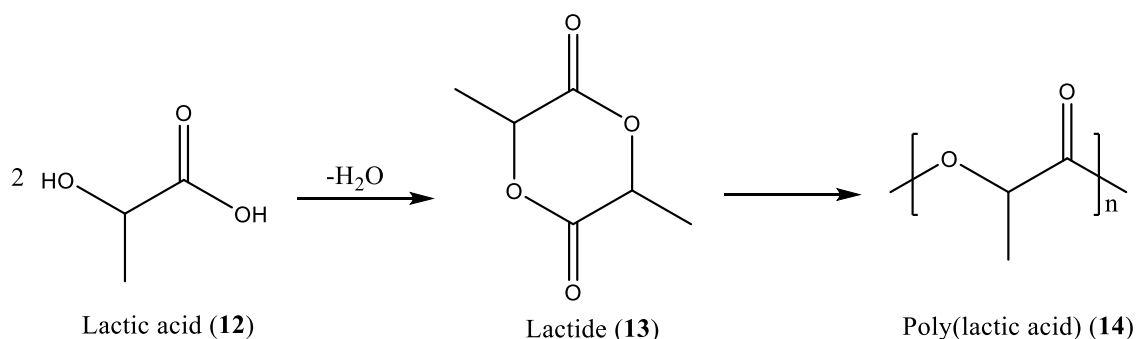
Figure 2.1. Condensation of lactic acid (**12**) to give lactide (**13**) and subjected to ring-opening polymerisation to give PLA **14**

Although the Carothers' method to produce PLA **14** was patented by DuPont, this biopolymer was not popular and more widely used in industry until the late 1990s by another company, Cargill.[122] Shortage of landfill space,[123] pollution and the environmental concersn of the plastics industry[124] had triggered more research activities with the goal of developing eco-friendly biopolymers. Cargill had overcome a cost issue which allowed them to synthesize both lactide (**13**) and PLA **14** in the melt instead of solution which also had environmental benefits.[125] The increased availability of PLA **14**

allowed more researchers to gain access to better understand the general pathway of producing PLA **14**, features of the precursors and products and, the importance of the optically active configurations as well as applications of PLA **14**. This polymer **14** was one of the strongest candidates to be developed amongst other biopolymers and one of the first reasons was due to the fact starting material **12** used to produce PLA **13** can be obtained from renewable natural sources. Lactic acid (**12**) itself can be synthesized from lactonitrile[126] but this method is not famously used and in fact, 95% of material **12** is derived from carbohydrate resources such as from corn starch.[127] Firstly, starch undergoes enzyme hydrolysis to become dextrose which is a type of glucose (sugar). Then, dextrose is fermented to give 2 equivalents of L-lactic acid which is polymerised to PLLA via polycondensation (Figure 2.2).[102] This direct polycondensation was first used and developed but this reaction is an equilibrium process but there are difficulties in removing the water as by-products that limit achieving the target molecular weight.[125] Producing high MW product with good mechanical properties using this route is challenging but it is still suitable for making biodegradable glue or lacquer.[128]

Starch (**15**)   Dextrose (**16**)   L-Lactic acid (**17**)   PLLA (**18**)
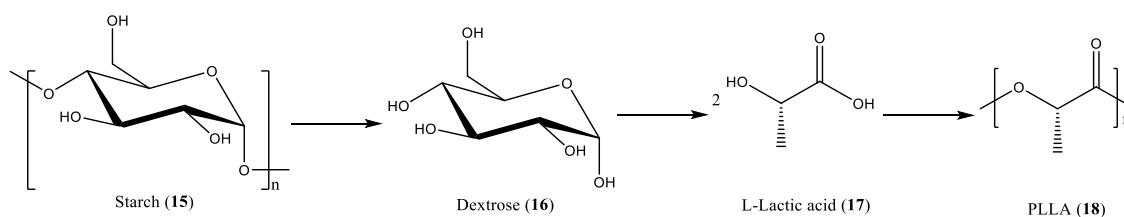
Figure 2.2. General pathway of corn starch (**15**) converted to dextrose (**16**), then L-lactic acid (**17**) and finally PLLA **18** via polycondensation[102]

As shown in Scheme 2 above, this microbial fermentation generally produces a stereo-specific L-(+) form of lactic acid **12** which gives majority of PLLA **18**.[127] Interestingly, lactic acid (**12**) can also be produced by mammals including humans[129] but mammalian cells only produce L-lactate dehydrogenase (L-LDH), an enzyme that can only produce L-lactic acid (**17**). Therefore, only the L(+) isomer can be produced in mammals exclusively.[130] Apart from the enzyme L-LDH, microorganism of the Lactobacilli family including, amylophilus, debruekii and helveticus strains can specifically yield L-lactic acid (**17**). Whereas other Lactobacilli strains such as bulgaricus can produce pure D-isomer.[131] The optical purity of lactic acid (**12**) is indeed very vital for PLA **14** production as small amounts of enantiomeric impurities can vastly alter certain properties such as crystallinity and, rate of biodegradation of the product.[132]   Not only can the optical configuration change the features of PLA **14**, this is also an important feature amongst

monomer **12** or **13**. Lactic acid (**12**) which consists of both racemic mixtures has the lowest melting point of 17 °C. Whereas the L(+) and D(-) isomers have higher m.p. of 53 °C. Similarly, meso-lactide which has both L(+) and D(-) configurations has a lower m.p. of 53 – 54 °C.[133] In contrast, its isomers which are optically pure have m.p. in the range of 95 – 98 °C (Figure 2.3).[134]
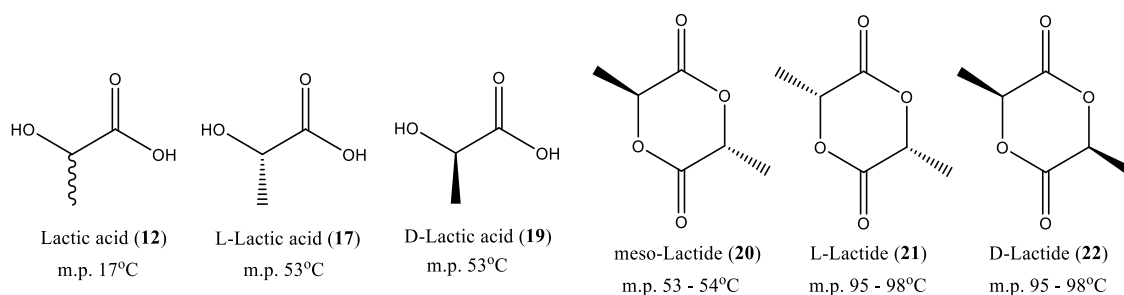
Figure 2.3. Isomers of lactic acids and lactides and their melting points

Upon recognition of the importance of the optical configuration of PLA **14**, the production method was further developed to produce polymers with controlled optical configuration as well as having higher molecular weights. As mentioned before, direct polycondensation to produce PLA **14** from lactic acid (**12**) has the drawback of not producing high MW polymer. Therefore, it is common that the low MW (1000 – 5000 Da) PLA **14** produced from polycondensation is often subjected to depolymerisation to produce 3 isomers of lactide. Backbiting reactions of PLA **14** produces different lactide isomers and the ratio depends upon the lactic acid (**12**) isomer feedstock, temperature and catalyst.[135] Typically, meso-lactide (**20**) can firstly be separated from D/L-lactide by repeated recrystallisation from various solvents, extraction, sublimation.[136] Lactide **21** & **22** can then can be further separated[137] and subjected to ring-opening polymerisation (ROP). Alternatively, catalysts can be utilised in order to produce PLA **14** with specific optical configurations. For instance, T. M. Ovitt *et. al*. reported an aluminium alkoxide complex that can catalyse meso-lactide (**20**) selectively to produce highly syndiotactic PDLLA with a yield of 94%.[138] C. Radano *et. al*. applied two chiral Schiff's base aluminium complexes to selectively polymerise L-lactide (**21**) and D-lactide (**22**) to produce pure isotactic PLLA and PDLA in paralell.[139] The mixture of 3 different polymers can be separated using a chromatographic method (Figure 2.4).[140]
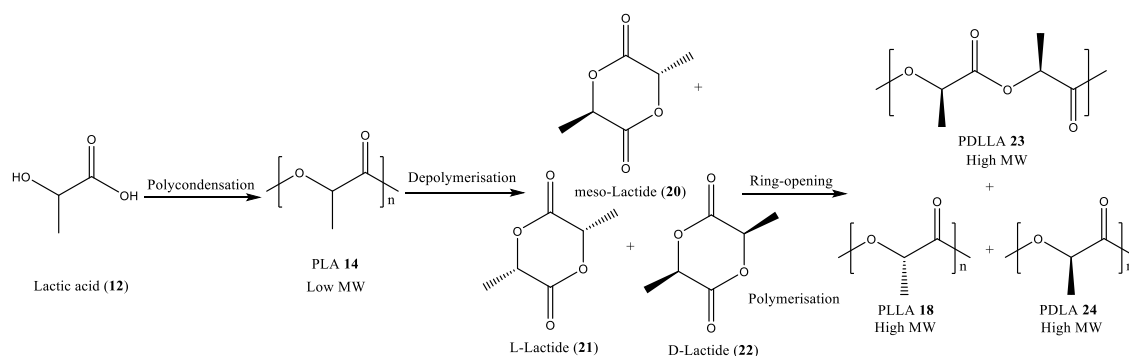
Figure 2.4. Production of high molecular weight PLA with controlled optical configuration via polycondensation, depolymerisation and ring-opening polymerisation

Production of PLA **14** using this pathway is more common as it can produce polymers with controlled stereochemistry and in addition, it can produce polymer with higher MW more easily. Another practical method that is often applied in the industrial process to overcome the limitation of producing low MW polymer from direct polycondensation of lactic acid (**12**) is via azeotropic dehydrative polycondensation. Generally, the most widely used method consists of reduced distillation pressure of LA **12** for 2 – 3 hours at 130 °C to remove water by-product of the condensation reaction. Catalyst and diphenyl ether as high boiling solvent are then added along with molecular sieves and this mixture was further refluxed for 30 – 40 hours at 130 °C. Finally, the polymer can be isolated for purification and the catalyst recovered by extraction with water and can be reused again.[141,142] This process can be summarised in the flow diagram below (Figure 2.5).
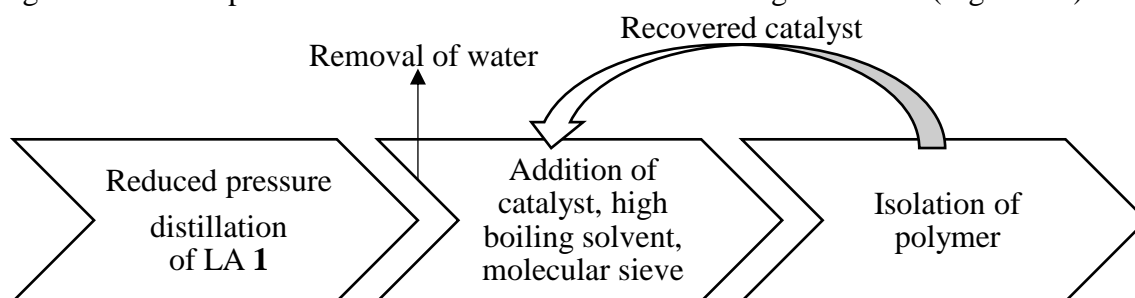
Figure 2.5. Flow diagram of PLA **14** production via azeotropic polycondensation

The use of high boiling solvent can further enhance the removal of water more effectively to obtain high MW PLA **14** and molecular sieves allows the isolation of polymer more easily from the solvent.[143] However, the use of high boiling solvent can increase the cost of production and removal of such solvent can be challenging and, is should be stated that the use of organic solvent has somehow created a contradiction of producing PLA **14** in an eco-friendly way.[144] Furthermore, it is also a concern that residual catalyst present in

the isolated polymer can negatively affect the properties of PLA **14**, such as degradation, uncontrolled or unreproducible hydrolysis rates as well as cyto-toxicity and different slow-release properties for products used in medical applications. Ideally, this issue should be resolved by using phosphoric or pyrophosphoric acid to deactivate the catalyst or addition of strong acid to precipitate or filter out the catalyst. By doing so, the weathering resistance, heat and storage stability of the polymer can be improved for various applications.[119] This method although popular and patented,[141] it is more focused on producing high MW PLA **14** and unlike using ROP, the stereochemistry of the polymer is often ignored.

2.2.1 Stereochemistry of PLA, PLLA, PDLA

Stereochemistry of the polymer is crucial as polymer with different configuration consists of different properties which are critical for further processing and application. However, this important piece of information is often ignored or only mentioned in passing by most researchers which can lead to contradiction or misunderstanding Much research conducted using PLA **14** has in the main been mostly concerned >90% with PLLA **18**. For instance, R. A. Auras *et. al*. studied 2 different PLA **14** but were in fact samples composed of 94 – 98% PLLA **7**.[145] The PLA **14** samples used by M. Murariu *et. al*. in their research actually contained 96% PLLA **18**.[146]

The properties of the polymer can be varied because of the stereochemistry and various research is on-going in order to tune the properties of PLA **14**. For example, very pure PLLA **18** and PDLA **24** have equilibrium crystalline melting points of 207 °C[147] but they often melt in the range of 170 – 180 °C very likely due to the presence of imperfect crystallites, slight racemization and impurities.[148,149] When a stereo-complex is formed with 1:1 PLLA **18** and PDLA **24**, the melting point was increased to 230 °C and crystallisation properties altered to give a high crystallisation rate and more stable crystals were observed.[150] In addition, this specific ratio of 1:1 PLLA:PDLA in the stereocomplex had more dense chain packing and induced stabilisation via stronger van der Waals interactions[151] between both polymer **18** and **24** and hence, the stereocomplex had increased tensile properties compared to pure PLLA **18** and PDLA **24**.[152] Although the stereocomplex is one of a popular type in the development of novel PLA **14** materials, it is not always the ideal type for all applications. It is more important to identify the needs and apply the suitable polymer.

2.2.2 PLLA as Biodegradable, Biocompatible Material

PLA **14** has been developed for packaging materials in the past 10 years. In comparison to other commonly used polymers such as polystyrene (PS) and poly(ethylene terephthalate) (PET), PLA **14** has a lower melting temperature which can reduce the cost of processing and the products can have improved mechanical properties.[153] As PLA **14** is also a thermoplastic this allows it to be subjected to multiple, reheat or reprocessing cycles with preserved mechanical properties.[154] Upon incineration, PLA **14** can be burnt without producing poisonous or corrosive gases and it can also be recycled to its monomers for remanufacturing again.[155] These features make PLA **14** a more attractive material to generate biodegradable and eco-friendly products. In this field, the stereochemistry of the polymer is not a major factor and often not specified at all. It is because when PLA **14** was further developed for biomedical applications, the optical configuration becomes a critical matter and more research studies have been conducted to confirm the relationship between PLA **14** stereochemistry and biocompatibility to produce safe and non-toxic materials.

Generally, PLLA **18** is more commonly utilised in the field of biocompatible and biodegradable applications. As it was mentioned in the previous section, the most famous pathway from corn starch can often ultimately lead to production of PLLA **18**.[127] L-LA **17** is indeed a biological metabolite as well as being the main fraction of PLA **14** derived from bio-renewable sources as the majority of LA **12** from biological sources exists in this form.[118] This naturally occurring L-LA **17** can also be used to make commercial PLLA **18** less expensive compared to that of PDLA **24**.[156] The fact that its monomer L-LA **17** can be produced by the human body[130] has caught the attention of researchers investigating the biocompatibility of PLLA **18** with humans. In fact, PLLA **18** is highly tolerated by the human body because degradation of PLLA **18** is a hydrolytic process which starts with the diffusion of water into the material then breaking of the polymer chains into small oligomers which can diffuse in and out of the polymer matrix.[157] The degradation product L-LA **17,** can be incorporated into tricarboxylic acid or Krebs' cycle and excreted by body as carbon dioxide and water. Therefore, PLLA **18** can undergo degradation and is completely resorbable in the human body.[158] Different research has shown that PLLA **18** was proven to be non-toxic for both rats[159] and human mesenchymal stem cells.[160] A further *in-vivo* study conducted with 20 human patients who had patellar tendon autograft anterior cruciate ligament reconstruction with PLLA **18** screws indicated

that all of the screws completely degraded after 89 to 124 months after insertion. More importantly, significant bone ingrowth that involves any bone formation within the screw site was not observed and additional surgery to remove the implant was not required.[161] PLLA **18** has been reported to have a tensile modulus as high as 16 GPa,[153] it can provide long retention of strength that is suitable for being applied in ligament and tendon reconstruction and, vascular or urological stents in the field of medical health care materials.[118]

Another reason for PLLA **18** being more popular than PDLA **24** for developing biocompatible and biodegradable products is that biodegradation of the former is more favourable. Is it because PLLA **18** has a lower crystallinity and PDLA **24** can actually act as a nucleating agent to increase the crystallisation rate and thereby slow down the rate of biodegradation of PLLA **18**.[162] This is a crucial factor in the design of biodegradable materials as the polymer chains in the amorphous phase are randomly arranged, or loosely packed, resulting in the polymer being more susceptible to degradation. In contrast, crystalline polymers are well-ordered and cause them to be more resistant to degradation.[163] Therefore, more research studies have been focused on applying PLLA **18** as the base material and associated with PDLA **24** in order to alter the thermal and mechanical properties[164] as well as customising the enzymatic[164] and hydrolytic[165,166] degradation of the resultant blend material.

2.2.3 Popular Industrial Processing Methods

After the unique properties and potential of PLA **14** as well as PLLA **18** and PDLA **24** were identified, interest was directed to techniques that could be used to generate PLAs by applying industrial manufacturing methods. Either polymer **14** was produced using polycondensation, ROP or azeotropic polycondensation and, the resin or pellets produced required drying prior to further processing. It is because the moisture present in the pellets can cause hydrolytic degradation that leads to reduced MW of the polymer during further processing.[167] Extrusion is a very common way of converting polymer pellets into different forms and is often the first step in the processing of PLA **14** and other materials in the polymer industry. This involves using a screw extruder which consists of an electrically heated metal barrel, a hopper for adding polymer pellets, a motor that can rotate the screw and a die for polymer melt to exit. Depending on the application, the polymer melt that exits the die can be subjected to further down-stream processing to make various materials (Figure 2.6).
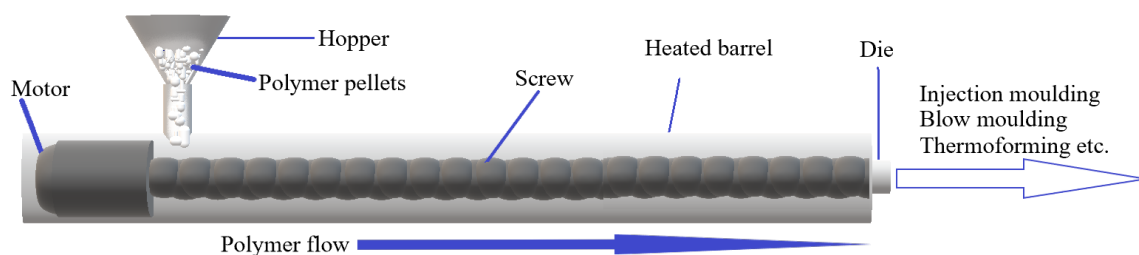
Figure 2.6. Diagram of polymer extrusion process

A combination of the thermal energy from the heated barrel and frictional energy between the pellets and screw melts the pellets prior to mixing. The ratio of flight length of the screw to its outer diameter commonly known as L/D ratio ($L/D = \frac{Flighted\ length\ of\ screw}{Outside\ diameter\ of\ screw}$) can influence the shear stress acting on the polymer and the residence time of the polymer melt in the extruder. Larger L/D ratio screws are favoured due to higher throughput, better mixing capability, pumping at higher die pressure, greater melting capacity with less shear heating and enhanced conductive heating via the barrel.[168] Modern extruders for processing one or more polymers or additives to give blends or composites are commonly equipped with double screws. This type of twin-screw extruder can be categorised as either co-rotating or counter rotating extruder. The former refers to screws that both rotate in one direction (both clockwise or anti-clockwise). The latter describes the extruder with one screw rotates clockwise and the other rotates anti-clockwise.[169] This technique is suitable and widely used to process PLLA **18** in which, barrel temperature and screw rotation speed are crucial factors to control to avoid degradation and ensure the MW of the resultant polymer does not decrease. V. Taubner *et. al.* have shown that severe damage can occur when PLLA **18** was extruded at 240 °C even at low rotation speed of 20 rpm that caused poor mechanical properties of the resultant product.[170]

After extrusion, injection moulding is often the next step in polymer processing and this is especially useful to produce products that require complex shape or high dimensional precision. The process involves injecting the polymer melt in to a mould at lower temperature and then ejecting the solidified polymer product. The extruder component contains a reciprocating screw to rotate as well as move forward and backward to fit the moulding cycle.[171] The mould is equipped with a cooling system that allows controlled cooling for solidifying the polymer. This technique simply requires the polymer melt can flow and fill the mould cavity easily[172] and is suitable for producing biodegradable scaffolds with complex shapes that consists of appropriate morphology with preserved

mechanical properties suitable for tissue engineering,[106] and biodegradable implants.[173] PLLA **18** has also been injection moulded with evidence shown that it can be used to produce PLLA **18** bio-absorbable interference screws. The authors noted that the crystallinity of the product was altered due to the cooling process within the mould.[174] As crystallinity is highly related to the rate of biodegradation, a different study conducted by Ghosh *et al.* also investigated the relationship between injection moulding parameters and crystallinity of injected PLLA **18**. It was observed that degree of crystallinity is directly proportional to shear stress but shear rate has a rather less effect which is inversely proportional to crystallinity.[175] However, PLLA **18** itself is a brittle material which has limited its application and the mechanical properties can only optimised up to a certain level via thermomechanical manipulation of conventional injection moulding (CIM).[176] In contrast, non-conventional methods such as shear controlled orientation in injection moulding can give additional degrees of freedom to manipulate the structure development of a solidifying polymer melt via an in-mould shearing action in order to tailor the morphology and controlling the mechanical properties of polymers.[176,177] This approach consists of an externally controlled in-mould unit, a SCORIM unit that includes two cylinders with each of them located on a different melt flow path leading to its corresponding gates (Figure 2.7).
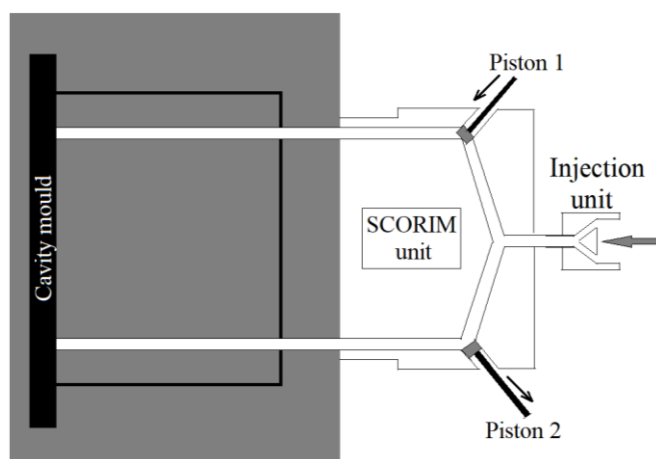
Figure 2.7. Schematic diagram of the SCORIM process

The cavity normally filled with one gate and melt manipulation can then be operated using three different modes. The first one is an out-of-phase mode that can control the forward and backward movement of cylinders to manipulate the melt inside the mould. Secondly, an in-phase mode that allows pumping of more polymer melt into the cavity. Finally, the hydrostatic pressure then applied by the cylinders to offset volumetric shrinkage.[176] PLLA **18** processed using this technique showed higher toughness as well as maximum stress

compared to that of CIM. Without the aid of polymer blending or plasticizers, mechanical properties of PLLA **18** products were promising without sacrificing stiffness.[178]

Apart from SCORIM, other techniques such as micro injection moulding has also been widely developed and applied in biomedical applications which can be used for producing polymeric products with high surface-to-volume ratios,[179] encapsulation with even further complex geometries for drug delivery[180] and in medical devices.[181] Hence, injection moulding is a versatile technique available for producing various polymeric products.

2.2.4 Common Methods for Modification of PLLA

PLLA **18** has great potential to be a green polymer being biodegradable and a biocompatible material. However, this material is well known to be brittle[176] which is indeed a major drawback and disadvantage for certain applications. As was discussed above, different approaches such as stereocomplexation can increase the melting temperature of PLLA **18** to 230 °C,[152] incorporation of PLLA **18** with PDLA **24** can also alter thermal and mechanical properties[164] and customise the degradation of the resultant material.[166]   Modification is commonly applied to overcome this disadvantage (brittleness) in order to diversify further the application of PLLA **18**.

Apart from PDLA **24**, different polymers can also be used for modifiy PLLA **18**. Commonly, copolymerisation can be used to introduce a different polymer along with PLLA **18** an example is poly(ethylene glycol) (PEG) which can be used to alter the thermal[182] or hydrolytic properties[183] as well as enhancing the hydrophilicity of PLLA **18** for drug delivery application.[184] Alternatively, physical blending is a more straight forward way to combine PLLA **18** with other polymers. With the aid of solvent, PLLA **18** can be blended with poly(ε-caprolactone) (PCL) resulting in improved thermal and mechanical properties.[185] The flexibility of PLLA **18** was improved after blending with poly(ester-urethane) (PEU).[186] Apart from using solvent, it is also possible to use melt mixing to obtain polymer blends[187] or composites.[188] Melt extrusion is a common tool which ensures the components are mixed thoroughly. This method is solvent-free which is more eco-friendly and then injection moulding can often be utilised in order to obtain products with designated shapes.[189] Therefore, melt extrusion along with injection moulding is a very convenient way to make polymer blends or composites and it these processes are more environmentally friendly than using solvents and can be used for large-scale production of PLLA **18** blends. Excluding improving or enhancing certain poor properties of PLLA **18**, blending can also be used to introduce new properties to the

polymer. For instance, incorporation of silver nano-particles to PLLA **18** can yield a composite material that exhibits anti-adhesion and antimicrobial properties.[190] Hence, with the appropriate choice of polymer or additive components, it is possible to generate novel PLLA **18** blends or composites that are eco-friendly, biodegradable, biocompatible with additional properties, such as antimicrobial efficacy. A selection of naturally occurring materials have many intrinsic properties, including antimicrobial offer great potential in biomedical applications when blended with PLLA **18** and will now be introduced. Most have not been blended with PLLA **18** before to produce novel biodegradable and biocompatible materials.

2.3 Lignin

In the world of plants, lignin is the major component that gives rigid structural support in vascular plants. It was first discussed in 1813 by Augustin Pyramus de Candolle who described lignin as a fibrous, tasteless material that cannot be dissolved in water or alcohol, is soluble in weak alkaline solutions and can be precipitated from solution with acid. He named this material "lignine" which was derived from the Latin word, "lignum".[191] Apart from being the support tissue in plants, it plays an important role in biosynthesis which can be initiated under biotic/abiotic stress conditions including wounding, pathogen infection, metabolic stress and perturbations in cell walls.[192] It is known that polysaccharides, such as cellulose in plants, can be protected by lignin against microbial degradation to impart decay resistance. Its chemical structure is a cross-linked matrix made up of aromatic phenol polymers which can be categorised by three types of mono-lignol building blocks, coniferyl (G), sinapyl (S) and *p*-coumaryl alcohol (H) (Figure 2.8).[193] Generally, lignin in plants is composed of all G/S/H lignin units but the ratios vary in different species, excluding gymnosperms which are mainly composed of G lignin, angiosperm dicots that are composed of G and S lignin and, the H lignin content is slightly higher in grasses.[194]
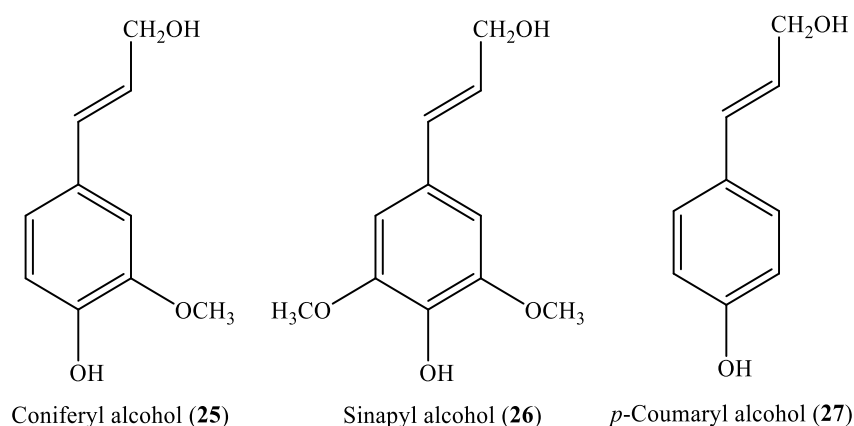
Figure 2.8. Chemical structures of coniferyl (**25**), sinapyl (**26**) and p-coumaryl alcohol (**27**)[195]

Lignin polymerisation or lignification occurs via oxidative radical coupling of monolignol involving enzymes such as peroxidases and/or laccases.[196] The former enzyme uses hydrogen peroxide as a substrate and the latter uses oxygen to oxidise its metal centre to enable catalytic phenol oxidation. When a monolignol is oxidised, the relative phenolic radical can be stabilised because of the delocalisation of the unpaired electron in the conjugated system. Two radicals may couple to form a new C-C or C-O bond which favour at their β positions to give β-β, β-5 and β-O-4 dimers (Figure 2.9).[195] Such radical-radical coupling occurs in a chemical combinatorial fashion and so, the orientation of the possible coupling products highly depend upon the chemical nature of each of the monolignol radical as well as the conditions in the cell wall.[197]
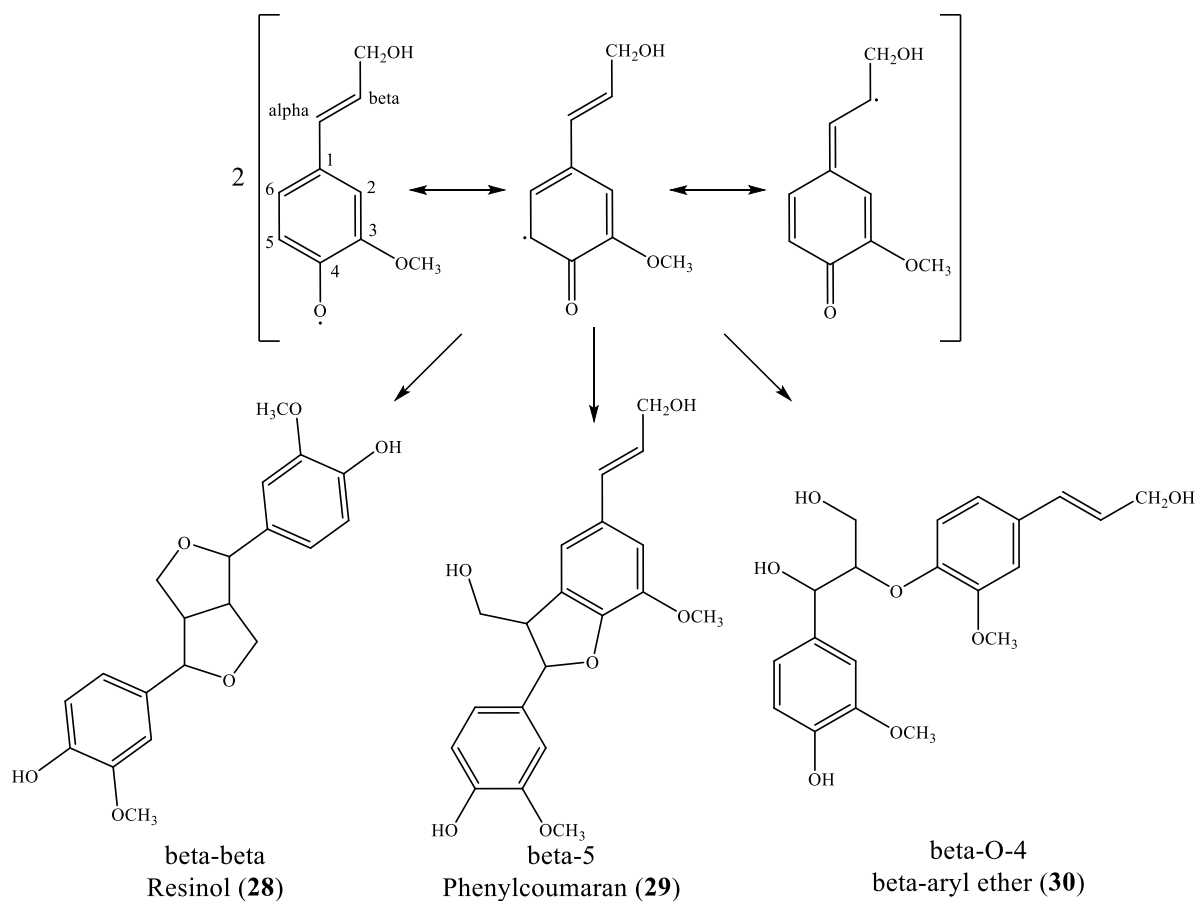
Figure 2.9. An example of delocalisation of the phenolic radical compound and possible resulting dimers[195]

The resultant dimers can be oxidised again to form a new radical and couple with another radical. This coupling can continue to occur between a new monolignol radical, a growing radical chain or two different growing racial chains. Therefore, unlike biopolymers such as chitin and cellulose, the structure of lignin is in effect a phenolic polymer network/matrix (Figure 2.10)[198] which can be irregular and, cannot be simply represented by repeating units. The average length of a lignin chain was estimated to be between 13 to 20 units.[199]
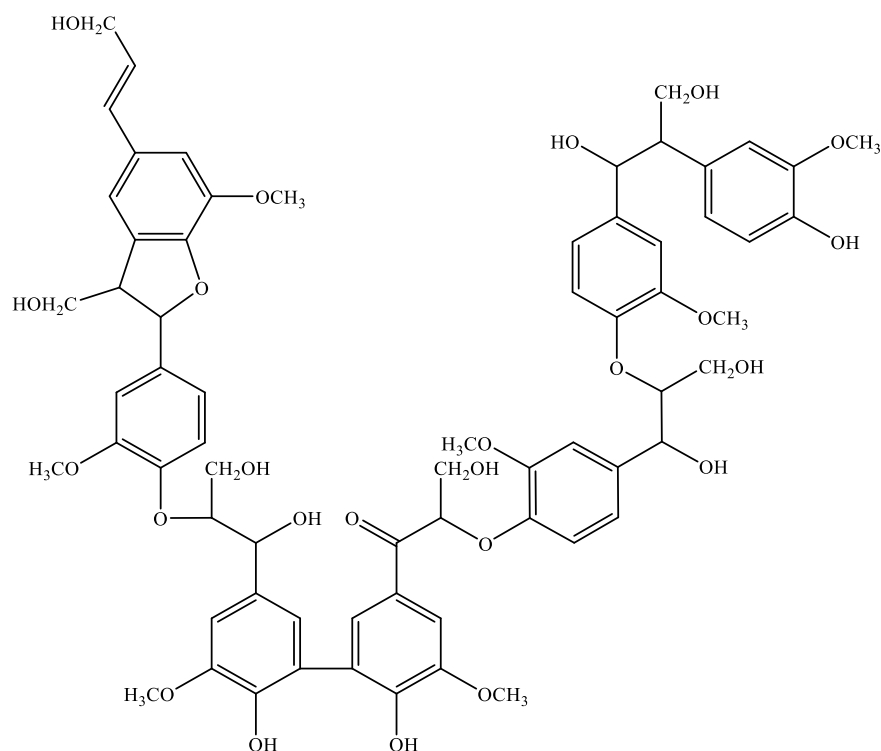
Figure 2.10. Partial structure of a lignin network[198]

In the cell wall, a linkage is formed between the lignin polymer network and the polysaccharide components, the resulting strong lignin-carbohydrate networks means the direct separation of individual polymers is very difficult.[200] In industry, the Kraft process or Kraft pulping is often applied which involves treating wood chips with sodium hydroxide and sodium sulphide to break the bonds between lignin, hemicellulose and cellulose.[201] Briefly, lignin from the process is removed from the fibre wall and solubilised in the mixture with a pH value that remains high due to the presence of ionised phenolic hydroxyl groups formed through reaction between lignin and the pulp mixture. Using a weak acid such as carbon dioxide, lignin can be protonated and then precipitated and filtered. However, the lignin separated during this process in most cases would normally be burned as a fuel in contrast to cellulose which can be turned to useful materials and used in packaging and paper.[202] Until recent years, it was reported that lignin can be a source to produce useful materials such as polyurethane foam[203] and carbon fibre.[204]

Although not widely reported, the fact that lignin acts as the structural support and is responsible for biosynthesis in plants, its biological properties have attracted some research interest. Zemek *et al*. studied model structures using bacteria, yeasts, yeast-like micro-organisms and moulds and observed that their growth was inhibited by G-lignin

25 and S-lignin **26**. Hence, it was concluded that lignin can exhibit antibiotic properties.[205] Recently, it was reported that Lig-8, a lignophenol derivative of lignin extracted from bamboo is a highly potent neuro-protectant for humans.[206] It was also reported that lignin derived from bamboo displayed antibacterial properties towards *Phyllostachys pubescens*;[207] and the lignin residue of corn stover (from ethanol production) showed strong antioxidant activity (based on results from hydrophilic oxygen radical absorbance capacity assay) as well as antimicrobial activity against *Listeria monocytogenes*, *MRSA* and yeast.[208] In other studies, extracts such as cellulose, hemicellulose did not show significant antibacterial properties. Therefore, it has been claimed that lignin could be the major component to provide antimicrobial properties in plants.[207] It is another biopolymer that can provide positive health benefits to humans and its antimicrobial properties explored further.

2.3.1 Previous Research on Blends of Lignin and Polymers

Although lignin is a bio-renewable biopolymer and has the potential to be developed for use in antimicrobial products but, its poor solubility in most common solvents is a drawback. In recent years, research has focused on the use of ionic liquids to dissolve lignin.[209] Alternatively, melt extrusion is a more commonly applied method especially in the preparation of polymer blends or composites. Kubo *et. al*. applied this method to prepare immiscible blends of PVOH and lignin[210] and Kadla *et. al*. also used the same method to produce a selection of lignin-based polymer blends.[211]

As PLLA **18** is becoming more and more popular due its eco-friendly, biocompatible and biodegradable properties, approaches were reported to combine PLLA **18** and lignin to prepare blends or composites. Li *et. al*. introduced lignin to PLLA **18** and aimed to lower the overall cost of products and adding some biodegradable characteristics to PLLA **18**. In this study, lignin and PLLA **18** were simply blended by hand using a mortar and the mixture compression moulded at 200 °C. However, it should be noted that the manual mixing is flawed and it failed to produce polymer blends at the molecular level and the actual applications of such blends was unclear.[212] Rahman *et. al*. also prepared PLLA/lignin blends using melt extrusion along with compression moulding but the authors observed that the introduction of lignin to PLLA **18** increased brittleness of the resultant composites. However, PEG was also introduced which acted as a plasticizer to provide flexibility and alter stiffness. The aim of this study was to understand the

influence of lignin as a filler and PEG as a plasticizer on the overall physico-mechanical behaviour of PLLA **18** but the potential uses of the composite was not discussed.[213]

There are other research groups who have prepared PLLA/lignin composites but the majority of research interest was mostly based upon addition of lignin to improve the thermal and mechanical properties of the PLLA-based composite.[212] Since lignin has exhibited antimicrobial efficacy, lignin can be introduced to polymers to provide additional antimicrobial properties. It was reported that lignin when incorporated into PVOH resultant composites exhibited a synergistic antioxidation response. Moreover, it could inhibit the growth of Gram-negative bacteria including *Erwinia carotovora subsp. carotovora* and *Xanthomonas arboricola pv. pruni*.[214] Yang *et. al*. used melt extrusion to prepare PLA **14** based composites with cellulose and lignin particles and observed that the composite materials exhibited a biocidal activity against a tomato bacterial plant pathogen.[215] The same research group conducted further experiments and confirmed that these composites have the potential to be developed for food packaging to provide protection against other bacterial plant pathogens such as *Xanthomonas axonopodis pv. vesica toria*.[216] Although PLLA **18** is more compatible with the human body, the antimicrobial property of PLLA/lignin composites has not been widely tested. Kai *et. al*. prepared nanofibers using PLA-lignin copolymer and PLLA **18** which exhibited antioxidant activity and with the optimal amount of lignin, the composites were compatible with human dermal fibroblasts and mesenchymal stem cells.[217] Hence, PLLA/lignin composites have the potential for use in the field of biomedicine and lignin can provide additional antimicrobial properties to PLLA **18,** which is not inherently antimicrobial.

2.4 Chitin

Amongst the reported biopolymers developed for food packaging, chitosan is inherently antimicrobial which can exhibit such efficacy even without the presence of antimicrobial additives. This is because it can promote cell adhesion via interactions with the negatively charged cell membrane particularly with residues of carbohydrates, lipids and proteins to cause leakage of intracellular constituents and thus inhibit the growth of microbes.[218] Chitosan is a linear polysaccharide, poly- β(1→4)-D-glucosamine[219] and there are often misconceptions with regards to the origin of chitosan. Precisely, chitosan does not naturally exist as it is derived from poly-β-(1→4)-N-acetyl-D-glucosamine, chitin (Figure

2.11). The word "chitin" originated from the French word "chitine" which was derived from the Greek word "χιτών: chiton" which means covering.[220] Commercially available chitin is often extracted from shrimp shell but it also exists in species such as Weinberg snail, baker's yeast (Saccharomyces cerevisiae), cockroach, lobster, mussel, squid, crab and its chemical structure was confirmed by Albert Hofmann in the late 1920s.[221,222] In an industrial process, extraction of chitin generally involves acid treatment of shrimp shell to remove minerals/salts, deproteinisation, removal of pigments with bleach and, chitosan can be further obtained by deacetylation with alkali.

Chitin (**31**)   Chitosan (**32**)
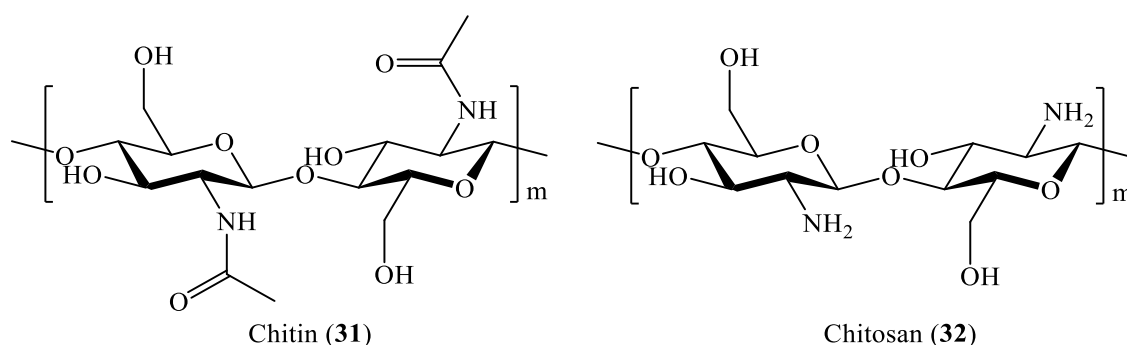
Figure 2.11. Chemical structures of chitin (**31**) and highly deacetylated chitosan (**32**)

Chitin (**31**) is placed as the second most abundant natural biopolymer after cellulose.[223] Its chemical structure consists of solely N-acetyl-D-glucosamine, whereas the structure of chitosan (**32**) is obtained from the deacetylation of chitin (**31**) which can compose of both N-acetyl-D-glucosamine and glucosamine.[224] It is always vital to distinguish between chitin and its derivatives but unfortunately, much of the reported literature claiming to use chitin was in fact chitosan[225] or some other derivative.[226] Chitin (**31**) is very thermodynamically stable, stability derived from the hydroxyl and N-acetyl-D-glucosamine units promoting a very complex hydrogen bonded network. The carbonyl (C=O) group of N-acetyl-D-glucosamine unit itself can promote two types of hydrogen bonding spontaneously, both intramolecular and intermolecular hydrogen bonding with an adjacent hydroxyl group and an amide (NH group), respectively (Figure 2.12) to provide extra strength and structural support.[227]
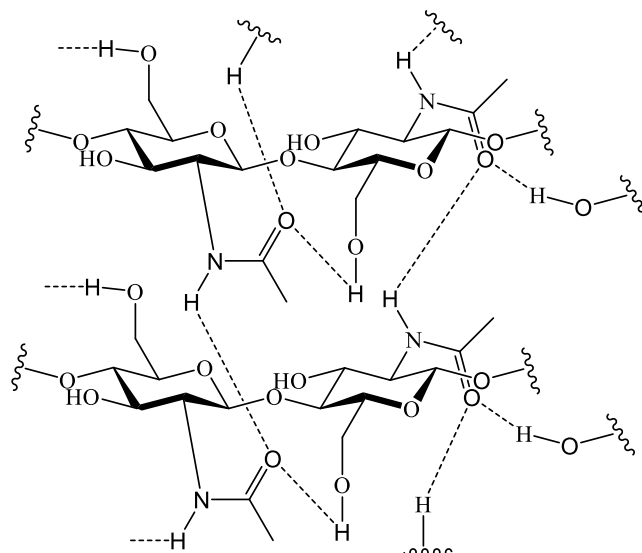
Figure 2.12. Schematic representation of the hydrogen bonding network in chitin (**31**)[227]

As a result, chitin (**31**) is often difficult to dissolve and processes in to various forms directly. So far, the most common solvents which have been used to dissolve chitin (**31**) include 1,1,1,3,3,3-hexafluoro-2-propanol (HFIP), a very corrosive, hazardous fluorinated solvent which is environmentally contentious and harmful to humans. Moreover, special laboratory equipment is required to tolerate such a corrosive solvent.[228] Alternatively, *N,N*-dimethylacetamide(DMAc) containing lithium chloride (LiCl) can also be used to dissolve chitin. However, DMAc can cause liver damage[229] where Li^+ in LiCl acts as Lewis acid to solvate the chitin amide group and it is uncertain whether this can be reversed by washing the resultant chitin group thoroughly.[230] It is also a concern that such harsh solvents can alter the nature of chitin (**31**) or even cause damage.[231] This is the main reason as to why chitin (**31**) is usually ignored and, is much less reported than chitosan but it is commonly used as a precursor and converted to different derivatives. Although it is very challenging to process chitin (**31**), the fact that it is naturally occurring in the exoskeleton of various species to provide protection and structural support has become its unique feature in biology. In spite of being described as the most insoluble polymeric forms of the substance, it has been proven that chitin (**31**) exhibits wound-healing effects[232] which has even been reported as a "potent pure chemical wound healing accelerator".[233] This property is attributed to the N-acetyl-D-glucosamine unit which can stimulate the production of hyaluronan and glycosaminoglycans in the extracellular matrix that are responsible for binding and regulating different proteins by cells such as fibroblasts.[234] As chitin (**31**) can be degraded by the enzyme, chitinase[222] which can be

produced by humans, this further supports the hypothesis that it is safe to be used in medical devices for application with humans.[235]

To further develop chitin (**31**) for use in medical devices, more research must be completed to fully investigate its potential. One of the common concerning aspects is whether chitin (**31**) can be used with humans who are allergic to shell fish. Fortunately, the source of the allergen of shell fish is a protein called tropomyosin, not chitin (**31**).[236] Recently, Benhabiles *et al.* tested the antibacterial activity of chitin (**31**) and confirmed that it showed inhibitory growth activity against two *MRSA* strains (Gram +); *E. coli*, *Vibrio cholera*, *Shigella dysenteriae* and *Bacteroides fragilis* [Gram-(–)]. The authors concluded that chitin (**31**) should be categorised as bacteriostatic (i.e. the ability to prevent or inhibit to growth instead of killing bacteria) rather than bactericidal (killing it instantly)[237] as the mechanism of antibacterial activity involved makes the bacteria flocculate and so killing it presumably through a lack of nutrients and oxygen.[238]

Researchers have demonstrated the potential of using chitin (**31**) for medical applications especially as an antimicrobial agent. Its insolubility in most organic solvents is indeed the major barrier to further development however, resultant chitin products would have very high tolerance towards most solvents as well as being a non-toxic, safe, renewable and biodegradable material.

2.4.1 Previous Research on Blends of Chitin and Polymers

As analogous to lignin, the difficulty of using chitin (**31**) is its very poor solubility in organic solvents. In addition, its strong micellular structure consists of strong intra- and intermolecular hydrogen bonding which results in no melting point for Chitin (**31**).[239] Thus, it is generally not the number one candidate to make polymer blends or composites. In contrast, chitosan (**32**) or other derivatives are more commonly reported and recognised.[240] As it was mentioned previously, harsh and very harmful solvents were used before the development of ionic liquid as powerful solvents.[241,242] For instance, Mi *et. al*. used DMAc/LiCl to prepare chitin/poly(lactic-co-glycolic) (PLGA) blend[243] and they later used the same reagent to prepare chitin/PLGA and chitin/PLA microspheres as biodegradable drug delivery systems.[244] Park *et. al*. used HFIP to prepare chitin/silk nanofibers.[245] Peesan *et. al*. prepared chitin/PVOH blend films via solution casting with concentratedformic acid. However, chitin (**31**) is insoluble in formic acid and so chitin (**31**) was only suspended in the strong acid prior to film casting.[246]

Alternatively, melt extrusion can be applied to prepare polymer blends or composites. Niño *et. al.* prepared starch-chitin/low density poly(ethylene)/ethylene-co-acrylic acid blends using extrusion to prepare new biodegradable films.[247] Yang *et. al.* prepared chitin/PCL blends using melt-blending.[248] Although these two early studies demonstrated the likelihood of applying melt extrusion, this method is not widely used to produce chitin-containing polymer blends and interest in applying these products in the biomaterials field was not a major focus.

In more recent years though production of polymer blends incorporating chitin (**31**) using melt extrusion have been more slightly targeted towards biomedical uses. Rizvi *et. al.* prepared PLA/chitin composites via melt-extrusion along with compression moulding. In this research, the authors noted that effective dispersion of chitin (**31**) could be a challenging issue and suggested an additional additive could be introduced to address this problem.[249] When N. Herrera *et. al.* prepared PLA/chitin blends, glycerol triacetate also known as triacetin (Figure 2.13) was introduced as a plasticizer during melt compounding. Triacetin itself can be used as an edible food additive[250] and it can also act as a plasticizer to reduce the brittleness of PLA **14** as well as a processing aid to facilitate the dispersion of chitin (**31**) during extrusion. This plasticized PLA/chitin blown film was expected to be a good packaging material and provide protection against fungi.[251]
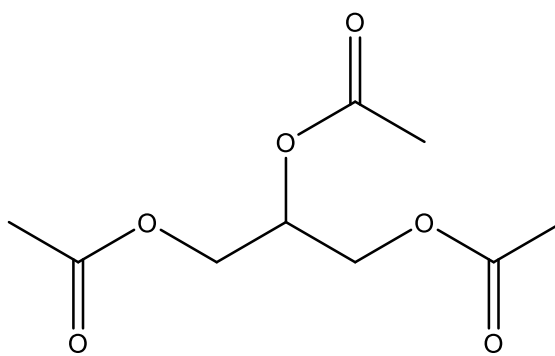
Triacetin (**33**)

Figure 2.13. Chemical structure of plasticizer, triacetin (**33**)

Although the toxicity or biocompatibility of the composites were not mentioned in this study, Mou *et. al.* confirmed that the composites did not cause allergic reactions as well as agitation or inanimate behaviour when tested with guinea pigs and rabbits.[252] Arunraj *et. al.* loaded a chemotherapeutic agent in a PLA/chitin composite and proved it to be an effective drug delivery system for cancer treatment.[253] On the other hand, few research studies have been published that describe the introduction of chitin (**31**) to PLLA

18 to develop new composite materials. For instance, Li *et. al.* prepared porous PLLA **18** scaffold reinforced by chitin (**31**) to achieve higher mechanical strength[254] and a further in vitro evaluation suggested that the material had the potential to be used in tissue engineering.[255] Their *in-vivo* tests showed the material was especially suitable for bone tissue engineering as it exhibited inductive bone formation by repairing bone defects. Kim *et. al.* prepared chitin-graft-PLLA and aimed to explore its potential for biomedical applications.[256] The former research group used dicyclohexylcarbodimide and organic solvent to link PLLA **18** and chitin (**31**)[254] and used DMAc/LiCl to prepare the copolymer.[256] Melt blending or extrusion is a more environmentally friendly approach that can avoid using organic solvents or harsh chemicals to generate new PLLA/chitin composites. Chitin (**31**) is biodegradable, biocompatible and exhibits antimicrobial properties. This material is a good candidate to introduce or improve various PLLA **18** properties for generating novel biomedical materials.

2.5 Tungsten Disulphide

Tungsten disulphide (WS_2, tungstenite) is a naturally occurring mineral[257] that was firstly used as a lubricant[258] that can withstand high temperatures and contact pressures up to 2068 MPa (300000 psi).[259] This material can also be prepared synthetically using controlled sulphidisation by reacting hydrogen sulphide (H_2S) with tungsten trioxide (WO_3) in a fluidised-bed reactor;[260] and direct synthesis from the vapour phase via chemical transport reactions consisting of the thermal decomposition of ammonium thiotungstate [$(NH_4)_2WS_4$] at 1200 – 1300 °C in hydrogen gas.[261] This inorganic nanomaterial has a structure that is analogous to multiwall carbon fullerenes and nanotubes which consist of layered one and two-dimensional molecular sheets that stacked and held together by van der Waals forces. In comparison to other two-dimensional nanoplatelets, WS_2 platelets are not stable because of the abundant dangling bonds on the rim of W and S atoms that are only four- and two- fold bonded respectively.[262,263] When the molecular sheets are being folded to cause the rim atoms to stitch together to stabilise nanotubular and spherical structures with all W and S atoms results in six- and three- fold-bonding respectively.[263] WS_2 nanotubes have outer diameters in the range of 10 – 30 nm with main size distribution centred from 15 – 20 nm. They are uniform in shape, open-ended and their lengths range from hundreds of nano-meters to several micro-meters with a hollow core that occupies up to 70% of their total volume and are found to be perfectly crystalline.[264,265]

Although the van der Waals forces between molecular layers are weak, they can bring benefit allowing easy, low-strength shearing. In addition to their chemical inertness and hollow structure, WS_2 has the ability to impart elasticity and allows particles to roll instead of slide when acting as a solid-state lubricant.[266] Apart from being developed as lubricants, WS_2 has also been used in the development of rechargeable batteries as it consists of fast-ion conductivity[267] and has been shown to improve the performance as lithium (Li) ion battery anodes.[268] WS_2 can be fabricated in to a well ordered mesoporous material with high surface area and narrow pore size distribution to deliver excellent high rate capability to Li ion batteries.[269] In addition, WS_2 remains chemically inert after being treated with super acid and such harsh treatment resulted in even large-area, few-layer WS_2 sheets in large quantities. Hence, increased Li-ion intercalation sites obtained lead to an improved reversible capacity.[270] WS_2 nanotubes exhibit superior mechanical properties as they have a Young's modulus up to *ca.* 150 GPa and tensile strength above 16 GPa. They can deform elastically to a large extent under both compression and tension but appear to be almost defect free. Furthermore, the interlayer shear modulus was found to be *ca.* 2 GPa and WS_2 is able to withstand shock waves of up to 21 GPa. This attractive mechanical behaviour and other properties such as tribological and conductive features mentioned above has attracted the attention of polymer scientists to further develop WS_2 as a filler or additive to produce polymer nanocomposites.

Using inorganic nanomaterials as reinforcing agents to improve tribological[271] and mechanical[272] properties of composites,[273] polymeric fibres[274] and nanocomposites becoming increasingly popular in polymer chemistry.[274] WS_2 is still a very new candidate in this field and related research has not been widely reported although WS_2 was first synthesised more than 20 years ago. As WS_2 was identified first as a solid lubricant, early studies included WS_2 being developed as a composite that exhibited adaptive lubricant behaviour that could withstand high temperature.[271] More research was then conducted to incorporate WS_2 into polymers, for instance, Sonker *et. al.* applied WS_2 as reinforcement to glutaric acid/poly(vinyl alcohol) (PVOH) to improve mechanical properties. As sulphur can act as a hydrogen bonding acceptor,[275] the outermost S atoms of WS_2 nanotubes can form hydrogen bonds with the hydroxyl groups of PVOH. As a result, WS_2 increased the tensile strength and toughness of PVOH by 86% and 102% respectively. This suggests the strong interaction between S and -OH groups facilitates stress to be transferred from the polymer network to the reinforcing WS_2 (Figure 2.14).[276]
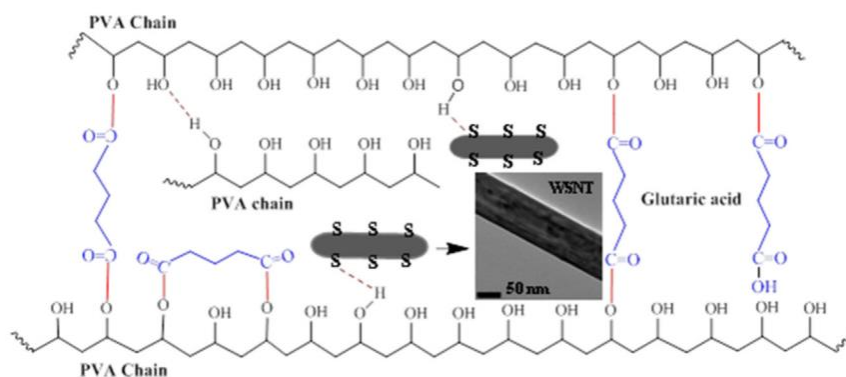
Figure 2.14. Schematic diagram of WS$_2$-PVOH composite which illustrates the hydrogen bonds between S and -OH groups between WS$_2$ and PVOH.[276]

Although Sonker *et al*.'s research confirmed that WS$_2$ was mainly responsible for improving the mechanical and not thermal properties, a different research concluded that WS$_2$ can influence the thermal behaviour of the polymer matrix. Naffakh *et. al*. observed that WS$_2$ can increase the onset degradation temperature of isotactic PP by up to 60 °C and so the resultant PP/WS$_2$ composites exhibited improved thermal stability compared to unfilled PP. Additionally, WS$_2$ can act as nucleating agent for some polymers and thereby, increase the crystalline content and crystallisation enthalpy of PP.[277] In very recent years, few researchers have studied WS$_2$ as new functional additive to modify the thermal and mechanical properties of polymers.[278]

Importantly and with relevance to this thesis, WS$_2$ is getting attention as a new reinforcing material for polymers because of it has been shown to be non-toxic. Appel *et. al*. tested WS$_2$ against human kidney cells HEK293f and a *Salmonella typhimurium TA10* strain and concluded that WS$_2$ did not cause cell death and mutation.[279] Preliminary toxicology tests also showed that WS$_2$ showed no toxic reactions via oral administration and inhalation in rats and no sensitisation in lymph nodes *via* dermal application.[280] Further research using the A5 and rat submandibular salivary gland cells had shown that WS$_2$ did not affect cell growth, proliferation kinetics as well as cell viability. More interestingly, uptake of WS$_2$ by the cells accumulated in the cytoplasmic vesicles but the cell morphology remained unchanged.[262] More research has showed that WS$_2$ can improve the fracture toughness, shear strength and peel strength of polymers [273] but knowledge in terms of its application as a biomaterial is still rather limited. As is can be dispersed easily in polymer matrices,[273] it is an ideal candidate as a polymer additive for tissue engineering.[281] Lalwani *et. al*. utilised WS$_2$ as a reinforcing agent to prepare poly(propylene fumarate) (PPF) composites and confirmed that WS$_2$

played a significant role enhancing the mechanical properties PPF. The authors suggested that the resultant higher compressive and flexural properties were as a consequence of increased crosslinking density of the WS$_2$ reinforced polymer combined with uniform WS$_2$ dispersion in the polymer matrix. Such results indicated that the WS$_2$ reinforced PPF is suitable in tissue engineering purposes for trabecular bone.[281] However, more research must be conducted to more deeply understand whether WS$_2$ can alter the toxicity, biocompatibility and biodegradability of the resultant composites.

2.5.1 Previous Research on Composites of WS$_2$ and Polymers

As it was discussed above WS$_2$ has been studied as a possible reinforcing agent for polymers such as poly(methyl methacrylate) (PMMA),[274] PVOH[275,276] and PP.[277] However, development of eco-friendly, biodegradable and biocompatible composites of PLLA **18** and WS$_2$ has not been investigated. Naffakh *et. al*. was first to report on composites of PLLA **18** with (0.1, 0.5 and 1.0 wt%) WS$_2$ prepared via melt extrusion without any modifiers or surfactants. WS$_2$ has a nucleating effect on PLLA **18** which altered both the melt and cold-crystallisation behaviour of as well as enhancing the mechanical properties of PLLA **18**.[282] Later research investigated the influence of WS$_2$ on isothermal crystallisation and melting behaviour of PLLA **18**. The authors concluded that WS$_2$ could act as highly effective nucleating agent which resulted in the acceleration of PLLA **18** crystallisation.[283] In another study conducted to understand the non-isothermal cold crystallisation and melting behaviour of PLLA/WS$_2$ composites at different heating rates and WS$_2$ loading it was again demonstrated that the presence of WS$_2$ nucleated PLLA **18**. Cold-crystallisation and crystallinity of PLLA **18** could be influenced by heating rates and WS$_2$ loading.[284]

In other studies, WS$_2$ was incorporated into PLLA/hydroxyapatite using melt blending without the use of a modifier or compatibiliser. WS$_2$ was shown once again to act as a nucleating aid and it also improved the dispersion of hydroxyapatite micro-particles in the PLLA **18** matrix reducing the mean particle size that led to a larger interfacial area between the particles and polymer matrix. In comparison to unfilled PLLA/hydroxyapatite composites, addition of WS$_2$ increased the thermal stability of PLLA as well enhancing mechanical properties. These nanocomposites exhibited good biocompatibility and non-cytotoxicity, they have great potential as scaffolding in tissue engineering.[285] Very recently, WS$_2$ was incorporated into PLLA/PP blends where it was

observed that that the WS$_2$ had a more prominent nucleating effect for the PLLA-rich composites and the overall composites exhibited an increase in storage modulus.[286]

These studies are indeed good evidence demonstrating the advantages of using WS$_2$ as a functional filler for polymers. The potential of WS$_2$ as an additive for PLLA **18** should be further explored to determine if these composites could be used as novel eco-friendly, biocompatible materials.

2.6 Banana leaf

The two biopolymers introduced above (chitin and lignin) can both have positive health benefits for humans, especially antimicrobial efficacy. They are commercially available but extraction with chemicals is required in order to separate and obtain the biopolymers from the biomass. Potentially, another material that could be introduced and used in dressings on human patients is banana leaf. Its potential and application as an antimicrobial agent in India is known, although the active ingredient(s) are not known.

Since 1976, V. Chongchet has used sterile, steamed banana leaves as inner non-adherent dressings to treat burn wounds on patients. This may be the first report that mentioned using banana leaves as dressings, but unfortunately statistical data is not available and detailed recording of their efficacy with patients was not professionally collected.[287]

In 1996, Gore *et al.* in the burns unit at the L.T.M.G. hospital, Mumbai decided to search for a new dressing material that was non-adhesive, pain-free, cheap and readily available. At that time, there was 7-8 million burn injuries which resulted in approximately 0.2 million deaths each year in India. Burn management is always under pressure due to the duration of patient stay in hospital, expensive medications, multiple operative procedures and prolonged periods of rehabilitation. Such burn care units are always facing increased costs and it would be ideal to find ways to reduce the total cost of treating burns. From a medical point of view, skin grafting is the integral component of burn management. If the patients experience significant pain, they might become reluctant to accept further treatments. Ideally, non-adhesive dressings should be used on burn areas to minimise pain as well as the damage that can be caused on the new epidermis during dressing removal to achieve better healing. Traditionally, petroleum jelly impregnated gauze/Vaseline gauze (VG) was often used as dressing for skin graft donor areas. However, such dressings are not completely non-adherent and patients often experience significant pain, which can make them anxious. Therefore, it is necessary to find alternative dressings to

solve all these issues, reducing the burden on burns units and ensure patients can heal more effectively in a comfortable way.

Banana trees are planted widely in India as banana is the second most important fruit crop after mango.[288] Gore *et al*. noticed the size of banana leaves (BL) and, that BL were very large, cheap and readily available throughout the year and that the surface of the leaves was waxy, smooth and non-adherent. In addition, BL in India are commonly used as plates to serve food; they can also be used as lining for cooking vessels because of their waxy surface which is impervious to water; patients with smallpox can lie on BL because of their coolness and non-adherence to wounds.[289] Hence, BL has been utilised previously, as V. Chongchet had applied BL as dressings on patients who were undergoing skin grafting and using VG as a control. Thirty patients took part in this study and all dressings were applied in the operating theatre when the patients were anaesthetised and they were blinded to the type of dressing used until the first dressing change. The BL were first cooked on thin paste made by cooking fine flour, then dried for 24 hours and autoclaved before being applied to the patients. The aim of the study was to observe the pain that was experienced by patients during the treatment and removal, the ease of removing the dressings from patients. The results were presented on a scale of 0-10 (0 being painless and 10 is extremely painful) (Table 2.1). Furthermore, another aim was to check likelihood of side effects/infections that might occur.

Table 2.1, Scores collected from all trials using BL and VG dressings[290]

Category	BL	VG
Pain during treatment		
Range, Mean $\pm$ SD	0-3, 1.1 $\pm$ 0.71	5-9, 6.9 $\pm$ 0.84
Pain during removal of dressing		
Range, Mean $\pm$ SD	0-3, 0.97 $\pm$ 0.61	8-10, 9.47 $\pm$ 0.77
Ease of removal of dressing		
Range, Mean $\pm$ SD	0-3, 1.1 $\pm$ 0.61	8-10, 9.53 $\pm$ 0.63

Overall, patients experienced much less pain, almost pain-free with BL dressings and removal of BL dressings was also almost painless and easy. In contrast, VG dressings did not ease patient pain, were much more difficult to remove and patients became reluctant to continue to use VG dressings. They regarded BL dressings as soft, smooth, cool and

comfortable. During this study, complete epithelisation was observed on 17 areas with the application of BL dressings. In contrast, application of VG dressings did not enhance epithelisation on patients. Finally, infections were not observed with BL dressings but three areas showed sign of infection when VG dressings were used.

BL has the potential to become a non-adherent, non-toxic, non-antigenic, cheap, effective alternative dressing on skin graft donor areas. Although it is known that BL cannot be stored for more than 7-10 days due to fungal growth, it has been observed that Gamma irradiation can extend the shelf life of BL for up 2-3 months.[290,291]

In 2012, Guenova et al. conducted various experiments to confirm the possibility of using BL as dressings. Their objectives included studying bacteria found on fresh BL, sterilisation methods that can be used without causing damage or affecting the wound-dressing properties and the application of dressings using mouse models for skin transplantation and, for human postsurgical patients. They reported the BL mainly contained $7 \times 10^3 - 5 \times 10^5$ colony-forming units (cfu) of aerobic spore-forming bacilli, Gram(+) cluster-forming cocci and moulds. To sterilise BL, BL was cooked in boiling water to kill all fungi and reduced bacteria to less than 100 cfu per 100 cm^2 of leaf area. BL can also be sterilised using a medical steriliser and a household pressure cooker which resulted a complete inactivation of mesophilic bacteria giving sterile BL. They had identified steam sterilisation/autoclaving as the most appropriate method and more importantly, these techniques did not damage the BL and the waxy surface of BL remained intact and non-adherent. They then used autoclaved BL on a mouse model for skin transplantation for seven days and the wound healed well without any signs of infection. Finally, clinical trials were performed on post-surgical patients with sterilised BL for approximately 7 to 14 days (Figure 2.15).
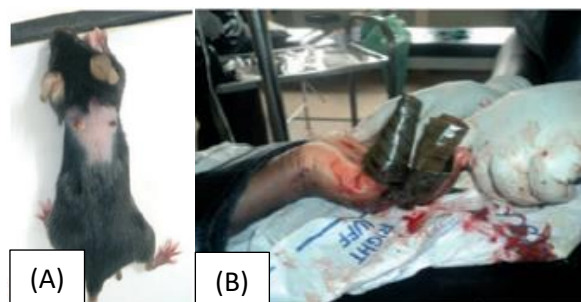

(A)   (B)

Figure 2.15. (A) Mouse with a healed wound after using BL dressings for 7 days; (B) post-surgical patient treated with a BL dressing

Patients can tolerate BL wound dressings without side effects and minimal or no discomfort. Pain experienced when the dressing was first changed was insignificant and no infections occurred even for up to 2 weeks treatment. From these results for mouse and post-surgical patients, the authors also confirmed that BL can be sterilised simply by autoclaving without affecting the wound dressing properties. In contrast, Gore *et al*. that applied BL on burnt patients only, these authors demonstrated that BL dressings can be used to treat different wounds. Thus, the overall results and patients' experience are consistent with those reported by Gore *et al*.

M. A. Gore and Guenova *et. al*. had shown how BL can be used as dressings in a direct manner. However, the contents or active ingredients that can be used to prevent infections in BL were not disclosed in their studies. Oliveira *et al*. studied the chemical composition of BL sheath and rachis and identified the major components as 31-37% cellulose, 13-18% extractives, 19-27% ashes, 8-12% hemi-celluloses and 10-13% lignin with G/S/H lignin ratio of (51-60)/(14-20)/(20-35).[292] It was proposed that lignin is chemically bonded to suberin-like components of cell tissues by β-O-4 and alkali-labile ester linkages.[292] Oliveira *et al*. had also conducted another study to identify the existence of bioactive compounds, steryl glucosides: Campesteryl 3-β-D-glucopyranoside, Stigmasteryl 3-β-D-glucopyranoside and Sitosteryl 3-β-D-glucopyranoside (Figure 2.16), in BL.
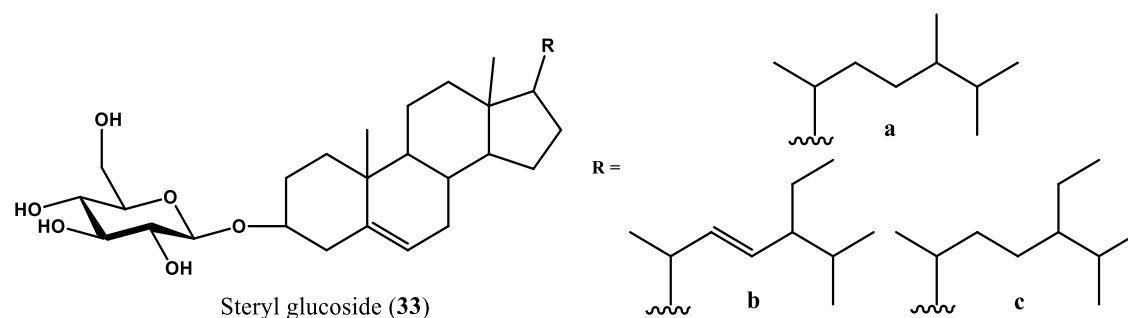
Figure 2.16. Chemical structures of steryl glucoside (**33a-c**)

Steryl glucosides (**33a-c**) accounted for 101-1350.5 mg/kg of BL and 838.4-1824.3 mg/kg of the whole banana plant (i.e. fraction(s) dry weight) which is unusual as only small amounts are normally present in other species. These compounds can bring various health benefits to humans and one of the well-known features is their ability to lower blood cholesterol.[293] They are also pharmacologically active having hepatoprotective,[294] anti-inflammatory,[295] anti-mutagenic and anti-cancer properties.[296] Overall, from clinical trials the health benefits that are available from BL (and its components) conclusively

prove that they have great potential to be further developed for medical device applications. Perhaps, the only concerns are the shelf life of the leaves, banana trees are less available in some countries and a method must be developed to process BL for converting them into long-life materials without destroying their intrinsic wound dressing, anti-inflammatory properties.

2.6.1 Previous Research on using Banana Leaf in Biomedicine

Although a small number of research studies have shown BL has the potential to useful for inclusion in antimicrobial devices, currently there is on-going research in this field. In fact, researchers have been more keen on identifying BL as biomass for energy resources.[297,298] On the other hand, the methods available for biomass processing are again a barrier to the development of BL for other applications. As mentioned above the major components of BL include 31-37% cellulose, 13-18% extractives, 19-27% ashes, 8-12% hemi-celluloses and 10-13% lignin,[292] but the high crystallinity of cellulose, high reactivity of lignin and the insolubility of cellulose and lignin in conventional organic solvents are technical challenging aspects in the conversion of BL biomass.[299] Fortunately, this issue is being tackled as ionic liquids (ILs) have been identified as powerful solvents for many biomass derived materials. Ionic liquids were firstly used for dissolution and processing of biopolymers, and with cellulose it was patented as early as 1930s.[300]

Up to this date, processing of BL using ILs has not been reported. There are examples which involved using ILs to process biopolymers and convert them into more versatile materials. Turner *et. al*. simply used microwaves to dissolve cellulose in 1-butyl-3-methylimidazolium chloride ([BMIM]Cl) to prepare a 4.75% (w/w) cellulose-IL solution. An enzyme was mixed with the solution thoroughly and upon casting and rinsed with distilled water, an enzyme incorporated cellulose membrane was obtained. Using this method, the enzyme was entrapped in the polymer matrix during casting which led to a low-leaching bioactive film and moreover, the enzyme activity was maintained in the casted cellulose membrane.[301] Phillips *et. al*. used 1-ethyl-3-methylimidazolium chloride ([EMIM]Cl) to dissolve silkworm cocoon silk and then regenerated the silk dope by extruding the silk-IL solution into a water or methanol coagulation bath.[302] Gupta *et. al*. also used [BMIM]Cl to dissolve silk fibroin. Silk films were then cast from a 7% (w/w) silk IL solution using a methanol rinse bath. The authors results indicated that the silk

film cast from IL did not alter the intrinsic cell viability, differentiation or gene expression of silk for tissue engineering.[303]

These experiments clearly demonstrated the use of IL for biopolymer processing. Using ILs, harsh reagents or solvents are not required and in addition, the regenerated biopolymer can be fabricated into desired forms/dimension such as beads,[301] fibres[302] depending upon the casting technique. As ILs are reported to be able to dissolve the major components of plants such as cellulose[301,304] and lignin,[209] ILs can be used to process BL and convert in to BL membrane with an extended shelf-life.

2.7 Ionic liquids

As stated above, an ionic liquid (IL) is defined as a salt with a melting temperature below the boiling point of water, 100°C. Most ILs consist of an organic cation, inorganic or polyatomic anion and the cation has a low degree of symmetry which causes the lattice energy of the crystalline form of the salt to be reduced and hence, lowering the melting point.[305] The chemical and physical properties of ILs can be tuned and varied for designated applications by carefully choosing the anion or cation with specific functional groups. It is indeed possible to combine different cations and anions to make new ILs therefore, the potential number of ILs possible is numerous, but thought to be about 1.2 million. Although ILs have been known for a long time, they were not widely reported until approximately 20 years ago. This is because when ILs were first introduced, it seemed that they could be synthesized relatively easy but their applications were uncertain. Eventually, instead of producing various ILs and investigating their potential applications, the new trend is to produce ILs, i.e. combine cations and anions with known properties to produce ILs with more predicted features.[52] Nowadays, categorisation and application of ILs has become very diverse especially as the chemical and physical properties of ILs can be readily altered and, tailored to suit use. In order to understand this unique feature, it is necessary to have a detailed understanding of IL chemistry and development.

2.7.1 The Origin and Major Events in the Development of ILs

The name "ionic liquid" was in fact not used until 1943. The exact date of the first IL synthesized is in dispute but it is believed it was first reported around the late 18th century. In 1877, Friedel and Crafts produced a liquid when aluminium chloride was added to

amyl chloride.[306] In 1888, Gabriel and Weiner discovered a protic IL, ethanolammonium nitrate.[307],[308] A more well-known event in IL history was the synthesis of ethylammonium nitrate (melting point: 52-55^{0}C) by Paul Walden and it is believed to be one of the earliest room temperature ILs.[309] In 1951, Hurley and Weir prepared ILs by mixing and warming aluminium chloride and ethylpyridinium halides which can be applied in the electroplating of aluminium.[310] In the 1960s, research by the United States Air Force Academy was on-going to develop molten salts (melting point close to 100^{0}C) for use as battery electrolytes.[52] In 1970-1980s, the development of ILs for battery use had become even more active[311] and in 1992, air and water stable imidazolium-based ILs were invented.[312] After that, major interest in ILs was strongly developed beyond the discovery of binary ILs which were made from mixtures of aluminium (III) chloride and N-alkylpyridinium or 1,3-dialkylimidazolium chloride. The field of ILs became even more popular in 2000s and studies have been further extended with task-specific and chiral ILs for various applications.[307]

Until now, ILs do not just simply consist of using aluminium(III) chloride and N-alkylpyridinium or 1,3-dialkylimidazolium chloride as they can be composed of a wide range of different ions (Figure 2.17). ILs have become of interest in inorganic chemistry, electrochemistry, catalysis, physical chemistry and engineering as they have not only involved in development of battery materials but also in cellulose processing,[304] production of polymers,[313] as solvents for synthesis and catalysis.[314,315]
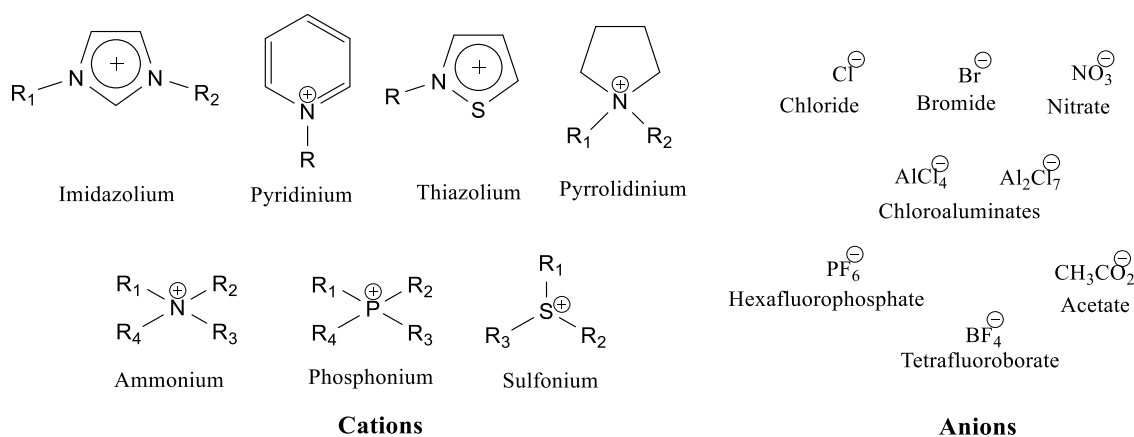
Figure 2.17. The most common cations and anions used in the production of ILs[52,307]

2.7.2 Ionic Liquids as Powerful Solvents for Dissolving Biopolymers (Chitin, Lignin)

As stated before, ILs display solvent properties and their thermal stability and negligible vapour pressure properties make them useful for 'green chemistry' as unlike many traditional organic solvents, they can be recycled and reused. IL use as solvents is the

most useful, important and well-known use of ILs to date. Most ILs are considered to be polar solvents but they have a non-coordinating feature highly dependent upon the type of anion used. Solvatochromatic studies have shown that ILs consist of similar polarities to that of short-chain alcohols, polar and aprotic solvents.[316] The solvation properties of ILs can be altered by changing the relative ions. The solvent features of ILs include the capability for hydrogen bond donation from the cation to polar or dipolar solutes, the hydrogen bond acceptor functionality of the anion, π-π or C–H… π interactions.

Apart from being able to dissolve simple molecules, metal salts do participate in chemical reactions. ILs can also be used in polymer synthesis and reactions can even be faster compared to other polar/co-ordinating solvents.[317] They have been used for dissolving biological macromolecules involved in intermolecular hydrogen bonding-networks such as in silk fibroin.[318] Traditionally, harsh conditions/chemicals[319] are often required to dissolve biopolymers but ILs are an alternative.

As mentioned before, chitin (**31**) consists of a complicated hydrogen bonding matrix resulting in structure that has high therm research related to the dissolution of chitin (**31**) but it should be noted that in some of the work reported the authors actually used chitosan instead of actual chitin (**31**).[320] ILs that can actually dissolve chitin (**31**) will now be introduced below.

Xie *et al*. used [BMIM]Cl (Figure 2.18) to dissolve chitin (**31**) and chitosan (**32**) with the aim of developing them as sorbents for carbon dioxide, CO_2. 10 wt% chitin/[BMIM]Cl and 10wt% chitosan/[BMIM]Cl were obtained. Although, neither [BMIM]Cl, nor chitin (**31**) and chitosan (**32**) themselves can capture CO_2, chitin/[BMIM]Cl and 10wt% chitosan/[BMIM]Cl mixtures showed 8.1% and 3.8% CO_2 fixing efficiency, respectively.[321] However, Wu *et al*. had doubted this report as 10 wt% chitin/[BMIM]Cl cannot be achieved. They managed to use [BMIM]Cl and [BMIM]OAc (Figure 2.18) to dissolve chitin (**31**) from crab and squid pen to prepare 1 wt% chitin/[BMIM]Cl and 4wt% chitin/[BMIM]OAc. The chitin/IL mixtures can be rinsed with methanol or water to remove the ILs and chitin sponges obtained.[322] Qin *et al*. tested [BMIM]Cl, [EMIM]Cl and [EMIM]OAc to dissolve chitin (**31**) and shrimp shells. The chitin/IL can be spun into water to remove the ILs and produce chitin fibres. It was concluded that practical grade chitin, which had a higher molecular weight and contained higher mineral content was more difficult to dissolve compared to pure chitin. IL with an acetate anion can enhance the dissolution of chitin (**31**) or shrimp shell which could be due to the increased hydrogen bonding basicity.[323] The authors also claimed that [EMIM]OAc can extract 94% available

chitin (**31**) from shrimp shell which can be recovered in higher molecular weight and a more pure form than that from industrial processes. The spun chitin fibres can be mechanically stronger if the polymer is first reconstituted and re-dissolved prior to spinning.[324] Barber *et al.* adapted this method to dissolve shrimp shell directly to obtain 6 wt% chitin/[EMIM]OAc. Dry-jet wet spinning involved soaking the spun chitin fibres into different solutions to obtain deacetylated, nitrile functionalised and amidoxime functionalised fibres. All fibres can be used to remove uranyl chloride, UO_2Cl_2 from very dilute aqueous solution.[325] The same research team then used [EMIM]OAc and [EEIM]OAc (Figure 2.18) to prepare 1-3wt% chitin/IL solutions for electrospinning and claimed that [EMIM]OAc can produce smooth, continuous fibres with this method.[326] Shamshina *et al.* also applied dry-jet wet spinning method to make chitin-calcium alginate composite fibres using [EMIM]OAc to dissolve shrimp shell and alginic acid spun into a saturated calcium carbonate, $CaCO_3$ bath.[327]
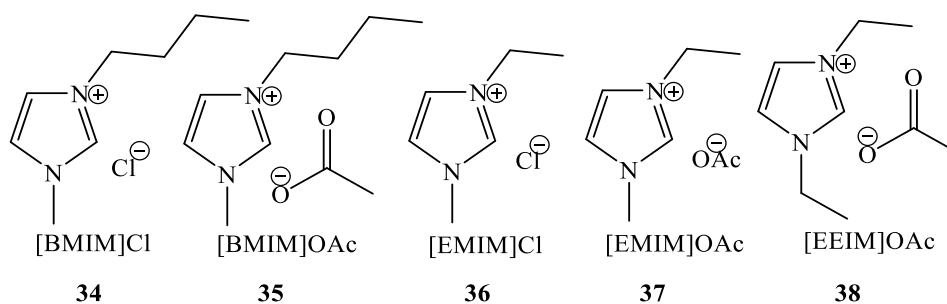

Figure 2.18. ILs that have been used to dissolve chitin (**31**)

It has been proven that some ILs are able to dissolve chitin (**31**) but it should be noted that some of the reports are not consistent and reliable. For instance, Wu *et al.* and Qin *et al.* showed that ILs consisting of an acetate ion are better candidates for dissolving chitin (**31**). It should be noted that Wu *et al.* was unable to obtain 10 wt% chitin/IL which was claimed to be feasible by Xie *et al.* Qin, Barber and Shamshina *et al.* claimed they had "extracted" chitin (**31**) from shrimp shell but in some of their experiments, they only dissolved the whole shrimp shell in ILs and most proteins, minerals still remained in their end products.

On the other hand, interest has been shown in the use of ILs to dissolve wood and lignin. Kilpelainen *et al.* synthesized 6 ILs (Figure 2.19) that dissolve wood chips, pine powder and saw dust. All 6 ILs can dissolve wood, especially [BMIM]Cl and [AMIM]Cl which had better performance (up to 7-8 wt %) but it was suggested that [BzMIM]Cl should be

better at solvating the lignin, due to π-π interactions, and give transparent solutions but, the viscosity of this IL was a major drawback (it is a hard jelly at room temperature).[328]

[BMIM]Cl   [AMIM]Cl   [BzMIM]Cl   [Bz(OMe)MIM]Cl   [Bz(Me)MIM]Cl   [BzMIM]DCA

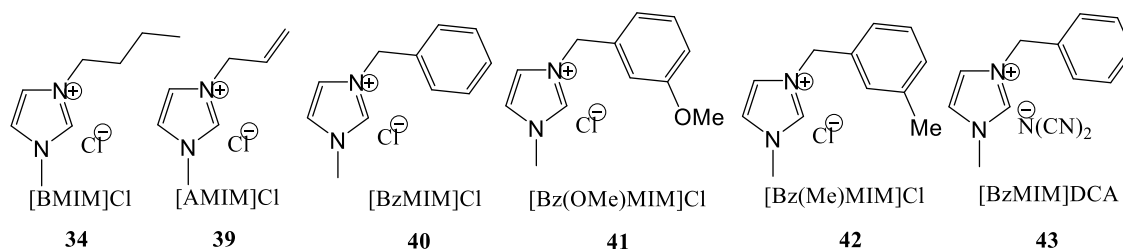**34**   **39**   **40**   **41**   **42**   **43**

Figure 2.19. ILs that can dissolve wood chips, pine powder and saw dust

Pu *et al*. examined a selection of ILs (Figure 2.20) and discovered that [HMIM][CF$_3$SO$_3$], [MMIM][MeSO$_4$], [BMIM][MeSO$_4$] can dissolve up to 20wt% lignin. Dissolution can be achieved by heating at 80-130 °C for 8-hours. The authors concluded that the solubility of lignin was influenced by anions in the order of [MeSO$_4$]$^-$ > Cl$^-$ ~ Br$^-$ >>> [PF$_6$]$^-$ but generally ILs with large, non-coordinating anions [PF$_4$]$^-$, [PF$_6$]$^-$ were not suitable. However, it should be noted that the lignin used was extracted by treating the wood with acid [196] and it was unclear if the lignin was oxidised/damaged.[209]

[MMIM][MeSO$_4$]   [HMIM][CF$_3$SO$_3$]   [BM$_2$IM][BF$_4$]   [BMPy][PF$_6$]   [BMIM]A (A = MeSO$_4$, Cl, Br, PF$_6$)

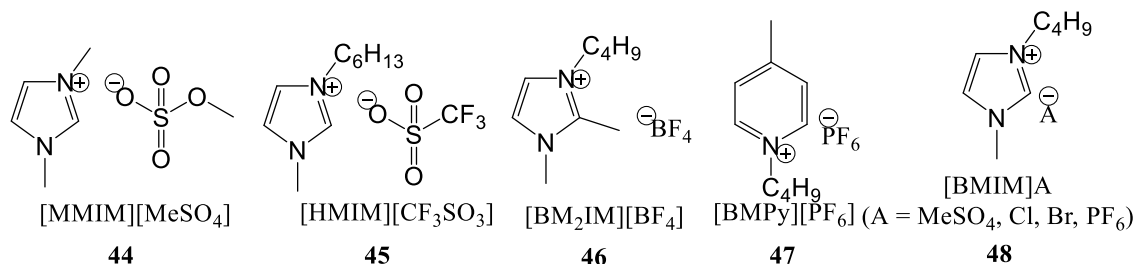**44**   **45**   **46**   **47**   **48**

Figure 2.20. ILs examined by Pu *et al*. for dissolution of lignin

Sun *et al*. utilised [BMIM]Cl **34** and [EMIM]OAc **37** and the latter had overall better performance as IL **37** can dissolve both hardwood and softwood lignin, even if the materials were only grinded mildly. Instead of heating the mixture on an oil-bath, the dissolution time can be shortened by using microwave pulse heating or ultrasound as a pre-treatment. In addition, reconstitution of dissolved wood can be achieved using acetone/water (1:1) to yield regenerated material that was richer in carbohydrates than the original material.[329] Wu *et al*. prepared biopolymer-based composite films using cellulose, starch and lignin with IL [AMIM]Cl **39**. Firstly, 6wt % cellulose (bamboo pulp), corn starch and lignin were heated in IL **39**. The mixture was then coagulated in water to make blend films. Since the three film components have good affinity for each other, excellent tensile strength was observed without sacrificing the extensibility of the

films. The films also had good thermal stability due to enhanced inter-molecular hydrogen bonding between the biopolymers. Moreover, the products can act as a gas barrier and different ratios of components can give $CO_2:O_2$ permeability ratios in the range of 1.05-1.67.[330] Fu *et al*. applied [EMIM]OAc **37** in the pre-treatment of straw in pure IL **37** as well as aqueous IL **37**. In comparison, higher fermentable sugar yields can be obtained with aqueous IL **37** under the same conditions as pure IL **37**. Fu *et al.* had shown that polysaccharides can be retained, the digestibility of cellulose and xylan can be enhanced (a cost-effective way to produce cellulosic biofuels) and the IL can be recycled easily.

Unlike chitin (**31**), the research conducted to date cannot provide the key properties ILs should have to effectively dissolve lignin but, there are more ILs available now that can be used to dissolve lignin. Moreover, these reports greatly demonstrated the potential applications of lignin when treated with ILs.

2.8 Electrospinning

Electrospinning is a versatile technique that can be employed to convert polymer solutions or polymer melts into fibres instantly. It is very well-known in the biomedical field but its application is starting to emerge in different areas such as in battery, clothing and cosmetic production. The fundamental aspects of electrospinning will be introduced and discussed next.

2.8.1 History of Electrospinning

It is believed the concept of electrospinning was first observed in the 16th century when W. Gilbert noticed the "electrostatic attraction of a liquid" when a piece of amber was electrically charged and came in close contact near a droplet of water. This resulted in a cone shape and small droplets were then ejected from the tip of the cone. This phenomenon is now known as electrospraying.[331] In 1887, C. Boy conducted an "electrical spinning" experiment which used molten rosin, beeswax, pitch, shellac, sealing-wax, Canada balsam, gutta-percha, burnt India-rubber, collodion or other viscous materials to make threads via an insulated small dish which was connected with an electrical machine.[332] In 1914, J. Zeleny reported on the behaviour of fluid droplets at the end of metal capillaries, this led to studies on the behaviour of fluids under electrostatic forces and resulted in several patent applications being submitted around 1930-40s.[333] *The major breakthrough was credited to N. D. Rozenblum and I. V. Petryanov-Sokolov*

as they produced electro-spun fibres. A special branch of industry was developed to produce efficient filtering materials based upon their work and named as Petryanov filters.[334] The next important person to make a contribution to electrospinning was Sir Geoffrey Ingram Taylor who is known because of his contribution to the theoretical underpinning of electrospinning. In 1964-9, he had mathematically modelled the shape of the cone formed during electrospinning when the fluid droplet was charged with an electric field.[335] Hence, the fluid cone that forms when an electric field is applied to the fluid droplet is called the 'Taylor' cone. In 1995, J. Doshi and D. H. Reneker investigated electrospinning in more detail and clearly stated the properties of the resultant fibres from the charged jet of polymer solution were free of solvent, had a variety of cross sectional shapes or sizes and a diameter in the rage of 0.05–5 microns. They had also reported the electrospinning process, conditions and potential applications of these fibres.[336] Since then, electrospinning has attracted much interest amongst polymer scientists, who wish to further explore polymers that can be electro-spun, and who wish to continue to improve and modify this technique for a variety of uses.

2.8.2 Principle of Electrospinning

In order to perform electrospinning, typically a polymer solution, syringe, metal needle with a small diameter/spinneret, high voltage supplier and a grounded metal collector are required (Figure 2.21). Although a vertical electrospinning set-up, as shown in Figure 2.21, can be used horizontally with the same principle applied to obtain the same products. The polymer solution can be prepared by dissolving the polymer with appropriate solvent before placing it into the syringe, (polymer melts are sometimes used in this process).[337] The high voltage supplier should be able to generate several tens of kilovolts(kV) and the syringe is often connected to a pump that can plunge the syringe to eject polymer solution at precise rate(s). During the electrospinning process, the spinneret is filled with polymer solution and when it reaches the tip of the spinneret, the fluid can be held by its surface tension. An electric field can then be supplied to the spinneret to generate electrically charged fluid. This causes the mutual charge repulsion and contraction of the surface charges to the counter electrode and results in an opposite force directly to the surface tension.[338] When the repulsive electrical forces overcome the surface tension of the fluid, a Taylor cone is formed with a charged jet ejected at the tip of spinneret. This ejected jet is stable for a very short time but then becomes unstable to undergo an elongation process and whip rapidly in the air between the spinneret and collector. The whipping jet becomes long and thin with solvent evaporating instantly to give dry polymer fibres on the

collector.[339] In the case when a polymer melt is used, the discharged jet solidifies in the air.[340] The syringe can be pumped to eject fluid constantly so that polymer fibres can be produced continuously. If all conditions are ideal, polymer fibres can be obtained easily.
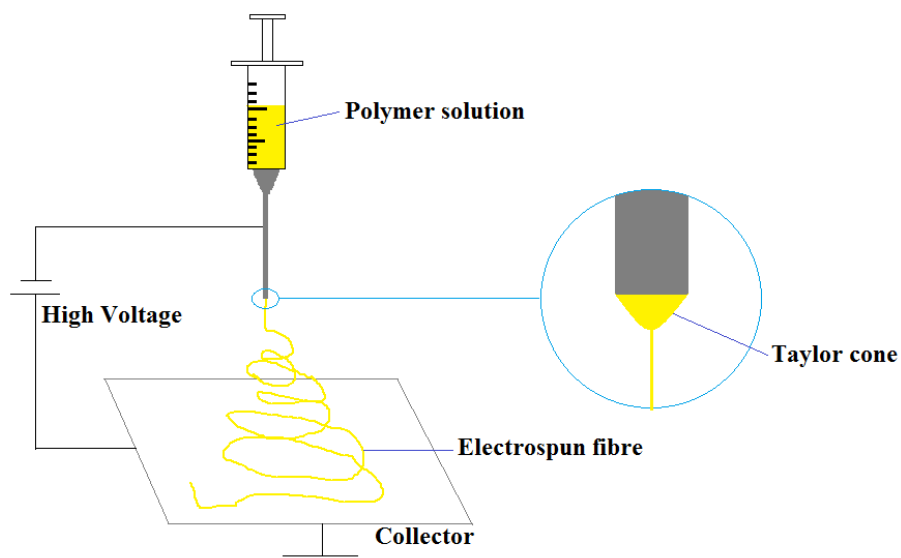

Figure 2.21. Illustration of an electrospinning apparatus and the appearance of a Taylor cone

2.8.3 Parameters that Influence the Electrospinning Process

Precise electro-spun nanofibers can offer properties such as high surface-to-volume ratio, tunable porosity, various sizes and shapes, controllable nanofiber composition to suit functionality.[341] Whether the resultant electro-spun fibres are nanofibers with consistent diameter (Figure 2.22A) or nanofibers with beads (Figure 2.22B), there are many parameters that can be controlled to achieve different fibre morphologies. Herein, the most common parameters that can influence the electrospinning process will be introduced and discussed in detail.
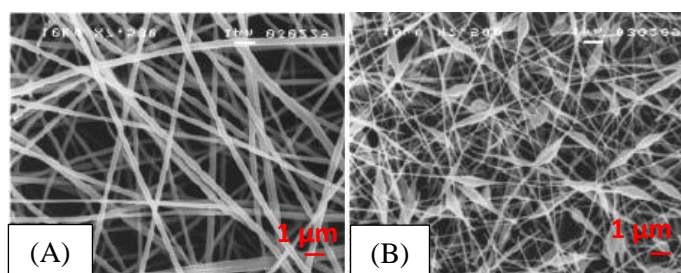

Figure 2.22. (A) Electro-spun fibres with similar diameters, (B) electro-spun fibres with beads[342]

The polymer solution itself can be affected by numerous parameters that can have an impact on the morphology of the nanofibers obtained. One of the most easily tunable parameters is the concentration of polymer solution, as a minimum solution concentration is required for fibre formation to occur. At low concentration, electro-spun fibres consist

of mixture of beads and fibres whereas, at higher concentration, formation of continuous fibres is favoured due to the ability to maintain the flow to give fibres with less beads, more uniform and often larger in diameter.[343] Similarly, the molecular weight(MW) of the polymer can have the same influence, as when molecular weight changes from low to higher, the electro-spun fibres change from being a mixture of beads and fibres to being bead-less, uniform fibres with larger diameter. However, high MWs are not always essential as MW reflects the level of polymer chain entanglement. When intermolecular interactions are sufficient, inter-chain connectivity can be obtained with chain entanglements to maintain a uniform jet.[344] Both concentration and molecular weight can affect another parameter, namely viscosity. In fact, these three parameters are actually correlated with each other. Generally, an increase in concentration can lead to higher viscosity and high molecular weight polymer often related to the greater number of chain entanglements to ensure a certain level of viscosity. Changing viscosity is another way to produce beaded or bead-less fibres during electrospinning. Very high viscosity polymer solutions tend to exhibit longer stress relaxation times to prevent fracturing of the ejected jets during electrospinning but if the viscosity is too high, it is likely that the fluid may coagulate at the spinneret tip. However, if the viscosity is too low, surface tension will become the dominant factor.[345] Surface tension can be regarded a function of solvent composition of the solution and, different solvents give rise to different surface tensions. High surface tension is usually avoided due to the occurrence of the instability of the jet and formation of sprayed droplets. Although lower surface tension is more preferred as it helps electrospinning to be operated at lower electric field, it does not imply low surface tension is suitable for all electrospinning processes. Surface tension can determine the upper and lower boundaries of electrospinning if all other parameters are kept constant.[346] Another potential polymer solution related parameter is electrical conductivity which depends upon the type of polymer, solvent and additives, such as ionisable salts. Generally, highly conductive fluids can generate fibres with smaller diameter but if conductivity is too high, fluids can be unstable that result in dramatic bending instabilities and broader fibre diameter distribution.[347] When the fluid's conductivity is low, it causes insufficient elongation of the jet and is more likely to produce beads. This can be overcome by adding ionic salt to produce uniform fibres without beads.[348]

Apart from changing the properties of polymer solutions, varying processing parameters is another widely used method to control the structure of electro-spun fibres. The applied voltage is another crucial parameter but the relative consequences of altering the voltage

have been inconsistent, from different studies. Generally, higher voltage should cause greater stretching of the polymer solution because of the higher columbic forces and a stronger electric field which then reduces fibre diameter when combined with the higher evaporation rate of the solvent. However, Reneker *et al*. believed electric field did not change the diameter of electro-spun fibres;[349] Demir *et al*. suggested that higher voltage can result in more fluid being ejected and hence, favoured formation of fibres with larger diameter.[340] In contrast, Deitzel *et al*. believed higher voltage tends to produce fibres with more beads. Therefore, a straight forward conclusion cannot be made and one could only suggest that voltage can of course influence the electrospinning process and the nature of the electro-spun fibres obtained. Perhaps, this parameter has different effects on different polymers and other variables must be considered with the applied voltage.[350] When the voltage is applied, polymer solution is ejected at a flow rate which can also affect the morphology of the spun fibres. Often, a minimum flow rate is required to maintain a continuous fluid ejection and allow the solvent sufficient time to evaporate. In contrast, higher flow rates generate fibres with beads because of the limited drying time before the polymer is deposited on the collector.[351] This would suggest that the type of collector used for electrospinning should also be considered. The collector used in the electrospinning set-up is best to be a conductive material. It was reported that a material that is less conductive than the polymer of interest would result in beaded fibres due to the reduced surface area available.[352] Aluminium, i.e. Al foil is the most commonly used collector because of its low cost, is easily purchasable, although the fibres deposited on it are not always removed easily as they consist of random arrangement of the fibres (Figure 2.23A) caused by the bending instability of the travelling charged jet.[353] Conductive paper, conductive cloth and wire mesh can replace Al as they can allow the collected mats to be removed more easily.[354] To collect aligned fibres (Figure 2.23B), a rotating wheel/drum[355] or rotating metal disk[356] can be used. Another common option is to use a non-solvent coagulation bath which can be used for removing excess solvent[326] and allow the spun fibres to be dispersed more uniformly.[357]
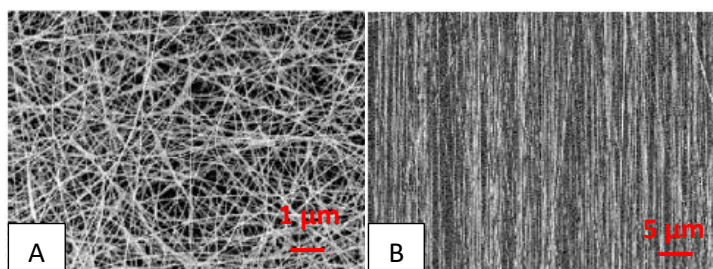
Figure 2.23. (A) Random fibres collected on Al, (B) aligned fibres collected on a rotating disk

After considering the type of collector that can be used, it is important to determine the distance between the collector and the tip of the spinneret. The fundamental aspect of having a distance between both is to allow the solvent enough time to evaporate before the fibres reach the collector. If the distance is too short the solvent cannot evaporate completely and this can result in beaded fibres,[358] smaller fibres,[359] flatter fibres[360] or fibres that are not completely dry.[361] However, some researchers reported that this distance was not so important and suggested that it is not a very major parameter for some polymers.[357,362]

Until now, the word solvent has been mentioned in this section many times. It is indeed very important in the electrospinning process and it can affect most parameters mentioned above, such as viscosity, surface tension, conductivity and the distance between the spinneret and collector has been highlighted because of how fast/slow solvent can evaporate. Thus, solvent can influence the morphology of electro-spun fibres. The choice of solvent cannot be easily generalised as it highly depends upon the intermolecular interaction between the polymer and solvent.[363] Perhaps the most vital factors when choosing the solvent is to consider whether it can dissolve the desired polymer to form an electrically charged jet as well as carrying the dissolved polymer molecules to the collector.[364] Finally, the electrospinning process is highly affected by environmental surroundings, e.g. ambient parameters such as temperature and humidity. Since there is an inverse relationship between temperature and viscosity, an increase in temperature results in decreased fibre diameter due to the decreased viscosity.[365] On the other, humidity often affects the rate of evaporation of the solvent. Low humidity causes solvent to evaporate quickly and in extreme cases, the spinnerets tip can clog when the solvent dries too quickly.[366] High humidity can sometimes favour the discharge of the electro-spun fibres but it is also possible to generate fibres with pores and even lead to pores coalescing when humidity is increased further.[367] Generally, optimal ambient parameters are preferred.

In summary, naturally occurring materials such as chitin, lignin and banana leaf have due to their combination of intrinsic antimicrobial properties and non-toxicity great potential when added to biopolymers, such as PLA, to be formed or shaped in to different constructs for use in many medical applications. Indeed, banana leaf that are composed of lignin were reported to be used as wound dressings. Albeit being difficult to dissolve these natural materials, ionic liquids can act as powerful solvents to dissolve them and used as a medium for use in electrospinning. Alternatively, melt extrusion and injection moulding can be used to produce composites with PLA which are biocompatible and biodegradable. However, as PLA is not intrinsically antimicrobial therefore, the key aim is to incorporate chitin, and lignin (with the assistance of triacetin as a plasticizer) to introduce antimicrobial properties to PLA. Finally, other non-toxic additives, such WS_2 can also be added as a reinforcing agent for PLA to produce novel composites that are also radio-opaque.

Chapter 3.
Experimental

3. Experimental
3.1 General Direction - Solvents and Reagents

Chitin (from shrimp shells), lignin (alkali), triacetin and DMSO were purchased from Sigma-Aldrich. WS_2 nanotubes were synthesised and provided by Professor Alla Zak from the Holon Institute of Technology, Israel. PLA was kindly supplied by Corbion which was made from European sugar beet and Thai sugarcane consist of at least 96% L-isomer and stored in a freezer. Molecular sieve (3Å) was purchased from Fluka. Banana leaves were purchased from the China Mini Market, Coventry, UK and stored in a refrigerator. [EMIM]OAc was purchased from Sigma-Aldrich, dried using a vacuum at 70 °C and stored using molecular sieve (3Å). [BMIM]Cl and DMF were purchased from Fisher Scientific, [AMIM]Cl from VMR International Ltd and both ionic liquids were stored under nitrogen gas. Aluminium SEM stubs, double stick carbon adhesive tape and 200 mesh TEM copper grids with lacey carbon film were purchased from Agar Scientific. Aluminium DSC pans and covers were purchased from PerkinElmer and alumina TGA crucibles were purchased from Mettler Toledo. All materials were used as received unless otherwise stated.

3.2 Preparation of composites
3.2.1 Preparation of PLLA based composites – melt extrusion and injection moulding

All melt extrusion was conducted using a Thermo Fisher HAAKE MiniLab II and injection moulding performed using a Thermo Fisher HAAKE MiniJet Pro Piston Injection Moulding System. Poly(lactic acid) pellets were cryogenic ground to a powder using liquid nitrogen for 15 minutes. PLA and filler in the ratio of (100/0, 99.5/0.5, 99/1, 98/2, 97/3, 95/5 and 90/10) were weighed and dry mixed. In the production of plasticized samples, 20 wt% of triacetin relative to the total polymer content (PLA/filler) was used for all plasticized composites. The mixes were then subjected to the twin conical screw extruder for compounding at 180 °C with a screw speed of 40 rpm for 4 minutes. The melt mixed PLA/WS_2 were re-circulated in the extruder for further compounding to achieve better dispersion of the fillers in the PLA matrix. Molten PLA-based composites were injected to moulds at 90 °C (800 bar, 8 s) to produce test specimens in the form of dog-bones/dumbbells, circular discs and rectangular bars.

Table 1. Quantities of PLA and filler used

1.1 Non-plasticized PLA/lignin composites

PLA/lignin ratio	PLA (g)	Lignin (g)
100/0	25	0
99.5/0.5	24.875	0.125
99/1	24.75	0.25
98/2	24.5	0.5
97/3	24.25	0.75
95/5	23.75	1.25
90/10	22.5	2.5

1.2 Plasticized PLA/lignin composites

PLA/lignin ratio	Triacetin (g)	PLA (g)	Lignin (g)
100/0	5	20	0
99.5/0.5	5	19.9	0.1
99/1	5	19.8	0.2
98/2	5	19.6	0.4
97/3	5	19.4	0.6
95/5	5	19	1
90/10	5	18	2

1.3 Non-plasticized PLA/chitin composites

PLA/chitin ratio	PLA (g)	Chitin (g)
100/0	25	0
99.5/0.5	24.875	0.125
99/1	24.75	0.25
98/2	24.5	0.5
97/3	24.25	0.75
95/5	23.75	1.25
90/10	22.5	2.5

1.4 Plasticized PLA/lignin composites

PLA/Chitin ratio	Triacetin (g)	PLA (g)	Chitin (g)
100/0	5	20	0
99.5/0.5	5	19.9	0.1
99/1	5	19.8	0.2
98/2	5	19.6	0.4
97/3	5	19.4	0.6
95/5	5	19	1
90/10	5	18	2

1.5 Non-plasticized PLA/WS$_2$ composites

PLA/WS$_2$ ratio	PLA (g)	WS$_2$ (g)
100/0	20	0
99.5/0.5	19.9	0.1
99/1	19.8	0.2
98/2	19.6	0.4
97/3	19.4	0.6
95/5	19	1

3.2.2 PLLA-based composite films, pure chitin and lignin discs

All thin films and chitin/lignin discs were prepared using a Collin Hot Press (P 200 PM). The dog-bone shaped fragments after completion of tensile tests were subjected to the hot press at 180 °C, 200 bar for 4 minutes to prepare 0.8 – 1 mm thick PLLA-based composite films. After they were cooled to room temperature, the films were cut into circular pieces with a diameter of 15 mm prior to use in the bioassay studies. Pure chitin or lignin powder was also subjected to the hot press at room temperature, 200 bar for 20 minutes to give pure chitin or lignin sheet which was then stamped into circular discs with a diameter of 8 mm prior to bioassays. FTIR confirmed that the samples did experience thermal degradation after being processed with the Hot press.

3.3 Characterisation of Composites
3.3.1 Scanning Electron Microscopy (SEM)

Fractured specimens were taken after completion of the tensile tests for examination in the SEM. All samples examined were first attached to Al stubs using double-stick carbon

tape which were subjected to gold coating using Agar manual sputter coater. They were then dried in vacuum and stored in a desiccator before being examined in the vacuum SEM chamber (Zeiss sigma field emission fitted with Gemini column). SE2 detector was used to examine the composites along with accelerating voltage of 5 kV, the aperture size of 30 µm and a working distance of 10 – 20 mm.

3.3.2 Transmission Electron Microscopy (TEM)

WS_2 powder was placed on 200 mesh TEM copper grids with lacey carbon film which were examined using a Talos F200X TEM with accelerating voltage of 200 kV (magnification x10000 to 100000). The 95 wt% PLLA/ 5 wt% WS_2 composite was cut into a square piece with dimensions of *ca*. 5 mm x 5 mm and thickness of *ca*. 0.8 mm. Samples were then inserted into the cryo specimen holder and trimmed using a trimming blade (Trim 45) to a depth of 100 – 300nm or until a shiny, reflective smooth surface could be seen. The samples were then sectioned using Diamond Knife (cryo 35°, wet, 3mm) to obtain film sections with a thickness of ~50 nm. The film sections were then transferred onto 200 mesh TEM copper grids with lacey carbon film which was examined using Talos F200X TEM with accelerating voltage of 200 kV (magnification x10000 to 100000).

3.3.3 Differential scanning calorimetry (DSC)

5 – 8 mg samples were accurately weighed and placed in sealed Al DSC pans. All measurements were carried out using a Mettler Toledo DSC 1 under a nitrogen atmosphere. In order to remove the thermal histories, the following procedures were performed: ramp 10 K/min from 25 to 180 °C, isotherm at 180 °C for 4 minutes and ramp 10 K/min from 180 to 25 °C. This procedure was repeated again so as to obtain the second heating and cooling curves which were then evaluated using STARe system software.

3.3.4 Dynamic mechanical thermal analysis (DMTA)

Rectangular samples prepared via injection moulding with dimensions of *ca*. 10 mm x 10 mm x 4 mm were used and measurements performed using a PerkinElmer DMA 8000 in single-cantilever mode. Liquid N_2 and standard dry air oven were applied to obtain the dynamic properties of the composites in the temperature range of 0 – 90 °C with a heating rate of 10 K/min and frequency of 1 Hz.

3.3.5 Tensile testing

The tensile tests were performed using a Shimadzu Autograph AGS-X series instrument with Trapezium X software. 5-7 dog bone shaped specimens were prepared and tested for each material or composite. Each specimen consisted of gauge length of 26 mm, thickness and width of 3.10mm–3.30 mm. During the measurements, a 10 kN load cells was used with stroke speed of 1 mm/min from 0 – 0.25% strain and at 50 mm/min above 0.25% strain according to ISO 527 standard.[368] In the case of errors occurring, faulty results were eliminated. Consistent results were then obtained to calculate the average values for Young's modulus, ultimate tensile strength, elongation at break.

3.3.6 Fourier-transform infrared spectroscopy (FTIR)

Dog-bone fragments of all PLLA composites were used and analysed using a Bruker Tensor 27 FTIR machine. Measurements were recorded in the wavenumber range of 500 – 4000 cm^{-1} and characteristic peaks quoted in cm^{-1}.

3.3.7 X-ray photoelectron spectroscopy (XPS)

WS_2 powder was placed on electrically-conductive carbon tape which in turn was placed on an Omicron sample plate and analysed using an Omicron Multiprobe. The sample was illuminated with an XM1000 monochromatic Al Kα X-ray source along with a Sphera electron analyser as the detector used a pass energy of 10 eV and a base pressure of 2 x 10^{-11} mbar. The spectrum was then analysed using CasaXPS software package with all binding energies calibrated using Fermi edge of a polycrystalline Ag sample as well as calibration of the transmission function of the spectrometer using a variety of clean metal foils.

3.3.8 X-ray diffraction (XRD)

Circular samples prepared by injection moulding were used for XRD measurements which were recorded on a Panalytical Empyrean equipped with a Co target with the wavelength of 1.79 Å in the scattering angle range of 2θ = 5 – 50° with a scanning speed of 4°/min..

3.3.9 Small-angle and wide-angle x-ray scattering (SAXS/WAXS)

Dog bone fragments were used to produce samples with a thickness of *ca*. 0.1 mm which were then cut into dimensions of 1 cm x 2 cm and analysed with a Xenocs Xeuss 2.0 instrument equipped with a Cu-Kα micro-focus source. The machine can run both SAXS and WAXS simultaneously with the SAXS detector, Pilatus 300k and WAXS detector, Pilatus 100k.

3.3.10 Raman spectroscopy

Renishaw inVia Raman microscope was applied and WS_2 sample was illuminated with Ar^+ laser (wavelength of 514.5 nm), a 785 nm solid state diode and a Renishaw CCD (visible to near infrared) InGaAs Detector (Infrared).

3.3.11 Oscillatory rheology

Circular discs with a diameter of 25 mm and thickness of 2 mm were used and measurements were performed using Thermo Scientific HAAKE MARS III equipped with a set of 2 parallel–plates with diameters of 25 mm and operating a gap size set to 1.8 mm. Amplitude sweep tests were performed at 145, 150 and 155 °C, at a frequency of 1 Hz and strain (%) range of 0.01 – 100 to determine the region in which the deformation was small enough for the storage moduli (G') to be independent of deformation. Frequency sweep measurements were then performed at 155 °C in the range of 0.1 – 100 Hz with a strain of 0.1%.

3.3.12 Polarised light microscopy (PLM)

Each $PLLA/WS_2$ sample was cut into a square piece with dimensions of *ca*. 5 mm x 5 mm and thickness of *ca*. 0.8 mm. Each piece was then embedded in OCT compound and frozen at -80 °C overnight and then sectioned into 20μm fine pieces using a cryo-microtome (Leica EM UC7). Each sample was placed between glass slides and mounted on a hot-stage for examination under a PLM (Carl-Zeiss KPL 10) equipped with a filter ($\lambda = 540$ nm). The hot-stage heated the sample to from room temperature to 180 °C at a rate of 10 K/min. and then cooled to room temperature at a rate of *ca*. 10 K/min. This procedure was repeated with a cooling rate of 1 K/min.

3.3.13 Thermo-gravimetric analysis (TGA)

5–8 mg samples were analysed using a thermos-gravimetric analyser, Mettler Toledo DSC 1. Dog-bone fragments of PLLA composites samples and WS_2 powder were used for this analysis. All composites were heated from 25 °C to 900 °C at a heating rate of 10 K/min under both N_2 and ambient atmosphere. WS_2 powder was heated from 25 °C to 1000 °C at a heating rate of 10 K/min and the temperature was maintained at 1000 °C for 10 minutes under both N_2 and ambient atmosphere.

3.3.14 Gel permeation chromatography (GPC)

Multi angle laser light scattering (MALLS) was used in conjunction with GPC which was equipped with a multi-angle laser light scattering (λ = 690 nm) and differential refractometer (λ = 930 nm) detector. Samples were dissolved in THF to prepare a polymer solution in a concentration of 5 mg/mL. The solutions were filtered once with a 0.45 μm PTFE filter as well as a 0.20 μm PTFE filter and then injected in to the column. Measurements were obtained using Agilent PLgel column with a flow rate of 0.9 mL/min.

3.4 Dissolution of Banana Leaves (BLs) in Ionic Liquids (ILs)

General procedure: 0.2 cm x 0.2 cm BL pieces were weighed and stirred with IL at 120 °C for 24 hrs. The undissolved residue was removed via decantation with the aid of a centrifuge (10000 rpm, 10 min.) and the supernatant was used for electrospinning. In the comparison of IL for dissolving BL, 1 cm x 1 cm BL (0.5 g) pieces were stirred in 8.5 g IL cut into 1 cm x 1 cm pieces and 0.5 g then placed in a 30 mL glass vial followed by addition of 8.5 g IL at 120 °C for 24 hrs. Then, the BL/IL mixture was poured on to a petri dish to assess the ability of the IL for dissolving the BL.

BL/[EMIM]OAc solutions (solution viscosity in brackets)

5 wt% BL/[EMIM]OAc – BL (0.569 g) and [EMIM]OAc (9.5 g, 55.81 mmol) were used to give a very dark greenish-brown solution (540 cP)

8 wt% BL/[EMIM]OAc – BL (0.91 g) and [EMIM]OAc (9.2 g, 54.05 mmol) were used to give a very dark greenish-brown solution (1437 cP)

10 wt% BL/[EMIM]OAc – BL (1.137 g) and [EMIM]OAc (9.2 g, 54.05 mmol) were used to give a very dark greenish-brown solution (1437 cP)

5 wt% BL/[BMIM]Cl solution

BL (0.782 g) and [BMIM]Cl (9.5 g, 54.39 mmol) were used to give a very dark greenish-brown solution (1584 cP)

5 wt% BL/[AMIM]Cl solution

BL (1.191 g) and [AMIM]Cl (9.5 g, 59.89 mmol) were used to give a very dark greenish-brown solution (447 cP)

3.4.1 Incorporation of co-solvent in BL/[EMIM]OAc solutions for electrospinning

General procedure: In a 10 mL glass vial, BL/[EMIM]OAc solution was weighed followed by addition of co-solvent and a magnetic stirrer bar. The glass vial was sealed

with a lid and the mixture was stirred at room temperature for 1 hour. The mixture can then be subjected to electrospinning.

8 wt% BL/(4:1)[EMIM]OAc-DMF – 10 wt% BL/[EMIM]OAc (2.5 g) and DMF (0.625 g, 8.55 mmol) were used to give a very dark green solution (780 cP)

8 wt% BL/(4:1)[EMIM]OAc-DMSO – 10 wt% BL/[EMIM]OAc (2.5 g) and DMF (0.625 g, 8.00 mmol) were used to give a very dark green solution (1011 cP)

5 wt% BL/(1:1)[EMIM]OAc-DMF – 10 wt% BL/[EMIM]OAc (1.5 g) and DMF (1.5 g, 20.52 mmol) were used to give a very dark green solution (72 cP)

5 wt% BL/(1:1)[EMIM]OAc-DMSO – 10 wt% BL/[EMIM]OAc (1.5 g) and DMSO (1.5 g, 19.20 mmol) were used to give a very dark green solution (168 cP)

5 wt% BL/(5:3)[EMIM]OAc-DMF – 8 wt% BL/[EMIM]OAc (2.0 g) and DMF (1.2 g, 16.42 mmol) were used to give a very dark green solution (139 cP)

5 wt% BL/(5:3)[EMIM]OAc-DMSO – 8 wt% BL/[EMIM]OAc (2.0 g) and DMSO (1.2 g, 15.36 mmol) were used to give a very dark green solution (252 cP)

3.5 Dissolution of Chitin in ILs for entanglement study

General procedure: In a 30 mL glass vial, chitin powder was weighed followed by addition of IL and a magnetic stirrer bar. The glass vial can be sealed with a lid and the mixture can then be heated and stirred at 120 °C for 24 hrs. It can then be subjected to electrospinning.

2 wt% Chitin/[AMIM]Cl – Chitin (0.2 g) and [AMIM]Cl (9.8 g, 61.78 mmol) were used to give a very dark orange solution (2958 cP)

2 wt% Chitin/[BMIM]Cl – Chitin (0.2 g) and [BMIM]Cl (9.8 g, 56.11 mmol) were used to give a very dark orange-brown solution (15910 cP)

2 wt% Chitin/[EMIM]OAc – Chitin (0.2 g) and [EMIM]OAc (9.8 g, 57.58 mmol) were used to give a yellow solution (1011 cP)

3.6 Dissolution of lignin in ILs for entanglement study

General procedure: In a 30 mL glass vial, lignin powder was weighed followed by addition of IL and a magnetic stirrer bar. The glass vial can be sealed with a lid and the mixture can then be heated and stirred at 120 °C for 24 hrs. It can then be subjected to electrospinning.

5 wt% Lignin/[AMIM]Cl – Lignin (0.5 g) and [AMIM]Cl (9.5 g, 59.89 mmol) were used to give a very dark brown solution (2583 cP)

5 wt% Lignin/[BMIM]Cl – Lignin (0.5 g) and [BMIM]Cl (9.5 g, 54.39 mmol) were used to give a very dark brown solution (1674 cP)

5 wt% Lignin/[EMIM]OAc – Lignin (0.5 g) and [EMIM]OAc (9.5 g, 55.81 mmol) were used to give a very dark brown solution (294 cP)

3.6.1 Viscometer

All viscosity measurements were recorded using a Brookfield DV2T viscometer using spindle LV4 (code: 64). Unless the polymer solution has a viscosity exceeding 3000 cP, all measurements were conducted using a rotation speed of 200 rpm. For samples with viscosities higher than 3000 cP, lower rotation speeds were applied. Single point averaging was applied using a measurement time of 1 min. and all measurements were conducted at 20 °C.

3.6.2 Electrospinning

Essential equipment includes Spraybase controller as the high voltage supplier, polytetrafluoroethylene tubing (inner diameter of 0.8 mm), 18 Gauge spinneret as the emitter, disposable BD plastic syringes, Spraybase Syringe pump module controlled by software (SyringePumpProV1) and camera (Chameleon USB 2.0 digital 1.3 megapixel monochrome camera, model: CMLN-13S2C-CS) controlled by software (Point Grey FlyCap2). Fibre collectors used included household aluminium foil and Spraybase circular stainless steel collector (diameter of 90 mm).

For each polymer solution, three (3) tables of the matrix as shown below were constructed for three(3) different tip-to-collector distances of 10, 15 and 20 cm. At each height, electrospinning experiments began using a fixed flow rate of 0.2 mL/h with voltage slowly varied from 8.5 kV – 22 kV to observe how the polymer solution responded to the applied voltage. The appearance of the polymer solution at the spinneret tip was captured by video and recorded. The experiment was then repeated using different flow rates also with voltages slowly tuned from 8.5 – 22 kV until all 6 flow rates were tested. The tip to collector distance as well as the camera position was then adjusted to conduct more trials with the same methods. This procedure was then repeated using other heights and thus, 108 trials were conducted using each polymer solution.

The polymer solution ejected from the needle tip can be focused and monitored clearly with the camera. The software, FlyCap2 was set to capture 10 images every second during the experiments. Blurry images were eliminated and clear images that show Taylor cones and polymer streams are saved and shown in the discussion chapters.

Table 2. General table to record the results of electrospinning experiments at different tip-to-collector distance, values of voltage and flow-rate

10/15/20 cm	8.5 kV	10 kV	12 kV	15 kV	18 kV	22 kV
0.2 mL/h						
0.5 mL/h						
0.8 mL/h						
1.0 mL/h						
1.5 mL/h						
2.0 mL/h						

3.7 Bioassays (Bacteria Studies)

Source of bacteria: *Escherichia coli (E. coli)* OR:H48:K- MG1655 (referred as K-12 MG1655) (ATCC 700926) was derived from parent strain W1485 by acridine orange curing of the F plasmid.[369] The enterohemorrhagic (EHEC) *E. coli* O157:H7 RIMD 0509952 (referred as O157 Sakai) (ATCC BAA-460) which produces two Shiga toxins, isogenic stx_1 and stx_2-negative nontoxigenic is a derivative of the Sakai strain isolated from human faeces during the Sakai outbreak in 1996.[370] *Staphylococcus aureus (S. aureus)* subsp. aureus, Strain JE2, Transposon Mutant NE100 (referred as MRSA JE2) is a plasmid-cured derivative of strain LAC which was isolated from a skin and soft tissue infection of an inmate in Los Angeles County Jail in California, USA during 2002.[371] *S. aureus* Newman D2C ATCC 25904 NCTC 10833 (referred to as MSSA Newman D2C) is a clumping factor-positive variant of the *S. aureus* strain Newman D2 deposited by J. Hawiger in 1972 to give the strain designation ATCC 25904.[372,373] *Candida albicans* SC5314 (referred as *Candida* SC5314) was isolated from a patient with generalised *Candida* infection by Margarita Silva Hunter at the Dermatology Department of Columbia College of Physicians and Surgeons in New York, USA.[374] *Pseudomonas aeruginosa* strain PAO1 (referred as *P. aeruginosa* PAO1), strain PA14 (referred as *P. aeruginosa* PA14) and strain LESB58 (referred as *P. aeruginosa* LESB58) were isolated from a six-year-period outbreak at Nottingham University Hospitals National Health Service (NHS) Trust – City Campus during 2001 to 2007.[375]

3.7.1 Reagents for Media and Cultures

Mueller Hinton (M-H) Broth (dehydrated powder), yeast extract (for microbiology), dextrose, sodium chloride, crystal violet and 0.2 μm syringe filter were purchased from

Sigma-Aldrich. Bacto-agar, Tryptic Soy Broth (TSB, Soybean-Casein Digest Medium, dehydrated powder) and peptone were purchased from BD. Isopropanol and ethanol were purchased from Fisher Scientific. Autoclaved phosphate buffer saline (PBS) solution was provided by Warwick Medical School. All materials were used as received unless otherwise stated.

3.7.2 Directions for use of media and cultures

As M-H agar is considered to be the best medium to use for routine susceptibility testing,[376] Kirby-Bauer disk diffusion tests were conducted using M-H agar plates for all microbes except for *Candida* SC5314. As *Candida albicans* require different nutrients to cultivate and prefer to form biofilms in yeast extract-peptone-dextrose (YPD), YPD agar was used when testing with *Candida* SC5314. To ensure reproducible robust biofilms can be generated in the anti-biofilm assay, TSB enriched with glucose and sodium was used as the only liquid culture.[377,378]

3.7.3 Protocols for media and cultures

M-H broth: 10.5 g M-H broth was weighed and dissolved in 500 mL of distilled water. The solution was then autoclaved at 121 °C and 0.5 bar for 15 mins. After it was cooled to room temperature, 250 μL $CaCl_2$ and 166 μL $MgCl_2$ were added and mixed thoroughly.

M-H agar plates: 10.5 g M-H broth and 7.5 g bacto-agar were weighed and dissolved in 500 mL distilled water. The solution was then autoclaved at 121 °C and 0.5 bar for 15 mins. After it was cooled to *ca*. 50–60 °C, 200 μL $CaCl_{2(aq)}$ and 133 μL $MgCl_{2(aq)}$ were added and mixed thoroughly. In a biological safety cabinet, the liquid M-H agar was poured into 15–18 petri-dishes. Each of the dishes should contain at least 25 mL of M-H agar or equivalent to a depth of 4 mm. They were then allowed to solidify and stored in a fridge.

YPD broth: 5 g yeast extract, 10 g peptone and 10 g glucose were weighed and dissolved in 500 mL distilled water. The solution was then autoclaved at 121 °C and 0.5 bar for 15 mins.

YPD agar plates: 5 g yeast extract, 10 g peptone, 10 g glucose and 10 g bacto-agar were weighed and dissolved in 500 mL distilled water. The solution was then autoclaved at 121 °C and 0.5 bar for 15 mins. After it was cooled to *ca*. 50–60 °C, the liquid M-H agar was poured into 15–18 petri-dishes in a biological safety cabinet. Each of the dishes should contain at least 25 mL of M-H agar or equivalent to a depth of 4 mm. They were then allowed to solidify and stored in a fridge.

TSB broth: 15 g TSB was weighed and dissolved in 500 mL distilled water. The solution was then autoclaved at 121 °C and 0.5 bar for 15 mins. After it was cooled to room temperature, 2.78 mL glucose$_{(aq)}$ and 13.97 mL NaCl$_{(aq)}$ were added and mixed thoroughly.

3.7.4 Kirby-Bauer disk diffusion test

For all microbes except *Candida* SC5314, a sterile inoculating loop was used to touch a colony of the organism. The inoculating loop was then dipped into 5 mL M-H broth which was then incubated at 37 °C overnight. OD (λ = 600 nm) of the overnight culture was measured, it was then diluted to achieve OD = 1 and incubated for another 4 hours at 37 °C. In the meantime, circular polymer samples with a diameter of 8 mm were sterilised using UV light (λ = 254 nm) for 10 minutes. ODs of the 4-hour cultures were measured, they were then diluted again to achieve OD = 0.01. A sterile inoculating loop was dipped into the diluted culture and then inoculate an M-H plate by streaking the swab in a back-and-forth motion. This action was repeated at least twice after rotating the plate to ensure even distribution of inoculum. The inoculated M-H agar plate then sat at room temperature for 3–5 minutes for drying and the sterilized polymer discs were placed on the dry inoculated agar. They were then incubated overnight at 37 °C. When the test was conducted using *Candida* SC5314, the same procedure was repeated but YPD broth was used instead of M-H broth.

3.7.5 Growth curves for bacteria

Bacteria strains were incubated in 5 mL M-H broth for overnight at 37 °C. ODs (λ = 600 nm) of these overnight cultures were measured, they were then diluted to achieve OD = 1 and incubated for another 4 hours at 37 °C. In the meantime, PLLA-based composites films were cut into a size of 1 cm x 5 cm. These films were then placed against the walls of 24-well plate with "labyrinth" lid and sterilised using UV light (λ = 254 nm) for 10 minutes. ODs of the 4-hour cultures were measured, they were then diluted again to achieve OD = 0.2. Excluding the wells that were designated to contain the blank M-H broth, 50 μL of the cultures were then added to the individual well in the 24-well plate that contained 950 μL M-H broth to ensure that each well contained culture with OD = 0.01. Growth curves were then obtained using FLUOstar Omega automatic plate reader after overnight at 37 °C. This procedure was repeated twice to obtain additional results.

3.7.6 Anti-biofilm assay

Bacteria strains were incubated in 5 mL TSB broth overnight at 37 °C. ODs ($\lambda = 600$ nm) of the overnight cultures were measured and, then diluted to achieve OD=1 and incubated for another 4 hours at 37 °C. In the meantime, PLLA-based composites films were cut into circular discs with a diameter of 15 mm. These films were then placed at the bottom of the wells with "labyrinth" lid and sterilised using UV light ($\lambda = 254$ nm) for 10 minutes. ODs of the 4-hour cultures were measured, they were then diluted again to achieve OD = 0.2. Excluding the wells that were designated to contain the blank TSB broth, 50 μL of the cultures were then added to the individual well in the 24-well plate that contained 950 μL TSB broth to ensure that each well contained culture with OD=0.01. This 24-well plate was then incubated undisturbed, without any shaking overnight at 37 °C. After incubation, the TSB broth in the wells was removed using a pipette very carefully. Each well was washed gently with 1 mL PBS three times and allowed to dry completely at room temperature. While the plates were drying, 0.5 g crystal violet was dissolved in 50 mL distilled water. After the crystal violet was dissolved completely, the solution was passed through a 0.2 μL syringe filter. After the multi-well plate was dried completely, 500 μL the filtered crystal violet solution was added to the wells. The plate was incubated again at 37 °C for 30 min. followed by removal of the crystal violet solution. Each well was then washed gently with 1 mL PBS twice. Ethanol, isopropanol and water in the ratio of 7:1:2 was mixed and added to the crystal violet. The crystal violet was allowed to dissolve in the 80% alcohol for 30 minutes at room temperature. They were then diluted 40-fold and their values of OD ($\lambda = 570$ nm) measured using a FLUOstar Omega automatic plate reader.

3.8 Bioassay (Endothelial Cell Culture)

Early passage human umbilical vein endothelial cells (HUVECs) were cultured in T-75 tissue culture flasks (Iwaki, Japan) at 37°C with 5% CO_2 in Human large vessel endothelial cell basal media (Cellworks, UK) supplemented with 1μg/ml hydrocortisone, 20% fetal bovine serum (FBS), 100 units/ml penicillin, 100μg/ml streptomycin and 2mM - L-glutamine (Sigma- Aldrich, UK). For all experiments, cells of passage number 2-5 were used.

3.8.1 Cell Viability and Cell Seeding Density

A qualitative assessment of HUVEC cell number and viability was made using the trypan blue exclusion assay method. Briefly, a HUVEC cell suspension was mixed with 0.4% trypan blue (1:1 by volume) and the cells counted using a TC-20 automated cell counter (Bio-Rad, UK). The breakdown in cell membrane integrity was determined by the uptake of trypan blue to which the normal cell is impermeable. Following assessment of number and viability, cells were seeded onto the polymer samples at a concentration of 5×10^5 cells/cm^2 and allowed to adhere and proliferate during incubation at 37°C in 5% CO_2.

3.8.2 Cell Adhesion Assay

Samples of sterile polymer (composite) were placed at the bottom of individual wells of a sterile 24-well polystyrene plate. Samples were then washed in three changes of PBS for 15 min each. The HUVEC suspension was added to the surface of the polymers at a concentration of 5×10^5 cells/disc in 1.0 mL of endothelial cell growth media. Triplicate samples were established for each composite with different PLA/WS$_2$ ratio to obtain multiple data. Polymer samples with cells so loaded were incubated at 37°C in a humidified atmosphere of 5% CO_2 in the air until the predetermined time point of 60 min at which time the polymer samples were removed to a clean well. At this stage, crystal violet staining of cells in culture was performed using a modification of the methods of Kueng *et. al.*[379] Briefly, cells were washed in PBS and fixed in ice-cold 10% Formalin (Sigma- Aldrich, UK) for 20 min. Cells were washed with PBS, permeabilized with 20% methanol for 20 min, and stained with 0.5% crystal violet (Sigma) in 20% methanol for 30 min. Cells were destained by three gentle washes in deionised water, followed by elution of the residual crystal violet with 10% acetic acid for 30 min during gentle agitation. Optical density was measured by spectrophotometry at 572 nm and 650 nm as a background (Tecan, UK). The optical density obtained with this assay has been shown to correlate directly with cell number and is thus useful for standardization of cell number between the experimental wells.

The number of adherent cells on each polymer derivative was expressed as a percentage (mean ± SD) of the number of cells seeded originally. The statistical significance of cell numbers in different serum treatments was tested by ANOVA (Prism Graphpad software) analysis.

3.8.3 Cell Proliferation.

Measurement of cell viability and proliferation forms the basis for numerous *in-vitro* assays of a cell population response to external factors. The MTT cell proliferation assay measures the cell proliferation rate and conversely, when metabolic events lead to apoptosis or necrosis, the reduction in cell viability. Cell proliferation was analysed by using 3-(4,5-dimethylthiazol-2-yl)-2,5-diphenyl tetrazolium bromide (MTT; Sigma-Aldrich, UK) mitochondrial reduction.[380,381] This assay is based on the ability of live cells to reduce a tetrazolium-based compound, MTT, to a purplish formazan product. The resulting intracellular purple formazan can be solubilized and quantified by spectrophotometric means. In brief, HUVECs (5×10^5 cells/cm^2) were seeded onto triplicate samples of control and modified polymer discs and incubated under normal cell culture conditions (37 °C in a humidified atmosphere of 5% CO_2 in air until the predetermined time point of 1 Day, 3 Days and 7 days. At each time point the polymers were washed with PBS, transferred into new cell culture plates containing 1 ml of culture medium containing no phenol red, and 5 mg/ml of MTT solution and incubated for 2–3 h at 37 °C. After removing the culture media, 0.5 ml of extraction solution (0.01 N HCl in isopropyl alcohol) was added. The polymers were washed extensively by pipetting up and down repeatedly to allow total colour release. The absorbance of the supernatant was read with a spectrophotometer at 572 nm with a background subtraction at 650 nm (Tecan, UK).

3.8.4 SEM of Cell Cultures

Cells remaining on the polymer substrate surface after culture for 1, 3 and 7 days were washed in PBS and fixed for 1 hr with 2.5% glutaraldehyde in 0.1 M sodium cacodylate buffer pH 7.4 (Agar, UK). Samples were then rinsed and fixed for another hour with 1% by volume osmium tetroxide in 0.1M sodium cacodylate buffer pH 7.4 (Agar, UK). Samples were then gently dehydrated through an aqueous replacement process by soaking in a series of graded alcohol of 50%, 60%, 70%, 80%, 90%, and 100% three times for 10 min each. To maintain ultra-structures on the biological specimens, the substrates were transferred to 100% hexamethyldisilazane, HDMS, (Sigma-Aldrich, Poole, UK) for 5 min and dried in a desiccator overnight. Scanning electron microscope (Jeol, UK) images were taken after sputtering samples with a 100 nm thick film of Au using a dual ion-beam sputter (Polaron, UK).

3.8.5 Immunocytochemistry

HUVECs were cultured on the polymer (composite) substrate for 1, 3 and 7 days under normal culture conditions, the medium being changed every 48h. The cells were then washed in PBS, and fixed in freshly prepared 3.7% paraformaldehyde for 15 min at 4°C and permeabilised with 0.1% Triton-X-100 in PBS for 10 minutes. Prior to the addition of the alexa-fluor phalloidin 543, cells were pre-treated with PBS containing 0.1% BSA and 0.01% sodium azide for 20 min. Cells were incubated with phalloidin for 30 minutes at room temperature. Cells were then washed and to visualise the nuclei, the cells were incubated with the DNA-binding 39 fluorochrome Hoechst 33258 (1mg/ml stock diluted 1:1000 in PBS, Sigma Chemical Co.) for 10 minutes at room temperature. The cells were mounted in glycerol-based mounting medium containing an anti-fade reagent and then studied under a confocal microscope LSM Pascal equipped with an inverted microscope Axiovert 100M and a 63 x (NA 1.2/w) water immersion objective (Zeiss, Göttingen, Germany).

3.8.6 Surface Wettability Study (Contact Angle Analysis)

Samples were placed flat on a glass microscope slide and then onto the stage of the KSV Contact Angle Instrument (CAM2000, KSV Instrument Ltd.). The camera for viewing the sessile drop was brought into focus and the stage base marked using CAM200 software. Using a modified method from Martins *et. al.*,[382] a 5 microliter drop of water was placed on the surface of the sample for 20 seconds and a recording taken. CAM200 software calculated the contact angle using Young's equation: $\gamma_{lv} \cos \theta_\gamma = \gamma_{sv} - \gamma_{sl}$ where θ_γ is the contact angle and whereas, γ_{lv}, γ_{sv} and γ_{sl} represent the liquid-vapour, solid-vapour and solid-liquid interfacial tensions respectively.[383]

Chapter 4.

Composites of PLA and Lignin

4. Composites of PLA and lignin

4.1. General Characterisations of PLA/lignin Composites

As lignin was reported to exhibit antimicrobial activity against *Listeria monocytogenes*, *MRSA* and yeast,[208] it was used as an additive for PLA to provide additional functionality to PLA-based composites with 0, 0.5, 1, 2, 3, 5 and 10 wt% lignin content prepared via melt-extrusion. In order to avoid embrittlement of the composites, another set of samples with the same composition profiles of PLA and lignin with addition of 20 wt% triacetin plasticizer were prepared. In this chapter, PLA/lignin composites and plasticized PLA/lignin composites will be compared. The points of interest are to determine the influence of lignin on the PLA and determine the influence of triacetin on the composites properties, such as mechanical and antimicrobial activity.

PLA/lignin composites in the form of dog bone shaped specimens were prepared using injection moulding for the tensile testing. After these tests, the fractured surface of the specimens were used for examination by SEM. Composites with the lowest and highest lignin loadings are shown and compared below. However, it should be noted that SEM examination was challenging as PLA is highly charging under the electron beam and it was difficult to obtain charge balance even when the samples were coated with conductive coatings such as gold or platinum. In addition, PLA itself is highly sensitive to the electron beam irradiation[384] and it was observed that the samples decompose very easily. High resolution imaging was impossible and the surface structure of the composites could be difficult to observe due to beam penetration effects.[384] As shown in Figure 4.1, a distinctive rectangular area can be seen which was actually damage caused by the electron irradiation beam.
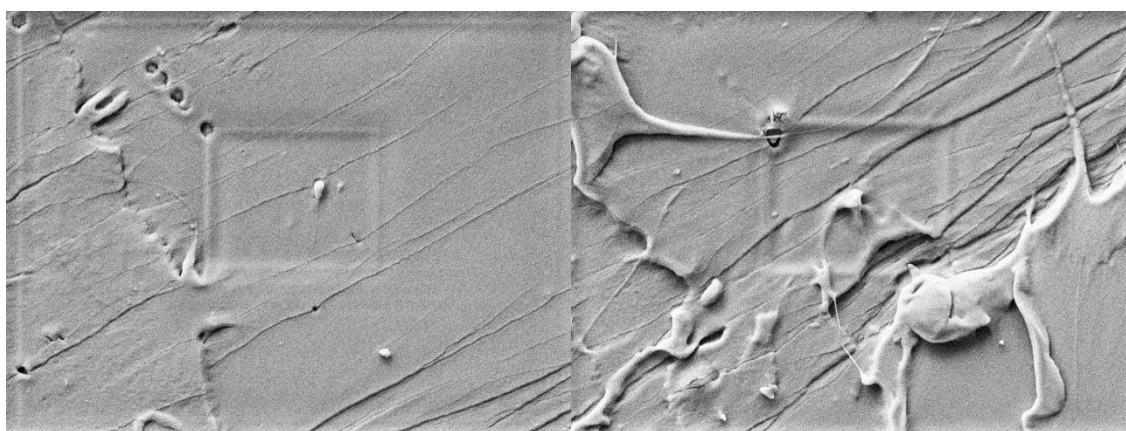
Figure 4.1. SEM images showing an area of damaged PLA composite caused by the irradiation beam.

This limitation could be slightly minimised by using a low voltage (i.e. a maximum of 5 kV), ensuring that the composites were not exposed to the irradiation beam for too long, i.e. a minimal time (less than 15 seconds) as well as apply low magnification.

For composites consisting of only 0.5 wt% lignin, the fractured surface appeared to be smooth and very few spherical granules can be seen which are likely to be lignin particles can be seen (red circles in Figure 4.2a, b). The size of these granules have diameters in the range of 300–500 nm. In contrast, most of the fractured surfaces of the other composite with 10 wt% lignin are much rougher with pores (Figure 4.2c). The pores may reflect a lack of wetting between the two components and the lignin phase is expelled during fracture. As the surface appear to be very uneven, it is actually harder to distinguish the presence of individual lignin particles (Figure 4.2d).
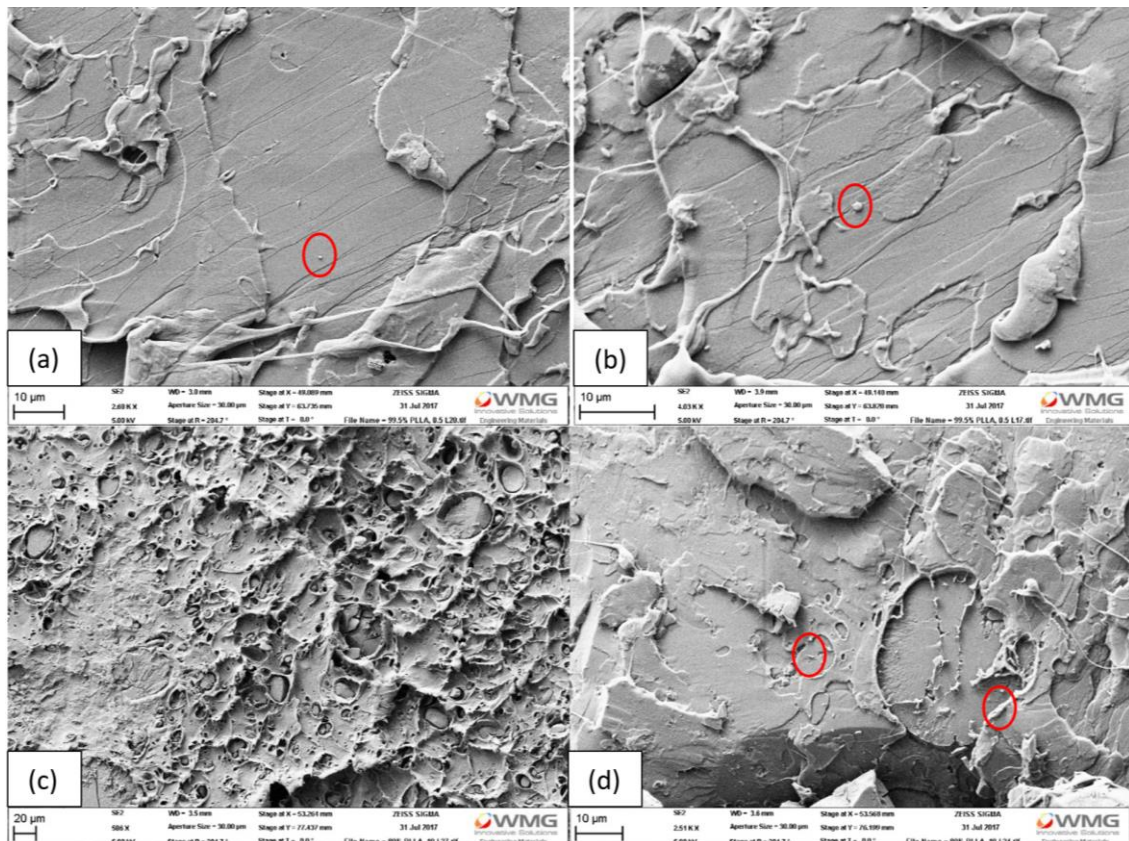
Figure 4.2. SEM images of (a) and (b) PLA with 0.5 wt% lignin and, (c) and (d) PLA with 10 wt% lignin

The same procedure was repeated for the plasticized PLA/lignin composites and gain as fractured specimens from dog-bones were examined by SEM, see Figure 4.3. The fractured surface of the plasticised composite appears to be smoother compared to the non-plasticized counterpart. In comparison to Figure 4.2(a, b), spherical granules seen in the plasticized composite are 2–3 times bigger but appear to be embedded within the PLA

matrix (Figure 4.3a, b red circles). Fracture of plasticized composite with 10 wt% lignin appears to have a rougher, very uneven surface which is similar to the image in Figure 4.2(c). It can be seen that there are spherical clusters on the surface (Figure 4.3c) and when a higher magnification was used to view the sample, it can be seen that the surface also consists of pores that are similar to those in Figure 4.2(c).
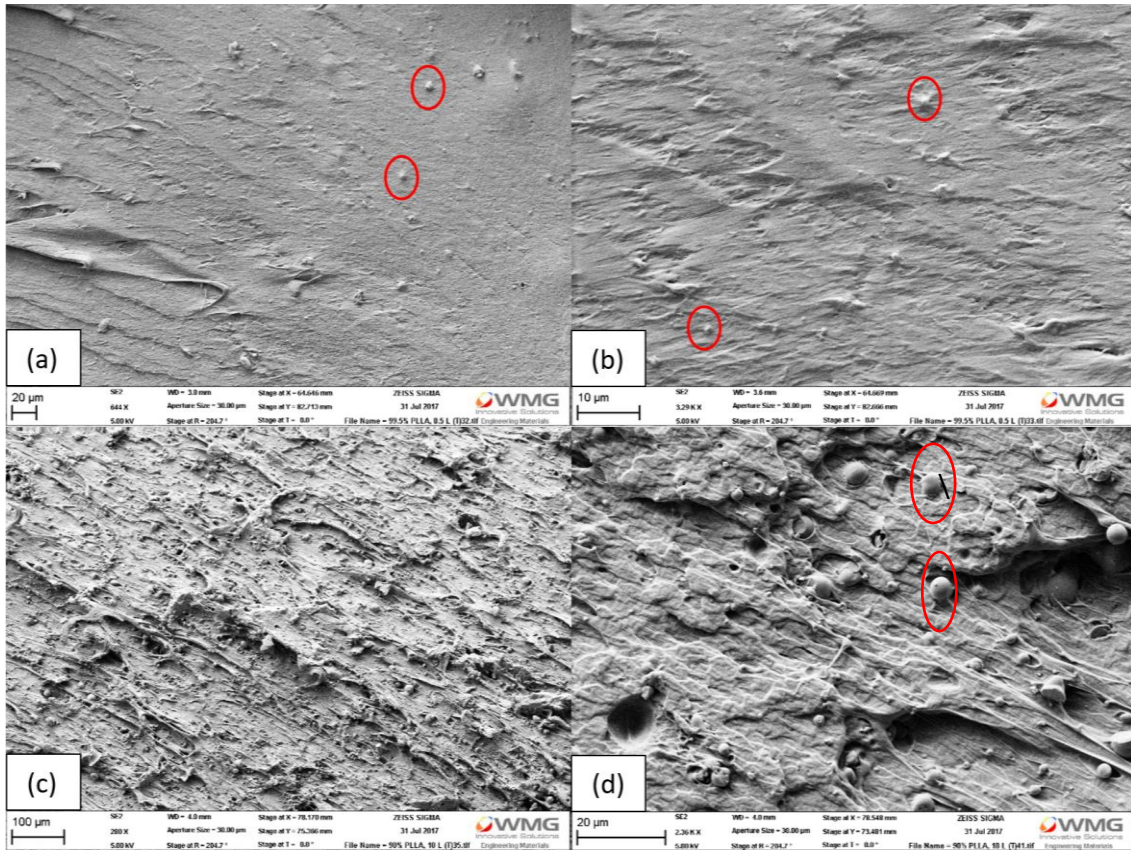
Figure 4.3. SEM images of plasticized (a) and (b) PLA with 0.5 wt% lignin and, (c) and (d) PLA with 10 wt% lignin

DSC measurements were conducted to determine the values of T_g, cold crystallisation temperature (T_{cc}), melting temperature (T_m) and crystallinity (X_c) of the composites. Lignin itself does not have a glass transition or display classical melting behaviour and so, the terms 'miscibility' and 'immiscibility' cannot be correctly applied in blend systems that involved lignin based upon T_g values.[212] In this case, the change of T_g and T_m of the PLA in the composites can be used to predict intermolecular interaction between PLA and lignin. Unlike T_{cc} and T_m, evaluation of T_g is more difficult because this involves the transition of the amorphous part from a high elastic state into a glassy state.[385] However, the amorphous rigid interfacial region can often be trapped between the crystalline lamellae after processing which causes the T_g value be harder to be detected

by DSC.[212,386] Fortunately, this parameter can be detected more easily by removing the thermal history. Therefore, the thermal histories of the composites were erased by heating from 25 °C to 180 °C, isotherm for 4 minutes and then cooling back to 25 °C at a heating rate of 10 K/min. This thermal cycle was repeated to obtain the second heating (Figure 4.4) and cooling curves (Figure 4.5) and the relevant parameter were obtained and shown in Table 1. Same procedure was used when plasticized samples were analysed but the samples were cooled to -30 °C instead of 25 °C. The values of T_g, T_{cc}, $T_{m,1}$, $T_{m,2}$ ($T_{m,1}$ is 1st melting peak and $T_{m,2}$ is 2nd melting peak) and X_c are listed below in Table 4.1

Table 4.1. Thermal parameters obtained from DSC measurements for composites of PLA and lignin

Composite	T_g	T_{cc}	$T_{m,1}$	$T_{m,2}$	X_c
Neat PLA	58 °C	126 °C	150 °C	-	0.99%
99.5% PLA/ 0.5% lignin	58 °C	121 °C	148 °C	-	1.06%
99% PLA/ 1% lignin	58 °C	120 °C	148 °C	-	0.91%
98% PLA/ 2% lignin	58 °C	122 °C	149 °C	-	0.81%
97% PLA/ 3% lignin	58 °C	121 °C	148 °C	-	1.06%
95% PLA/ 5% lignin	57 °C	122 °C	148 °C	-	0.37%
90% PLL/ 10% lignin	57 °C	117 °C	146 °C	152 °C	1.10%

The T_g of plasticized PLA was recorded as 22 °C and it remained unchanged when up to between 0.5 and 3 wt% lignin was added. When the weight percentage of lignin was further increased to 5 and the 10 wt%, the T_g increased to 57 °C. Pure PLA had a small cold crystallisation peak at 126 °C but the peak became more intense but the maximum decreased to the range of 120 – 122 °C for composites that consisted of 0.5 – 5 wt% lignin. For the composite with 10 wt% lignin an even bigger cold crystallisation peak centred at 117 °C (Figure 4.4b) was obtained. Pure PLA has a small melting peak at 150 °C but the melting peaks increased in size and T_m decreased (allowing for instrument error) to 148 – 149 °C for composites with 0.5 – 5 wt% lignin. Interestingly, when lignin content was increased to 10 wt%, the PLA exhibited 2 melting peaks with maxima at 146 °C and 152 °C (Figure 4.4c). This double-melting behaviour can occur in semicrystalline

polymers.[387] Samples with 0 – 5 wt% of lignin consist of single melting peak which is likely to be more perfect crystals presented that could melt more directly and gave rise to a single melting peak.[388] In the case of a double-melting behaviour, their lower melting peak was attributed to melting of primary crystals,[389] formation of thickened lamellae[390] or fusion of think lamellae formed.[284] The second, higher temperature peak attributed to melting of recrystallized crystals[389] or fusion of newly formed lamellae via melting-recrystallisation of primary thin lamellae.[284] In addition, PLA itself consists of different crystalline polymorphs and it was reported that such double-melting peak can emerge when T_{cc} is below 120 °C.[391] While a single melting correspond to a more stable α crystalline phase, double-melting peak can often be seen when T_{cc} below is 120 °C corresponding to melting of α crystal phase (lower melting peak) and melting of a less stable α' crystal phase (higher melting peak).[391] Therefore, it is possible that incorporation of 10 wt% lignin had resulted T_{cc} below 120 °C as well as induce formation of the α' crystal phase of PLA.

The degrees of crystallinity of all composites were determined based upon the second heating cycles with extra enthalpy absorbed by crystallites formed during heating which had to be subtracted from the endothermic heat flow because of the melting of the whole crystallites and hence, the following equation was applied, $X_c = \frac{\Delta H_m - \Delta H_{cc}}{\omega PLLA \times \Delta H_m^0} \times 100\%$ (where ΔH_m stands for enthalpy of melting, ΔH_{cc} is enthalpy of cold crystallisation, $\omega PLLA$ is weight fraction of PLA and ΔH_m^0 is the melting enthalpy of a theoretically 100% crystalline PLA which has been reported to be 93.7 J/g).[389,392] The composite with 5 wt% lignin has the lowest crystallinity of 0.37% and the rest of the samples consist of X_c within 0.81 – 1.10%. Overall, all composites have degrees of crystallinity less than 2% which is possibly due to the slow crystallisation rate of PLA and so, very few crystals generated in PLA resin which caused the polymer content remained amorphous under the most practical processing and moulding procedures.[393]
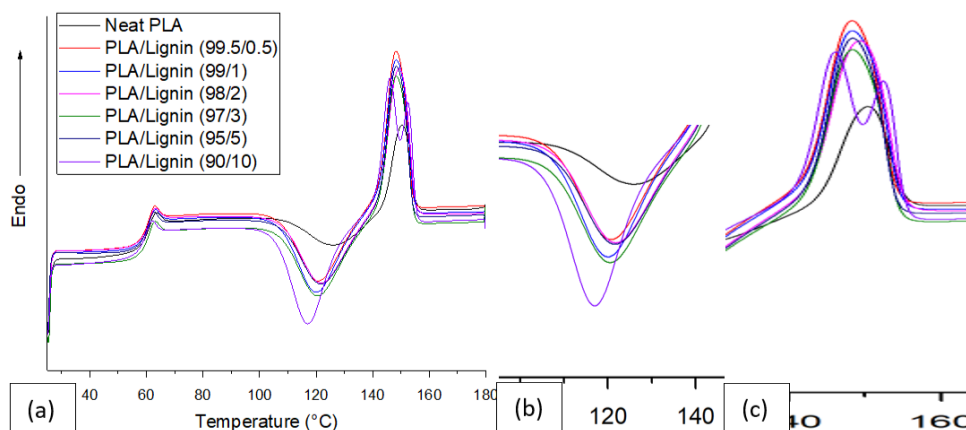
Figure 4.4. DSC (a) second heating curves, (b) enlarged cold crystallisation peaks & (c) enlarged melting peaks of PLA/lignin composites

The second cooling curves of the PLA/lignin composites are shown in Figure 4.5. As PLA crystallises slowly[394] and this is the reason why only glass transition steps appeared in all cooling curves of PLA/lignin composites. Precisely, the formation of critical nucleus required for nucleation demands some time, slow crystallisation leads to absence of crystal formation and hence, crystallisation was prevented which resulted in all PLA-based composites being fully amorphous and showing only glass transition steps in their cooling curves.[394]
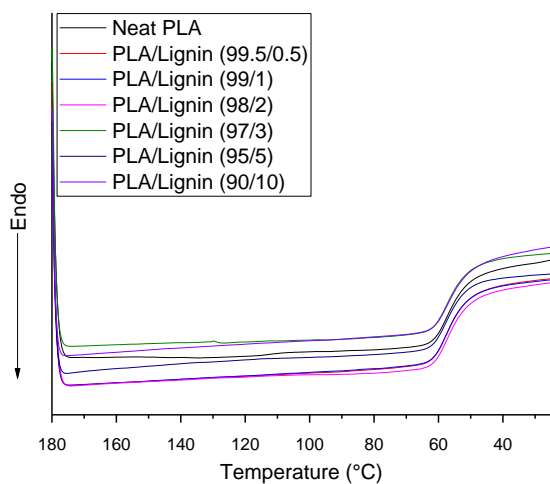
Figure 4.5. DSC second cooling curves of PLA/lignin composites

The second heating (Figure 4.6) and cooling curves (Figure 4.7) of the plasticized samples were obtained and their relevant results are listed in Table 4.2 on the next page.

Table 4.2. DSC data for plasticized PLA/lignin composites

Plasticized composite	T_g	T_{cc}	$T_{m,1}$	$T_{m,2}$	X_c
100% PLA	22 °C	96 °C	143 °C	-	1.26%
99.5% PLA/ 0.5% lignin	22 °C	96 °C	141 °C	-	1.08%
99% PLA/ 1% lignin	21 °C	100 °C	141 °C	-	0.44%
98% PLA/ 2% lignin	22 °C	99 °C	142 °C	-	0.82%
97% PLA/ 3% lignin	21 °C	98 °C	142 °C	-	0.59%
95% PLA/ 5% lignin	21 °C	96 °C	142 °C	-	0.93%
90% PLA/ 10% lignin	19 °C	96 °C	127 °C	141 °C	0.05%

Plasticized composites with 0 – 5 wt% lignin had the same T_g. When the lignin composition was further increased to 10 wt%, the T_g decreased to 19 °C. In comparison to the non-plasticized composites, T_g values of these plasticized samples were decreased by more than 50%. This is because when plasticizer was incorporated into the polymer matrix, the free volume between polymer chains increased allowing them to move or rotate more freely. Therefore, plasticized materials tend to have a lower T_g and melt viscosity[395] compared to their non-plasticized counterparts.[395] Similarly, there is only a little difference between the overall T_{cc} values for plasticized PLA/lignin allowing instrumental errors. In addition, the plasticized composites with 0, 1 and 2 wt% lignin have broader cold crystallisation peaks (Figure 4.6b) and it is possible to be due to the major changes in the phase separation behaviour as well as more diverse sizes of lignin particles in the polymer matrix.[396] In the comparison of T_m values, there was a very little change as the values are in the range of 141 – 143 °C but it was also noticed that it consisted of a very small shoulder peak at 127 °C (Figure 4.6c). This seems to be the double-melting behaviour that was observed also for the non-plasticized PLA composite with 10 wt% but presence of the plasticizer enhanced the composite to melt more directly and gave rise to a peak that is analogous to a single melting peak. PLA indeed consists of different crystalline polymorphs and it was reported that such double-melting peak can emerge when T_{cc} is below 120 °C.[391] All plasticized samples consist of T_{cc} below 120 °C and they all consist of shoulder peaks within their melting peaks. It can be seen that

plasticized sample with 10 wt% lignin has a first melting peak at 127 °C (Figure 4.6c). The presence of plasticizer as well as 10 wt% lignin should induce formation of different crystal phase of PLA to give the double-melting peak effect. The degrees of crystallinity of all plasticized samples were also determined based upon the second heating cycles with extra enthalpy absorbed by crystallites being subtracted and hence, the following equation was applied, $X_c = \frac{\Delta H_m - \Delta H_{cc}}{\omega PLA \times \Delta H_m^0} \times 100\%$ (where ΔH_m stands for enthalpy of melting, ΔH_{cc} is enthalpy of cold crystallisation, ωPLA is weight fraction of PLA and ΔH_m^0 is the melting enthalpy of 100% crystalline PLA which reported to be 93.7 J/g).[389,392] Sample with the lowest and highest composition of lignin had the highest and lowest X_c of 1.26% and 0.05% respectively. The rest of the samples consist of X_c values in the range of 0.44 – 1.08%. Both non-plasticized and plasticized PLA samples have very low crystallinity according to the DSC data. This is very highly to be due to the optical purity of the PLA matrix. 100% pure isotactic and optically active PLLA and PDLA are both crystalline polymer and in contrast, atactic and optically inactive PDLLA is amorphous.[118] The PLA matrix used in this project consists of only 96% pure isotactic and optically active PLLA and the rest are mixture of PDLA and PDLLA which led to the low crystallinity values of all composite materials.[397]
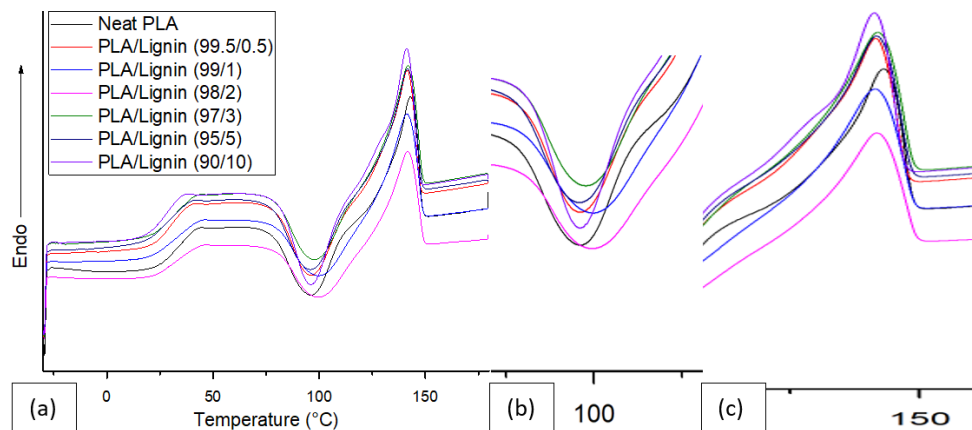
Figure 4.6. (a) Second heating curves, (b) cold crystallisation peaks & (c) melting peaks of plasticized PLA/lignin composites

The second cooling curves of plasticised PLA/lignin composites are shown in Figure 4.7. As PLA consists of slow crystallisation,[394] only the glass transition process appeared in all cooling curves of the plasticized composites. This observation is identical to that attained for the non-plasticized PLA/lignin systems suggesting that the plasticizer does not affect such slow crystallisation behaviour. Hence, the plasticized samples also

exhibited nearly fully amorphous features and showing only glass transition steps in the their cooling curves.[394]
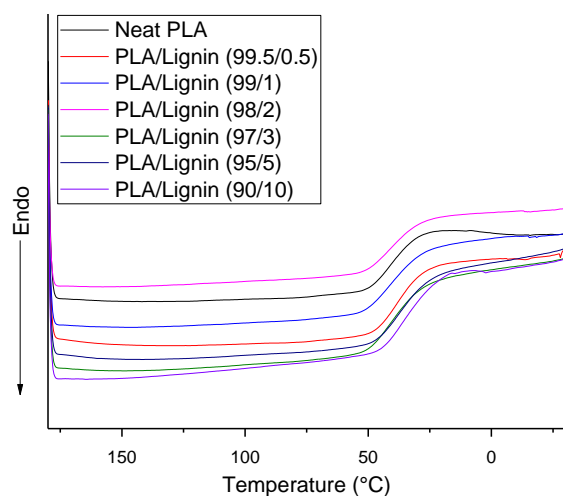
Figure 4.7. Second cooling curves of PLA/lignin composites

DMTA measurements can provide insights to the dynamic mechanical properties of the composites and changes in viscosity and storage modulus as a function of lignin and plasticizer content. The tan δ curves and dynamic modulus as a function of temperature are shown in Figure 4.8. The T_g of the composites can easily be identified as the maxima in the tan δ curves which indicate transition of the amorphous part from a high elastic state into a glassy state.[385] Alternatively, the slopes of the dynamic modulus curves show the transition from solid to rubber which can also be used to show the T_g of the composites.[398,399] All tan δ curves have very similar shapes with a sharp peak typically having a maximum in the narrow range 66 – 68 °C (Figure 4.8a). Temperatures of the tan δ peaks vs lignin content (wt%) with a best fit line was drawn in Figure 4.8c to indicate that the T_g values did not change dramatically with increasing lignin content. Taking the instrumental error into account, there is no difference in these T_g values. On the other hand, the dynamic modulus curves have slopes in the range of 58 – 65 °C (Figure 4.8b). Overall, the DMTA data also seem to imply that presence of lignin did not alter the mechanical properties of PLA composites too dramatically according to the tan δ and dynamic modulus curves obtained. Although DMTA data of PLA/lignin composites materials are not reported, Rahman *et. al.* recorded DMTA data PLA/lignin systems. It was reported that the T_g values of the PLA/lignin composites only shifted to higher temperatures when the materials were prepared at 200 °C.[213] Similarly, the T_g values of PLA/lignin composites that were prepared at 180 °C do not consist of major difference.
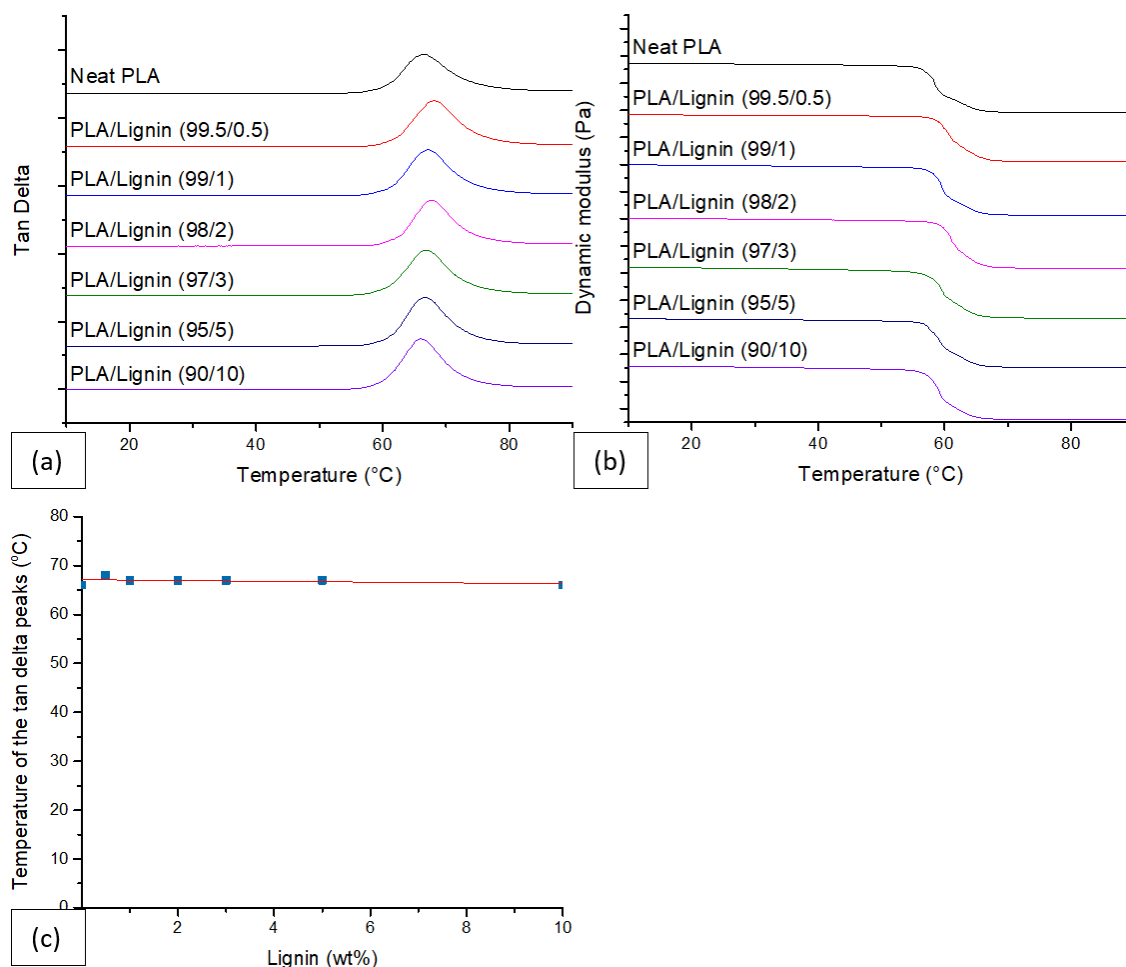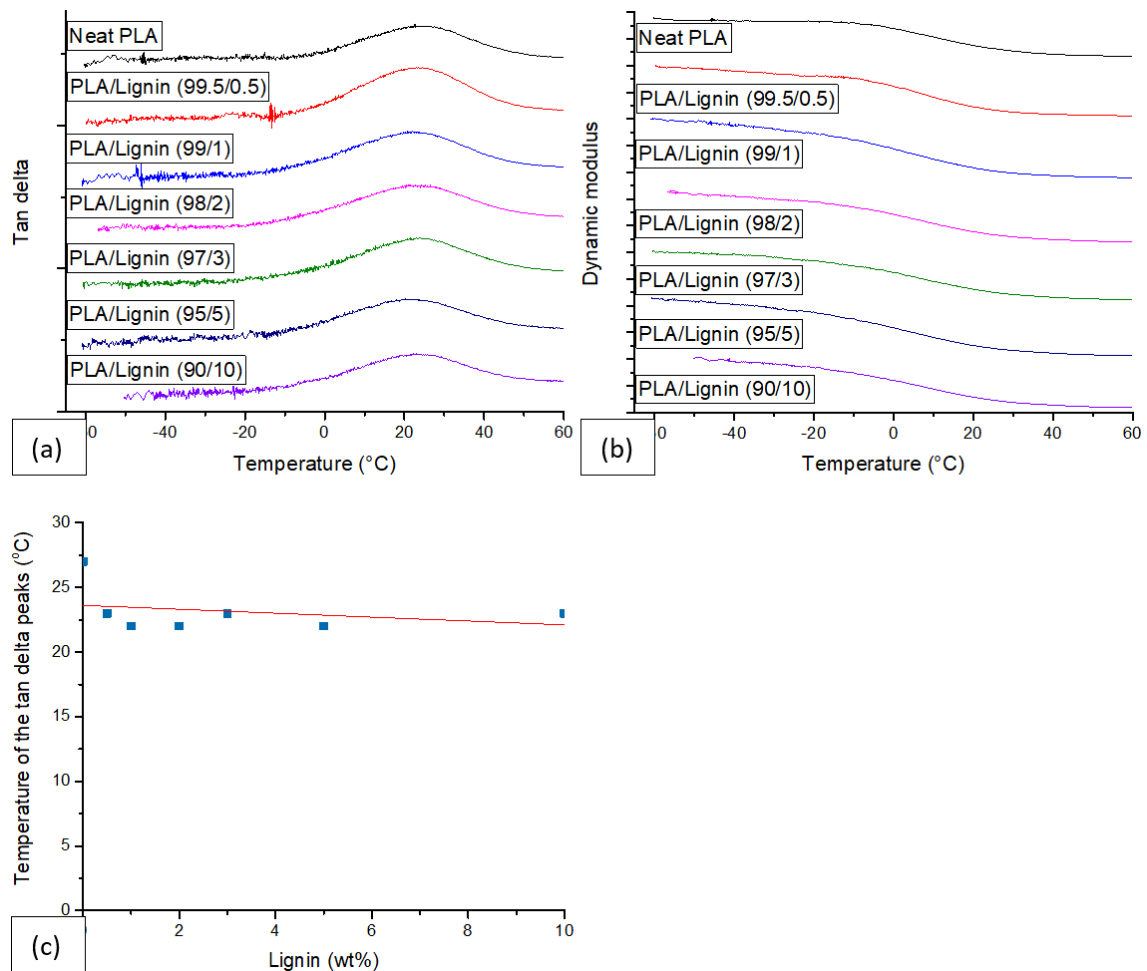
Figure 4.8. (a) Tan δ curves, (b) dynamic modulus vs temperature of PLA/lignin composites; changes of T_g with % of lignin according to (c) tan δ curves, (d) dynamic modulus curves

The DMTA measurements were repeated with the plasticized PLA/lignin composites. From the DSC data, the plasticized composites consist of lower T_g values and hence, the measurements started at -60 °C. As mentioned above, addition of plasticizer can increase the free volume between polymer chains and allow more free movement, increased chain dynamics and rotation.[395] In these systems, this made DMTA measurements more challenging compared to that of the non-plasticized composites as a consequence of slippage of samples between the clamps during measurements. In Figure 4.8, all curves obtained with the non-plasticized composites are smooth. In contrast, the curves obtained with plasticized samples contain noise (Figure 4.9), particularly below 0 °C. From the peak maxima peak of the tan δ curves, plasticized PLA **7** had the highest T_g at 27 °C. The T_g decreased with addition of lignin but the T_g for all these composites was in the range 22 – 23 °C (Figure 4.9a, Table 4.3). T_g values of these plasticized PLA/lignin composites are much lower than that of non-plasticized counterparts. Temperatures of the tan δ peaks

vs lignin content (wt%) with a best fit line was drawn in Figure 4.9c to indicate that the T_g values have an overall slight descending trend with the incorporation of lignin. On the other hand, the slopes of dynamic modulus curves are in the range of -20 – 20 °C (Figure 4.9b) which are also in a much lower range compared to that of non-plasticized PLA/lignin composites.

All T_g values for both non-plasticized and plasticized PLA/lignin composites are listed in Table 4.3 below. It can clearly indicate the reduction of T_g values of the composites after plasticization which is consistent with the DSC data. Plasticization results in an increase the free volume between polymer chains allowing them to move or rotate more freely. Therefore, the plasticized composites have lower T_g compared to their non-plasticized counterparts.[395]

Figure 4.9. (a) Tan δ curves, (b) dynamic modulus vs temperature of plasticized PLA/lignin composites; changes of T_g with % of lignin according to (c) tan δ curves, (d) dynamic modulus curves

Table 4.3. T_g of both non-plasticized and plasticized PLA/lignin composites obtained from tan δ and dynamic modulus curves

Compositions		Non-plasticized composites	Plasticized composites
PLA/wt%	Chitin/wt%	T_g / °C (tan δ)	T_g / °C (tan δ)
100	0	66	27
99.5	0.5	68	23
99	1	67	22
98	2	67	22
97	3	67	23
95	5	67	22
90	10	66	23

The static mechanical performance of these composites was determined from tensile tests and the ultimate tensile strength (MPa), Young's modulus (MPa) and elongation at break (%) of the composites determined. For each composite, 5 – 6 dog bone shaped specimens were used during the tests and their average results are shown in Figure 4.11(a) which can be seen that all composites are brittle materials.[400] The results are tabulated in Table 4.4 and the trends shown in Figure 4.11(b – d).

Table 4.4. UTS, YM, EB and their standard deviations of PLA/lignin composites

Composite	UTS (MPa)	YM (MPa)	EB (%)
Neat PLA	66.78 ± 0.53	3084.19 ± 201.67	3.45 ± 0.24
PLA/lignin (99.5/0.5)	67.13 ± 1.73	2885.90 ± 81.41	4.12 ± 0.83
PLA/lignin (99/1)	65.32 ± 1.34	3149.76 ± 217.73	3.42 ± 0.64
PLA/lignin (98/2)	64.75 ± 0.70	2834.91 ± 187.01	3.76 ± 0.30
PLA/lignin (97/3)	61.02 ± 0.75	2813.84 ± 77.96	3.56 ± 0.48
PLA/lignin (95/5)	56.82 ± 2.16	3074.38 ± 228.67	2.84 ± 0.23
PLA/lignin (90/10)	55.57 ± 3.86	2981.97 ± 88.62	2.50 ± 0.35

The ultimate tensile strengths (U.T.S) are determined from the maximum in the stress-strain curves. The unfilled PLA and 0.5wt% lignin composite had very similar tensile strengths of 66.78 ± 0.53 and 67.13 ± 1.73 MPa, respectively. When the lignin content was increased further the ultimate tensile strength gradually decreased to 55.57 ± 3.86 MPa. It is very clear that the ultimate tensile strengths decrease with increasing lignin content (Figure 4.11b). This reduction of tensile strengths with increasing lignin content was observed by other studies.[401,402] In the study completed by O. Gordobil *et. al*., two sets of PLA-based composites were prepared with both acetylated and unmodified lignin at different compositions. Although both systems experience reduction of tensile strengths with increasing lignin contents, it was noticed that the extent of decrease was much smaller for the samples that incorporated with acetylated lignin and this was very likely to be responsible for a better interaction between acetylated lignin and PLA.[401] Hence, a descending trend of tensile strengths observed in Figure 4.11b for the PLA-based composites with higher lignin content (wt%) is due to a poorer interfacial interactions in the polymer matrix. Neat PLA, composites with 1wt% and 5 wt% lignin had similar Young's moduli 3084.19 ± 201.67, 3149.76 ± 217.73 and 3074.38 ± 228.67 MPa respectively. In comparison, composites with 0.5 wt% (2885.90 ± 81.41 MPa), 2 wt% (2834.91 ± 187.01 MPa), 3 wt% WS_2 (2813.84 ± 77.96 MPa) and 10 wt% (2981.97 ± 88.62 MPa) have lower Young's moduli. Unlike the tensile strengths, a clear trend of was not observed for Young's moduli with increasing lignin content (Figure 4.11c) Therefore, an ANOVA (Analysis of Variance) statistical test were performed to analyse the differences among group means. The ANOVA results is shown below (Figure 4.10) and reported the p-value that is smaller than 0.05 which indicated that statistically, at least two of the entire groups have significantly different means.[403,404] Therefore, incorporation of lignin to PLA matrix is likely to alter the Young's Modulus of the composites.

One Way ANOVA

Overall ANOVA

	DF	Sum of Squares	Mean Square	F Value	Prob>F
Model	6	529631.51382	88271.91897	2.5233	0.04437
Error	28	979516.01104	34982.71468		
Total	34	1.50915E6			

Null Hypothesis: The means of all levels are equal.
Alternative Hypothesis: The means of one or more levels are different.
At the 0.05 level, the population means are significantly different.

Fit Statistics

R-Square	Coeff Var	Root MSE	Data Mean
0.35095	0.06287	187.03667	2974.99429

Figure 4.10. ANOVA results for Young's Modulus of non-plasticized PLA/lignin composites

In the comparison of elongation at breaks, the value increased from 3.45 ± 0.24 (0 wt% lignin) to 4.12 ± 0.83 % (0.5 wt% lignin) but decreased to 3.42 ± 0.64 % with 1 wt% lignin. The composite with 2 wt% lignin added has a slightly higher elongation at break at 3.76 ± 0.30 % but gradually decreased to 2.50 ± 0.35 % when lignin content increased to 10 wt%. Hence, the values fluctuate at low lignin content but decrease when lignin content was further increased (Figure 4.11d). A trend line was drawn which can clearly indicate that overall elongation at break decrease with increasing lignin content which should be due the poor interactions between PLA and lignin.[401]
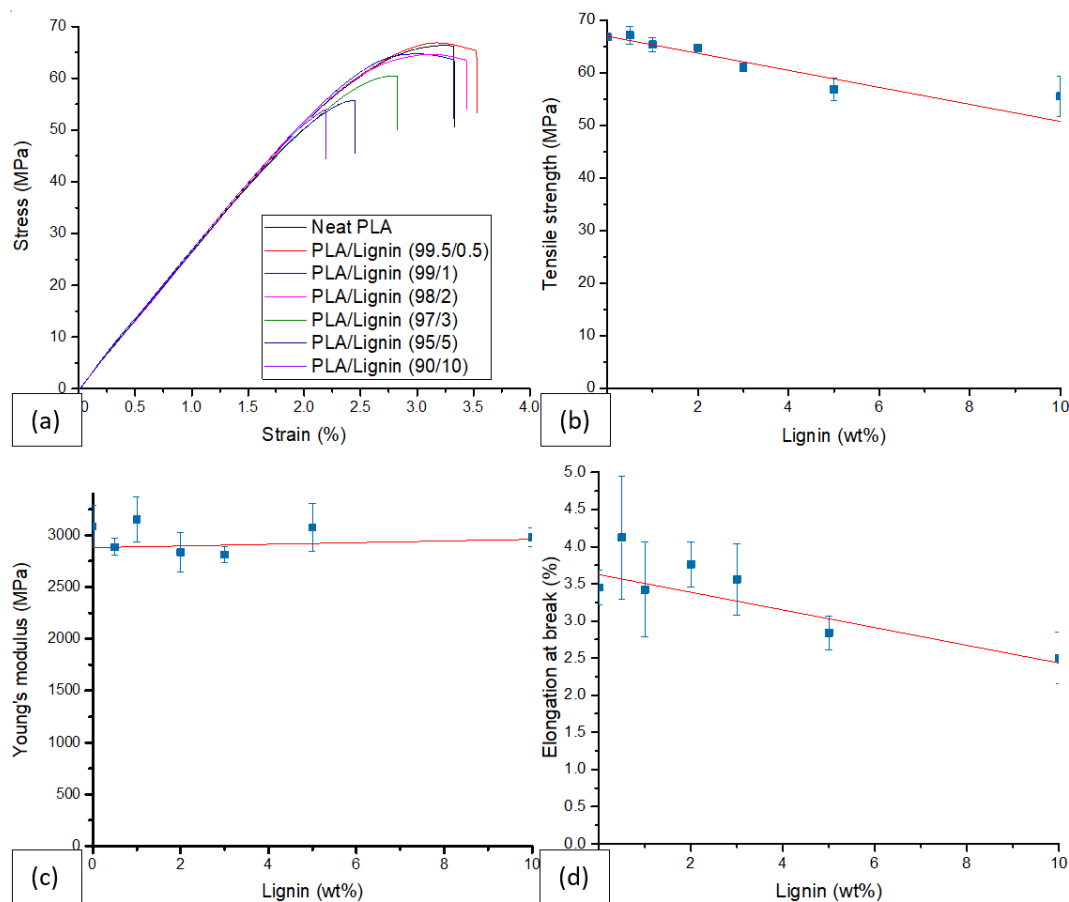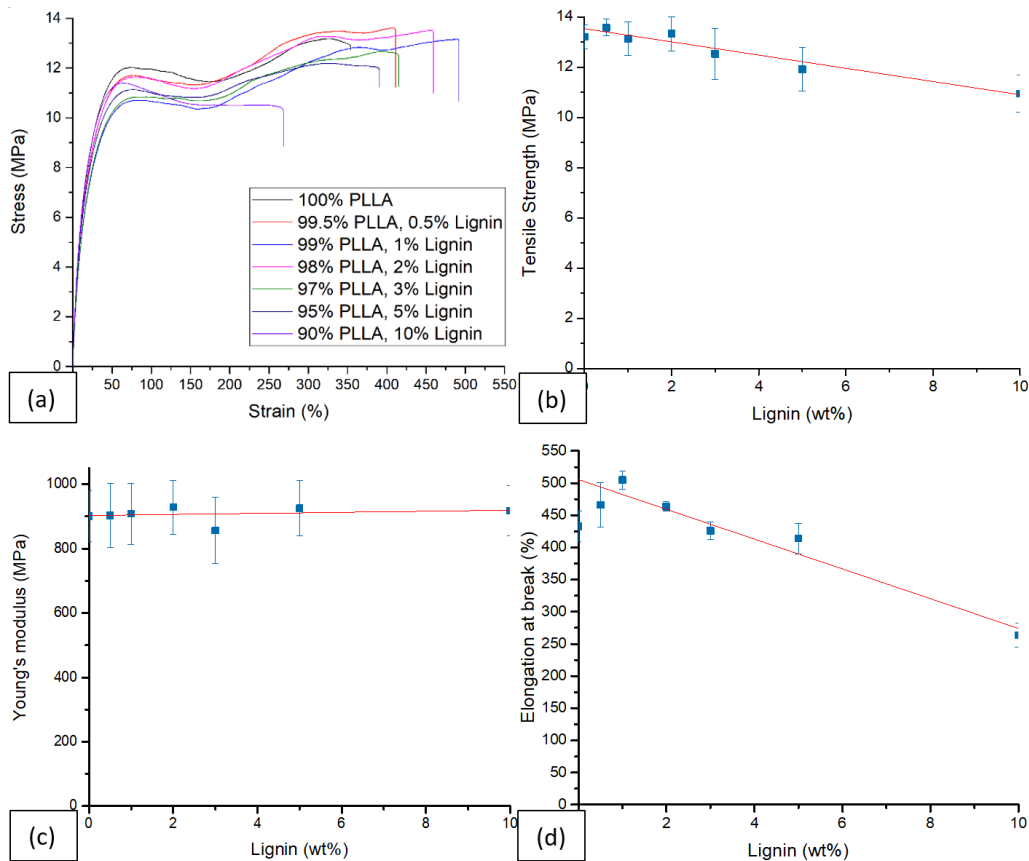

Figure 4.11. (a) Stress-strain curves of PLA/lignin composites and, variation in (b) tensile strength; (c) young's modulus and (d) elongation with percentage lignin content

Tensile testing using the same parameters were repeated for the plasticized PLA/lignin composites and again the ultimate tensile strength (MPa), young's modulus (MPa) and elongation at break (%) determined to study the effect of triacetin addition on the mechanical properties of the PLA. For each composite, 5 – 6 dog bone shaped specimens were also used during the tests and their average results are shown in Table 4.5 and Figure 4.11(a) which can be seen that all curves of the plasticized composites look very different from their brittle non-plasticized counterparts (Figure 4.13a).

Table 4.5. Tensile strength, young's modulus, elongation at break and their standard deviations of plasticized PLA/lignin

Composition	UTS (MPa)	YM (MPa)	EB (%)
Neat PLA	13.20 ± 0.48	900.78 ± 79.14	432.76 ± 23.62
PLA/lignin (99.5/0.5)	13.57 ± 0.33	903.04 ± 98.42	466.16 ± 34.91
PLA/lignin (99/1)	13.13 ± 0.67	908.20 ± 94.81	504.79 ± 13.71
PLA/lignin (98/2)	13.33 ± 0.68	928.13 ± 84.25	463.56 ± 7.39
PLA/lignin (97/3)	12.53 ± 1.02	856.02 ± 103.02	425.75 ± 13.82
PLA/lignin (95/5)	11.91 ± 0.86	925.14 ± 85.73	413.92 ± 23.71
PLA/lignin (90/10)	10.94 ± 0.73	918.26 ± 79.50	263.43 ± 18.37

In terms of the ultimate tensile strengths, the values fluctuated in the range of 13.20 ± 0.48 to 13.33 ± 0.68 MPa when composition of lignin increased from 0 – 2 wt% lignin. When lignin content was further increased to 10 wt%, tensile strength decreased gradually to as low as 10.94 ± 0.73 MPa (Figure 4.11b). In comparison to the non-plasticized composites, it can be observed that incorporation of plasticizer led to reduction of ultimate tensile strengths by approximately 5 times. Similarly, tensile strengths of plasticized samples are also lowered than that of non-plasticized composites. The plasticized unfilled PLA had a YM of 900.78 ± 79.14 MPa which increased to 928.13 ± 84.25 MPa when composition of lignin increased to 2 wt%. When the lignin composition further increased to 3, 5 and 10 wt%, the value varied between 856.02 ± 103.02 to 918.27 ± 78.24 MPa (Figure 4.11c). The ANOVA statistical test was performed to analyse the differences among group means. The ANOVA results is shown below (Figure 4.12) and reported the p-value that is higher than 0.05 which indicated that statistically, these groups are considered to have equal variance.[403,404] Therefore, incorporation of lignin did not alter the Young modulus of plasticized PLA-based composites.
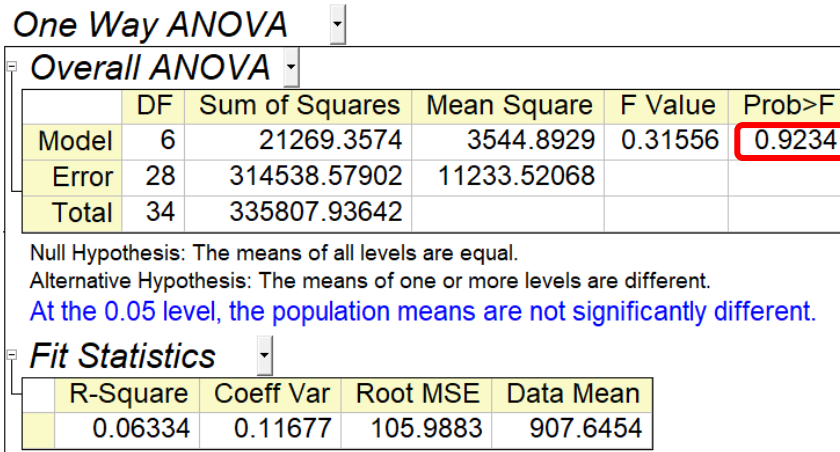
Figure 4.12. ANOVA results for UTS of non-plasticized PLA/lignin composites

In the comparison of the elongation at break, the plasticized composites increased from 432.76 ± 23.62 to 504.79 ± 13.71 % when lignin composition increased from 0 to 2 wt%. When lignin composition increased further, all values of elongation at break decreased to 263.43 ± 18.37 % (Figure 4.13d). Therefore, incorporation of plasticizer reduced the values of both tensile strength and Young's modulus but extended the elongation at breaks by more than 100 times. In addition, plasticized PLA/lignin are rubbery, flexible materials in contrast to the non-plasticized PLA/lignin that are brittle.

Figure 4.13. (a) Stress-strain curves of PLA/lignin composites and, variation in (b) tensile strength; (c) young's modulus and (d) elongation with percentage lignin content

FTIR was used to examine whether damage occurred due to the processing (melt-extrusion, injection moulding) as well to determine if there are interactions between PLA, lignin and triacetin as plasticizer amongst the composites. The repeat unit of PLA contains a carbonyl group which can give a strong C=O stretching band at 1750 – 1760 cm^{-1}. Although lignin also consists of absorption band in the same region, its influence on the PLA/lignin composites is too weak that it could be neglected.[212] In addition, both polymers consist of hydroxyl groups that should give O–H stretching bands in the region of 2800 – 3400 cm^{-1}. When J. Li. *et. al.* used FTIR to analyse composites of PLA and lignin, the absorption bands associated with lignin could not be seen when the lignin content was less than 20 wt%.[212] Therefore, any changes in these regions would be attributed directly to hydrogen bonding in carbonyl and hydroxy groups of PLA itself.[212] In comparison for the PLA/lignin FTIR spectra (Figure 4.14), they all consist of characteristic peaks at 1044 cm^{-1} (C-CH_3 vibration), 1082 cm^{-1} (C-O-C stretching), 1128 cm^{-1} (CH_3 rocking band), 1180 cm^{-1} (C-O-C vibration), 1750 cm^{-1} (C=O vibration) that are correspond to PLA.[389] As all composites consist of less than 20 wt% lignin content, intermolecular bonds correspond to lignin cannot be observed using FTIR which is also consistent with the results reported by J. Li *et. al.*[212]
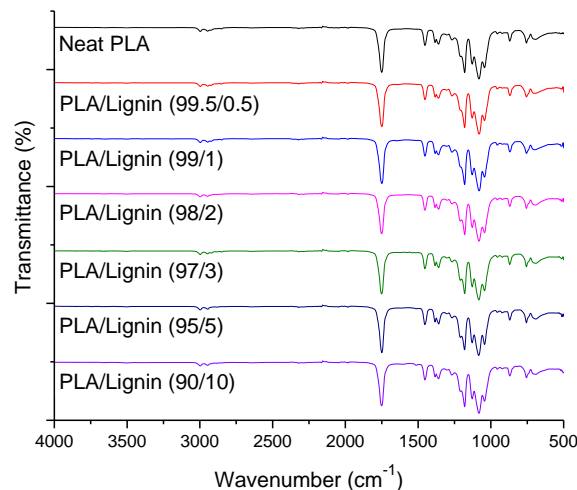
Figure 4.14. FTIR spectra of composite of PLA and lignin

FTIR spectra were also recorded for the plasticized PLA/lignin composites. Similarly, IR absorption bands attributed to lignin cannot be seen in the spectra (Figure 4.15). With addition of plasticizer, some of the IR bands shifted slightly especially the C=O band at 1750 cm^{-1} which was shifted to 1747 cm^{-1}. This could indicate that the C=O bonds were weakened due to the incorporation of plasticizer. Overall, all plasticized samples consist of characteristic peaks at 1043 cm^{-1} (C-CH_3 vibration) 1080 cm^{-1} (C-O-C stretching),

1129 cm^{-1} (CH$_3$ rocking band), 1181 cm^{-1} (C-O-C vibration), 1747 cm^{-1} (C=O vibration).[389]
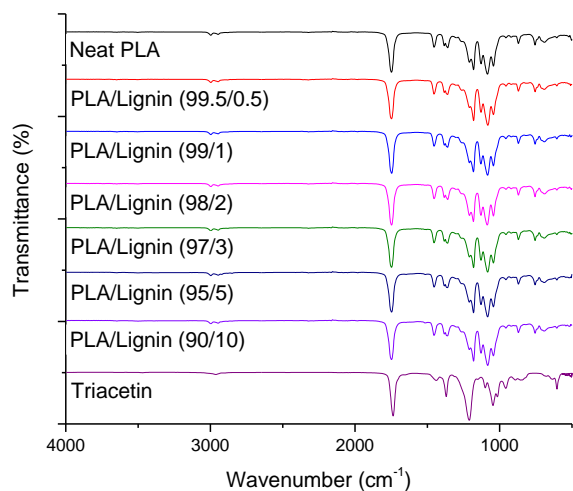
Figure 4.15. FTIR spectra of composites of triacetin plasticized PLA and lignin

4.2 Antimicrobial Behaviour of Composites of PLA and Lignin (Bioassay Study)

As it was reported that lignin exhibits antimicrobial property,[208] bioassays utilising a small selection of microbes on the composites were performed. The microbes were firstly tested on neat lignin to confirm antimicrobial activity. Two *Escherichia coli* (*E. coli*) strains, two *Staphylococcus aureus* (*S. aureus*) strains, one *Candida* strain and three *Pseudomonas* strains were tested using the Kirby-Bauer disk diffusion method. This disk diffusion method can provide qualitative results so as to categorise antimicrobial susceptibility as resistant, intermediate or sensitive/susceptible.[405] Ideally, mathematical curves or algorithms are required for such categorisation or determination of MIC.[406,407] Pure lignin discs were sterilised with UV light ($\lambda = 254$ nm) and placed on agar gels that were swabbed with microbes. After incubation at 37 °C for overnight, inhibition zones can be seen in the medium that contained *S. aureus* (USA 300 Lac 200 JE2, MRSA) and *S. aureus* (Newman, MSSA). This procedure was repeated 2 times on 2 different days to confirm the results. The lignin discs incubated on *MRSA JE2* had an average diameter of 8.38 mm and an average inhibition zone of 11.03 ± 0.56 mm (Figure 4.16a). Lignin discs with average diameters of 8.03 mm were used and the inhibition zone on *MSSA Newman* had an average diameter of 11.18 ± 0.22 mm (Figure 4.16b). Although the inhibition zones are small, they indeed indicate that lignin can inhibit the growth of both *MRSA JE2* and *MSSA Newman*.
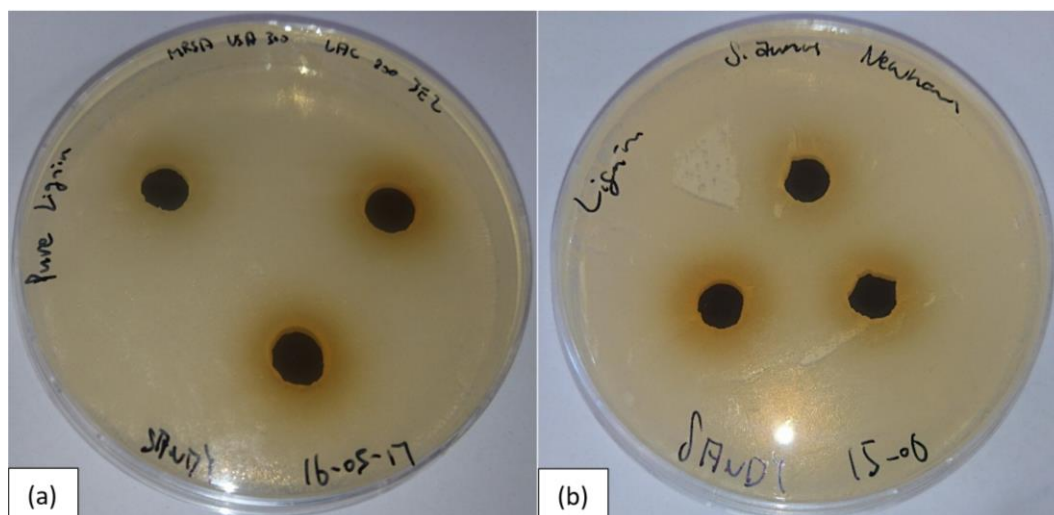
Figure 4.16. Pure lignin discs on incubated (a) *MRSA JE2* and (b) *MSSA Newman*

As neat lignin successfully inhibited the growth of both *S. aureus* strains and hence, the composites of PLA and lignin were further tested. As the inhibition zones induced by pure lignin are small, more precise and quantitative methods were used to assess antimicrobial properties. Firstly, growth curves were obtained using an automatic plate reader. A multi-well plate was used with non-plasticized and plasticized PLA/lignin composite films placed against the walls of some of the wells. As shown in Figure 4.17, 3 wells were the controlled broth that didn't contain any composite materials. 3 wells contained neat PLA film, 3 wells contained plasticized neat PLA film, 3 wells contained 90wt% PLA/ 10wt% lignin film and 3 wells contained plasticized 90wt% PLA/ 10%wt lignin film. The remaining wells were finally filled with pure broth without any bacteria and composites as the blank references. The multi-well plate was shaken continuously in the reader at 37 °C overnight and the optical density (OD, $\lambda = 600$ nm) of each well was recorded every 5 minutes so as to obtain the growth curves. This procedure was repeated on 2 different days in order to get triplicate data.
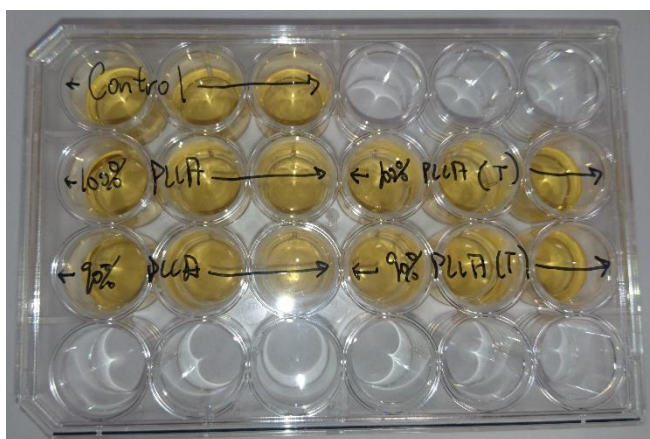
Figure 4.17. Photograph of the multi-well plate with 3 control wells and wells that contained non-plasticized and plasticized composites placed against the wall of the wells.

Growth curves for *MRSA JE2* are shown in Figure 4.18 (a) and it can be seen that *MRSA JE2* grew at the same rate in the control wells and in those that contained non-plasticized PLA and non-plasticized 90wt% PLA/10wt% lignin samples. When incubation was increased further, the curves deviated and interestingly the curves corresponding to both non-plasticized samples had slightly higher optical densities at the end. In contrast, plasticized PLA and plasticized composites of PLA and 10wt% lignin slightly suppressed the growth of *MRSA JE2*. The curves had lower optical densities throughout the incubation especially for the plasticized composite containing lignin. When the incubation time exceeded 600 mins., both curves plateaued instead of continuing to increase upwards. The growth curves for *MSSA Newman* are shown in Figure 4.18 (b) and it is obvious that the plasticized composite with 10 wt% lignin could slightly suppress growth throughout the whole incubation period. This is because the curve deviated from other curves and often consisted of lower optical densities compared to other samples. Although it seems that other composites had slightly lower optical densities compared to the control curve after an incubation time of 500 mins., the effects were very small and insignificant compared to that of the plasticized PLA/10wt% lignin composite.
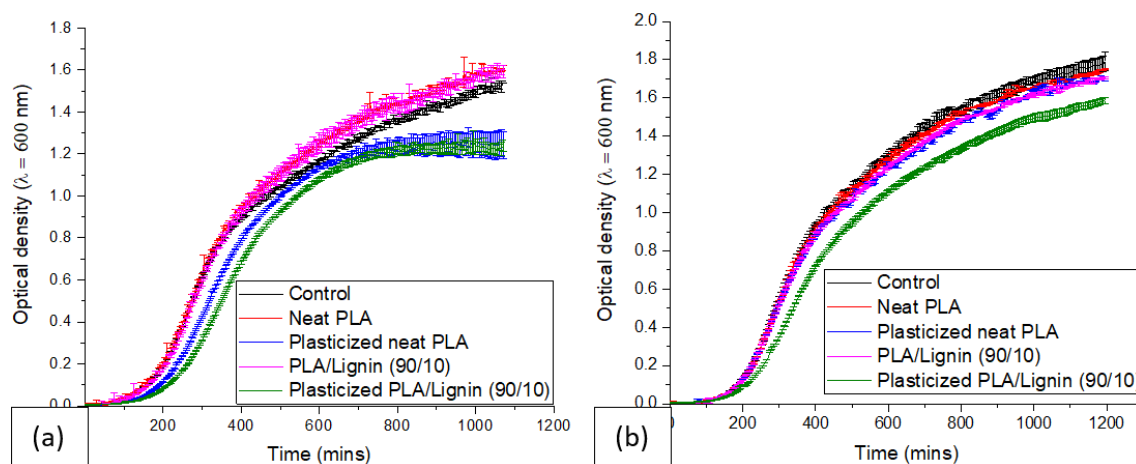
Figure 4.18. Growth curves of (a) *MRSA JE2* and (b) *MSSA Newman* in the presence of neat PLA and 90wt% PLA/ 10wt% lignin films

These growth curves indicate that some composites of PLA and lignin can affect the growth of bacteria although the effect seems to be very small. In comparison, for the growth curves for *MRSA JE2*, both plasticized samples (PLA itself, 10 wt% lignin) can slightly suppress the growth especially the composite containing lignin. In comparing the growth curves for *MSSA Newman*, it is quite obvious that the plasticized composite with

10wt% lignin can suppress the bacteria growth although the effect is not hugely significant. Hence, further experiments were conducted to confirm the effect.

The last experiment provided insight with regard to how the bacteria grow in the presence of the composites within the broth. The next experiment aimed to observe whether the bacteria can growth on the surface of the composites. Similarly, non-plasticized PLA and the composite with 10 wt% lignin and the plasticized equivalents were used to compare the effect of lignin and plasticizer addition to the PLA matrix on antimicrobial properties. In the multi-well plate, each sample was placed in 3 different wells along with 3 wells which contained no samples as the control. Unlike the previous experiment, all composites were placed at the bottom of the wells and the automatic plate reader was not used for this experiment. Instead, the plate was placed in an incubator (37 °C, overnight) without shaking to allow the formation of biofilm on the composites. After several washings with phosphate-buffered saline (PBS) solution the biofilm formed was allowed to dry. Finally, crystal violet was used to stain (Figure 4.19) the biofilm and the values of OD ($\lambda = 570$ nm) were recorded to compare the formation of biofilm on the composites. This whole procedure was repeated 3 times on 3 different days to get multiple data.

Figure 4.19. Photograph of a multi-well plate with stained biofilm on the composite materials.

The values of OD ($\lambda = 570$ nm) were recorded and the reduction of biofilm calculated via $\frac{OD_{Control} - OD_{Sample}}{OD_{Control}} \times 100\%$ which are listed in Table 4.6. Comparing biofilm formation of *MRSA JE2*, non-plasticized PLA reduced biofilm formation by 11.82% and its plasticized counterpart performed slightly worse as it reduced biofilm formation by 9.45%. The non-plasticized composite with 10wt% lignin reduced biofilm formation by 13.25% but when the plasticizer was incorporated into the composite, biofilm reduction was improved to 46.42%. In the comparison of *MSSA Newman* biofilm formation, non-

plasticized PLA reduced biofilm formation by 11.83%, but when the plasticizer was incorporated into the composite, biofilm formation reduced further to 58.63%. For composites that contained 10wt% lignin, the non-plasticized sample reduced biofilm formation by 17.15% but the plasticized sample reduced biofilm formation by 64.59%. Hence, biofilm formation of *MRSA JE2* can be reduced more effectively when the composite contained both plasticizer and lignin. In contrast, biofilm formation of *MSSA Newman* can be reduced when composites contained plasticizer and the performance could be further improved with addition of lignin. Indeed, biofilm formation can vary depend on the bacteria species. This set of results can indicate that biofilm formation was definitely reduced when PLA-based composites contain both plasticizer as well as lignin.

Table 4.6. Values of OD ($\lambda = 570$ nm) and reduction of biofilm formation on different composites

Composite	MRSA JE2		MSSA Newman	
	OD ($\lambda = 570$ nm)	Reduction of biofilm formation	OD ($\lambda = 570$ nm)	Reduction of biofilm formation
Control	0.60 ± 0.30	-	0.48 ± 0.21	-
Neat PLA	0.53 ± 0.27	11.82%	0.42 ± 0.11	11.83%
Neat plasticized PLA	0.55 ± 0.11	9.45%	0.20 ± 0.13	58.63%
PLA/Lignin (90/10)	0.52 ± 0.15	13.25%	0.40 ± 0.07	17.15%
Plasticized PLA/Lignin (90/10)	0.32 ± 0.05	46.42%	0.17 ± 0.10	64.59%

Although future studies are required to further confirm the antimicrobial effect of composites of PLA/lignin, this study has shown that lignin as a phenolic biopolymer can indeed inhibit the growth of two *S. aureus* strains. It was confirmed that PLA composites incorporated with 10 wt% lignin could reduce biofilm formation of up to 17%. More importantly, the antibiofilm effect was improved if the composites were plasticized with triacetin. This clearly shows that the incorporation of plasticizer can enhance the antimicrobial effect of lignin in the PLA composites.

Chapter 5.
Composites of PLA and Chitin

5. Composites of PLA/chitin

As mentioned in Chapter 2, research has shown that chitin can exhibit bactericidal efficacy against *MRSA* strains, *E. coli*, *Vibrio cholera*, *Shigella dysenteriae* and *Bacteroides fragilis*.[237] Hence, it was explored as a filler for PLA with the target of transferring antimicrobial properties to PLA-based composites with 0, 0.5, 1, 2, 3, 5 and 10 wt% chitin prepared via melt-extrusion. From a rheology perspective in is known to be difficult to melt mix polymers and chitin and related materials (e.g. chitosan) therefore, another batch plasticized PLA-chitin blends with the same composition range were prepared using triacetin as a 20 wt% plasticiser. In this chapter, the preparation and characterisation of both sets of composites (PLA/chitin) and plasticized (PLA/chitin) are described. The first aim of this work was to determine the influence of chitin on the properties of PLA. Second, was to determine the change in composite properties on the incorporation of plasticizer with a particular emphasis on mechanical properties and antimicrobial activity.

5.1. General characterisations of PLA/chitin composites

Melt extrusion or melt compounding was used to prepare PLA/chitin composites but it is always a concern that the dispersion of chitin is likely to be poor due to its high surface area and hydrogen bonding which leads aggregation.[408] In addition, compatibility between the two polymers is poor as PLA is hydrophobic and chitin is relatively hydrophilic.[408,409] Therefore, effective dispersion and distribution of chitin in the PLA matrix can be challenging. SEM imaging was employed to check whether the plasticizer can act as a dispersing aid in these composites.

PLA/chitin in dog bone shaped specimens were prepared from extrudate using a mini-injection moulding machine. After the completion of the tensile tests, fractured specimens were taken and coated with gold prior to examination in the SEM. By way of example, the SEM images of composites with the lowest and highest chitin loadings are shown and compared. Generally, chitin particles can exist in irregular or rod shapes and have sizes on the micro-scale.[410] In figure 5.1(a,b), SEM images of PLA-composites contained 0.5 wt% chitin are shown. As the chitin content was only 0.5 wt%, chitin particles are not easily found and the fracture surface appears to be smooth and mostly even. Overall, there are very few rod shape granules of lengths of 1 – 1.2 μm (red circles in Figure 5.2.1a,b). In contrast, the fracture surface of composite contained 10 wt% chitin appears to be more

rough and uneven. In addition, larger rod-shaped clusters with length 1.8 – 2 μm can be seen (red circles, Figure 5.1c,d).
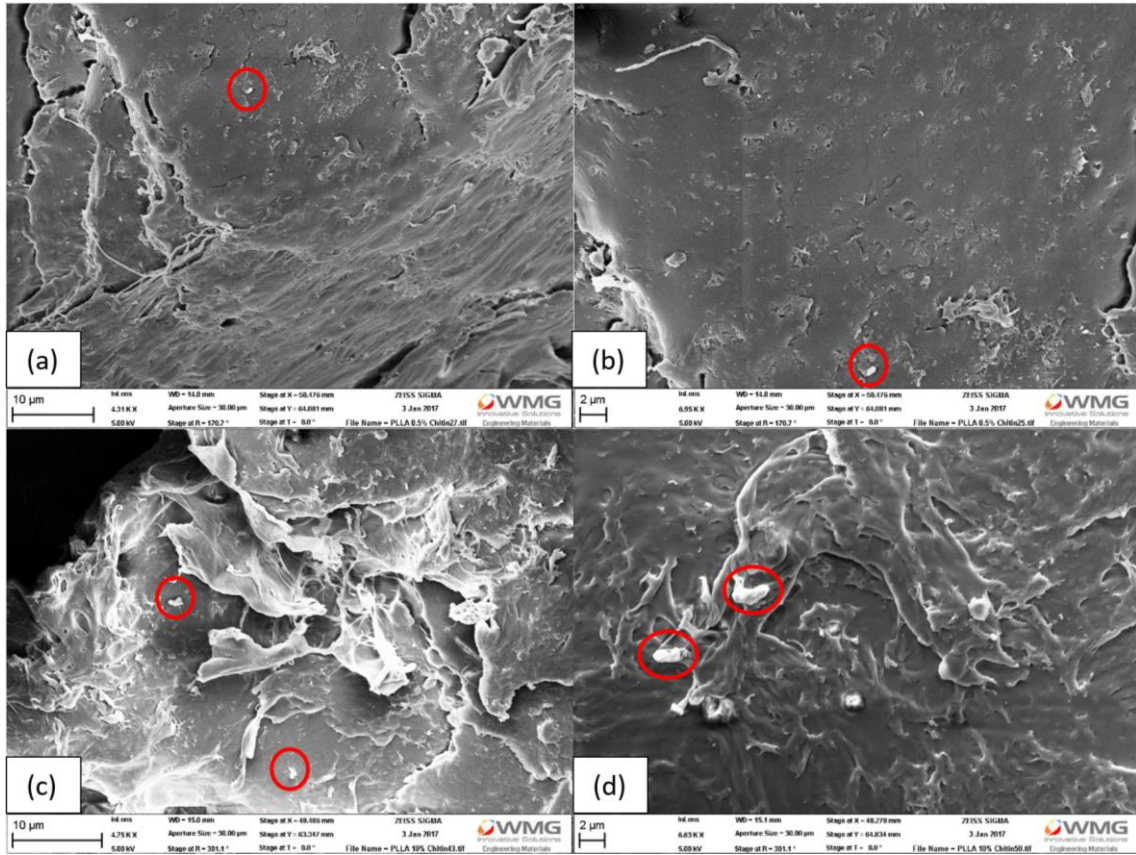
Figure 5.1. SEM images of (a) and (b) PLA with 0.5 wt% chitin and, (c) and (d) PLA with 10 wt% chitin

The same specimen procedure for SEM was repeated for the plasticized PLA/chitin composites. The plasticized composites with 0.5 wt% chitin and 10 wt% chitin are shown in Figure 5.2 (a,b). The fracture surface of the composite with lower chitin content is very smooth and some granules with diameters of 300 nm – 500 nm can be observed. In the comparison from the SEM images for the plasticized composite with 10 wt% chitin, the fracture surface appears to be smoother compared to the non-plasticized sample. Granules and clusters with diameters in the range of 800 nm – 2 μm can be seen (Figure 5.2c,d). Overall, plasticized composites consist of fracture surfaces that are smoother even when the chitin loading is 10 wt%. In addition, most of the chitin particles were reduced in size. This could suggest that the plasticizer fills the void volume between the PLA and chitin as well as improving the level of chitin dispersion and reducing chitin aggregation.
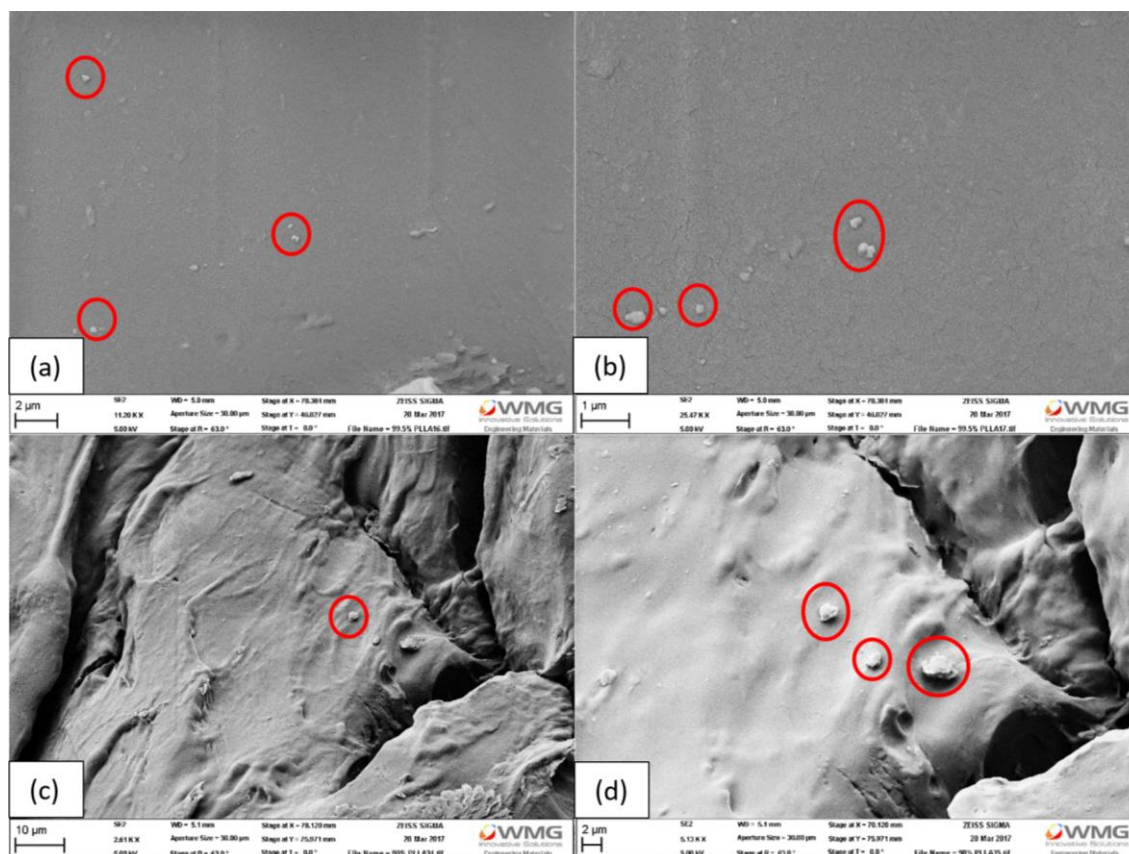
Figure 5.2. SEM images of plasticized (a), (b) PLA with 0.5 wt% chitin; (c), (d) PLA with 10 wt% chitin

DSC measurements were performed to determine the effect of chitin addition on the thermal properties of PLA, including T_g, cold crystallisation temperature (T_{cc}), melting temperature (T_m) and the crystalline content (X_c). Chitin also has a glass transition temperature or melting behaviour[411] but its DSC curve consists only of a wide but weak endothermic peak between 50 – 140 °C caused by the evaporation of water molecules bound to the hydrophilic functional groups.[248] Hence, miscibility with polymers cannot be defined for polymer blends that consist of chitin, from DSC. The DSC data of PLA/chitin composites can be used to predict whether the intermolecular interactions between PLA and chitin could influence the values of T_g, T_{cc}, T_m and X_c of the PLA matrix. All DSC measurements were conducted by erasing the thermal histories of the composites via heating from 25 °C to 180 °C, isotherm for 4 minutes and then cooling back to 25 °C at a heating rate of 10 °C/min. This cycle was repeated to obtain the second heating (Figure 5.3) and cooling curves (Figure 5.4) and the relevant thermal parameters are tabulated and shown in Table 5.1.

Table 5.1. DSC data for PLA/chitin composites

Composite	T_g	T_{cc}	$T_{m,1}$	$T_{m,2}$	X_c
Neat PLA	60 °C	117 °C	147 °C	152 °C	1.68%
PLA/chitin (99.5/0.5)	60 °C	121 °C	149 °C	-	2.15%
PLA/chitin (99/1)	60 °C	117 °C	147 °C	153 °C	1.23%
PLA/chitin (98/2)	60 °C	118 °C	149 °C	-	2.21%
PLA/chitin (97/3)	60 °C	117 °C	147 °C	-	1.72%
PLA/chitin (95/5)	60 °C	119 °C	149 °C	-	1.27%
PLA/chitin (90/10)	60 °C	116 °C	146 °C	152 °C	2.45%

The T_g of pure PLA was recorded at 60 °C and it remained unchanged with the addition of chitin at loadings between 0.5 – 10 wt% chitin. Neat PLA had a cold crystallisation peak at 117 °C which increased to 121 °C when 0.5 wt% chitin was incorporated. Composites with 1 – 5 wt% chitin had T_{cc} values within 117 – 119 °C and composite with 10 wt% chitin had the lowest T_{cc} of 116 °C (Figure 5.3b). In the comparison the melting temperatures, T_m values were in the range 146 – 149 °C. Three composites (0, 1, 10 wt% chitin) consist of a second melting peak at 152 – 153 °C (Figure 5.3c) which may be attributed to melting of recrystallized crystals[389] or fusion of newly formed lamellae via melting-recrystallisation of primary thin lamellae.[284] The values of crystallinity were calculated using the formula, $X_c = \frac{\Delta H_m - \Delta H_{cc}}{\omega PLA \times \Delta H_m^0} \times 100\%$ (where ΔH_m stands for enthalpy of melting, ΔH_{cc} is enthalpy of cold crystallisation, $\omega PLLA$ is weight fraction of PLA and ΔH_m^0 is the melting enthalpy for a theoretically 100% crystalline PLA which reported to be 93.7 J/g).[389,392] PLA/chitin composites have values of X_c in the range of 1.23 – 2.45% and these low degrees of crystallinity are likely due to the slow crystallisation rate of PLA. Therefore, very few PLA crystals were formed, the composites being predominately amorphous under the most practical processing and moulding procedures.[393]
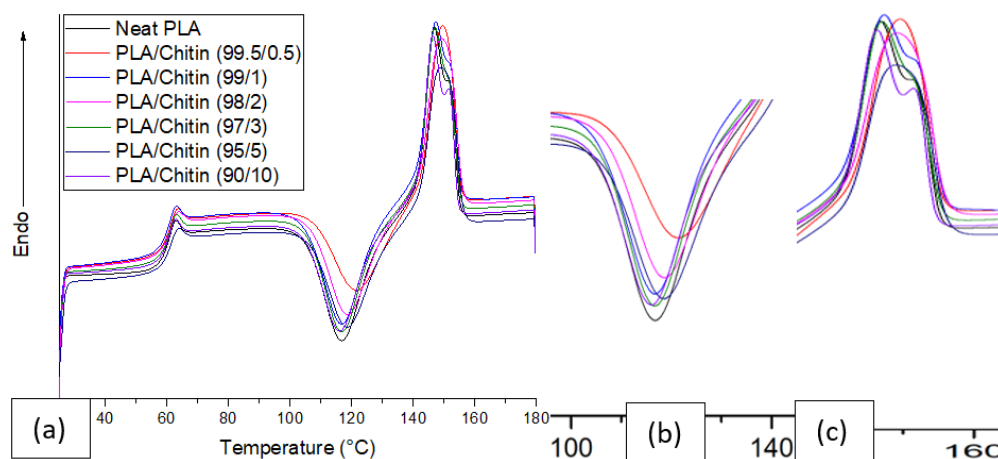
Figure 5.3. DSC (a) second heating curves, (b) cold crystallisation peaks & (c) melting peaks for PLA/chitin composites

The second cooling curves for the PLA/chitin composites are shown in Figure 5.4. As PLA undergoes very slow crystallisation[394] and so, only the glass transition process can be observed in all cooling curves of the PLA/chitin composites. Since the formation of the critical nucleus required for nucleation demands some time, slow crystallisation leads to the absence of crystal formation. As a result, crystallisation was prevented which led to all the PLA-based composites having nearly fully amorphous features with only glass transition steps recorded in their DSC cooling curves.[394]
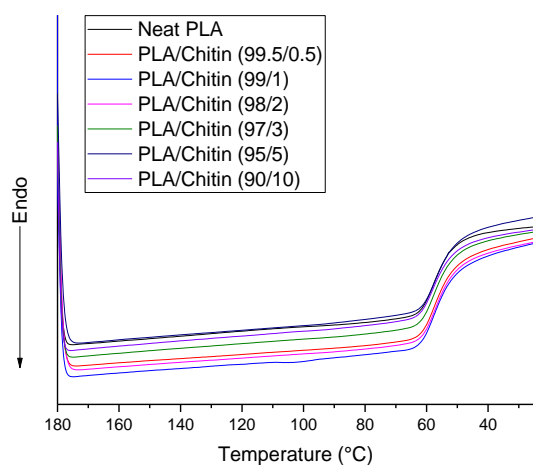
Figure 5.4. Second cooling curves of PLA/lignin composites

The DSC measurements were repeated with the plasticized (triacetin) PLA/chitin composites. The thermal histories of these plasticized composites were erased by heating the samples from -30 °C to 180 °C, isotherm for 4 minutes and then cooling back to -30 °C at a heating rate of 10 K/min. This cycle was repeated to obtain the second heating (Figure 5.6) and cooling curves (Figure 5.7) and the relevant results are listed in Table 5.2 on the next page.

Table 5.2. DSC data for plasticized PLA/chitin composites

Composition of plasticized composite	T_g	T_{cc}	T_m	X_c
Neat PLA	25 °C	94 °C	142 °C	2.03%
PLA/chitin (99.5/0.5)	23 °C	91 °C	142 °C	2.95%
PLA/chitin (99/1)	23 °C	79 °C	139 °C	5.01%
PLA/chitin (98/2)	27 °C	90 °C	141 °C	3.69%
PLA/chitin (97/3)	26 °C	89 °C	141 °C	4.08%
PLA/chitin (95/5)	23 °C	83 °C	138 °C	3.07%
PLA/chitin (90/10)	24 °C	83 °C	139 °C	4.67%

The T_g of plasticized PLA was recorded as 25 °C, 23 °C for (0.5, 1 wt% chitin), 27 °C for (2 wt% chitin), 26 °C for (3 wt% chitin), 23 °C for (5 wt% chitin) and 24 °C (10 wt% chitin), suggesting addition of chitin to plasticised PLA had little effect on the T_g of the polymer, allowing for instrument error (±5%). In comparison to the non-plasticized composites, the T_g values of the triacetin plasticized samples decreased by more than 50%. Plasticization results in an increase the free volume between polymer chains allowing them to move or rotate more freely. Plasticized materials often have lower T_g and melt viscosity compared to their non-plasticized counterparts.[395] Comparing the T_{cc} values, they are also lower than that for the non-plasticized composites. Plasticized pure PLA had the highest T_{cc} at 94 °C which decreased to 91 °C on addition of 0.5 wt% chitin and to 79 °C for 1 wt% chitin, but T_{cc} increased again to 90 °C (2 wt% chitin), 89 °C (3 wt% chitin) and 83 °C (5, 10 wt% chitin) with further increasing chitin content. The variation of T_{cc} values for plasticized samples is more significant and it was also noticed that some plasticized composites have broader cold crystallisation peaks (Figure 5.5b). This is likely to be due to the major changes in the phase separation behaviour as well as more diverse sizes of chitin particles in the polymer matrix.[396] Moreover, this variation may be associated with different levels of interaction between chitin and PLA as a consequence of different levels of chitin dispersion and distribution achieved during mixing. Compared to T_g and T_{cc}, T_m values of plasticized PLA/chitin did not decrease dramatically as all of them melted at close to 140 °C. Precisely, the plasticized samples

melted in the range of 138 – 142 °C, most probably within the error range of DSC. In addition, all blends consisted of only one melting peak which was slightly sharper than that for neat PLA (Figure 5.5c). This could indicate that are more well defined crystalline structure present in these plasticized composites.[412] Indeed, values of X_c increased for all plasticized samples, but it should be noted that this PLA has a very low crystalline content. Plasticized pure PLA had the lowest $X_c = 2.03\%$ and the plasticized composites were in the range 2.95 – 5.01%. Overall, incorporation of plasticizer into the PLA/chitin composites resulted in decreases of T_g, T_{cc} and T_m values but increase in X_c values which could indicate formation of more well defined crystalline structure in the composites.[412]
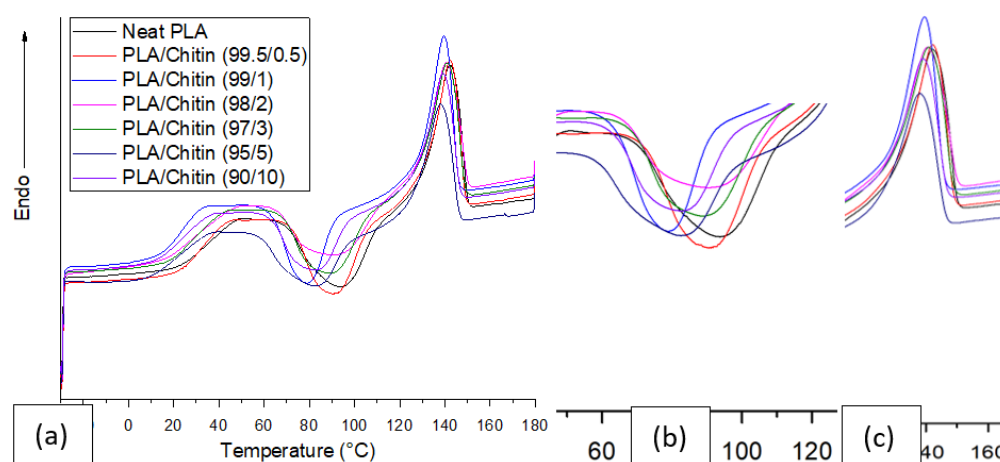
Figure 5.5. DSC (a) second heating curves, (b) cold crystallisation peaks and (c) melting peaks of plasticized PLA/lignin composites

The second cooling curves of plasticized PLA/chitin composites are shown in Figure 5.6a. As PLA crystallises slowly,[394] mostly glass transition steps can be seen in all the cooling curves of plasticized PLA/chitin composites. Crystallisation was prevented which led to all PLA-based composites having nearly fully amorphous features with only glass transition steps observed from the cooling curves.[394] Excluding the plasticized composite with 1 wt% chitin, its second cooling curve consists of a very small, weak endothermic peak within 60 – 85 °C (Figure 5.6b). As it has the highest X_c of 5.01%, it should be attributed to the cold crystallisation. Overall, incorporation of plasticizer to PLA/chitin composites reduces all values of PLA T_g, T_{cc} and T_m but having a bigger impact on the T_g as all T_g values were decreased by more than half. Moreover, the plasticizer can give a slightly more well defined crystalline structure to higher values of crystallinity.[412]
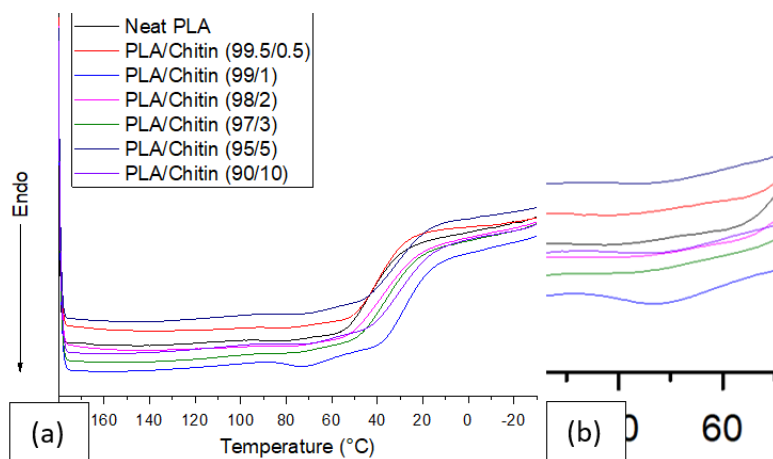
Figure 5.6. DSC second cooling curves of PLA/lignin composites

DMTA measurements were then conducted to gain insights into the dynamic mechanical properties of the composites and assess the effect the presence of chitin and plasticizer has on T_g. The tan δ curves and dynamic modulus as a function of temperature are shown in Figure 4.2.7. The maxima in the tan δ curves, by convention, is a measure of the T_g of the polymers. On the other hand, the change in the slope of the storage modulus curves indicates the transition from solid to rubber like behaviour which can also indicate the values of T_g.[398,399] All curves exhibited a sharp peak with maxima around 67 – 69 °C (Figure 5.7a, c). Composites with 0, 0.5, 1, 2 and 3 wt% chitin have sharp peaks at 67 °C and composites with 5 and 10 wt% chitin have sharp peaks at 68 and 69 °C respectively. Overall, the T_g values increase very slightly with increasing chitin content. Although, not expected the T_g values obtained from the tan δ curves are similar to those determined from DSC data.[399,413] According to this DMTA data, chitin as a filler did not significantly influence the dynamic mechanical properties of this PLA matrix.
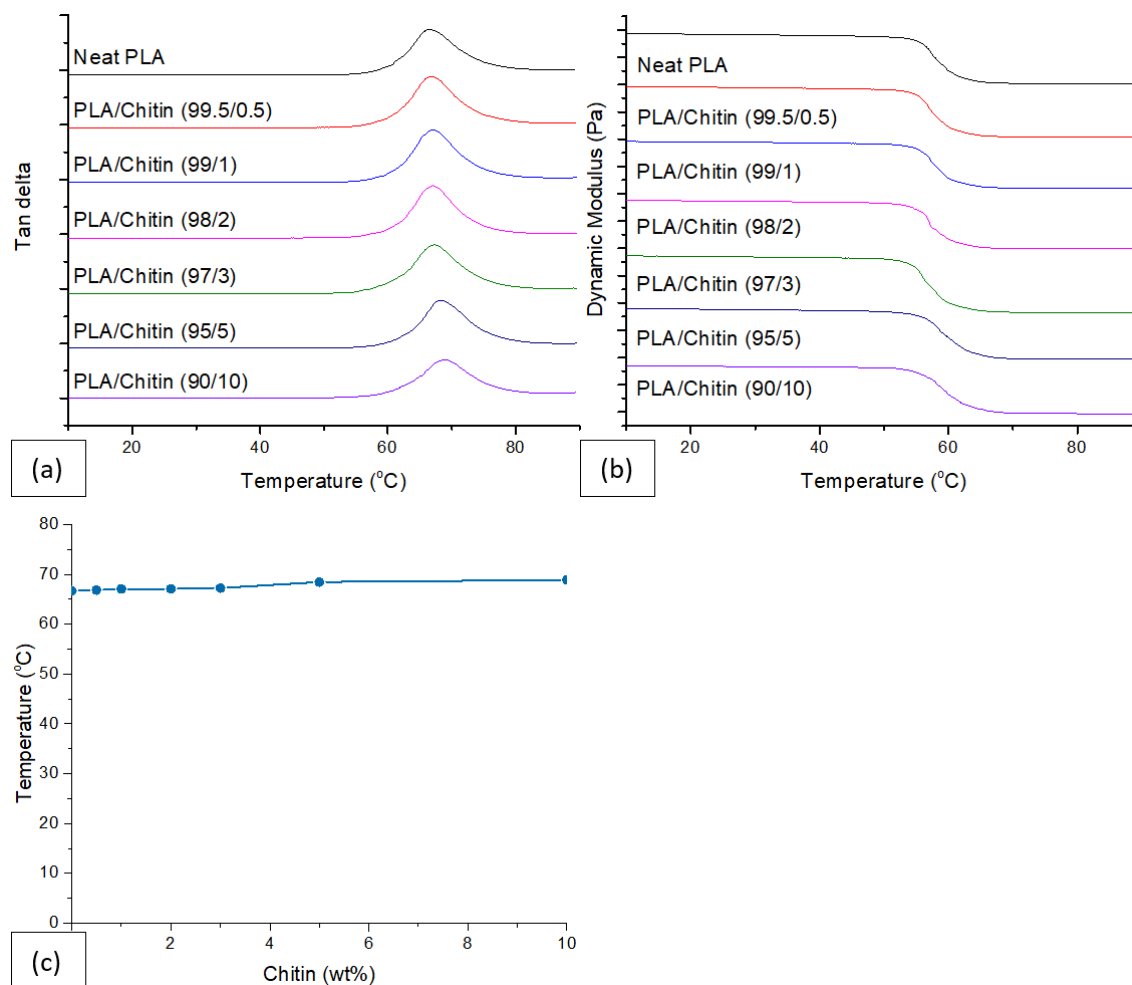
Figure 5.7. (a) Tan δ curves, (b) Storage modulus vs temperature of PLA/chitin composites; changes of T_g with % of chitin according to (c) tan δ curves obtained according to the tan δ peaks

The DMTA data for the plasticized PLA/chitin composites was also recorded. As the DSC data indicated that the T_g of the plasticised PLA sample was likely to be below 30 °C (see p.102 – 103), the DMTA measurements were started at -60 °C. Since plasticizer increases the free volume between polymer chains to allow more free movement and chain rotation,[395] slippage of samples occurred (as a consequence of sample contraction during cooling) during the DMTA experiments. In addition, all tan δ and dynamic modulus curves of the plasticized samples were contained noise at lower temperatures (Figure 5.8a, b). For the plasticised blends, plasticized PLA had the highest T_g value at 27 °C and plasticized composite with 5 wt% chitin had the lowest T_g at 18 °C. The rest of the plasticized samples had T_g's in the range 19 – 23 °C (Figure 5.8a, c). A trend line was drawn on Figure 5.8c which can be seen that overall the T_g values decreases with increasing chitin content. All T_g values for both non-plasticized and plasticized composites are listed in Table 5.3.
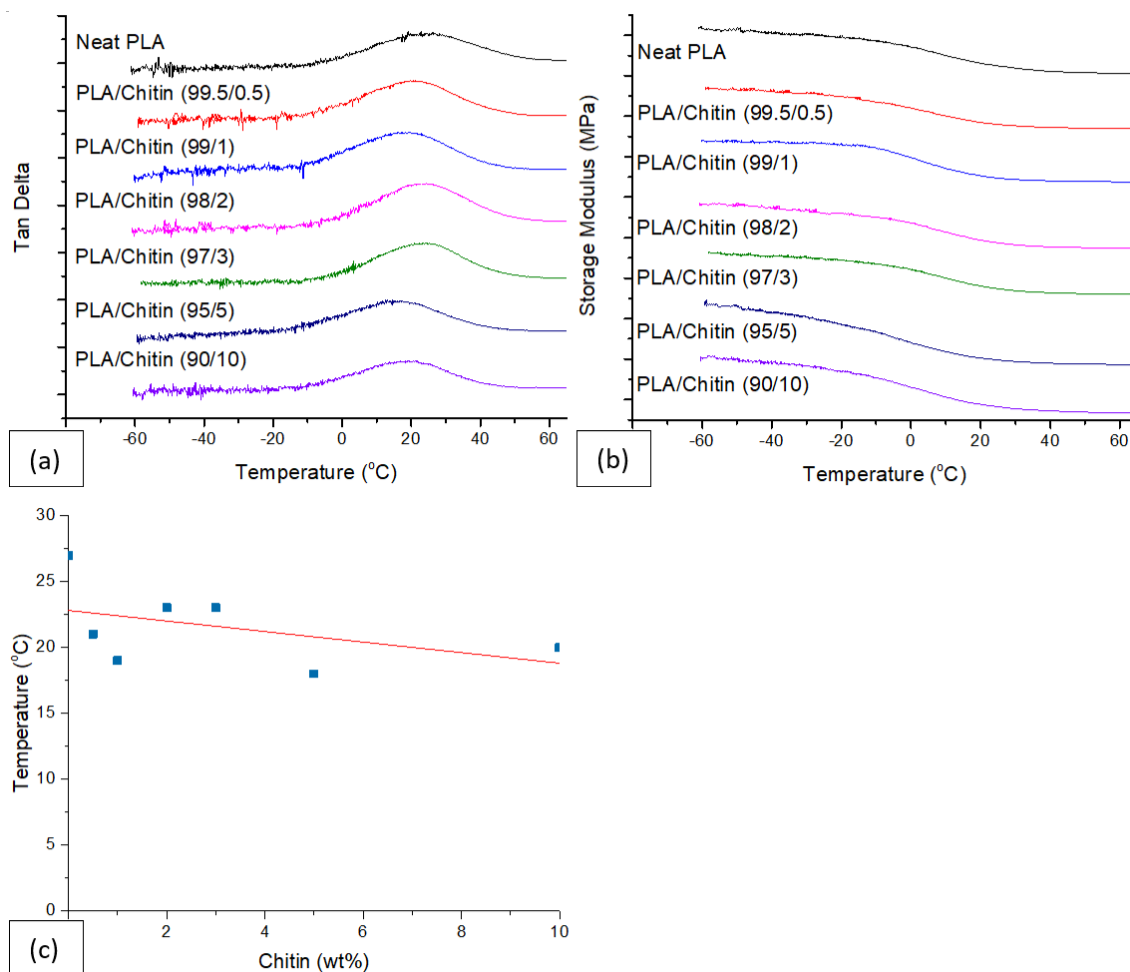
Figure 5.8. (a) Tan δ curves, (b) storage modulus vs temperature of plasticized PLLA/chitin composites; changes of T_g with % of chitin according to (c) tan δ curves obtained from the tan δ peaks

Table 5.3. T_g of all non-plasticized and plasticized PLA/chitin composites obtained from peaks of tan δ curves

Composite	Non-plasticized composites	Plasticized composites
	T_g / °C (tan δ)	T_g / °C (tan δ)
Neat PLA	67	27
PLA/chitin (99.5/0.5)	67	21
PLA/chitin (99/1)	67	19
PLA/chitin (98/2)	67	23
PLA/chitin (97/3)	67	23
PLA/chitin (95/5)	68	18
PLA/chitin (90/10)	69	20

Tensile tests were conducted to determine the ultimate tensile strength (MPa), Young's modulus (MPa) and elongation at break (%) of the PLA/chitin composites. For each composite with specific concentration (wt%) of chitin, 5 – 6 dog bone shaped specimens were tested and their average stress-strain curves are shown in Figure 5.11(a) which indicate that they are all brittle materials.[400] The changes of ultimate tensile strength, Young's modulus and elongation at break with increasing chitin content (wt%) are shown in Figure 5.9(b – d) with the relevant parameters listed in Table 5.4.

Table 5.4. Change in tensile strength, Young's modulus, elongation at break with standard deviations for composites of PLA and chitin

Composite	UTS (MPa)	YM (MPa)	EB (%)
Neat PLA	69.68 ± 1.26	2881.11 ± 117.18	3.49 ± 0.36
PLA/Chitin (99.5/0.5)	67.17 ± 2.08	2709.48 ± 119.91	3.46 ± 0.43
PLA/Chitin (99/1)	63.85 ± 1.12	2746.39 ± 106.48	2.89 ± 0.31
PLA/Chitin (98/2)	63.49 ± 1.87	2962.56 ± 25.83	2.72 ± 0.09
PLA/Chitin (97/3)	65.36 ± 2.22	2926.09 ± 78.65	2.73 ± 0.08
PLA/Chitin (95/5)	66.45 ± 1.67	2950.73 ± 69.62	2.80 ± 0.14
PLA/Chitin (90/10)	63.35 ± 1.54	3122.51 ± 127.66	2.47 ± 0.02

In the comparison of ultimate tensile strength values, the overall variation is small as their values varied in the range of 63.35 ± 1.54 – 69.68 ± 1.26 MPa only. Therefore, an ANOVA (Analysis of Variance) statistical test were performed to analyse the differences among group means. The ANOVA results is shown below (Figure 5.9) and reported the p-value that is smaller than 0.05 which indicated that statistically, at least two of the entire groups have significantly different means. In Figure 5.11b, a trend line was drawn on the ultimate tensile strengths vs chitin (wt%) graph to show a slight descending trend with increasing chitin content.

One Way ANOVA

Overall ANOVA

	DF	Sum of Squares	Mean Square	F Value	Prob>F
Model	6	138.02228	23.00371	7.50172	1.12798E-4
Error	25	76.66143	3.06646		
Total	31	214.68372			

Null Hypothesis: The means of all levels are equal.
Alternative Hypothesis: The means of one or more levels are different.
At the 0.05 level, the population means are significantly different.

Fit Statistics

R-Square	Coeff Var	Root MSE	Data Mean
0.64291	0.02669	1.75113	65.61719

Figure 5.9. ANOVA results for UTS of non-plasticized PLA/chitin composites

Similarly, ANOVA performed again when comparing the Young's moduli of the composites. Their values are in the range of 2709.48 ± 119.91 – 3122.51 ± 127.66 MPa and the ANOVA also reported the p-value that is less than 0.05 which indicated that statistically, at least two of the entire groups have significantly different means. A trend line was also drawn on the Young's modulus vs chitin (wt%) graph to show a slight ascending trend with increasing chitin content.

One Way ANOVA

Overall ANOVA

	DF	Sum of Squares	Mean Square	F Value	Prob>F
Model	6	552281.17536	92046.86256	9.63486	1.31309E-5
Error	26	248391.69214	9553.52662		
Total	32	800672.8675			

Null Hypothesis: The means of all levels are equal.
Alternative Hypothesis: The means of one or more levels are different.
At the 0.05 level, the population means are significantly different.

Fit Statistics

R-Square	Coeff Var	Root MSE	Data Mean
0.68977	0.03367	97.74214	2902.82697

Figure 5.10. ANOVA results for YM of non-plasticized PLA/chitin composites

In contrast, their elongation at breaks exhibited a more obvious descending trend and hence, the ANOVA was not performed. Neat PLA has the highest elongation at break at 3.49 ± 0.36 % but the value decreased to 2.72 ± 0.09 % when chitin content was increased to 2 wt%. Although the elongation at break increased slightly to 2.73 ± 0.08 and 2.80 ±

0.14 % when composite consisted of 3 and 5 wt% chitin respectively, it dropped to the lowest value at 2.47 ± 0.02 % when chitin was increased to 10 wt% (Figure 5.11d). Therefore, the overall trend for elongation at break also decrease with increasing chitin concentration.
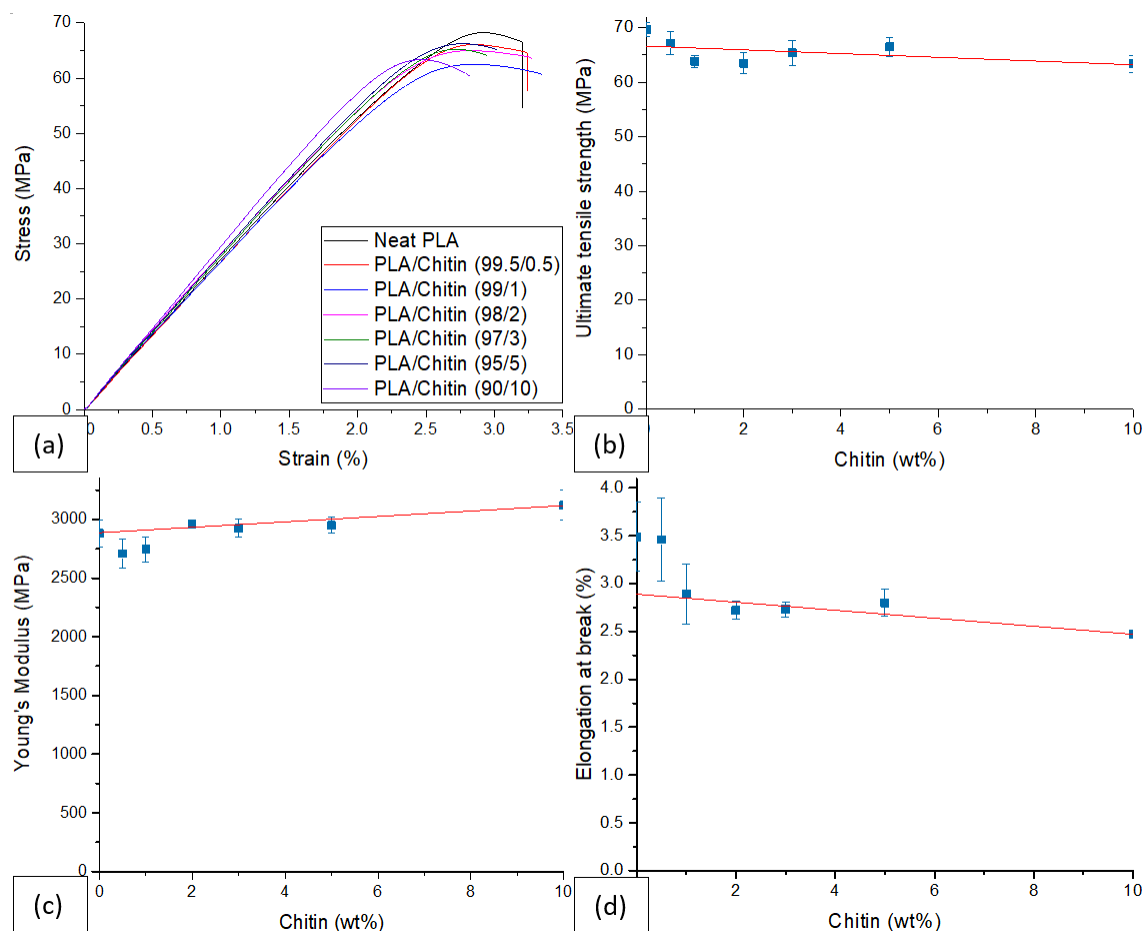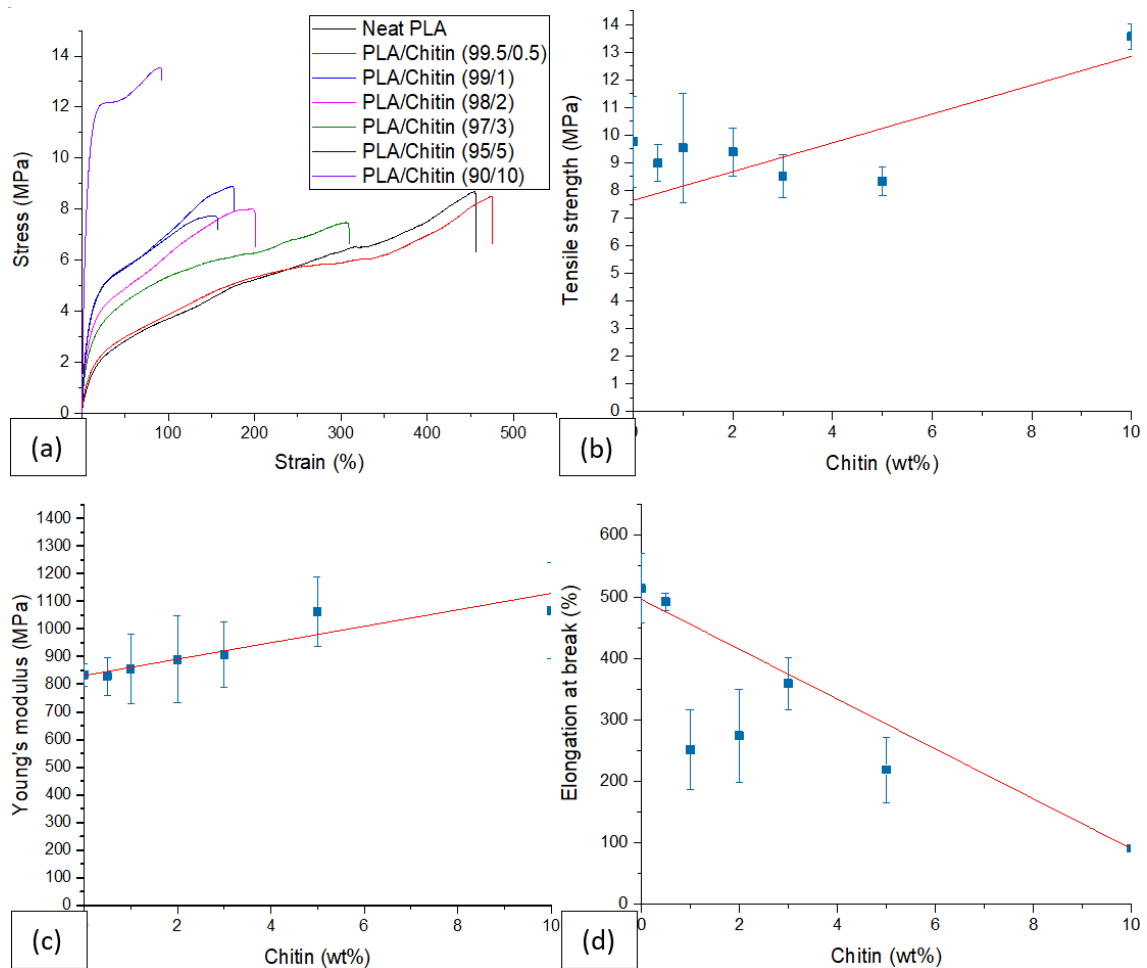

Figure 5.11. (a) Stress-strain curves for PLA/chitin composites and, the change in (b) tensile strength; (c) Young's modulus and (d) elongation with weight percentage chitin content

The mechanical tests were repeated for the plasticized PLA/chitin composites to determine their ultimate tensile strength (MPa), Young's modulus (MPa) and elongation at break (%). Compared to the non-plasticized composites (Figure 5.11a), stress-strain curves of the plasticized composites look very different which indicate that the composites are less brittle after plasticization. In comparison of ultimate tensile strengths, plasticized pure PLA had a value of 9.76 ± 1.63 MPa and this parameter decreased with the addition of chitin up to 5 wt% as plasticized composites with 0.5 – 5 wt% chitin consist of tensile strength in the range of 8.33 ± 0.53 – 9.54 ± 1.97 MPa. However, when chitin content was further increased to 10 wt%, the tensile strength increased to the highest at 13.58 ± 0.46 MPa (Figure 5.12b). In terms of Young's modulus, plasticized

samples with 0, 0.5 wt% chitin have similar value as the former is 834.59 ± 40.95 MPa and the latter is 829.46 ± 68.33 MPa. As chitin content further increased, the value of Young's modulus gradually increased to 1066.40 ± 174.51 MPa (10 wt% chitin) (Figure 5.12c). Finally, plasticized pure PLA has the highest elongation at break at 513.57 ± 56.71% which decreased to 251.96 ± 64.46% when chitin content increased to 1 wt%. Although this parameter increased again to 274.44 ± 75.28% and 359.07 ± 42.41% when plasticized composites incorporated with 2 and 3 wt% chitin respectively, it gradually decreased again to the lowest at 90.96 ± 2.98% when chitin concentration was further increased up to 10 wt%. Overall, incorporation of plasticizer had lowered the tensile strengths and Young's moduli but increased the values of elongation at break of the materials. Plasticization of the PLA/chitin composites resulted the materials to flexible and soft nature compared to the non-plasticized PLA/chitin composites that are rigid and brittle.

Figure 5.12. (a) Stress-strain curves of plasticized PLA/chitin composites, trends of (b) tensile strength; (c) Young's modulus and (d) elongation with percentage of chitin

Table 5.5. Tensile strength, Young's modulus, elongation at break and their standard deviations of 20 % plasticized PLLA/chitin

Plasticized composite	UTS (MPa)	YM (MPa)	EB (%)
Neat PLA	9.76 ± 1.63	834.59 ± 40.95	513.57 ± 56.71
PLA/Chitin (99.5/0.5)	8.99 ± 0.66	829.46 ± 68.33	491.95 ± 14.16
PLA/Chitin (99/1)	9.54 ± 1.97	855.63 ± 124.78	251.96 ± 64.46
PLA/Chitin (98/2)	9.39 ± 0.88	890.03 ± 158.06	274.44 ± 75.28
PLA/Chitin (97/3)	8.53 ± 0.77	907.02 ± 118.92	359.07 ± 42.41
PLA/Chitin (95/5)	8.33 ± 0.53	1061.91 ± 126.15	219.01 ± 53.27
PLA/Chitin (90/10)	13.58 ± 0.46	1066.40 ± 174.51	90.96 ± 2.98

FTIR was recorded to see whether there are new interactions between PLA matrix, chitin and plasticizer in the composites. In the FTIR spectrum of pure PLA, characteristic peaks at 1043 cm^{-1} (C-CH$_3$ vibration) 1081 cm^{-1} (C-O-C stretching), 1128 cm^{-1} (CH$_3$ rocking band), 1181 cm^{-1} (C-O-C vibration), 1749 cm^{-1} (C=O vibration) that corresponds to PLA are clearly observed.[389] However, no significant changes were observed when chitin was incorporated in PLA. Although chitin exhibits strong bands at 1010 cm^{-1}, 1068 cm^{-1} (C-O-C/C-O stretching in cyclic ring), 1203 cm^{-1}, 1260 cm^{-1}, 1309 cm^{-1} (amide bond), 1621 cm^{-1}, 1652 cm^{-1} (C=O bond in amide group and broad peaks at 3260 cm^{-1}, 3426 cm^{-1} (-NH, -OH stretching),[414] their influence on the composite materials is too insignificant. Hence, significant changes of intermolecular bonds cannot be clearly observed in the FTIR spectra (Figure 5.13).
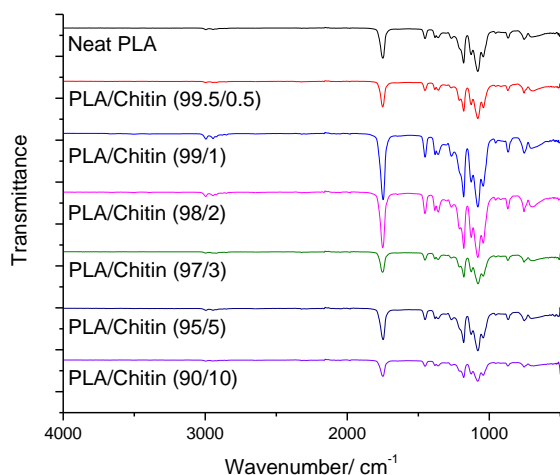
Figure 5.13. FTIR of PLA/chitin composites

The FTIR spectra for the plasticized PLA/chitin composites were also recorded. Similarly, IR absorption bands attributed to chitin cannot be seen in the spectra (Figure 5.14). With the addition of plasticizer, some of the IR bands shifted slightly especially the C=O band at 1750 – 1751 cm^{-1} was shifted to 1748 cm^{-1}. This could indicate that the C=O bonds were slightly weakened due to the incorporation of plasticizer. Overall, all plasticized samples consist of characteristic peaks at 1043 cm^{-1} (C-CH$_3$ vibration) 1081 cm^{-1} (C-O-C stretching), 1130 cm^{-1} (CH$_3$ rocking band), 1181 cm^{-1} (C-O-C vibration), 1748 cm^{-1} (C=O vibration).[389] In comparison to the non-plasticized composites, the changes are also very insignificant.
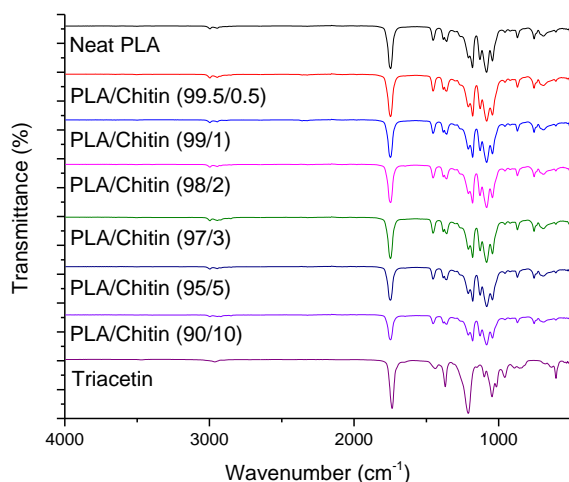
Figure 5.14. FTIR of plasticized PLA/chitin composites

5.2 Antimicrobial Behaviour of Composites of PLA/chitin (Bioassay study)

As report had shown that chitin can exhibit antimicrobial activity,[236] but bioassays with a small selection of microbes were conducted. These included two *Escherichia coli* (*E. coli*)

strains, two *Staphylococcus aureus* (*S. aureus*) strains, one *Candida* strain and three *Pseudomonas* strains. A screening test using the Kirby-Bauer disk diffusion method was performed with pure chitin discs to see whether any microbes are sensitive to chitin. Firstly, pure chitin discs were sterilised with UV light (λ = 254 nm) and placed on agar gels that were swabbed with microbes. Pure lignin discs were sterilised with UV light (λ = 254 nm) and placed on agar gels that were swabbed with microbes then incubated at 37 °C for overnight. However, inhibition zones were not clearly seen for any microbes.

According to the study conducted by Benhabiles *et al.*, chitin showed inhibitory growth activity against two *MRSA* strains (Gram +); *E. coli*, *Vibrio cholera*, *Shigella dysenteriae* and *Bacteroides fragilis* [Gram-(–)] and it was suggested that chitin could be bacteriostatic.[238] Therefore, some PLA/chitin composites were tested against two *E. coli* strains, *MRSA JE2* and *MSSA Newman* to check whether incorporation of chitin can influence the antimicrobial activity of PLA. Then, growth curves of these microbes were obtained in the presence of non-plasticized and plasticized PLA composites with the lowest (0 wt%) and highest (10 wt%) chitin loading.

All growth curves were obtained using automatic plate reader with stripes of non-plasticized and plasticized PLA/chitin films. In an 18-well plate, three wells had the control broth that did not contain any composite materials. Three wells contained 100% neat PLA films, three wells contained plasticized 100% PLA films, three wells contained 90% PLA/10wt% chitin films and three wells contained plasticized 90% PLA/ 10% chitin films. The remaining wells were filled with pure MH-broth without any bacteria and composites as the blank reference. The multi-well plate was shaken continuously in an automatic reader at 37 °C overnight and the optical density (OD, λ = 600 nm) of each well was recorded every 5 minutes so as to obtain the growth curves. This procedure was repeated on two (2) different days in order to get triplicate data.

Growth curves for *E. coli*. *K12* was firstly obtained on three different days. However, the patterns of the curves were very not consistent with each other. On the first attempt, the bacterial activity deviated after incubation of 200 minutes as the growth of the *K12* strain was clearly suppressed by the plasticized composite with 10 wt% chitin. Values of OD recorded in the presence of 100% PLA were higher than that of the plasticized composite with 10 wt% chitin but slightly lower than the control. The growth curve for plasticized 100% PLA displayed the same trend compared to the control. Although the growth curve of non-plasticized composite with 10 wt% chitin showed the same trend as the control until incubation of 500 minutes, values of OD became the highest (Figure 5.15a). On the

second attempt, the trend for all curves started to deviate after incubation of 250 minutes. It can also be seen that values of OD tend to be lower in the presence of plasticized composite with 10 wt% chitin addition. Growth curves for non-plasticized and plasticized PLA display very similar trends but their OD values are slightly lower than that of control after 600 minutes incubation. Growth curve for non-plasticized composite with 10 wt% chitin has higher values of OD after incubation of 250 minutes and even higher than that of control curve after incubation of 600 minutes (Figure 5.15b). On the third attempt, patterns of the curves are different from the first and second attempt. Both plasticized composite (0, 10 wt% chitin) have very similar trend throughout the incubation period as their curves slightly deviated after incubation of 250 minutes and clearly consist of lower OD values when the bacteria was incubated further. On the other hand, growth curves of the control and both non-plasticized composites (0, 10 wt% chitin) consist of the same trend as they all have higher OD values after incubation of 500 minutes (Figure 5.15c). Overall, trends are not consistent when comparing all attempts together and the only consistent phenomenon that can be seen is the bacterial growth was always slightly suppressed when the plasticized composite with 10 wt% chitin presented indicated by the lower OD values of the relevant curves at later incubation time in all attempts.
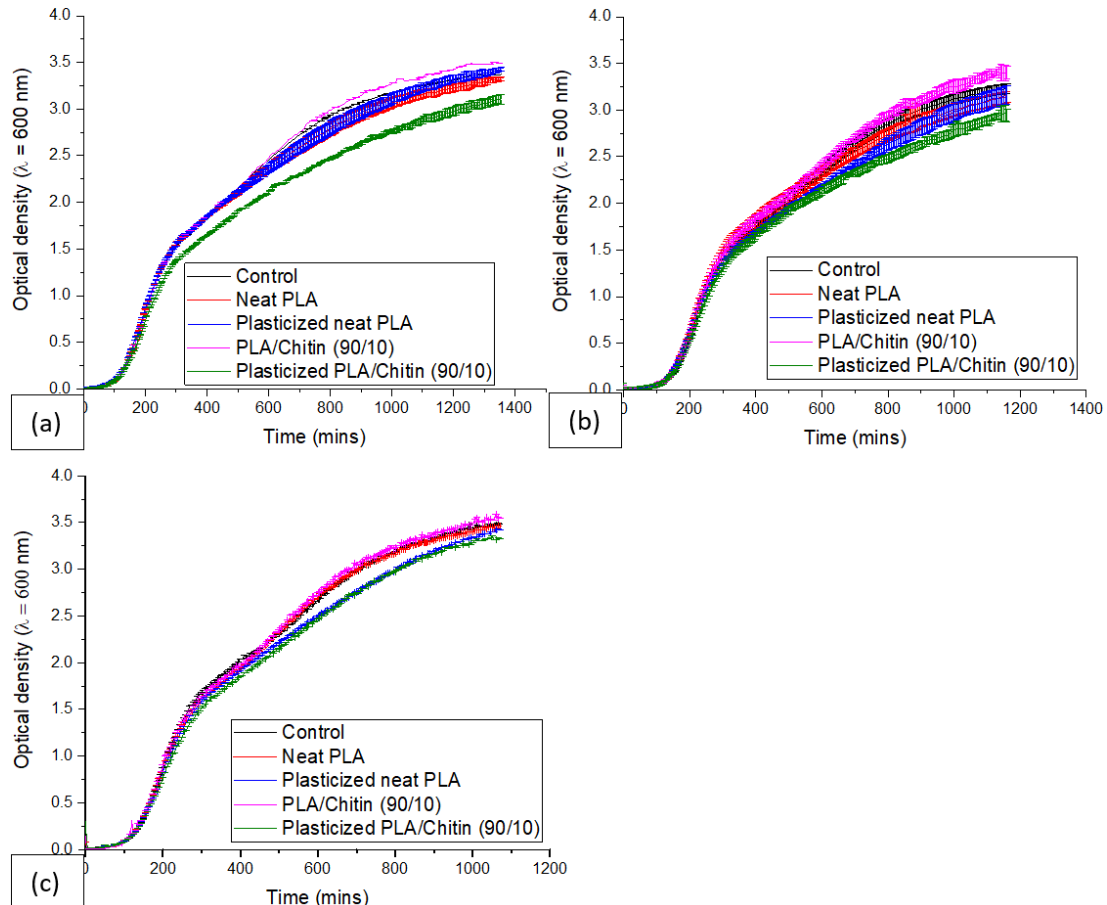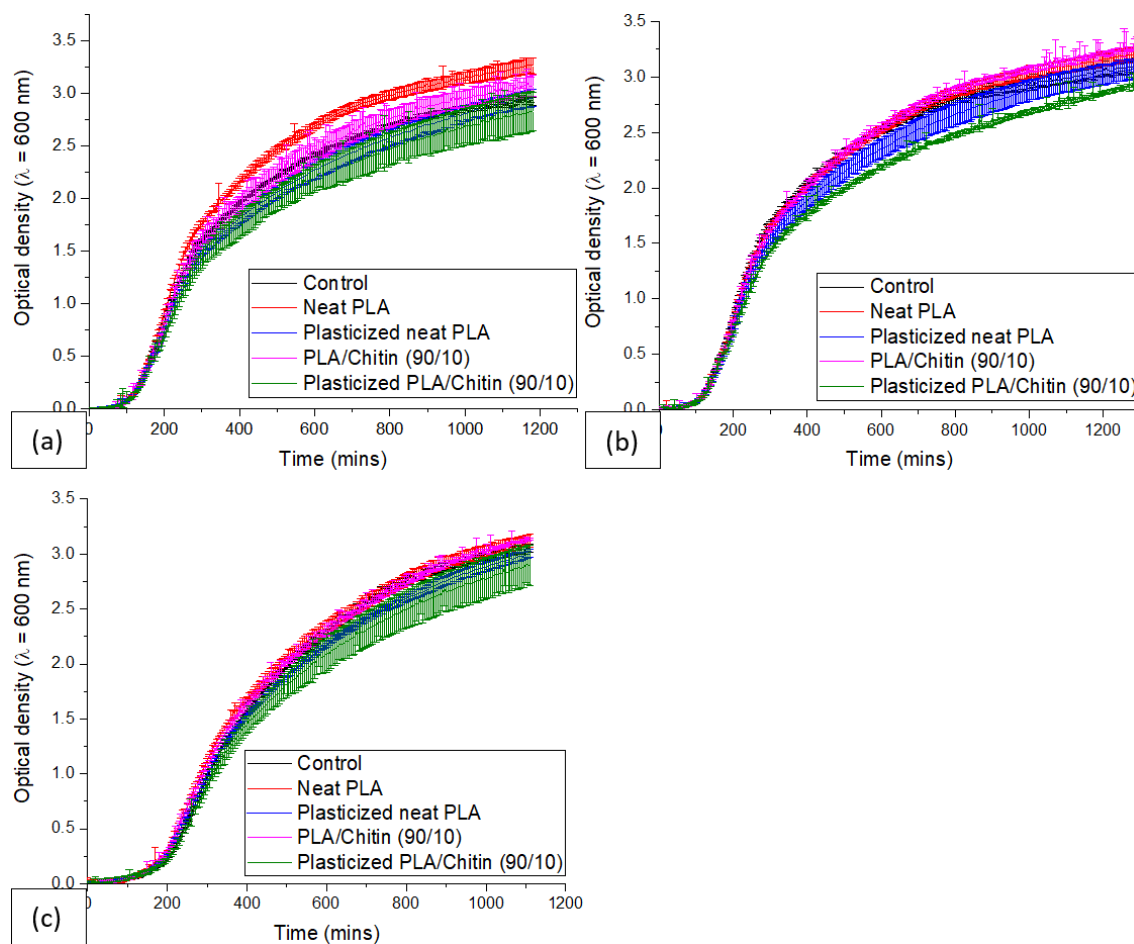

Figure 5.15. Growth curves for *E. coli. K12* in the presence of 100% PLA and 90 wt% PLA/ 10-wt% chitin films on the (a) first, (b) second and (c) third attempts

119

The growth curves for *E. coli Sakai* were also constructed with the same procedures and materials. The overall trends for all curves also seemed slightly inconsistent when comparing them in all attempts. On the first attempt, the curves started to deviate after incubation of 250 minutes which can be seen that both plasticized composites (0, 10 wt% chitin) have lower OD values. In the ascending order, the curves represent the control, non-plasticized composite with 10 wt% chitin and non-plasticized PLA have higher values of OD with increasing incubation time (Figure 5.16a). On the second attempt, curves deviated also after incubation of 250 minutes. In comparison to the first attempt, it is slightly more obvious that plasticized composite with 10% chitin can slightly suppressed the bacterial growth indicated by the slightly lower OD values at higher incubation time. Both curves for the control and plasticized PLA have very similar OD values during later incubation and whereas the both non-plasticized samples (0, 10 wt% chitin) have even higher OD values during higher incubation time (Figure 4.2.16b). On the third attempt, the difference between the curves became less distinguish. The curves deviated after incubation of 250 minutes which can be seen that both plasticized composites (0, 10% chitin) display very similar trends during longer incubation time. Whereas, the curves for the control as well as non-plasticized composites (0, 10 wt% chitin) show very similar trends, OD values with increasing incubation time (Figure 5.16c). Although growth curves for the plasticized composite with 10 wt% chitin tend to have slightly lower OD values at longer incubation time, the overlapping error bars in the first and third attempt (Figure 5.16a,c) make the deviation of the correspond growth curves become less distinctive. Hence, the effect of the plasticized composite with 10 wt% chitin towards bacterial growth is very minimal and negligible and it is inconclusive about whether it can inhibit the growth of *E. coli Sakai* until further additional experiments are completed.

Figure 5.16. Growth curves of *E. coli. Sakai* in the presence of 100% PLA and 90% PLA/ 10% chitin films on the (a) first, (b) second and (c) third attempt

Finally, growth curves for *MRSA JE2* and *MSSA Newman* were also constructed using the same procedures on three different days with same set of materials. Unlike the growth curves obtained for *E. coli. K12* and *Sakai*, the curves obtained display the same trends for all attempts. All the growth curves are shown in Figure 5.17(a) and it can be seen that all three curves have identical trends throughout the incubation period. This can clearly indicate that bacterial growth was not affected by the presence of any of the composite materials. When constructing the growth curves for *MSSA Newman*, trends were also consistent for the different attempts. All curves consist of the same trend until an incubation time of 350 minutes as the curve represents plasticized composite with 10 wt% chitin deviated and has a slightly lower OD values at higher incubation time. The other growth curves correspond to the control and rest of the samples consist of the same trend but slightly higher OD values with increasing incubation time (Figure 5.17b). Although it seems that plasticized composite with 10wt% chitin can slightly suppress the growth of *MSSA Newman*, the effect is indeed very insignificant.
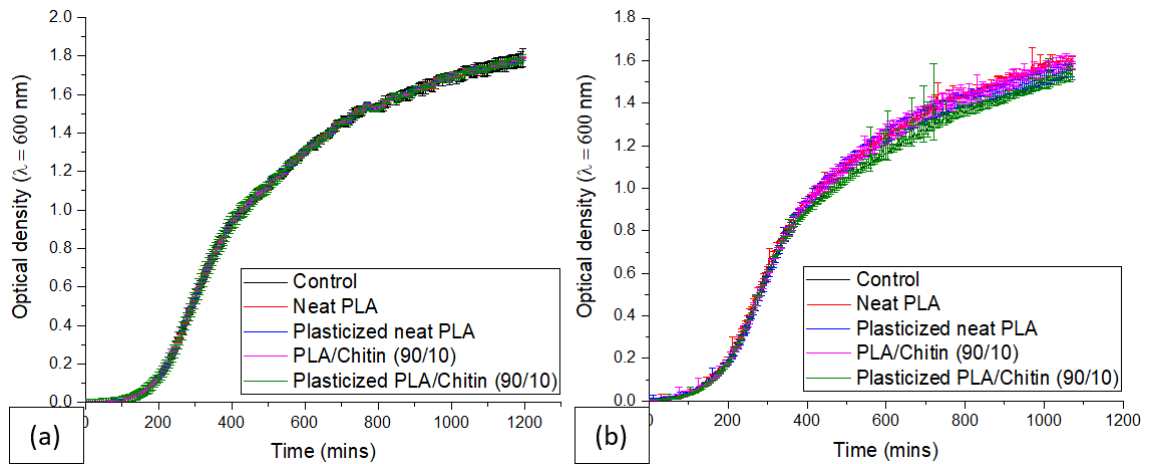
Figure 5.17. (a) Growth curves of *MRSA JE2* and (b) *MSSA Newman* in the presence of 100% PLA and 90% PLA/ 10% chitin films

In summary, the plasticized composite with 10wt% chitin seems to show very small antimicrobial efficacy towards *E. coli K12*, *Sakai* and *MSSA Newman* compared to other samples. However, the effect is indeed insignificant and there is insufficient information to make a certain conclusion. Therefore, additional experiments are required to confirm the antimicrobial activities of the PLA/chitin composites with chitin loadings in excess of 10 wt%.

Chapter 6.

Composites of PLA and WS$_2$

6. Composites of PLA/WS$_2$

6.1 General Characterisations for composites of PLA/WS$_2$

The WS$_2$ powder was firstly examined using SEM and TEM. From SEM images it can be seen that the WS$_2$ consist of tubes of length from 1 – 2 µm (Figure 6.1a). From TEM the hollow structure of a WS$_2$ nanotube can be seen.[415] (Figure 6.1b). In addition, it can be seen that each WS$_2$ nanotube has a diameter of between 40 – 60nm and composed of approximately 20–23 layers (Figure 6.1b).
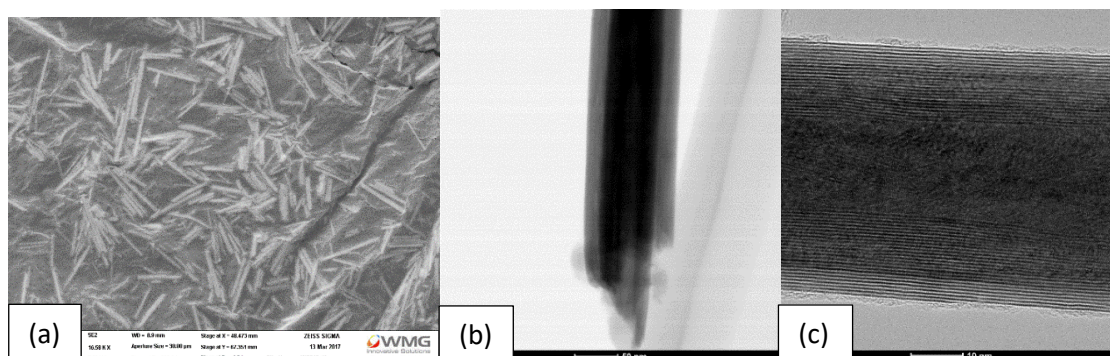
Figure 6.1. (a) SEM image of pure WS$_2$; (b) & (c) TEM images of single WS$_2$ nanotube

The atomic and mass fraciton of WS$_2$ was analysed using TEM-EDS. The spectrum is shown in Figure 6.2 and elemental composition listed in Table 6.1. The ratio of W to S is 1:2.2 which indicates that there is more free sulphur present, possibly as a consequence of residual sulphur on the surface of the WS$_2$ nanotubes from the growth process.[416] The copper signal is likely to be the result of electrons scattering due to the interaction between the sample and the Cu grid used to support the sample.[417] It was somewhat surprising that carbon and oxygen was also present at 16.41% and 2.81% atomic fraction, respectively. However, their relative mass fraction (%) are only 3.55% for C and 0.82% for O.
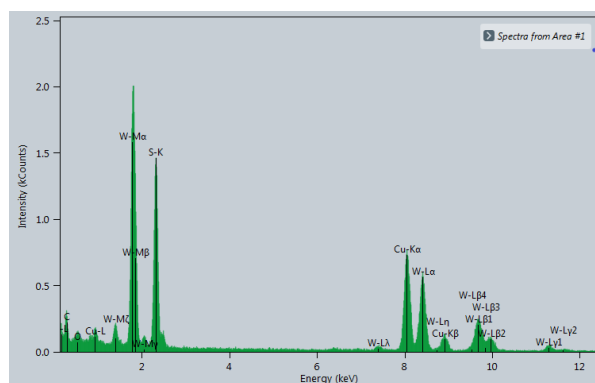
Figure 6.2. EDS spectrum of WS$_2$

Table 6.1. Atomic and mass fraction of EDS

Element	Atomic %	Mass %
C	16.41	3.55
O	2.81	0.82
S	36.89	20.21
Cu	27.26	27.55
W	16.64	47.87

TEM mapping was conducted and images are shown in Figure 6.3 below. It can be seen in Figure 6.3(b) that the green dots that represent W are dense especially in the WS$_2$ tubes. Similarly, the purple dots that represent S are dense and can be clearly seen in the nanotubes (Figure 6.3c). In contrast, the yellow dots representing the C are mostly shown on the surface of the Cu grid but there is only a thin layer surrounding the WS$_2$ tube (Figure 6.3d). Hence, it is suggested that the C signal is mostly also caused by scattering because of the grid and it is unlikely that there are C contaminants on and just inside the nanotube surfaces.
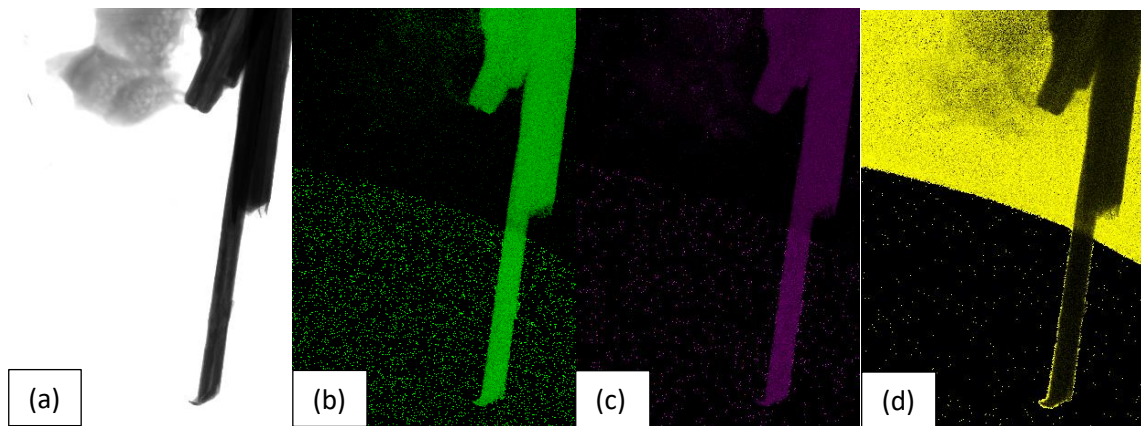
Figure 6.3. TEM mapping (a) blank, (b) tungsten, (c) sulphur and (d) carbon

By way of example, the morphology of the composite of PLA and 5wt% WS$_2$ was also examined using a combination of SEM (Figure 6.4a,b) and TEM (Figure 6.4c, d, e). From Figure 6.4 (a) & (b), the WS$_2$ nanotubes are distributed uniformly within the PLA matrix. Voids can alo be observed suggesting that the wetting of the nanotubes by the polymer was limited. There was also a concern that the size of WS$_2$ nanotubes was changed by the electron beam during examination in the SEM. Therefore, a specimen was sectioned by ultra-microtome into thickness of ~50nm and studied in theTEM to further examine the structure of the tubes.
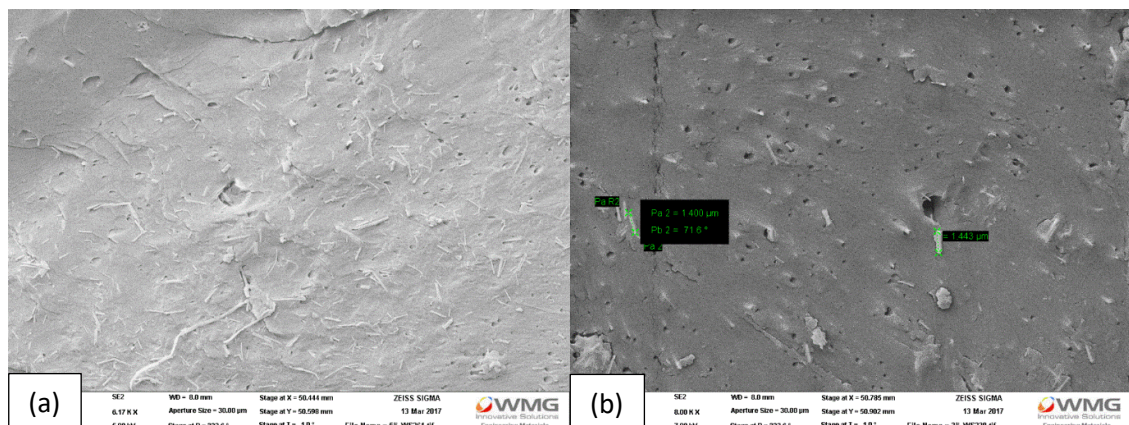
Figure 6.4. (a) & (b) SEM images of PLA/WS$_2$

From the images in Figure 6.5 (b – c), it can be seen that some of the WS$_2$ nanotubes appeared to be shorter which could be a consequence of melt processing, microtoming or both. The overall diameter of nanotubes was still between 40–60 nm but the length of some of the nanotubes had been significantly fragmented and reduced to *ca.* 50 nm from *ca.* 1.5 μm.
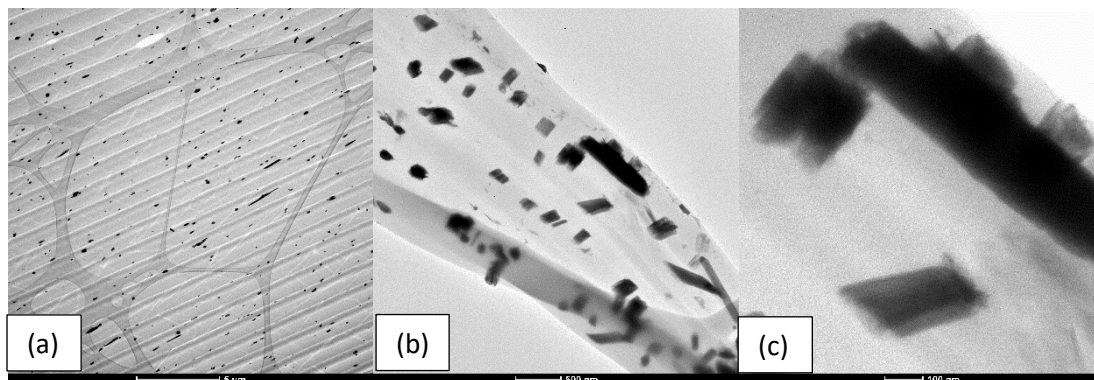
Figure 6.5. (a), (b) & (c) TEM image of PLA/WS$_2$ (95/5)

Finally, the TEM diffraction patterns of pure WS$_2$ and the PLA/WS$_2$ (95/5) were also collected. As WS$_2$ is a crystalline material[265] its diffraction appears as sharp symmetric rings (Figure 6.6a) which demonstrate the high crystallinity order.[418] In contrast, the diffraction pattern of the composite appear to be very weak and distorted rings that implies that the composite is highly amorphous (Figure 6.6b). This observation is confirmed from DSC and XRD data below.
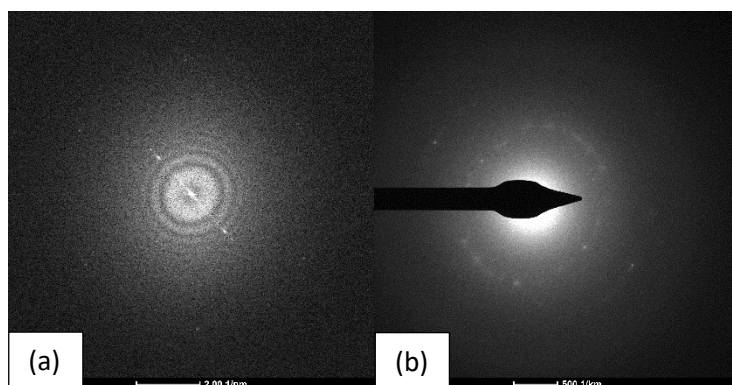
Figure 6.6. TEM diffraction pattern of (a) pure WS$_2$ and (b) PLA/WS$_2$ (95/5)

Pure WS$_2$ was analysed using XPS to measure the atomic percentage of each element in the sample and determine if there are impurities present in the as received powder. A XPS survey spectrum is shown in Figure 6.7. The composition was determined to be 37.16% sulphur, 9.95% oxygen, 16.7% tungsten and 36.19% carbon, see Table 6.2. Although the WS$_2$ powder was heated overnight to 120°C prior to XPS analysis, the impurities (C, O)

were detected. It is likely that sample had aged which involved the adsorption of airborne contaminants on the surface.[416] In addition, the ratio of S:W was 69:31, which is greater than 2 and is possibly due to residual sulphur on the surface of the WS$_2$ nanotubes from the growth process,[416] as observed in the TEM map.
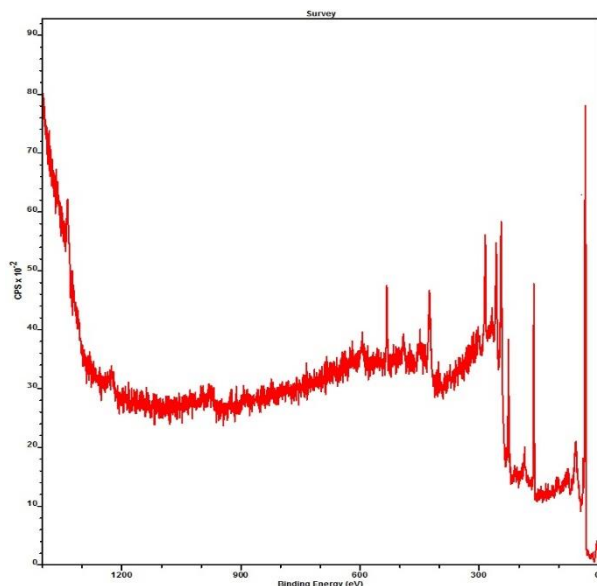
Table 6.2. Atomic percentage of XPS

Element	Position	Atomic %
S	162	37.16
O	532	9.95
W	32	16.70
C	284	36.19

Figure 6.7. XPS spectrum of WS$_2$

The interpretation of the four individual peaks obtained in Figure 6.7 and their assignment is shown in Figure 6.8. With regard W, the peak at 32.4 eV correspond to WS$_2$, the peak at 35 eV correspond to W itself and at 38.2 eV corresponds to WO$_3$.[419] For S, there is a clear splitting at 163 eV of a spin-orbit doublet that correspond to WS$_2$.[420]

Apart from the likelihood of adsorption of airborne contaminants on the surface of WS$_2$,[416] it is also very likely that this could be caused by adventitious carbon contamination (a thin layer of carbon on the material's surface).[421] Indeed the C1s spectrum for contamination typically consisting of C-C, C-O and O=C-O components[421] and so, there is a relative O1s spectrum consisting of C-O and O=C-O components. The same phenomenon was reported on various XPS analysis and in vacuo, such that contamination rates can even be 10 times greater when the x-ray source is in operation which indicates that the radiation damage of hydrocarbon species occurs via secondary electron flux which can cause an over-layer deposition.[422] Therefore, a signal for C and O is detected in the XPS analysis.
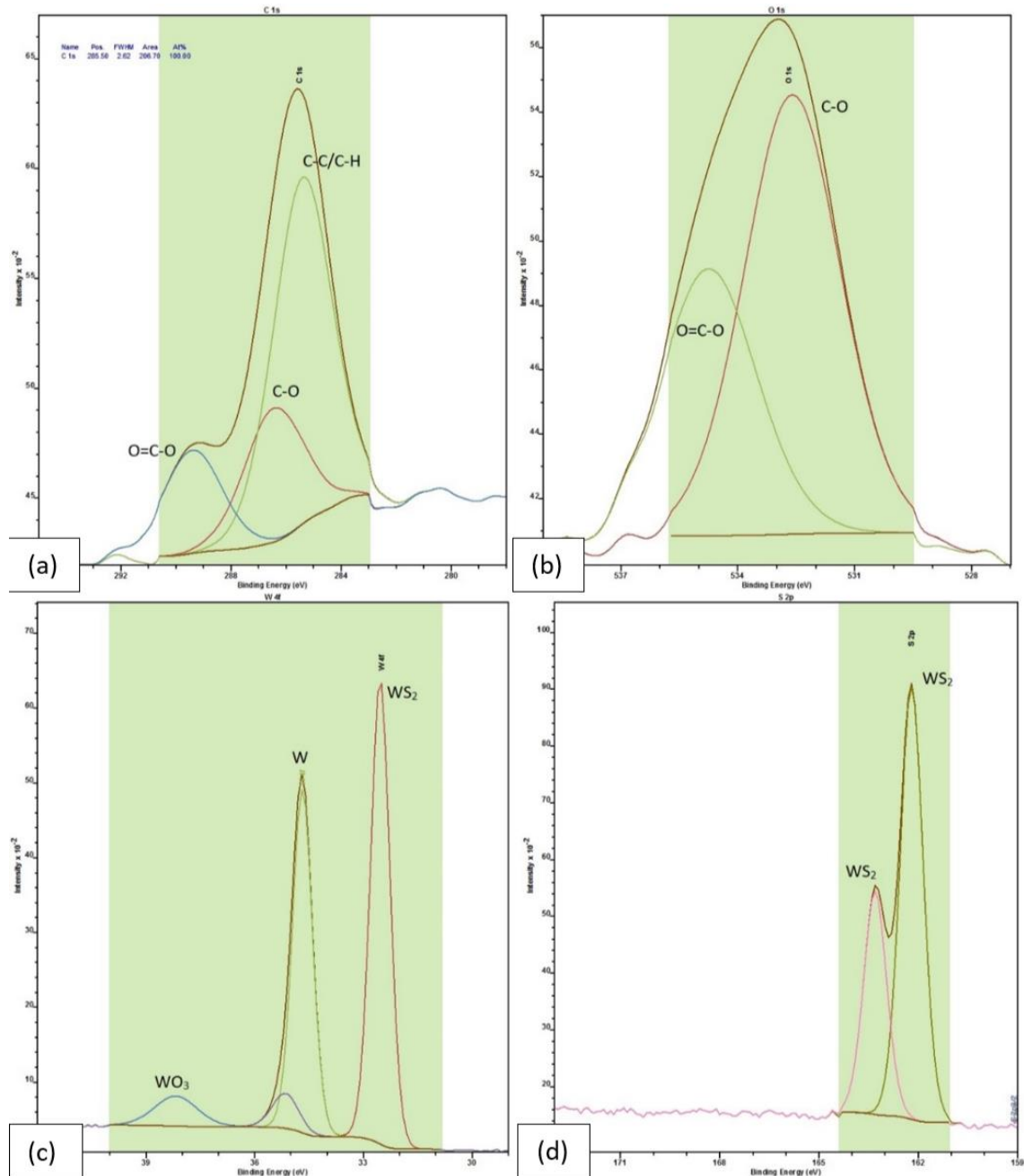
Figure 6.8. Interpretation of individual element (a) carbon, (b) oxygen, (c) tungsten and (d) sulphur – deconvolution spectra.

The Raman spectrum for WS$_2$ was obtained using 514.5 nm laser excitation. Most of the peaks obtained correspond to WS$_2$ itself. The peak at 173 cm^{-1} corresponds to the longitudinal acoustic LA(M) mode and the other peaks are associated with longitudinal acoustic, in-plane LA(M) at 267 cm^{-1}; longitudinal acoustic LA(M), in-plane E$^1_{2g}$(Γ) modes at 295 cm^{-1}; basal plane at 321 cm^{-1}; in-plane E$^1_{2g}$(Γ) at 354 cm^{-1} and out-of-plane A$_{1g}$(Γ) at 418 cm^{-1}.[423] The peak at 518 cm^{-1} corresponds to sulphur[423] whereas the peaks at 710 and 807 cm^{-1} corresponds to tungsten oxide (Figure 6.9).[424]
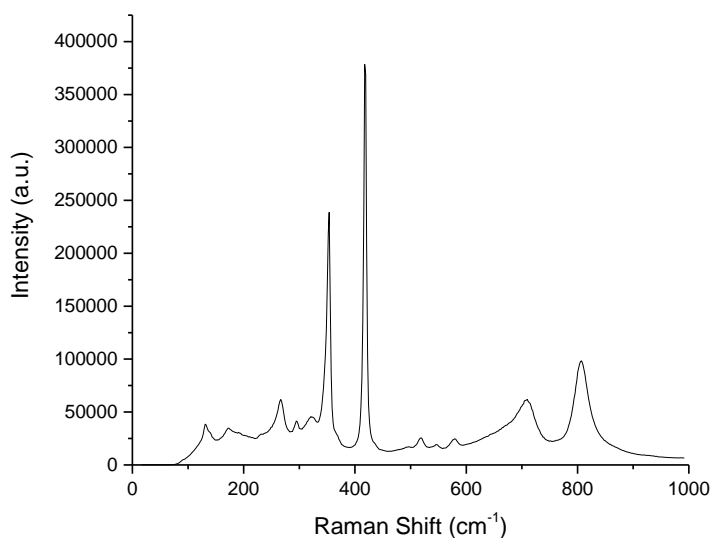
Figure 6.9. Raman spectrum of WS$_2$

DSC measurements were carried out in order to determine the values of T$_g$, cold crystallisation temperature, melting temperature (T$_m$) and crystallinity (X$_c$) of the composites. The thermal histories of the composites were removed by heating from 25 °C to 180 °C, isotherm for 4 minutes and then cooling back to 25 °C at a heating rate of 10 K/min. This cycle was repeated again in order to obtain the heating (Figure 6.10) and cooling curves (Figure 6.11) and the relevant results are tabulated and shown in Table 6.3.

Table 6.3. DSC data for PLA/WS$_2$ composites

Composite	T$_g$	T$_{cc}$	T$_{m,1}$	T$_{m,2}$	X$_c$
Neat PLA	58 °C	118 °C	147 °C	152 °C	0.39%
PLA/WS$_2$ (99.5/0.5)	58 °C	116 °C	147 °C	152 °C	0.28%
PLA/WS$_2$ (99/1)	58 °C	116 °C	147 °C	152 °C	0.01%
PLA/WS$_2$ (98/2)	58 °C	116 °C	147 °C	152 °C	1.57%
PLA/WS$_2$ (97/3)	58 °C	116 °C	147 °C	152 °C	0.18%
PLA/WS$_2$ (95/5)	58 °C	117 °C	147 °C	152 °C	0.55%
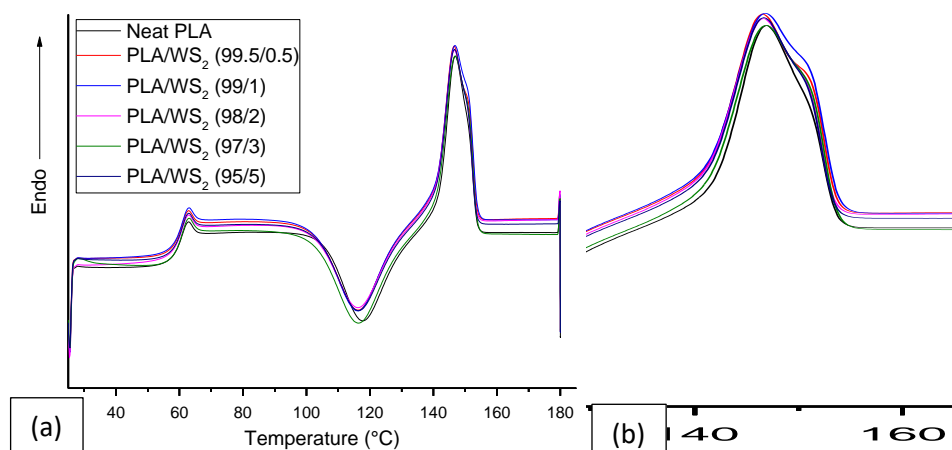
Figure 6.10. (a) Second heating curves; (b) melting peaks of PLA/WS$_2$ composites

The T$_g$ of PLA remained constant at 58 °C on addition of WS$_2$ and it can also be seen that the slopes of the curves at 55 – 60 °C remained the same (Figure 6.10a). Pure PLA had a cold crystallisation peak at 118 °C, which decreased slightly to 116 °C on addition of 0.5, 1, 2 and 3 wt% WS$_2$, but increased again to 117 °C when the percentage of WS$_2$ was increased to 5 wt%. These variations are within experimental error of the DSC instrument. The shape of the cold crystallisation peaks are identical but became slightly broader when WS$_2$ was increased to and above 3 wt% which could be due to major changes in phase separation behaviour as well as more diverse WS$_2$ sizes in the PLA.[396] All the composites had a melting temperature at 147 °C and albeit not obvious, it was noticed that they all display a second melting process centred at about 152 °C especially with the presence of WS$_2$ (Figure 6.10b). This double-melting behaviour is a common phenomenon that occurs in semi-crystalline polymers.[387] Pure PLA has a slightly higher T$_{cc}$ peak and smaller T$_{m,2}$ peak associated with more perfect crystals present and give rise to a peak that is analogous to a single melting peak. In the case of the PLA/WS$_2$ composites, the lower melting peak is attributed to melting of primary crystals,[389] formation of thickened lamellae[425] or fusion of think lamellae formed[284] and the higher temperature peak can be attributed to melting of recrystallized crystals[389] or fusion of newly formed lamellae via melting-re-crystallisation of primary thin lamellae.[284] The degrees of crystallinity for all the composites was determined based upon the second heating cycles with extra enthalpy absorbed by crystallites being subtracted. Hence, the following equation was applied,

$X_c = \frac{\Delta H_m - \Delta H_{cc}}{\omega PLA \times \Delta H_m^0} \times 100\%$ (where ΔH_m stands for enthalpy of melting, ΔH_{cc} is enthalpy of cold crystallisation, ωPLA is weight fraction of PLA and ΔH_m^0 is the melting enthalpy of 100% crystalline PLA which reported to be 93.7 J/g).[389,392] All composites were shown

to have degrees of crystallinity less than 2%, possibly due to the slow crystallisation rate of PLA and so, very few crystals are generated in the PLA resin. Therefore, the composites remained amorphous under the most practical processing and moulding procedures.[393]

This slow crystallisation of PLA is also the reason only glass transition steps appeared in all cooling curves of the PLA/WS$_2$ composites (Figure 6.11). Since formation of the critical nucleus required for nucleation demands some time, slow crystallisation leads to the absence of crystal formation and hence, crystallisation is prevented which resulted in all the PLA/WS$_2$ composites having being almost fully amorphous and showing only glass transition steps in the cooling curves.[394]
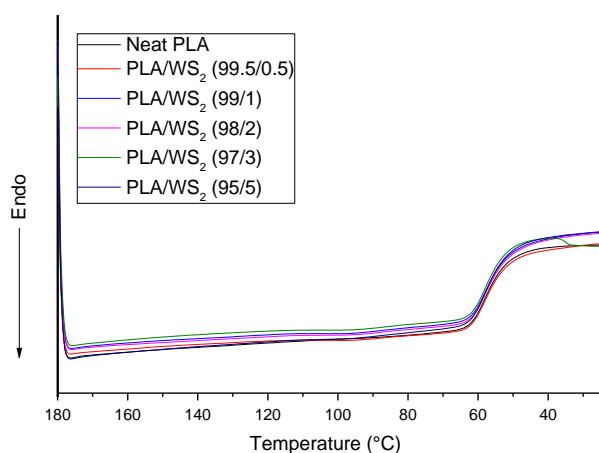
Figure 6.11. Second cooling curves of PLA/WS$_2$ composites

The limited crystallisation behaviour of these composites was also studied using controlled cooling experiments under POLM equipped with a hot stage and filter ($\lambda = 540$ nm) and, to also examine the birefringent crystals at different temperatures. When the samples were heated from room temperature to 180 °C at a rate of 10 K/min, the changes in birefringence were consistent with the DSC data. Images of unfilled PLA during certain temperatures in the heating ramp are shown in Figure 12 below as examples. At 30 °C, the Michel-Levy colour of the birefringent crystals[426] can clearly be seen (Figure 6.12a). When the sample was heat to 60 °C which is at the T$_g$ of PLA, the sample softened and the colours started to disappear. When 70 °C was reached, the sample become transparent (Figure 6.12b). When the temperature was increased to 115 °C which is the cold crystallisation temperature of PLA, Michel-Levy colours can be seen again (Figure 6.12c). When the sample was heated further and reached 150 °C (melting of PLA), the colours once again disappeared and sample became transparent again (Figure 6.12d).

131

When sample was cooled at rate of 10 K/min to room temperature, the sample remained transparent and birefringent crystals could not be seen. This observation during cooling is also consistent with the DSC results as re-crystallisation were not seen from the DSC curves at the same cooling rate.
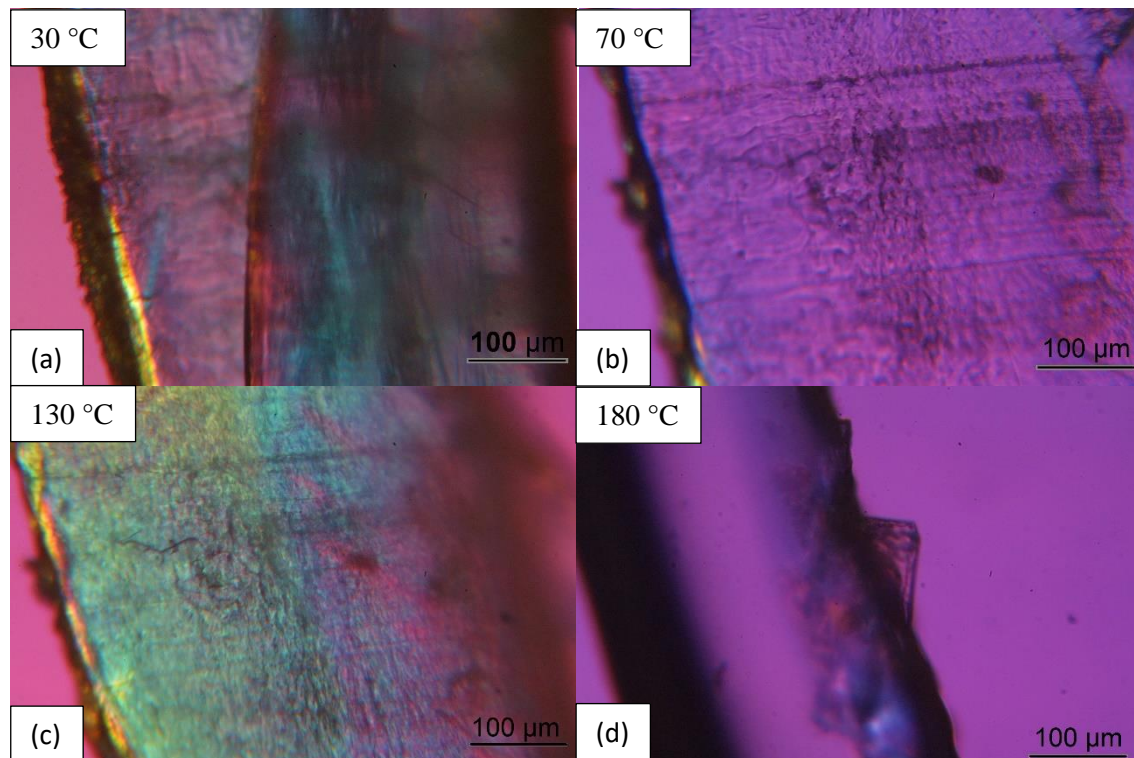

Figure 6.12. Birefringent crystals of PLA at (a) 30 °C, (b) 80 °C, (c) 130 °C & (c) 180°C

As it was discussed in the previous chapter, this PLA crystallises very slowly. Therefore, POLM experiments were repeated for all the PLA/WS$_2$ composites to investigate if crystal formation could be induced. All samples were heated to 180 °C at the 10K/min and the temperature held at 115 °C for 10 mins during cooling. The appearance of all samples changed when the temperature was maintained at 115 °C. By way of example, POLM images of neat PLA are shown in Figure 6.13 and indicate that the surface of sample appeared to be blue and red which is very likely to be derived from positive and negative-type birefringence spherulites[427] after the holding the temperature at 115 °C for 3–4 minutes (Figure 6.13a). When this temperature was held for 5 mins, the appearance of the sample remained as shown in Figure 6.13b. Similar observations were made when the other PLA/WS$_2$ composites were examined, confirming the presence of WS$_2$ did not affect the formation of birefringent spherulites under these conditions.
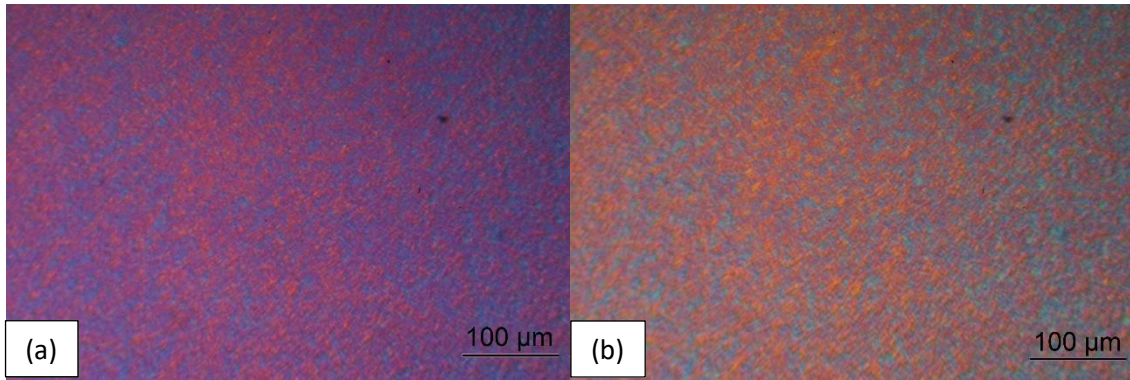
Figure 6.13. PLA being held at 115 °C for (a) 3 – 4, (b) 5 minutes

These experiments were repeated but now the cooling rate was reduced to 1 K/min. and spherulites started to appear in all the composites at 125 °C. Interestingly, it was noticed that presence of WS$_2$ can promote the formation of PLA spherulites under these conditions. Some images are shown in Figure 6.14 to demonstrate this behaviour with and without WS$_2$ added. Both images were taken at 120 °C and spherulites were still growing in pure PLA which can still be seen clearly even when filter was removed (Figure 6.14a). In contrast, the spherulites were already fully formed and distributed evenly in composite with 0.5wt% WS$_2$. Positive and negative-type birefringence spherulites can be seen using the filter but these became less distinguishable without the filter due to the high volume (Figure 6.14b). This phenomenon occurred for all other composites with WS$_2$ incorporated. Hence, it is possible for WS$_2$ to act as nucleation sites for this PLA under certain cooling conditions.
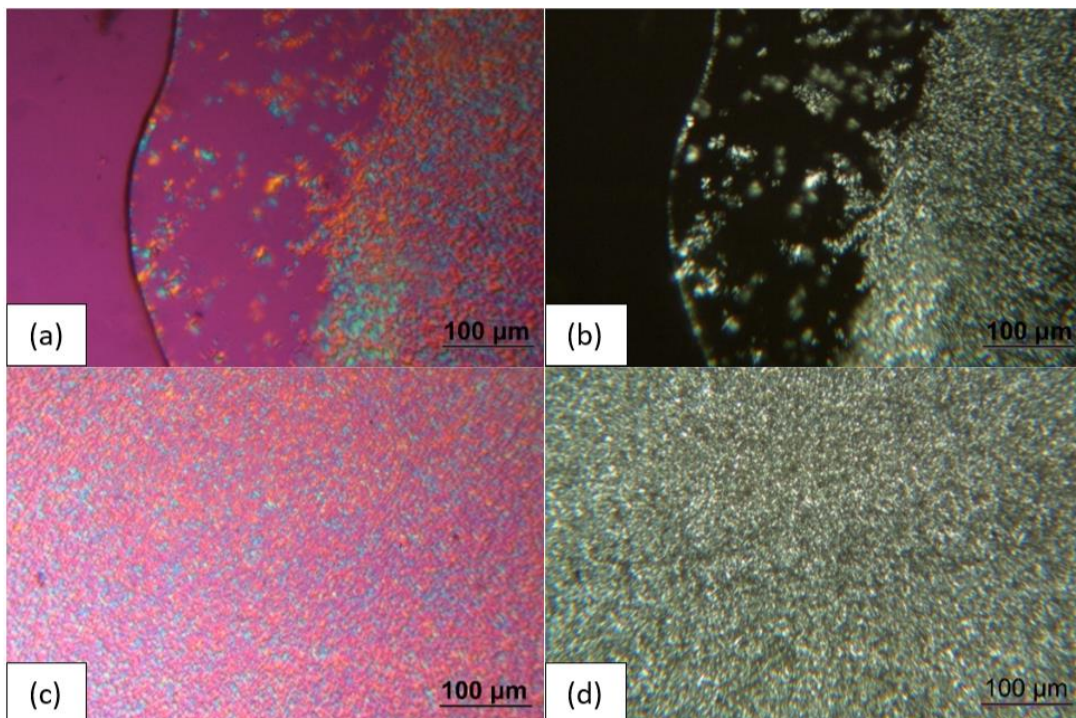
Figure 14. POLM images of unfilled PLA examined under (a) filter, (b)without filter; and composites of PLA and WS$_2$ (99.5/0.5) examined under (c) filter, (d)without filter at 125 °C[133]

XRD measurements were then conducted and the diffraction curves for pure PLA appear to be very broad which indicates that the pure PLA sample is an amorphous material.[428] At $2\theta = 18.4°$, a weak crystalline diffraction peak appeared which is assigned to the (200) and/or (110) planes of PLA crystals in the α-phase.[429] This peak then became smaller in the XRD curve of the composites (PLA/WS$_2$ (99.5/0.5)) and even became indistinguishable when the WS$_2$ content was further increased to between 1wt% and 5wt%. In the XRD curves of composites, there is a high intensity peak at $2\theta = 16.3°$, weak broad peaks at $2\theta = 33.3°$ and very small broad perks at $2\theta = 38.0°$ which are assigned to the WS$_2$ (002) plane of successive S-W-S sandwiches,[430] WS$_2$ (100/101) planes cause network rotation along the nanotube axis,[431] and WS$_2$ (103) plane which often appears to be very small and broad.[430] In comparison, all these peaks increased in intensity with increasing WS$_2$ content which is specifically more significant and obvious for the peak of WS$_2$ (002) plane (Figure 6.13). For that peak of WS$_2$ (002) was originated at $2\theta = 14.2°$ and peak of WS$_2$ (103) plane was originated at $2\theta = 39.0°$. For WS$_2$ the (002) plane shifted to higher angles in the composites, this indicated that this plane experienced tensile stress in the composites.[432] Oppositely, the WS$_2$ (103) plane shifted to slightly lower angles in the composites suggesting the 103 plane experiences some compressive stress when added to the polymer.[432]
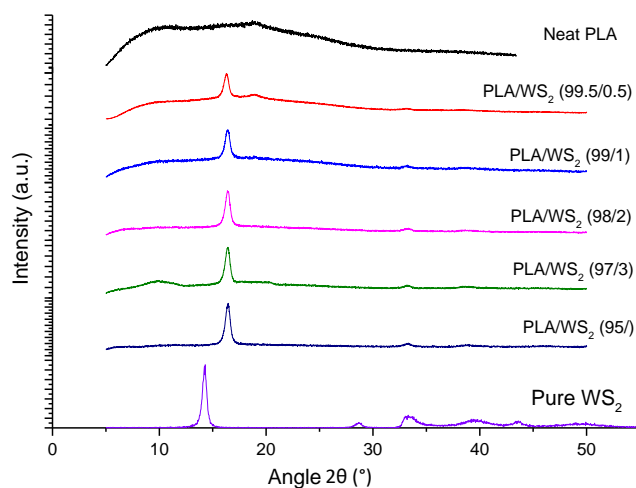
Figure 6.13. XRD curves for PLA/WS$_2$ composites

SAXS as well as WAXS curves were collected simultaneously. From the SAXS curves no scattering maxima were observed (Figure 6.14a). This again confirms the composites are highly amorphous as any lamellar stacks are highly disordered and could not give any scattering peaks. Whereas, the trend observed in the WAXS curves are similar to XRD

data. It is because the curve of pure PLA was broad and two peaks at 2θ = 33.7°, 39.6° appeared when WS$_2$ was present in the composites.
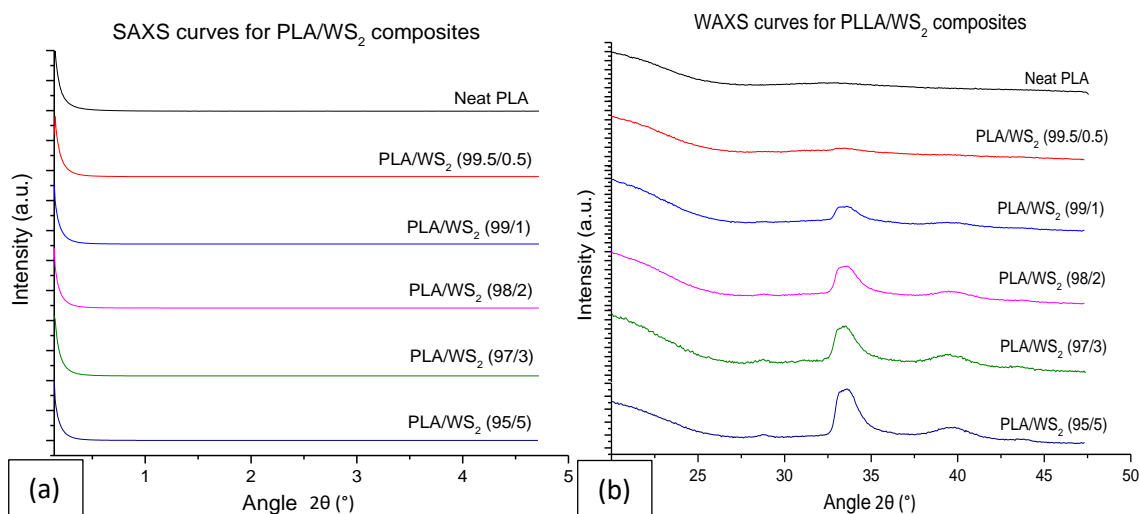

Figure 6.14. (a) SAXS curves and (b) WAXS curves for PLA/WS$_2$ composites

Oscillatory rheology measurements were performed to determine the storage/elastic (G') and loss/viscous (G") moduli of the PLA/WS$_2$ composites and to asses if a rheological percolation had been achieved. An amplitude sweep test was conducted at close to the melt state (155 °C) of PLA to confirm the linear viscoelastic region in the range of 0.1 – 100 Hz. Their storage modulus curves were combined and shown in Figure 6.15(a) below which can be seen that composites with 0%, 0.5%, 1% and 2% WS$_2$ consist of very similar G' values in the range of frequency applied. Whereas, composite with 3% WS$_2$ has the highest magnitude of G' and 5% sample with WS$_2$ has the lowest magnitude of G' which indicates the former has the strongest mechanical strength and the latter has the strongest mechanical strength compared to other composites. It is possible that this highest mechanical strength of composite 95/5 PLA/WS$_2$ was attributed by stronger interactions between PLA and WS$_2$. However, further increase in concentration of WS$_2$ has negative effect on the interactions between the two components and so, the mechanical strength decreased.[433] A similar trend is seen in their loss moduli curves as composites with 0%, 0.5%, 1% and 2%; composite with 3% WS$_2$ has the highest magnitude of G" and sample with 5% WS$_2$ has the significantly lowest magnitude of G". Further, loss modulus of 95/5 PLA/WS$_2$ decreased with increasing frequency (Figure 6.15b). With incorporation of WS$_2$ up to 5 wt%, transition to more elastic (solid-like) behaviour of the composite can be seen when higher frequency was applied.[434]
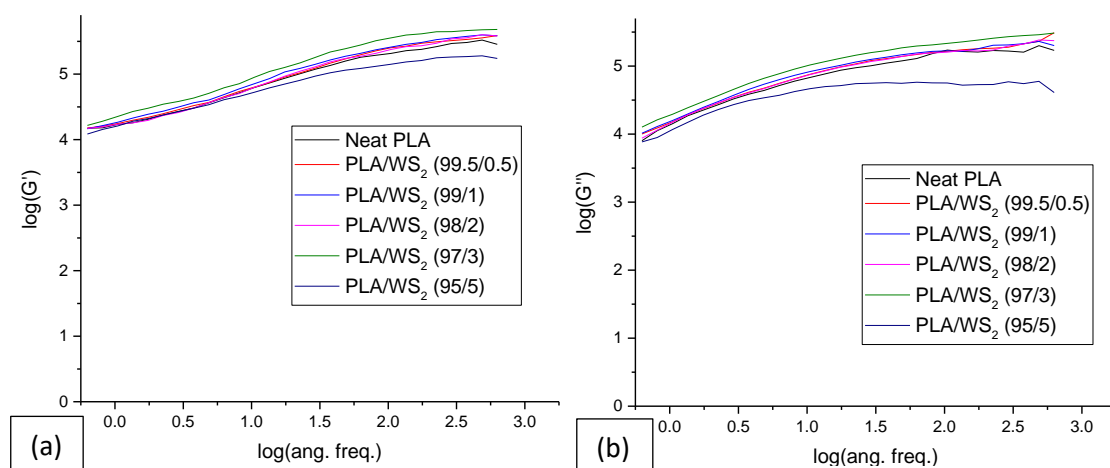
Figure 6.15. (a) Storage moduli and (b) loss moduli of PLA/WS$_2$ composites

DMTA measurements can provide insights to the mechanical properties of the composites as well as whether physical properties of PLA were altered with the presence of WS$_2$. The tan δ curves and dynamic modulus as a function of temperature are showed in Figure 6.16. T$_g$ of the composites can easily be identified as the peaks of the tan δ curves which indicate domination of liquid behaviour over solid. Alternatively, the slopes of the dynamic modulus curves show the materials' transition from solid to rubber which can also be used to show the T$_g$ of the composites.[398,399] All tan δ curves have very similar shapes with very sharp peak at 68 – 70 °C (Figure 6.16a). In which composite with 3% WS$_2$ has T$_g$ of 68 °C, those with 0, 0.5 and 2 % WS$_2$ have T$_g$ values of 69 °C and composite with 1% WS$_2$ has T$_g$ of 70 °C (Table 6.4). Similarly, all PLA/WS$_2$ composites have very similar dynamic modulus with increasing temperature and consist of T$_g$ values at 59 °C (Figure 6.16b, Table 6.4).

Table 6.4. T$_g$ of composites obtained from tan δ and dynamic modulus curves

Composite	T$_g$ / °C (tan δ)
Neat PLA	69
PLA/WS$_2$ (99.5/0.5)	69
PLA/WS$_2$ (99/1)	70
PLA/WS$_2$ (98/2)	69
PLA/WS$_2$ (97/3)	68
PLA/WS$_2$ (95/5)	69

Although T_g values obtained from Figure 6.16(b) are very close to values obtained from DSC, they are indeed lower than that of tan δ curves by *ca*. 10 °C. and this difference was apparently also observed for various polymer.[399,413] Overall, the DMTA data also seem to indicate that presence of WS$_2$ did not significantly alter the mechanical properties of PLA composites according to the tan δ and dynamic modulus curves obtained.
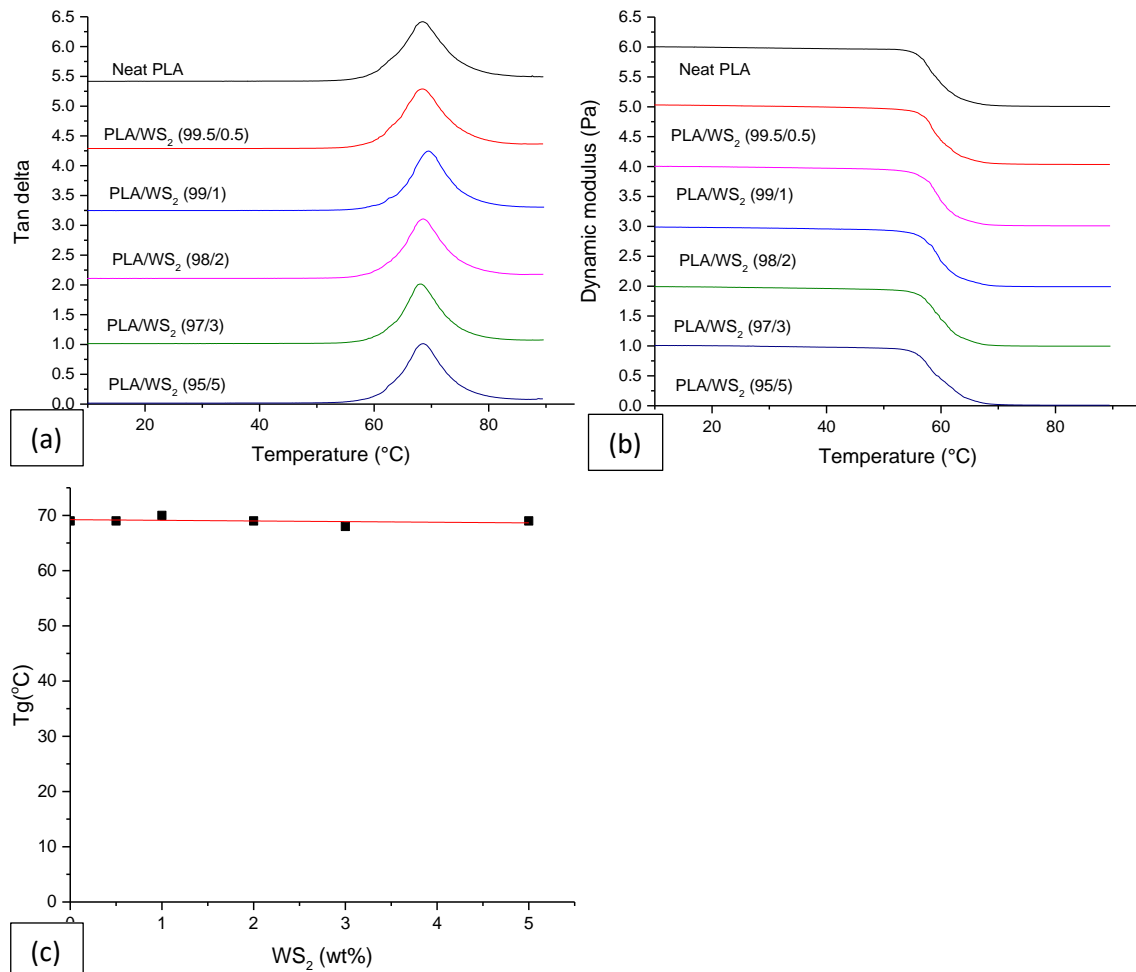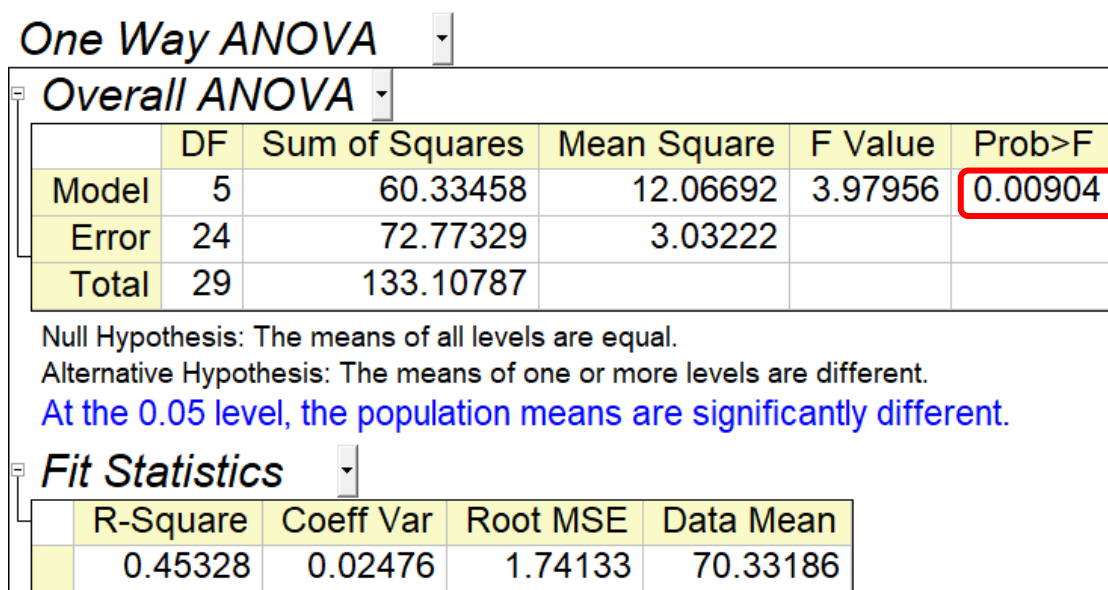

Figure 6.16. (a) Tan δ curves, (b) dynamic modulus vs temperature of PLA/WS$_2$ composites; (c) change in T_g of PLA on addition of WS$_2$

Further mechanical tests were conducted in order to determine the ultimate tensile strength (MPa), young's modulus (MPa) and elongation at break (%) of the composites. For each composite, 5 – 6 dog bone shaped specimens were used during the tests and their average results are shown in Figure 6.20 which can be seen that all composites are brittle materials.[400] Overall results were tabulated in Table 6.5 and the trends are also shown in Figure 6.20(b-d).

Table 6.5. Tensile strength, Young's modulus, elongation at break and their standard deviations of PLA/WS$_2$

Composite	UTS (MPa)	YM (MPa)	EB (%)
Neat PLA	69.37 ± 0.78	3378.99 ± 137.68	3.40 ± 0.12
PLA/WS$_2$ (99.5/0.5)	71.22 ± 1.60	3461.01 ± 85.57	3.37 ± 0.15
PLA/WS$_2$ (99/1)	71.99 ± 0.59	3316.63 ± 140.08	3.69 ± 0.12
PLA/WS$_2$ (98/2)	70.81 ± 2.04	4022.83 ± 587.56	3.73 ± 0.38
PLA/WS$_2$ (97/3)	70.91 ± 1.10	3719.76 ± 586.18	3.93 ± 0.42
PLA/WS$_2$ (95/5)	67.68 ± 2.38	4119.91 ± 379.73	3.73 ± 0.06

The ultimate tensile strengths are the highest points of the stress-strain curves which increased from 69.37 ± 0.78 to 71.99 ± 0.59 MPa when WS$_2$ increased from $0 - 1\%$ which then decreased from 70.81 ± 2.04 to 67.68 ± 2.38 MPa when WS$_2$ further increased from $2 - 5\%$. An ANOVA (Analysis of Variance) statistical test were performed to analyse the differences among group means. The ANOVA results is shown below (Figure 6.17) and reported the p-value that is smaller than 0.05 which indicated that statistically, at least two of the entire groups have significantly different means.[403,404] Therefore, incorporation of WS$_2$ to PLA matrix had altered the UTS of the composites.
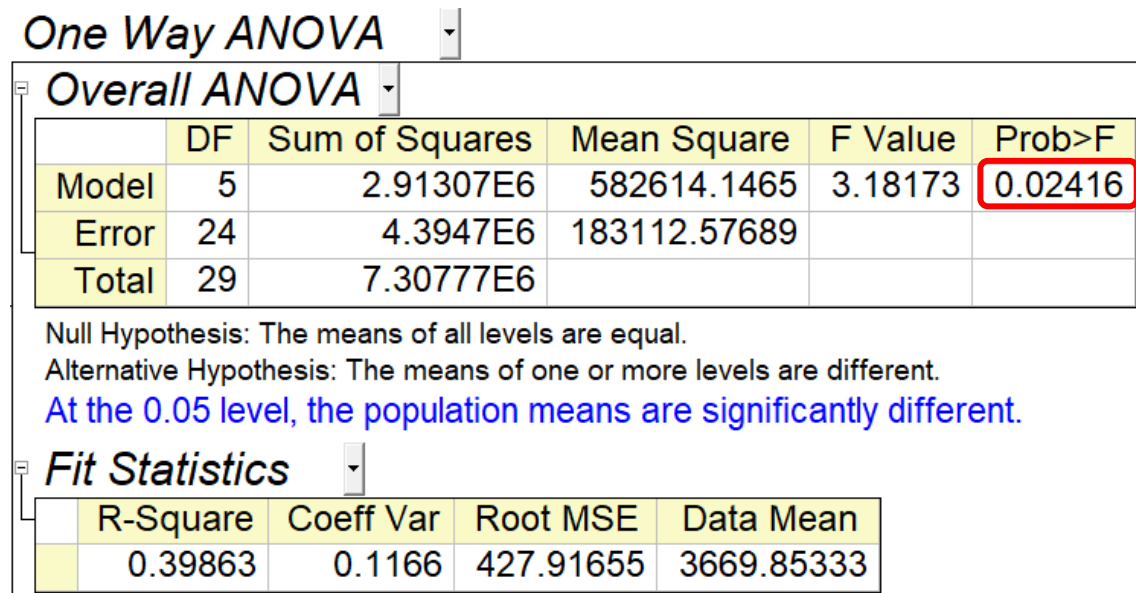

One Way ANOVA

Overall ANOVA

	DF	Sum of Squares	Mean Square	F Value	Prob>F
Model	5	60.33458	12.06692	3.97956	0.00904
Error	24	72.77329	3.03222		
Total	29	133.10787			

Null Hypothesis: The means of all levels are equal.
Alternative Hypothesis: The means of one or more levels are different.
At the 0.05 level, the population means are significantly different.

Fit Statistics

R-Square	Coeff Var	Root MSE	Data Mean
0.45328	0.02476	1.74133	70.33186

Figure 6.17. ANOVA results for UTS of non-plasticized PLA/WS$_2$ composites

Composites with 0, 0.5 and 1% WS$_2$ have similar Young's modulus which are 3378.99 ± 137.68, 3461.01 ± 85.57 and 3316.63 ± 140.08 MPa respectively. In comparison, composites with 2% (4022.83 ± 587.56 MPa), 3% (3719.76 ± 586.18 MPa) and 5% WS$_2$ (4119.91 ± 379.73 MPa) have higher Young's moduli and so, it seems that the overall Young's modulus increases with increasing WS$_2$. An ANOVA statistical test was also performed which shown below (Figure 6.18) and reported the p-value that is smaller than 0.05 which indicated that statistically, at least two of the entire groups have significantly different means.[403,404] Therefore, incorporation of WS$_2$ to PLA matrix had altered the YM of the composites.

One Way ANOVA

Overall ANOVA

	DF	Sum of Squares	Mean Square	F Value	Prob>F
Model	5	2.91307E6	582614.1465	3.18173	0.02416
Error	24	4.3947E6	183112.57689		
Total	29	7.30777E6			

Null Hypothesis: The means of all levels are equal.
Alternative Hypothesis: The means of one or more levels are different.
At the 0.05 level, the population means are significantly different.

Fit Statistics

	R-Square	Coeff Var	Root MSE	Data Mean
	0.39863	0.1166	427.91655	3669.85333

Figure 6.18. ANOVA results for Young's Modulus of non-plasticized PLA/WS$_2$ composites

Finally, the overall elongation also increases slightly with increasing percentage of WS$_2$. Composites with 0 and 0.5 % WS$_2$ have elongation at break at 3.40 ± 0.12 and 3.37 ± 0.15 %. When WS$_2$ increased, composites can elongate to 3.69 ± 0.12% (1% WS$_2$), 3.73 ± 0.38% (2% WS$_2$), 3.93 ± 0.42% (3% WS$_2$) and 3.73 ± 0.06% (5% WS$_2$). Similarly, an ANOVA statistical test was also performed which shown below (Figure 6.19) and reported the p-value that is higher than 0.05 which indicated that statistically, these groups are considered to have equal variance.[403,404] Therefore, incorporation of WS$_2$ to PLA matrix did not alter the elongations of the composites.

One Way ANOVA

Overall ANOVA

	DF	Sum of Squares	Mean Square	F Value	Prob>F
Model	5	0.79069	0.15814	2.00412	0.11436
Error	24	1.89376	0.07891		
Total	29	2.68445			

Null Hypothesis: The means of all levels are equal.
Alternative Hypothesis: The means of one or more levels are different.
At the 0.05 level, the population means are not significantly different.

Fit Statistics

R-Square	Coeff Var	Root MSE	Data Mean
0.29454	0.07807	0.2809	3.59826

Figure 6.19. ANOVA results for Elongation at break of non-plasticized PLA/WS$_2$ composites
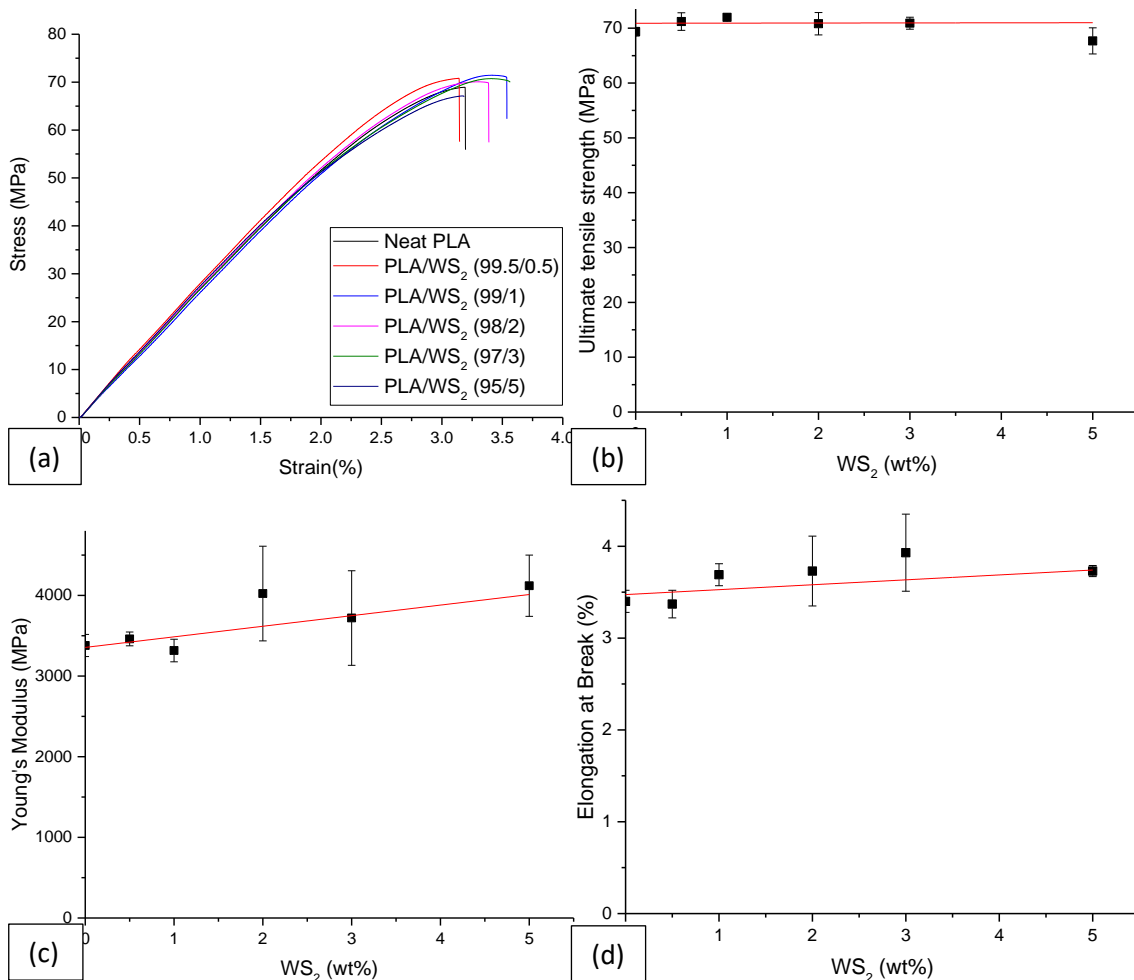
Figure 20. (a) Stress-strain curves of PLA/WS$_2$ composites, trends of (b) ultimate tensile strength;

(c) Young's modulus and (d) elongation with content of WS$_2$ (wt%)

During the TGA measurements, all PLA/WS$_2$ composites and pure WS$_2$ were heated up to 1000 °C with N$_2$ as a carrier gas. TGA curves and their 1st derivative curves as function of temperature are shown in Figure 6.21 below. For neat PLA as well as all PLA/WS$_2$ composites, all curves were identical as samples started to degrade at 440 °C and degradation was completed after heating to 580 °C. This indicated that the presence of WS$_2$ did not influence the thermal stability of PLA under N$_2$ atmosphere. On the other hand, WS$_2$ itself did not degrade in N$_2$ even when heated to 1000 °C and held at this temperature for 10 mins.
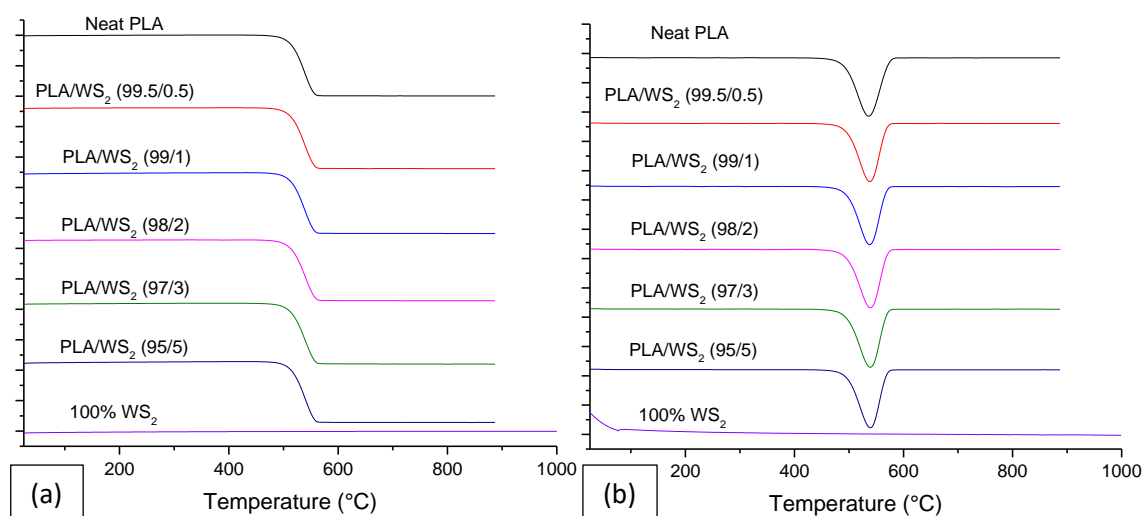
Figure 6.21. (a) TGA curves (b) 1st derivative curves for PLA/WS$_2$ under N$_2$

Same TGA experiments were repeated under air. TGA curves and their 1st derivative curves as a function of temperature are shown in Figure 6.22. Pure PLA degraded at 500 °C and all the sample had completely degraded after heating to 640 °C. Although WS$_2$ appeared to be thermally unstable under ambient atmosphere, only 1.35% of the sample degraded in the temperature range of 460 °C to 610 °C. For the composites with WS$_2$, they all have identical TGA curves as they all degraded completely in the temperature range of 310 – 410 °C. These results show that WS$_2$ can decrease the thermal stability of PLA when tested under ambient atmosphere as the composites degraded at a much lower temperatures compared to both pure PLA and WS$_2$ alone. Polymer degradation can indeed be accelerated in the presence of oxygen which produces radicals that lead to scission and fragmentation of polymer chains. However, the actual reasons of lower thermal stability with the incorporation of WS$_2$ in the presence of oxygen are unknown and further studies are required in order to gain deeper understandings.
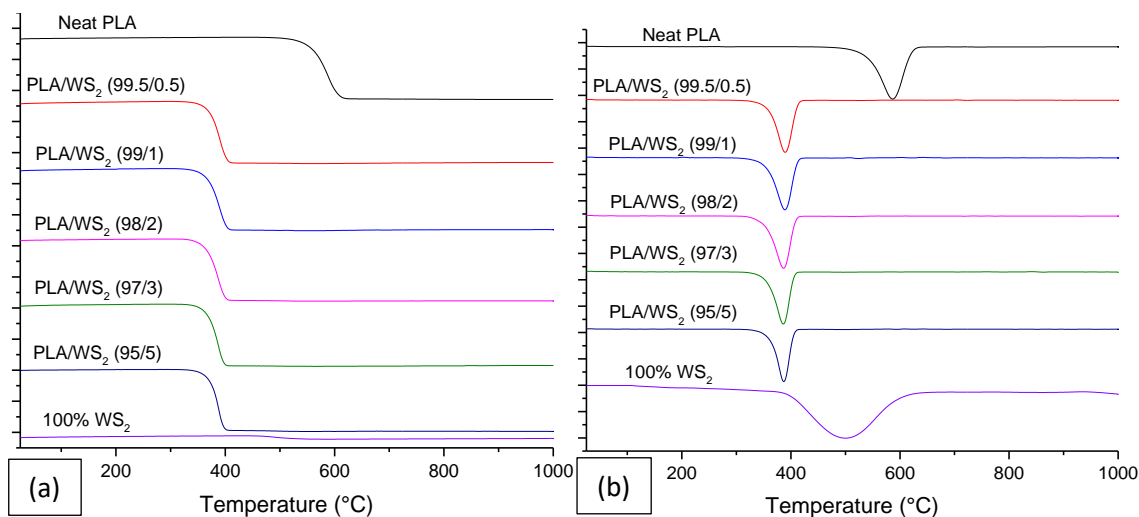
Figure 6.22. (a) TGA curves (b) 1st derivative curves for PLA/WS$_2$ under ambient atmosphere

The FTIR spectra of the materials were collected in an attempt to see if there are any interactions between the nanotubes and the polymer. Although WS$_2$ is Raman active, it is not IR active and its FTIR spectrum cannot be recorded. This is because WS$_2$ exhibits no dipole moment due to its symmetry[435] which causes a change of polarizability.[436] The FTIR spectra of the PLA and the composites were recorded, see Figure 6.23. They all display characteristic peaks at 1043 cm^{-1} (C-CH$_3$ vibration) 1081 cm^{-1} (C-O-C stretching), 1128 cm^{-1} (CH$_3$ rocking band), 1181 cm^{-1} (C-O-C vibration), 1749 cm^{-1} (C=O vibration) associated with PLA.[389]
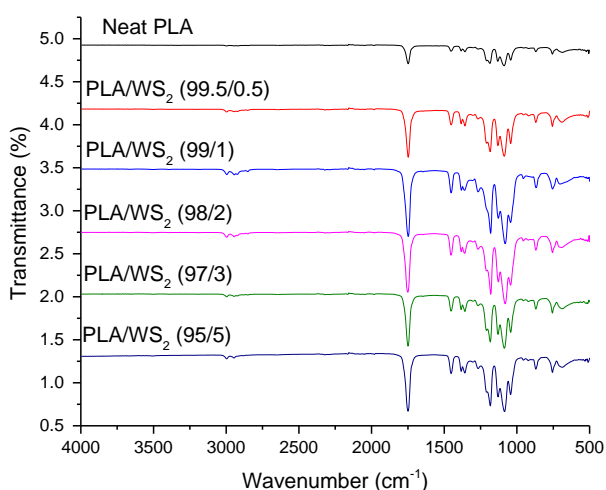
Figure 6.23. FTIR of PLA/WS$_2$ composites

The molecular weight of PLA was measured as there was some concern the impurities in the WS$_2$ could initiate the degradation of PLA when melt mixed at elevated temperatures. Therefore, the molecular weight of the unfilled PLA (before and after melt mixing) and

its composites with WS$_2$ were analysed by GPC analysis. All composites were filtered twice in order to remove insoluble WS$_2$. The GPC curves were obtained using both a light scattering detector and a refractive index detector are shown in Figure 6.24. The values for M$_w$, M$_n$ and DP were tabulated in Table 6.6.

Table 6.6. Values of M$_w$, M$_n$ and DP of different samples

Composite	M$_w$ (kg/mol)	M$_n$ (kg/mol)	DP
Neat PLA	129.85	77.24	1.68
PLA/WS$_2$ (99.5/0.5)	132.55	10.19	1.30
PLA/WS$_2$ (99/1)	132.25	94.35	1.40
PLA/WS$_2$ (98/2)	120.25	76.55	1.57
PLA/WS$_2$ (97/3)	135.75	95.63	1.42
PLA/WS$_2$ (95/5)	126.45	88.54	1.43
Unprocessed PLA	130.25	101.76	1.28

From Figure 6.24, it can be seen that all samples were detected at the same retention time. There are very small differences between the width of the peaks From Figure 6.24(a) the unfilled PLA has a slightly wider peak and a higher DP of 1.68. The composite samples have very similar peak width and DP values within the range 1.30 – 1.57. The unprocessed PLA has the narrowest peak width and a DP of 1.28. Extrusion had a modest effect on the molecular weight of PLA. The difference was not seen in Figure 6.24(b) and when both detectors are complementary to each other, the data showed that all PLA samples have a M$_w$ within the range of 120 – 136 kg/mol. Hence, PLA had higher DPs after processing but the values of M$_w$ were not significantly altered due to the incorporation of WS$_2$.
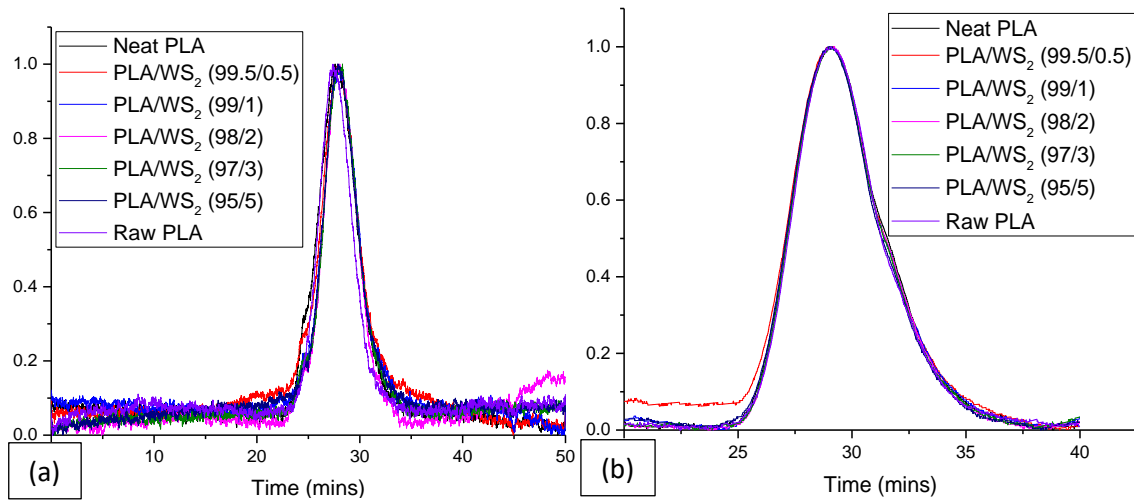
Figure 6.24. GPC curves of PLA obtained by (a) light scattering and (b) refractive index detector

6.2. Bioassays of Composites of PLA and WS$_2$ (bacterial and HUVEC cells studies)

The PLA/WS$_2$ composites were tested against some living organisms to predict the biocompatibility of the composite materials. Experiments were done using *E. coli K-12 MG1655* and *O157 Sakai* strains. After overnight incubation of liquid cultures at 37 °C with and without the composite materials, growth curves were obtained (Figure 6.25). It can be seen that the growth curves of *K-12 MG1655* are identical in the control cultures as well as in the presence of the composite materials. The same phenomenon was observed when experiments were conducted with *O157 Sakai* and so, this demonstrate that neither PLA nor WS$_2$ influence the growth of these two *E. coli* strains.
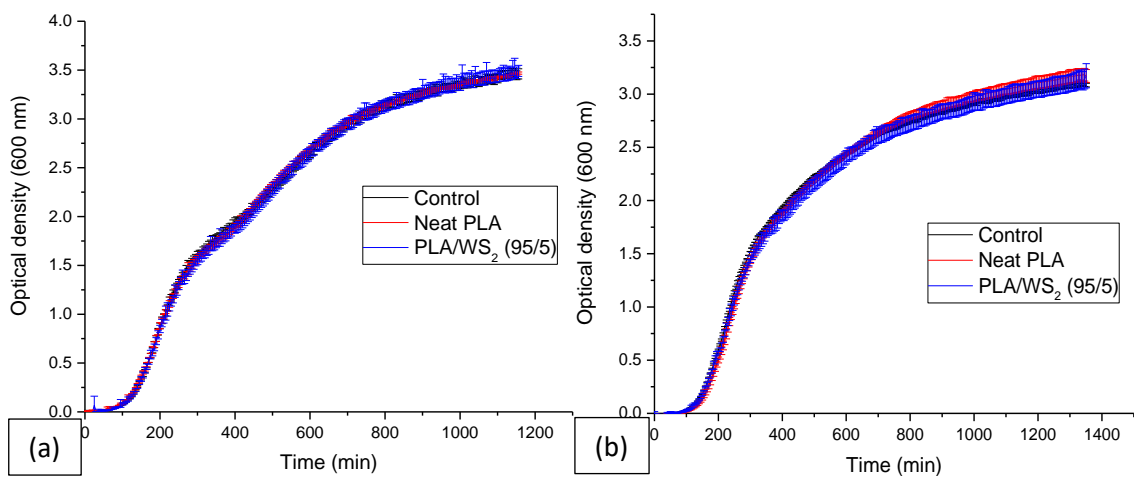
Figure 6.25. (a) Growth curves of *E. coli K-12* and (b) *E. coli Sakai* in the presence of 100% PLA and 95% PLA/ 5% WS$_2$ films

Further experiments were also conducted using HUVEC to predict the biocompatibility and cell attachment on the surface of the composites. The studies were conducted over a period of 7 days and a bar chart of the cell viability assay on days 1, 3 and 7 plotted, see

Figure 6.26. Overall, the cells can survive in the presence of all composite materials. On day 1, cell viability was higher on the composites containing 0, 0.5, 3 and 5% WS$_2$. On day 3, the viability decreased by approximately 50% on all samples in which, the composites with 0.5wt%, 1wt% and 2wt% WS$_2$ had slight cell growth compared to other samples. On day 7, cells activity increased 2 times compared to that of day 3 and it can be seen that the composites with 0, 0.5wt% and 1% WS$_2$ had lower cell viability compared to composites with 2, 3 and 5% WS$_2$.
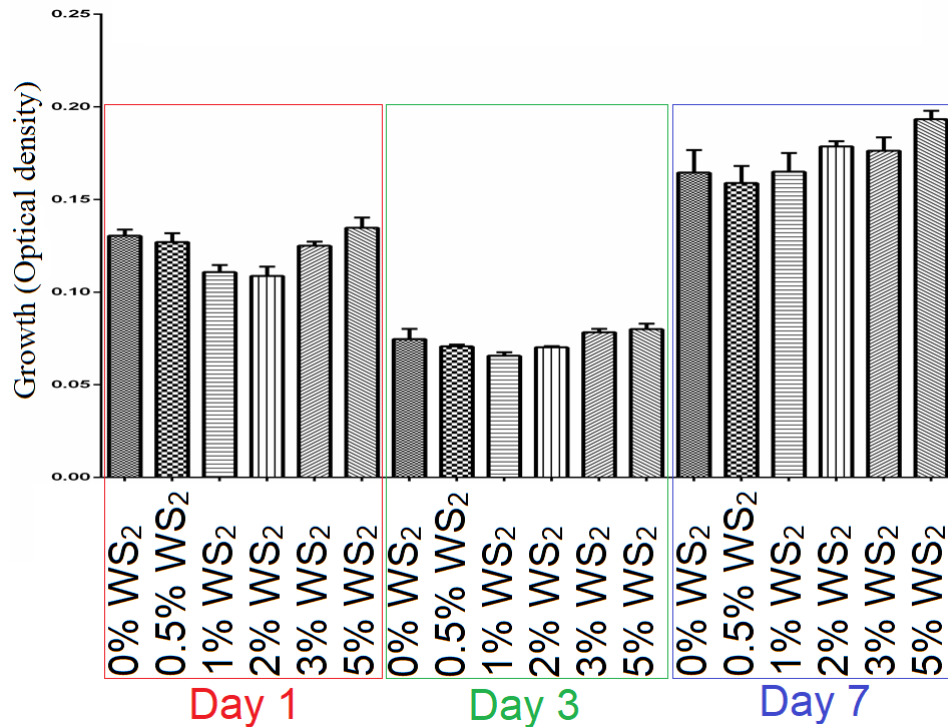
Figure 6.26. Bar chart of endothelial cell viability assay on PLA/WS$_2$ composites

With the aid of fluorescence, images were taken to compare whether the cells can attach on the surface of the composites (Figure 6.27). Overall cell attachment was strong on pure PLA as some cells were larger and more willing to spread out on the surface of the PLA sample (Figure 6.27a). However, very few cell counts were observed on the composites that contained 0.5wt%, 1wt% and 2wt% WS$_2$ (Figure 6.27 b – d). In contrast, more cells attached to the composites with 3wt% and 5% WS$_2$ but they were small and not spread out on both of the surfaces (Figure 6.27e,f). Compare to that of neat PLA (Figure 6.27a), cell attachment on composites with 3wt% and 5wt% are weaker.

This result shows that PLA/WS$_2$ composites did not inhibit the growth of HUVEC. Interestingly, the presence of WS$_2$ in the composites influenced cell attachment at the surface. Overall the survival of endothelial cells was preferred on neat PLA. Incorporation

of 0.5, 1 and 2 wt% WS$_2$ decreased the cell attachment on the composites. However, when WS$_2$ loadings were further increased to 3 and 5wt%, cell attachment became favourable on the composites but their interaction on the surface was very weak compared to that of neat PLA surface.
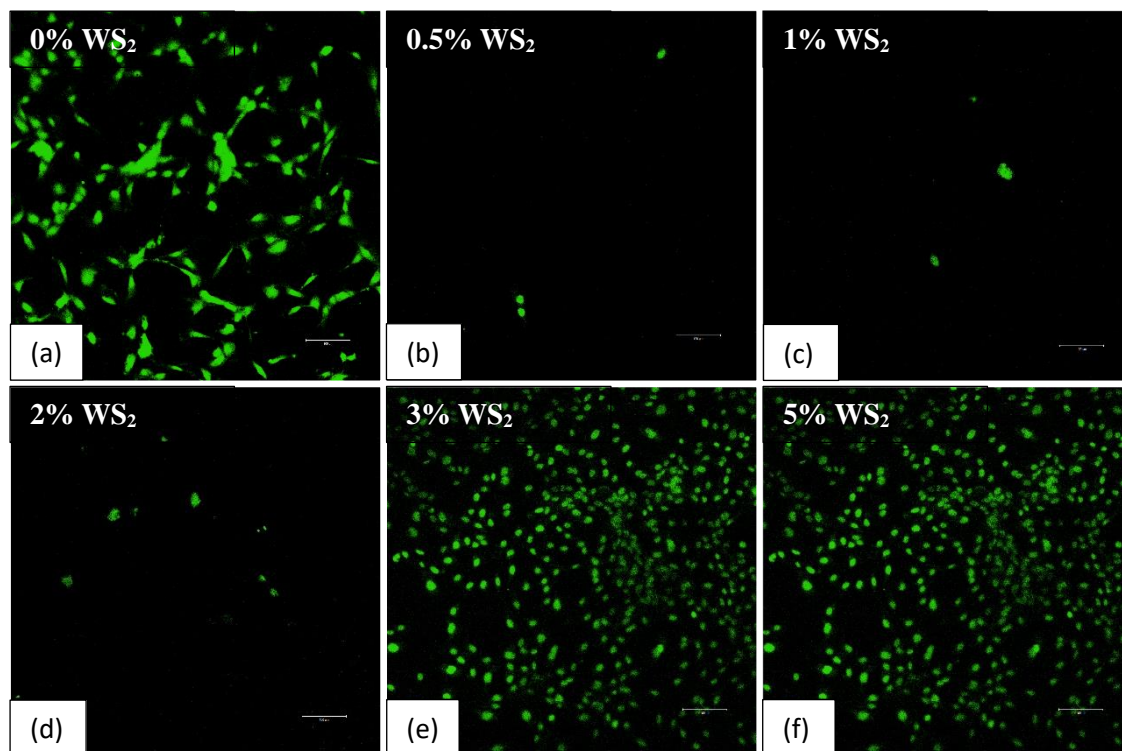
Figure 27. Fluorescent microscope images of HUVEC on PLA composites with (a) 0% WS$_2$, (b) 0.5% WS$_2$, (c) 1% WS$_2$, (d) 2% WS$_2$, (e) 3% WS$_2$, (f) 5% WS$_2$ after incubation for 7 days

Finally, surface wettability (contact angle analysis) was conducted to compare the surfaces' contact angles of the composites. The term "wettability" refers to the ease with which a fluid spreads across a solid surface or more specifically how the fluid adheres to the solid surface[437] and it plays a critical role in the biocompatibility of a biomaterial.[438,439] Hydrophobic surfaces with high contact angles do not serve as good substrates for cellular culture, a water contact angle less than 90 degrees in classed as hydrophilic and most polymers have a contact angle greater than 120 degrees natively.[440,441] The contact angle is the angle created by the air fluid interface on the surface of a test material and is digitally calculated using software that measures the drop on the surface at a particular time point following application to a surface. This wettability study should provide an explanation of the changes in cell attachment on the surface of the PLA/WS$_2$ composites. The addition of WS$_2$ nanoparticles has a varying effect on contact angle as the dose is increased. With the addition of 0.5wt% WS$_2$ the contact angle increased significantly,

however when the concentration increased beyond 1wt% the opposite response was observed with a significant decrease in contact angle to just above the hydrophilic range (Figure 6.28). As the nanoparticle concentration was increased further an increasing trend of contact angle back to control levels is observed. These changes could be attributed to increased surface roughness from the nanoparticles on the surface or the disruption of the crystalline structure of the surface by nanoparticle infiltration. Changes in the nano-topography of biomaterial surfaces and certainly a decreased contact angle into the hydrophilic range is associated with better cellular attachment and proliferation for tissue culture and engineering. This variance in contact angle could explain the MTT assay results obtained at day 1, 3 and 7.
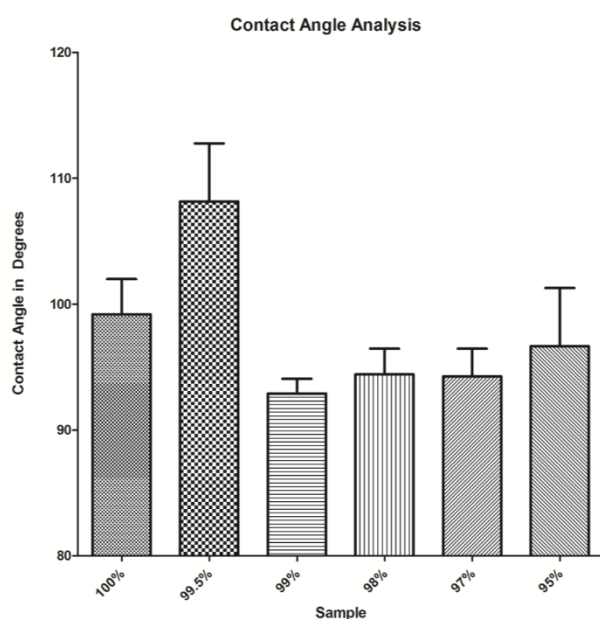
Figure 6.28. Contact angle values for composites of PLA and WS$_2$

In summary, a selection of PLA/WS$_2$ composites were produced and their physical properties were analysed in detail to understand the features of these composites. Composites of PLA and WS$_2$ did not inhibit any growth of *E. coli*. tests and hen further bioassays were conducted using HUVEC cells, the results indicated that the composites did not inhibit the growth of the HUVEC cells. Contact angle measurements of the composites surface confirmed that the incorporation of WS$_2$ to PLA can alter the surface properties and influence cellular attachment and proliferation of tissue culture. However, further tests, such as cytotoxicity, should be conducted so as to explore the full potential of these composite materials.

Chapter 7. Electrospinning of Biopolymer/IL and their Entanglement Prediction

7. Electrospinning of Biopolymer/IL and their Entanglement Prediction

This chapter involves mostly electrospinning and can be divided be three parts which can be expressed in the flow diagram (Figure 7.1) below:

1. Comparison and identification of and ionic liquid that can dissolve BL for electrospinning. Further electrospinning of BL/IL with co-solvents.
2. Study of biopolymer entanglement in ILs with oscillatory rheological and FTIR data.
3. Production of BL membranes by film casting for bioassays with bacteria.

Dissolution of BL in [EMIM]OAc, [BMIM]Cl and [AMIM]Cl ILs	Electrospinning of BL/IL solutions	Electrospining of BL/[EMIM]OAc with co-solvents
Oscillatory rheological studies of biopolymer/IL solutions	Comparison of FTIR spectra of biopolymer/IL solutions	Prediction of entanglement of biopolymer in ILs
Dissolution of BL in [EMIM]OAc	Film casting of BL using coagulation bath	Bioassays using bacteria

Figure 7.1. Key procedures involved in this chapter

7.1 Dissolution of BL in ILs for Electrospinning

As described in the literature review, studies have shown that banana leaves (BLs) have the potential to be developed for wound-dressings.[290] As BL contains 10 – 13% lignin which has been shown in this work to inhibit the growth of *MRSA JE2* and *MSSA Newman*, the aim of this work was to investigate whether BL can also inhibit bacterial growth. However, the shelf-life of BLs can be a drawback in any development as ait is a plant material. Generally, it is known that BL cannot be stored for more than 7-10 days due to fungal growth and it was observed that Gamma irradiation can extend the shelf life of BL for up to 2-3 months.[290,291] Hence, the goal was to use a combination of electrospinning and ionic liquids to process BL to further extend this shelf life as well as remove small molecules (e.g. minerals such as calcium, magnesium; glucose) that can act as nutrients for microbes.

To date, no ILs were reported to be used for dissolving banana leaves. However, the ILs used in this project include [EMIM]OAc, [BMIM]Cl and [AMIM]Cl and have been proven to dissolve lignin. ILs have also been reported for the dissolution of cellulose a major component in plants and therefore, a simple experiment was conducted to check whether these ILs are able to dissolve BL.

The BL were cut into pieces with dimensions of 1 cm x 1 cm and these were then heated in ILs overnight at 120 °C with the target of preparing 5wt% BL/IL solutions. When [EMIM]OAc was used, it was significant that BL pieces started to dissolve within 2–3 hours. Whereas for [BMIM]Cl and [AMIM]Cl, dissolution of BL were not significant and obvious. All BL/IL mixtures were heated overnight and then poured into petri dishes for examination and comparison. Most BL pieces dissolved in [EMIM]OAc and a greenish-brown liquid was obtained (Figure 7.2a) although very small amount of precipitated presented and this was likely to be starch as its interaction with [EMIM]OAc is often limited.[442] When [BMIM]Cl was used, a paler greenish-brown liquid was also obtained but it could be seen that some BL pieces remained in the mixture (Figure 7.2b). When [AMIM]Cl was used, the BL pieces were not dissolved effectively and in fact, most remained intact (Figure 7.2c). Actual % of yield of BL dissolved in ILs was calculated as $\frac{Weight\ (BL\ added-undissolved\ BL)}{Weight\ of\ BL\ added} \times 100\%$ (Table 7.1).
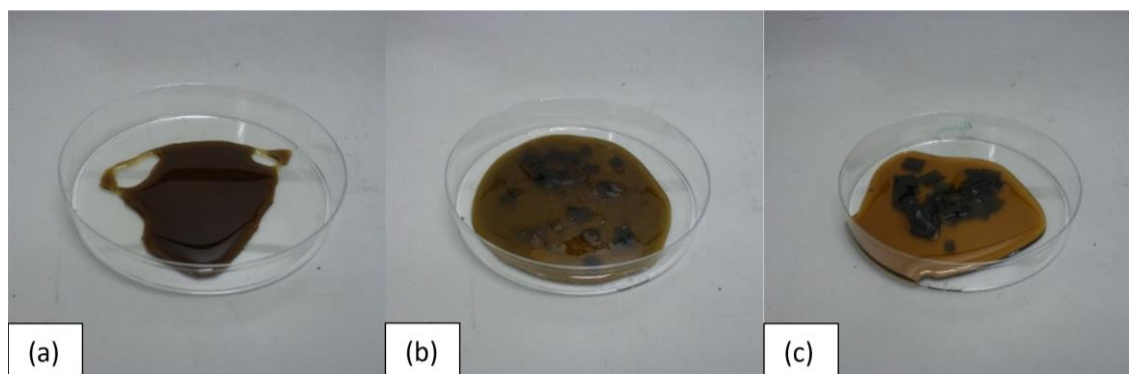
Figure 2. BL dissolved in (a) [EMIM]OAc, (b) [BMIM]Cl, (c) [AMIM]Cl

In order to dissolve BL using [BMIM]Cl and [AMIM]Cl, BL pieces should be ground to finer solids. Therefore, [EMIM]OAc seemed to be the most effective solvent to dissolve BL as it dissolved larger BL pieces easily. It was then attempted to prepare 8 wt% BL/IL and 10 wt%/BL for electrospinning using heights of 10, 15, 20 cm, flow rates of 0.2, 0.5, 0.8, 1.0, 1.5, 2.0 mL/h and voltages of 8.5, 10, 12, 15, 18, 22 kV. A total of 108 trials were conducted for each solution and the details with regard to the dissolution, viscosities and observations during electrospinning will be discussed.

With [EMIM]OAc, 5, 8 and 10 wt% BL/IL solutions were prepared the undissolved solid removed via decantation with the aid of a centrifuge. However, the 8 and 10 wt% BL/IL cannot be prepared using [BMIM]Cl and [AMIM]Cl. The viscosities of the 5 wt% BL/IL were measured prior to electrospinning. It was observed that the 5 wt% BL/[EMIM]OAc could be electro-spun although the Taylor cone appeared to be very unstable and the polymer stream was not continuous. Whereas in the experiments using [EMIM]OAc and [AMIM]Cl, the Taylor cone and polymer stream were not observed at all, as spattering of polymer solution was observed in all trials. Therefore, the focus was on [EMIM]OAc for the electrospinning of BL/IL which was further continued using 8 and 10 wt% BL/IL. In both cases, electrospinning occurred as the Taylor cone appeared to be slightly more stable but further improvement was not observed when 10 wt% BL/[EMIM]OAc was used. Observations are briefly listed in Table 7.1 and details are discussed below.

Table 7.1. Dissolution of BL in ILs and their values of viscosity

IL	[EMIM]OAc 54	[BMIM]Cl 51	[AMIM]Cl 56
Dissolution of BL	88% soluble	64% soluble	42% soluble
	Big pieces (1 cm x 1 cm) can be dissolved easily	Grinded BL pieces required for dissolution	Grinded BL pieces required for dissolution
	5, 8, 10 wt%/IL were prepared	Only 5 wt% BL/IL can be prepared	Only 5 wt% BL/IL can be prepared
Viscosity	5 wt% - 540 cP 8 wt% - 1437 cP 10 wt% - 2574 cP	5 wt% - 1584 cP	5 wt% - 447 cP

Brief information about electrospinning using BL/IL solutions were listed in Table 7.2 below. When 5 wt% BL/IL solutions were subjected to electrospinning, only 5 wt% BL/[EMIM]OAc can be used to produce polymer stream. Therefore, BL/[EMIM]OAc solutions were continued to be used for further electrospinning. Indeed, 8 wt% BL/[EMIM]OAc was able to form a more stable Taylor cone but the ejected polymer stream still appeared to be discontinuous. Finally, 10 wt% BL/[EMIM]OAc was subjected for electrospinning and unfortunately, both Taylor cone and polymer stream appeared to be very unstable.

Table 7.2. Information of BL/[EMIM]OAc solutions with the addition of co-solvents

BL/IL solution	Viscosity	Observations	Relative figure
5 wt% BL/[EMIM]OAc	540 cP	Unstable Taylor cone, discontinuous stream produced	2
5 wt% BL/[BMIM]Cl	1584 cP	No continuous stream produced	3
5 wt% BL/[AMIM]Cl	447 cP	No continuous stream produced	4
8 wt% BL/[EMIM]OAc	1437 cP	Stable Taylor cone, discontinuous stream	5
10 wt% BL/[EMIM]OAc	2574 cP	Unstable Taylor cone, discontinuous stream produced	6

When 5wt% BL/[EMIM]OAc was used in electrospinning for a tip to collector distance of 10 cm, the Taylor cone with an ejected polymer stream was observed in some trials but were very unstable since the Taylor cones induced were wagging severely and so, the Taylor cone ejected polymer stream was moving from side to side very quickly. As shown in Figure 7.3a, the trial was conducted at 10 cm, 1.5 mL/h and 15 kV, the polymer stream ejected was moving from left to right very quickly. When the flow rate was increased to 2.0 mL/h, the motion was suppressed but not too significantly as the unstable Taylor cone and moving polymer stream could still be seen (Figure 7.3b). In order to further suppress the motion, the height was increased and a much greater flow rate used. In Figure 7.3c, a still Taylor cone with a polymer stream is shown when the trial was conducted using 15 cm, 4.0 mL/h and 12 kV. However, this phenomenon only occurred for 2–3 s and a large flow of droplets were produced continuously at this flow rate.
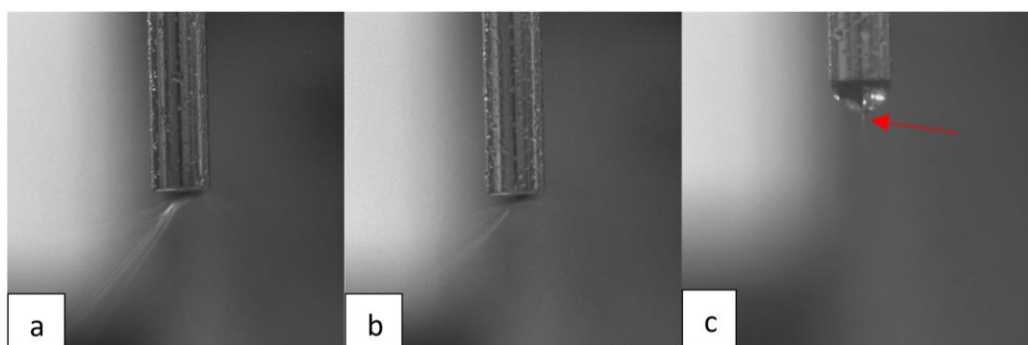
Figure 7.3. Electrospinning of 5wt% BL/[EMIM]OAc at conditions, (a) 10 cm, 1.5 mL/h, 15 kV; a(b) 10 cm, 2.0 mL/h, 15 kV and (c) 15 cm, 4.0 mL/h, 12 kV

It was not possible to electrospin 5 wt% BL/[BMIM]Cl at all. As demonstrated by the trials using a height of 10 cm and flow rate of 0.2 mL/h, the polymer solution was stretched in to a long conical shape at 8.5 – 12 kV to produce fine droplets (Figure 7.4a); the size reduced at 15 kV but a Taylor cone was not induced (Figure 7.4b); and when voltage was further increased to 18 – 22 kV, multi-jet spattering and splashing of polymer solution occurred and a Taylor cone was not observed (Figure 7.4c).
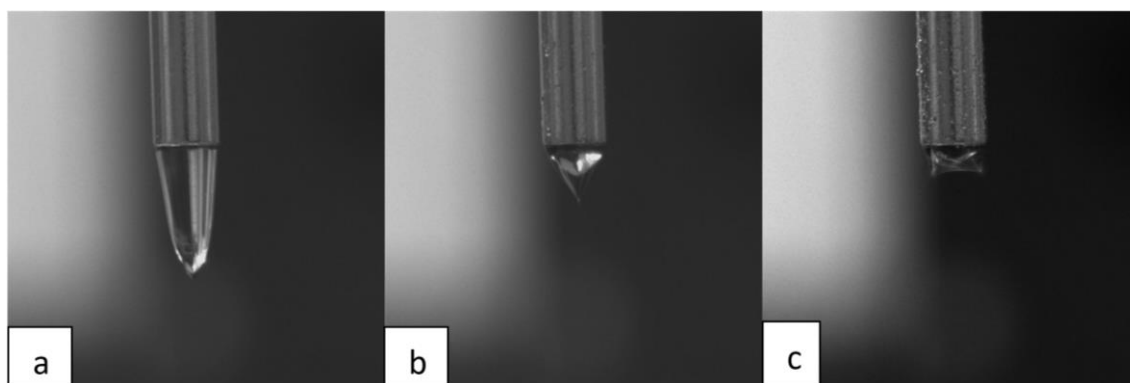
Figure 7.4. Transition of polymer solution to Taylor cone of 5 wt% BL/[BMIM]Cl at condition at 10 cm, 0.2 mL/h, (a) 8.5 – 12 kV; (b) 15 kV and (c) 18 – 22 kV

It was not possible to electrospin 5 wt% BL/[AMIM]Cl. A trend can be demonstrated using the trials at a height of 10 cm and flow rate of 0.2 mL/h: an oscillating cone was observed for a voltage of 8.5 – 10 kV to produce fine droplets (Figure 7.5a); the cone stopped oscillating at a voltage of 12 – 15 kV to spatter polymer solution (Figure 7.5b); and for a voltage of 18 – 22 kV, a Taylor cone was not observed and the polymer solution was only spattered more quickly and vigorously (Figure 7.5c).
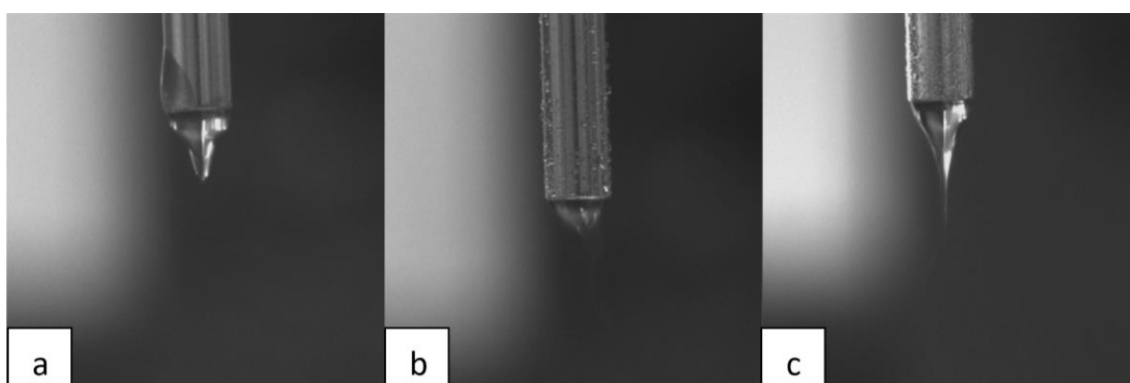
Figure 7.5. Transition of polymer solution to Taylor cone for 5wt% BL/[AMIM]Cl at condition at 10 cm, 0.2 mL/h, (a) 8.5 – 10 kV; (b) 12 – 15 kV and (c) 18 – 22 kV

Therefore, dissolution as well as electrospinning of BL were not further conducted using [BMIM]Cl and[AMIM]Cl.

An attempt was made to electrospin 8wt% BL/[EMIM]OAc with the specific goal to see if a more stable Taylor cone, with continuous flow stream could be spun, due to the increased concentration of BL. The spinnability was improved and Taylor cones were observed at all heights although the parameters applied were not the same when different tip to collector distances were used. For example, it is very clear that a big Taylor cone was induced at 10 cm, 0.5 mL/h and 10 kV with a constant moving polymer stream ejected (Figure 7.6a); at 15 cm, a Taylor cone was observed which was stable at 0.5 mL/h and 12 kV to eject a polymer stream (Figure 7.6b); and at 20 cm, the Taylor cone induced at 2.0 mL/h and 15 kV also appeared to be very stable and a polymer stream was ejected (Figure 7.6c). Although stable Taylor cones were observed with this polymer solution, the stream ejected was not continuous. In addition, the BL fibres could not stay intact when they reached the water coagulation bath.
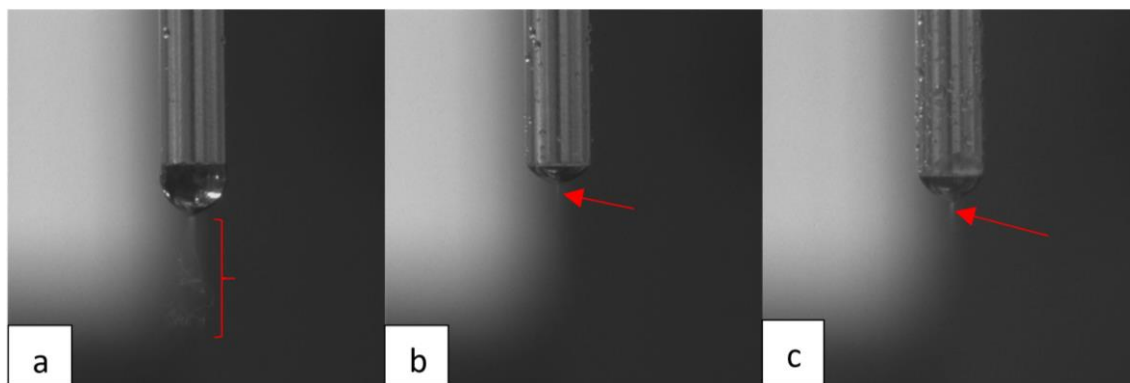
Figure 7.6. Taylor cones of 8 wt% BL/[EMIM]OAc at condition at (a) 10 cm, 0.5 mL/h, 10 kV; (b) 15 cm, 0.5 mL/h, 12 kV and (c) 20 cm, 2.0 mL/h, 15 kV

Finally, 10wt% BL/[EMIM]OAc was subjected to electrospinning to check whether the performance of electrospinning with higher BL content. However, almost all the Taylor cones appeared using this polymer solution were very unstable. Typically, when a Taylor cone was induced the ejected polymer stream wagged from side to side and spattered in random directions. For example, a clear picture was taken at 10 cm, 0.8 mL/h, 15 kV for which it can be seen that a cone and a ejected stream was moving from side to side (Figure 7.7a). The only stable Taylor cone with a constant polymer stream was observed in a particular trial conducted using 15 cm, 0.8 mL/h and 12 kV (Figure 7.7b). When a height of 20 cm was used, all Taylor cones and the ejected polymer streams wagged from side to side, as demonstrated by the trials with parameters of 0.8 mL/h and 8.5 kV (Figure 7.7c). Unfortunately, the fibres produced were weak and broke easily in the coagulation bath.
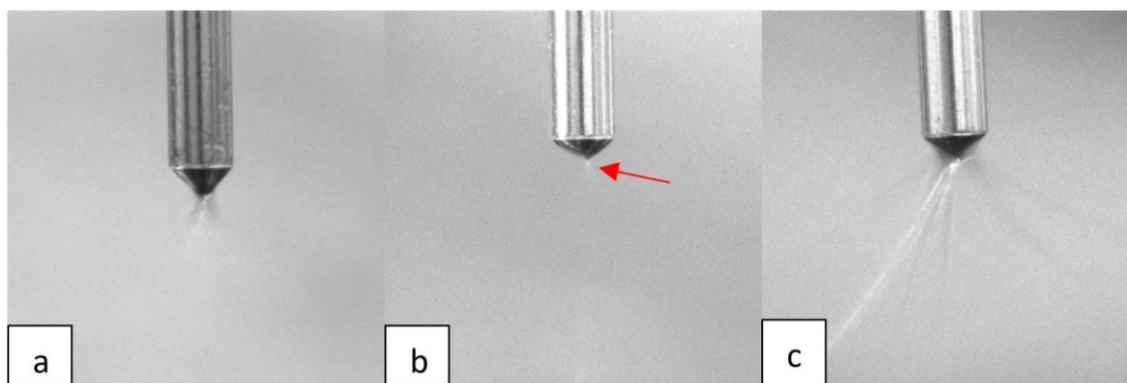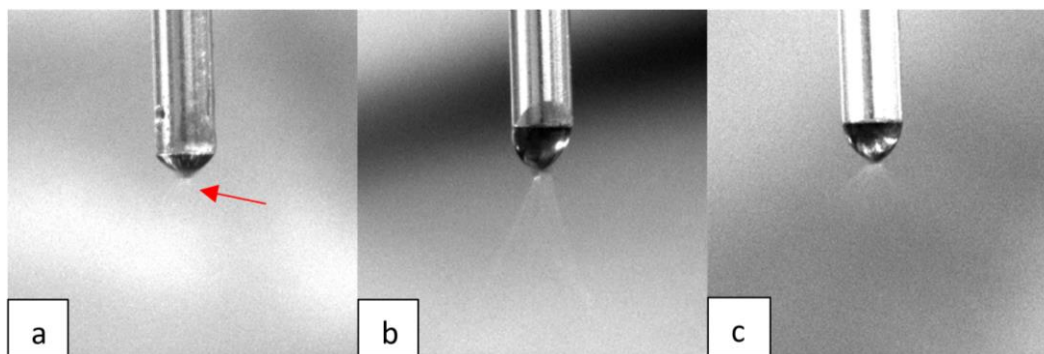
Figure 7.7. Taylor cones of 10 wt% BL/[EMIM]OAc at condition at (a) 10 cm, 0.8 mL/h, 15 kV; (b) 15 cm, 0.8 mL/h, 12 kV and (c) 20 cm, 0.8 mL/h, 8.5 kV

7.2 Electrospinning of BL/[EMIM]OAc with co-solvents

In comparison to using [BMIM]Cl and [AMIM]Cl to electrospin BL, [EMIM]OAc was a better choice as a solvent because of the formation of polymer stream. However, the polymer fibres ejected were discontinuous and cannot be coagulated in the water bath. Hence, co-solvents were introduced in the later stage of electrospinning with BL/[EMIM]OAc. Y. Ahn *et. al*. electrospun lignocellulosic biomass from hemp using [EMIM]OAc as the solvent with the aid of DMF as co-solvent. The purpose of introducing a co-solvent was to decrease the surface tension of the spinning solution. In addition, this could increase the conductivity but decrease the viscosity of the IL solution.[443] Consequently, DMF and DMSO chosen as co-solvents and added to the 10 wt% BL/[EMIM]OAc solutions and this solution electrospun and relevant observation are listed in Table 3 below. DMF and DMSO were chosen as the co-solvents as they do not induce the precipitation of the dissolved BL in IL especially lignin. As lignin is a key polymer to enhance antimicrobial properties, the choice of co-solvents were chosen carefully. All samples listed in Table 7.3 below were prepared by adding co-solvent to 10wt% BL/[EMIM]OAc and detailed observations are discussed below. After testing electrospinning at different conditions such as tip-to-collector distances, voltages and flow-rates, images of the stable Taylor cones were capture and shown below.

Table 7.3. Information of BL/[EMIM]OAc solutions with the addition of co-solvents

Concentration of BL	Ratio of IL/co-solvent	Viscosity	Observations in electrospinning
8 wt%	4:1 – IL **54**/DMF	780 cP	Electrospray, unstable stream
8 wt%	4:1 – IL **54**/DMSO	1011 cP	Electrospray, unstable stream
5 wt%	1:1 – IL **54**/DMF	72 cP	Electrospray, very unstable stream
5 wt%	1:1 – IL **54**/DMSO	168 cP	Electrospray, unstable stream
5 wt%	5:3 – IL **51**/DMF	139 cP	Electrospray, unstable stream
5 wt%	5:3 – IL **51**/DMSO	252 cP	Electrospinning, fibres can be collected for SEM

7.2.1 Electrospinning of 8 wt% BL in 4:1 IL/co-solvent

DMF was added to 10wt% BL/[EMIM]OAc to prepare a 8wt% BL/(4:1)[EMIM]OAc-DMF solution for electrospinning. The Taylor cone and polymer stream observed were unstable because the ejected streams were often wagging from side to side and discontinuous. Some Taylor cones appeared to be slightly more stable, e.g. at 10 cm, 2.0 mL/h and 11 kV which was small and the ejected stream was discontinuous (Figure 7.8a). At 15 cm, 0.2 mL/h and 8.5 kV, a bigger Taylor cone was induced with a long polymer stream that was wagging quickly below the cone (Figure 7.8b); and at 20 cm, 1.0 mL/h and 8.5 kV, a Taylor cone was seen but the polymer stream was wagging so severely to give discontinuous fibres (Figure 7.8c). Unfortunately, such phenomenon was not persistent and fibres could not stay intact and dispersed in the water coagulation bath.
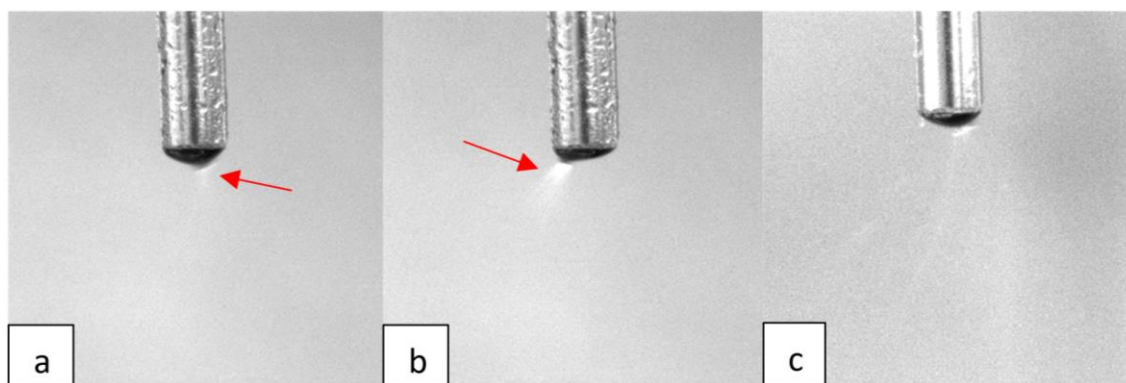

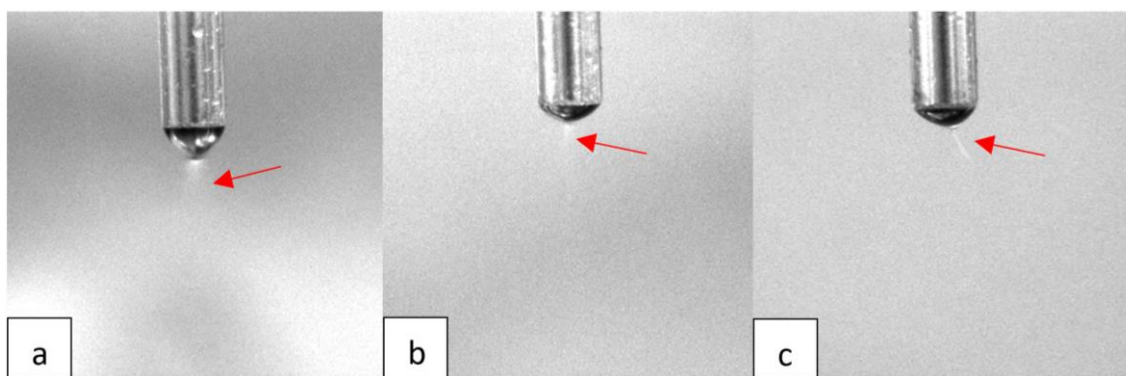*Figure 8*. Taylor cones of 8 wt% BL/(4:1)[EMIM]OAc-DMF at condition at (a) 10 cm, 2.0 mL/h, 12 kV; (b) 15 cm, 0.2 mL/h, 8.5 kV and (c) 20 cm, 1.0 mL/h, 8.5 kV

Similarly, DMSO was added to 10 wt% BL/[EMIM]OAc to prepare a 8 wt% BL/(4:1) [EMIM]OAc-DMSO but again the electrospinning process was often unstable. As demonstrated by the trial for a distance of 10 cm, 1.5 mL/h and 10 kV, a Taylor cone was formed and the polymer stream was wagging (Figure 7.9a); at 15 cm, 0.5 mL/h and 8.5 kV, a smaller Taylor cone formed but an ejected stream of polymer moved from side to side (Figure 7.9b); the Taylor cone seemed slightly more stable at 20 cm, 1.0 mL and 22 kV but the it was not persistent and the ejected stream of polymer was discontinuous (Figure 7.9c). Overall improvements were not significant and it proved difficult to produce continuous fibres.
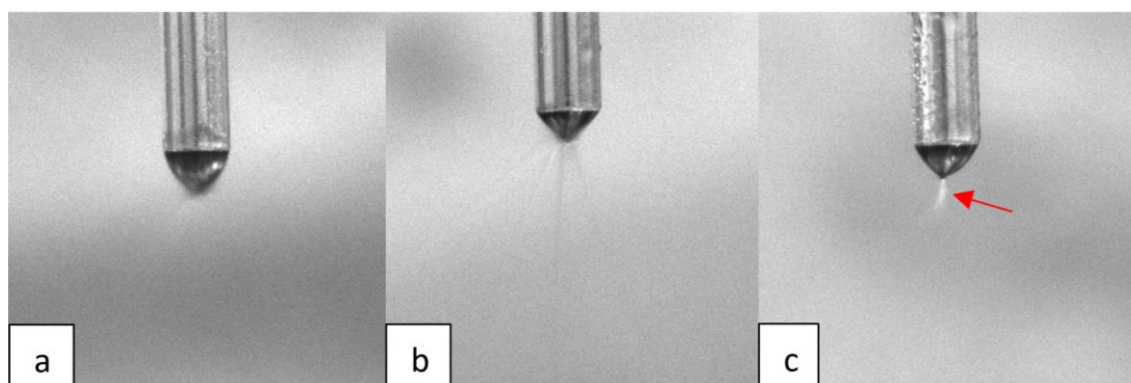
Figure 7.9. Taylor cones for 8 wt% BL/(4:1)[EMIM]OAc-DMF at condition at (a) 10 cm, 1.5 mL/h, 10 kV; (b) 15 cm, 0.5 mL/h, 8.5 kV and (c) 20 cm, 1.0 mL/h, 22 kV

7.2.2 Electrospinning of 5 wt% BL in 1:1 IL/co-solvent

After examining 8 wt% BL in 4:1 IL/co-solvent for electrospinning, more co-solvents were introduced to prepare 5 wt% BL in 1:1 IL/co-solvent. These samples prepared consisted of the highest ratio of co-solvent compared to the rest. The aim was to see the consequences of further introduction of co-solvent which led to low values of viscosity of polymer solution in the electrospinning.

First, DMF was added to 10 wt% BL/[EMIM]OAc to prepare a 5 wt% BL/(1:1) [EMIM]OAc-DMF however, electrospinning was even more difficult and the Taylor cone with a polymer stream appeared only in a few trials. At the height of 10 cm, the Taylor cone with a polymer stream was only seen for a flow rate of 1.5 mL/h and an applied voltage of 10 kV were applied but again the polymer stream wagged (Figure 7.10a); at 15 cm, the Taylor cone was seen at 0.8 mL/h and 15 kV but the stream was also unstable and discontinuous (Figure 7.10b); although the Taylor cone appeared in more than one trial when a height of 20 cm was used but, the ejected stream moved erratically and more vigorously (Figure 7.10c).
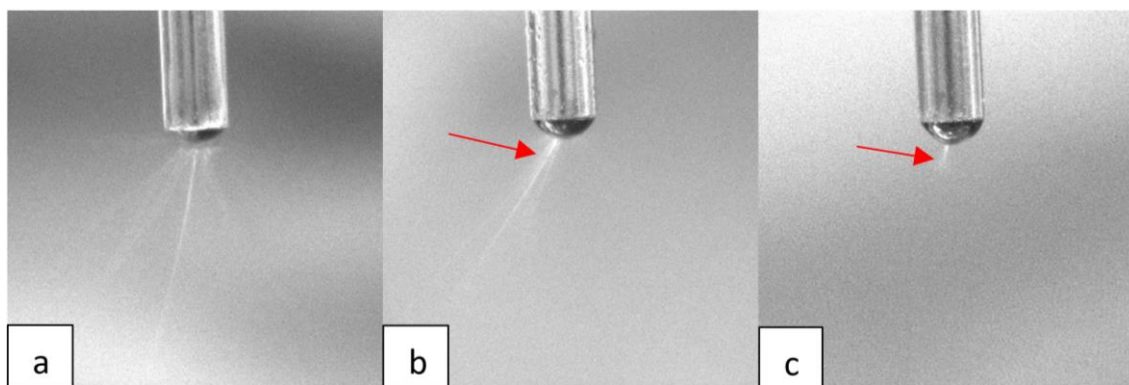
Figure 7.10. Taylor cones of 5 wt% BL/(1:1)[EMIM]OAc-DMF at condition at (a) 10 cm, 0.8 mL/h, 15 kV; (b) 15 cm, 0.8 mL/h, 15 kV and (c) 20 cm, 0.5 mL/h, 10 kV

When DMSO was used instead of DMF to dilute 10 wt% BL/[EMIM]OAc to make 5 wt% BL/(1:1) [EMIM]OAc-DMSO, spinnability improved although Taylor cones appeared to be unstable with a discontinuous polymer stream. Taylor cone induced with polymer stream was wagging more severely at height of 10 cm such as the trials at 1.0 mL/h, 10 kV (Figure 7.11a). When the tip to collector distance was increased, the motion of the Taylor cone and polymer stream was suppressed but, the effect was not persistent as droplets were often produced constantly. For example, a stationary Taylor cone was formed when the parameters were set to 15 cm, 0.8 mL/h and 10 kV and a polymer stream was ejected (Figure 7.11b) and a very similar effect was observed for parameters of 20 cm, 0.2 mL/h, 12 kV (Figure 7.11c). However, the difficulty of producing a smooth continuous fibre was remained a challenge.
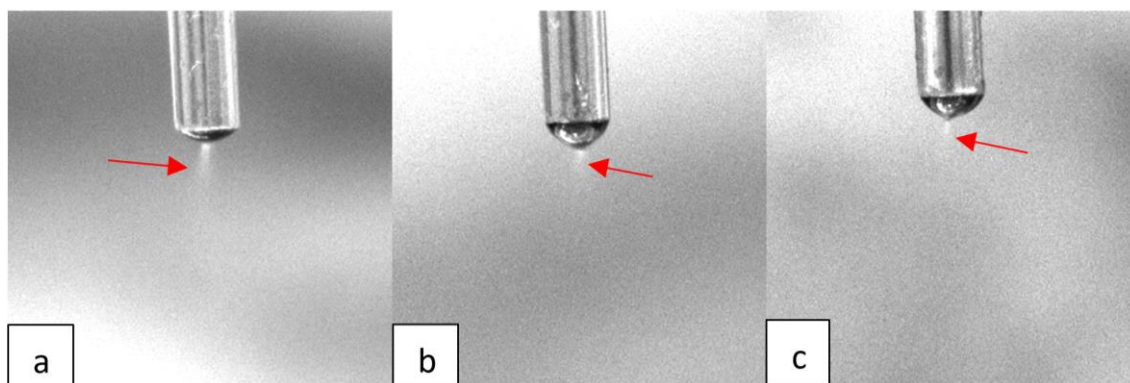

Figure 7.11. Taylor cones of 5 wt% BL/(1:1)[EMIM]OAc-DMF at condition at (a) 10 cm, 1.0 mL/h, 10 kV; (b) 15 cm, 0.8 mL/h, 10 kV and (c) 20 cm, 0.2 mL/h, 12 kV

7.2.3 Electrospinning of 5 wt% BL in 5:3 IL/co-solvent

After testing two different IL/co-solvent ratios for electrospinning, the difficulty of having discontinuous stream continued to occur. In fact, BL solution with IL/co-solvent in the ratio of 1:1 appeared to be more unstable compared to the ratio of 4:1 IL/co-solvent

because it was noticed that electrospraying occurred that led to formation of droplets instead of polymer stream. Hence, ratio of IL/co-solvent was changed to 5:3 to increase the viscosity of the BL solutions.

5 wt% BL/(5:3)[EMIM]OAc-DMF was prepared by diluting 8 wt% BL/[EMIM]OAc with DMF and an attempt to electro-spin this solution. Taylor cones were observed but most were unstable at heights of 10 and 15 cm. A clear image of Taylor cone was captured for the trial conducted at 10 cm, 0.5 mL/h, 8.5 kV for which it can be observed that the Taylor cone and ejected was wagging severely (Figure 7.12a); similarly, wagging cone observed at 15 cm, as demonstrated when trial conducted at 0.2 mL/h and 18 kV (Figure 7.12b). When the height increased to 20 cm, the motion of the Taylor cone and polymer stream was suppressed in some trials such as with 0.5 mL/h, 15 kV (Figure 7.12c).

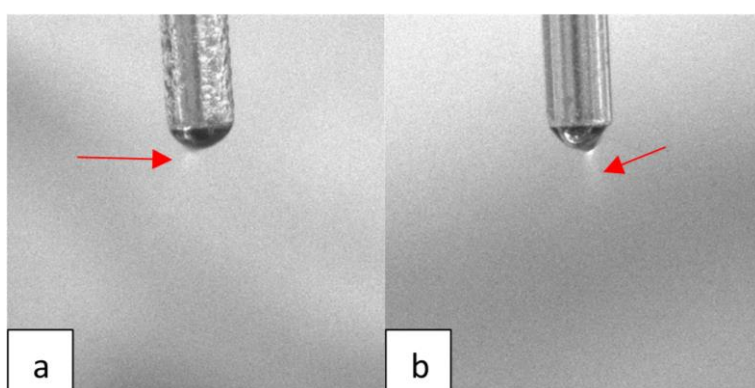*Figure 7.12.* Taylor cones of 5 wt% BL/(5:3)[EMIM]OAc-DMF at condition at (a) 10 cm, 0.5 mL/h, 8.5 kV; (b) 15 cm, 0.2 mL/h, 18 kV and (c) 20 cm, 0.5 mL/h, 15 kV

When DMSO was used instead of DMF to prepare 5 wt% BL/(5:3)[EMIM]OAc-DMSO for electrospinning, most Taylor cones appear to be stable and wagging polymer stream were observed less often. In some trials, the electrospinning processes were more persistent which could lasted for 6 – 8 s. At height of 10 cm, parameters of 1.0 mL/h and 8.5 kV were applied to result a small Taylor cone with a polymer stream ejected (Figure 7.13a); at 15 cm, parameters of 1.0 mL/h and 8.5 kV were used to give a slightly bigger Taylor cone with polymer stream (Figure 7.13b); and at 20 cm with the parameters of 1.0 mL/h 12 kV, the Taylor cone induced was also very stable and a polymer stream was ejected (Figure 7.13c).

Figure 7.13. Taylor cones of 5 wt% BL/(5:3)[EMIM]OAc-DMSO at condition at (a) 10 cm, 1.0 mL/h, 8.5 kV; (b) 15 cm, 1.0 mL/h, 8.5 kV and (c) 20 cm, 1.0 mL/h, 12 kV

Electrospinning process using 5 wt% BL/(5:3)[EMIM]OAc-DMSO appeared to be the most stable compared to other BL/IL solutions. Although the polymer stream ejected was discontinuous and further improvements are required in order to produce fibre-mat or membrane, two BL fibres were collected and examined using SEM. Only two BL fibres could be collected due to the discontinuous streams with high amount of droplets produced during the electrospinning process. In addition, most electrospun fibres could not stay intact after being soaked in the water coagulation bath for removing the IL **54**. The first fibre was collected using parameters of 10 cm, 1.5 mL/h and 22 kV (Figure 7.14a) which had a length of *ca*. 7 cm and the second fibre was collected using parameters of 15 cm, 1.0 mL/h and 18 kV which had a length of *ca*. 1 cm. They were soaked in distilled water for 24 h to remove IL **54** and followed by drying in a vacuum dessicator for overnight. They were then examined using SEM.

Figure 7.14. Taylor cones of 5 wt% BL/(5:3)[EMIM]OAc-DMSO at condition at (a) 10 cm, 1.5 mL/h, 22 kV; (b) 15 cm, 1.0 mL/h, 18 kV

The first fibre collected at the tip to collector distance of 10 cm is composed of beaded fibres (Figure 7.15a). When higher magnification was applied, it can be seen that the

fibres consist of uneven surface with diameter typically range in 600 – 1000 nm and they tend to connect to each other tightly (Figure 7.15b). When higher magnification was applied further, fibres with diameter of *ca*. 300 cm was found and it can be seen that they are bent and knotted fibre (Figure 7.15c).
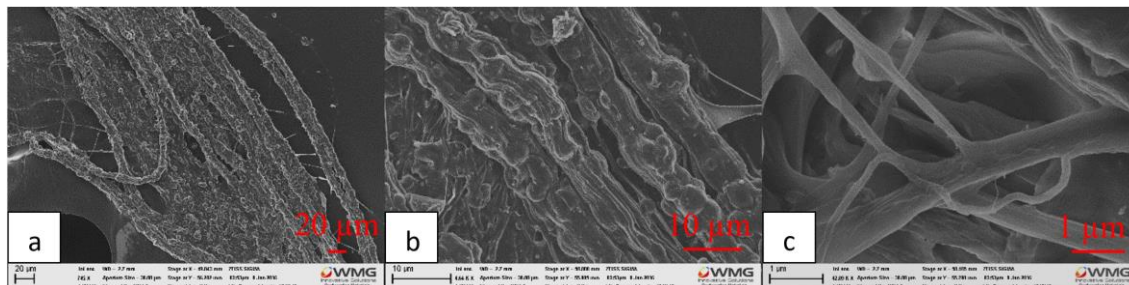
Figure 7.15. SEM images of BL fibres collected at 10 cm: (a) low magnification, (b) higher magnification (c) high magnification to show the details of BL fibres

The BL fibre collected at the tip to collector distance of 15 cm which is also composed to beaded fibres with very uneven surface (Figure 7.16a). When higher magnification was used to examine the fibre, it can be seen that the fibres have diameters in the range of 600 – 1900 nm (Figure 7.16b, c). Unlike the fibre collected at height of 10 cm, individual fibre can be seen more clearly and it can also be observed that the fibres are aligned in the same direction.
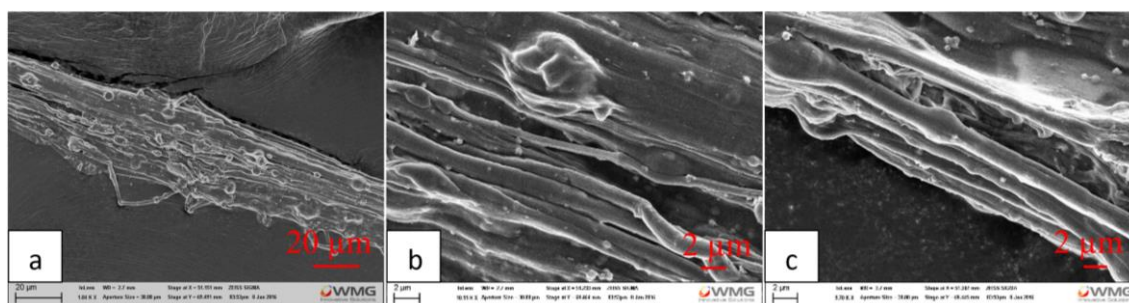
Figure 7.16. SEM images of BL fibres collected at 15 cm: (a) low magnification, (b), (c) higher magnification

It is indeed the first set of experiments conducted that used BL and IL in electrospinning to produce fibres. Although further improvements are required to achieve better spinnability in order to prepare fibres with uniform morphology, the likelihood of electrospinning using BL is clearly shown.

In summary, various electrospinning conducted using bio-materials/IL solutions. Before bio-materials/IL solutions were used in electrospinning, experiments were conducted using 10 wt% PVA/H$_2$O with addition of ILs which demonstrated the influence of ILs in

electrospinning process as well as morphology of the polymer structures. Electrospinning of chitin/IL solutions were proven to be very challenging as chitin/IL solutions that were available for electrospinning were limited due to the low solubility of chitin (**8**) as well as high viscosities of certain solutions. Moreover, formation of gel with the applied voltage was the major drawback during the electrospinning of chitin/IL. Electrospinning of lignin/IL solutions were shown to be difficult and addition of co-solvents could not improve the electrospinning process at all. Finally, [EMIM]OAc was a more effective solvent to dissolve BL and albeit unstable, electrospinning of BL/[EMIM]OAc was observed to give BL fibres. Addition of co-solvents to BL/[EMIM]OAc could improve the electrospinning but further work ought to be done in order to produce continuous BL fibres.

7.3 Entanglement of Ionic Liquids and Biopolymers

In order to gain further understanding with regards to biopolymer/IL electrospinning. Additional measurements such as oscillatory rheology and FTIR were completed. In addition, different biopolymers such as chitin, lignin are also included in this section to provide different comparisons. Herein, values of viscosity of various biopolymer/IL solutions as well as the brief electrospinning observations are shown below. As seen on the graphs, viscosity of solutions increases linearly with increasing biopolymer concentration. Unfortunately, most of these biopolymer/IL solutions are not suitable for electrospinning. Generally, formation of gel was a very major drawback when electrospinning chitin/IL solutions. On the other hand, electrospray and vigorous spatting of lignin/IL solutions occurred that prevented the formation of lignin polymer stream. In contrast, electrospinning using BL/[EMIM]OAc was shown to be possible although co-solvents are required to assist to formation of continuous polymer stream. Although viscosity of the polymer solution is a key factor to be considered during electrospinning, knowing the values of viscosity of the polymer solutions are not good enough when trying to explain the failure of electrospinning of most biopolymer/IL solutions. Therefore, oscillatory rheological data and FTIR data were collected for predicting the polymer entanglement and ultimately, the aim is to apply these data to understand the importance of polymer entanglement required for electrospinning.

Firstly, viscosities of the biopolymer/IL solutions were measured to determine whether they are suitable to be tested on the oscillatory rheometer.

In Figure 7.17, it can be seen that viscosity of [EMIM]OAc increased with increasing chitin content. Overall, formation of gel occurred when voltage applied during electrospinning (Table 7.4) that prevented the formation of chitin fibres.
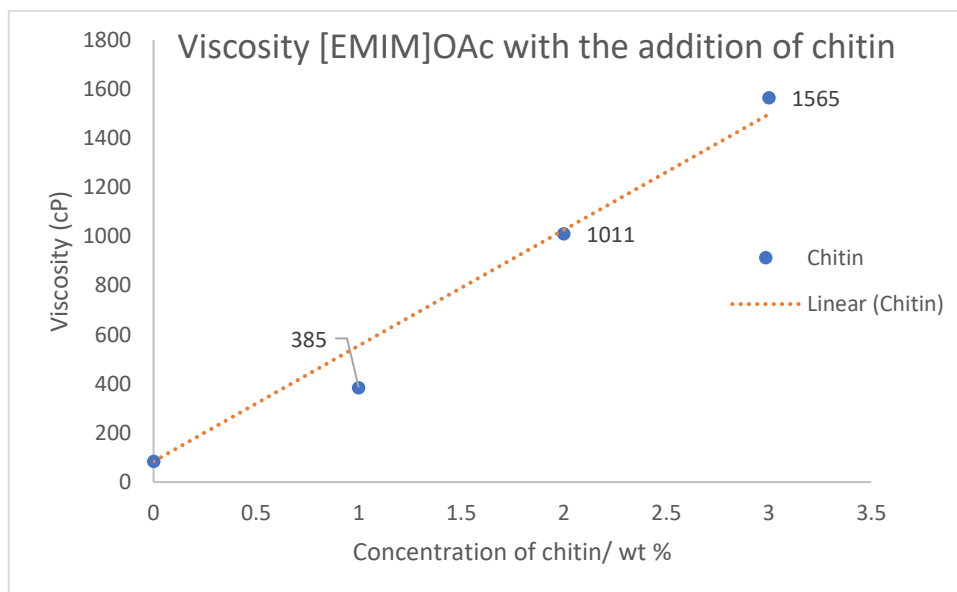

Figure 7.17. Variation in viscosity with concentration for chitin/[EMIM]OAc

Table 7.4. Results of electrospinning of 1-3 wt% chitin/[EMIM]OAc

Concentration of chitin	Observations during electrospinning
1 wt%	Formation of short, discontinuous gel when voltage was applied but Taylor cone and stable stream were not induced successfully
2 wt%	Formation of longer but also discontinuous gel when voltage was applied but Taylor cone and stable stream was not induced successfully
3 wt%	Formation of gel when voltage was applied but it coagulated at the spinneret's tip to cause clogging. The gel had to be wiped out in order to continue the process

In Figure 7.18, it can be seen that viscosity of [AMIM]Cl increased with increasing chitin content. Using chitin/[AMIM]Cl, electrospraying and formation of gel occurred when voltage applied during electrospinning (Table 7.5) that prevented the formation of chitin fibres. Electropsinning using 3 wt% chitin/[AMIM]Cl was particular challenging due to its very high viscosity as the polymer solution got stuck in the syringe.
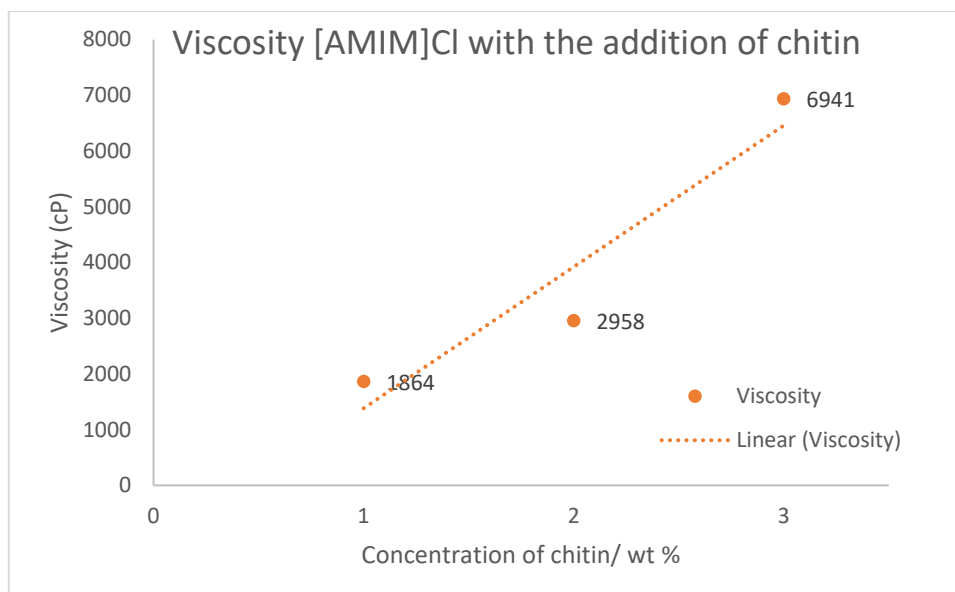
Figure 7.18. Graph of viscosity vs concentration of chitin/[AMIM]Cl

Table 7.5. Results of electrospinning of 1-3 wt% chitin/[AMIM]Cl

Concentration of chitin	Observations during electrospinning
1 wt%	Electrospraying occurred at lower heights using certain conditions but a continuous stream were not ejected and fibres were not produced
2 wt%	Taylor cones were observed but gelation occurred very quickly. Soft gels were ejected but continuous streams not ejected to produce fibres at all
3 wt%	Polymer solution is too viscous as it was stuck in the tubing and the syringe snapped when pressure was applied to push the polymer solution further

Unfortunately, chitin/[BMIM]Cl solutions were not available for electrospinning due to their very high values of viscosity as 1 wt% chitin/[BMIM]Cl has viscosity of 12250 cP and 2 wt% chitin[BMIM]Cl has viscosity of 15910 cP and 3 wt% chitin/[BMIM]Cl is a gel at room temperature.

Lignin was dissolved in [EMIM]OAc and the viscosities were measured (Figure 7.19) and solutions were subjected to electrospinning (Table 7.6). Although a stable Taylor cone with a continuous polymer stream produced during the electrospinning of 4 wt% lignin/[EMIM]OAc, such result could not be repeated and lignin fibres produced could not be collected successfully. Overall, spattering of lignin/[EMIM]OAc solution occurred

to prevent formation of lignin fibres were the major drawback when lignin/[EMIM]OAc was subjected to electrospinning.
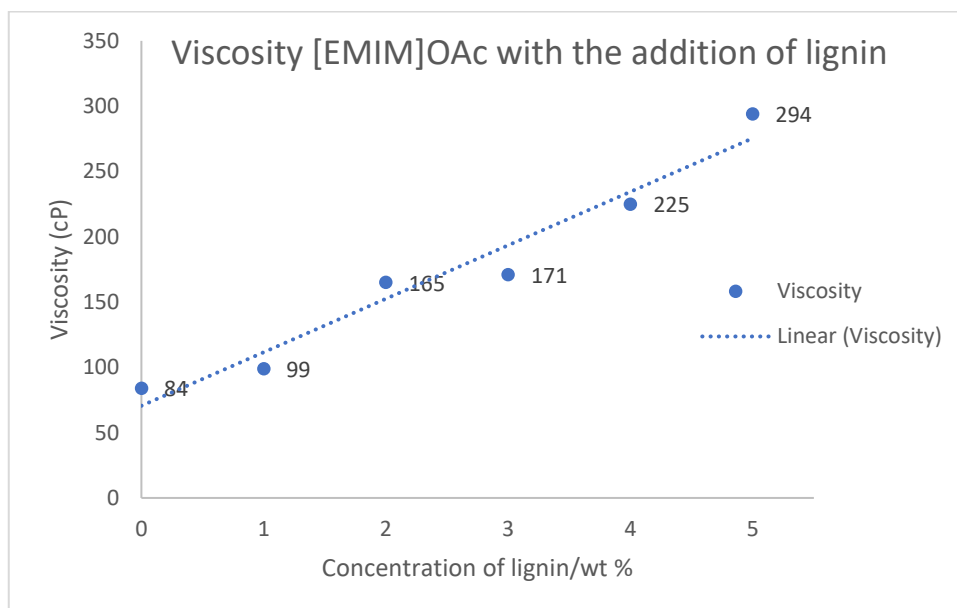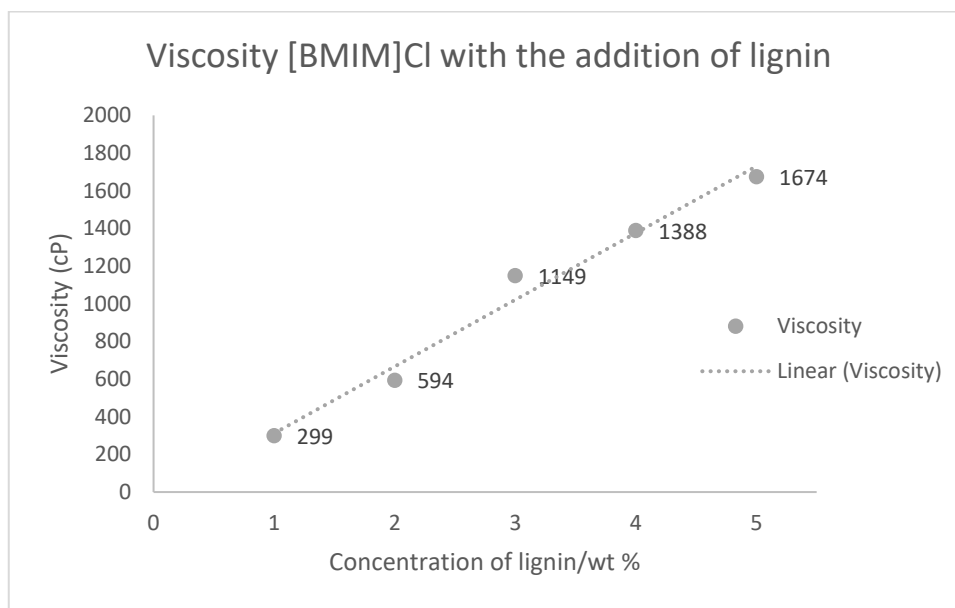

Figure 19. Graph of viscosity vs concentration of lignin/[EMIM]OAc solutions

Table 6. Results of electrospinning of 1-5 wt% lignin/[EMIM]OAc

Concentration of lignin	Observations during electrospinning
1 wt%	Continuous stream was not observed and only lignin/IL solution was spattered
2 wt%	Continuous stream was not observed and only lignin/IL solution was spattered
3 wt%	Continuous stream was not observed and only lignin/IL solution was spattered
4 wt%	A stable Taylor cone formed and continuous ejected at one condition but it only lasted for 20 s and such result was not repeatable to produce more fibres
5 wt%	Continuous stream was not observed and only lignin/IL solution was spattered

Similarly, lignin was also dissolved in [BMIM]Cl and the viscosities were measured (Figure 7.20) and solutions were subjected to electrospinning (Table 7.7). When lignin/[BMIM]Cl solutions were subjected to electrospinning, stable Taylor cone with a continuous polymer stream could not be induced. Electrospraying occurred when 1 and

3 wt% lignin/[BMIM]Cl solutions were used but lignin fibres could not be and collected in a water bath.
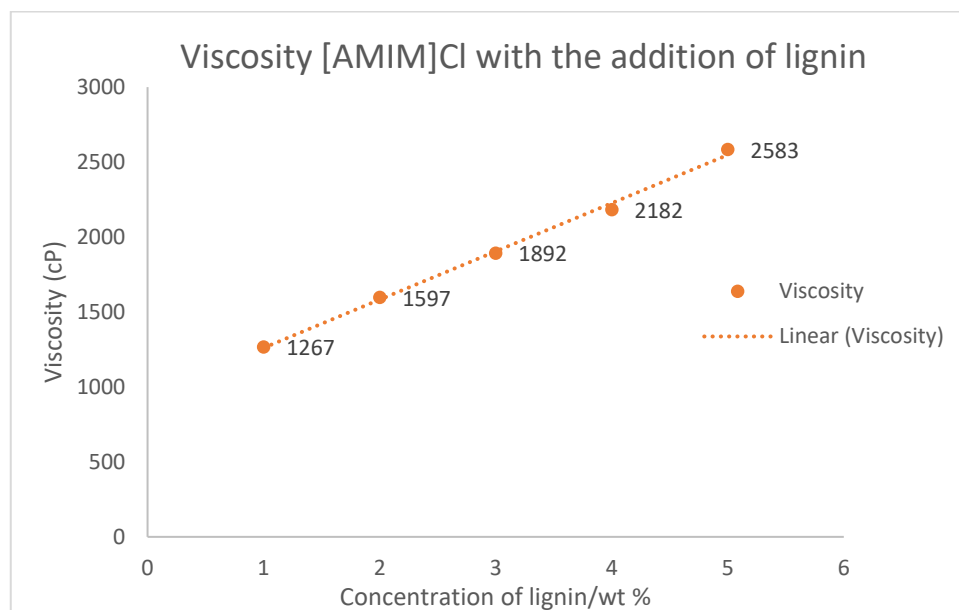

Figure 7.20. Graph of viscosity vs concentration of lignin/[BMIM]Cl solutions

Table 7.7. Results of electrospinning of 1-5 wt% lignin/[BMIM]Cl

Concentration of lignin	Observations during electrospinning
1 wt%	Electrospraying occurred but stable Taylor cone, continuous stream was not observed to produce fibres
2 wt%	Continuous stream was not observed and only lignin/IL droplets were spattered
3 wt%	Electrospraying occurred but stable Taylor cone, continuous stream was not observed to produce fibres
4 wt%	Continuous stream was not observed and only lignin/IL droplets were spattered
5 wt%	Continuous stream was not observed and only lignin/IL droplets were spattered

Solutions of lignin/[AMIM]Cl were also prepared and the viscosities were measured (Figure 7.21) and solutions were subjected to electrospinning (Table 7.8).The observations for electrospinning of lignin/[AMIM]Cl solutions were very similar to that of lignin/[BMIM]Cl. Overall, lignin/[AMIM]Cl solutions consist of much higher values of viscosity compared to all lignin/[EMIM]OAc and lignin/[BMIM]Cl with the same

lignin content. When 2 and 3 wt% lignin/[EMIM]OAc were used, electrospraying occurred but lignin fibres cannot be produced and collected in the coagulated bath.

Figure 7.21. Graph of viscosity vs concentration of lignin/[AMIM]Cl solutions

Table 7.8. Results of electrospinning of 1-5 wt% lignin/[AMIM]Cl

Concentration of lignin	Observations during electrospinning
1 wt%	Continuous stream was not observed and only lignin/IL droplets were spattered
2 wt%	Electrospraying occurred but stable Taylor cone, continuous stream was not observed to produce fibres
3 wt%	Electrospraying occurred but stable Taylor cone, continuous stream was not observed to produce fibres
4 wt%	Continuous stream was not observed and only lignin/IL droplets were spattered
5 wt%	Continuous stream was not observed and only lignin/IL droplets were spattered

Finally, a graph of viscosity vs concentration of BL/[EMIM]OAc solutions was also drawn and shown in Figure 7.22 below. As discussed, [EMIM]OAc is a much powerful solvent to dissolve BL compared to using other two ILs. When [AMIM]Cl and [BMIM]Cl were used to dissolve BL, most BL pieces remained intact. Moreover, electrospinning of BL/[EMIM]OAc was shown to be possible to produce BL fibres although incorporation

of co-solvent is required to produce continuous stream. Their oscillatory rheological data of these BL/IL solutions are then compared in order to further understand the different outcomes of electrospinning.
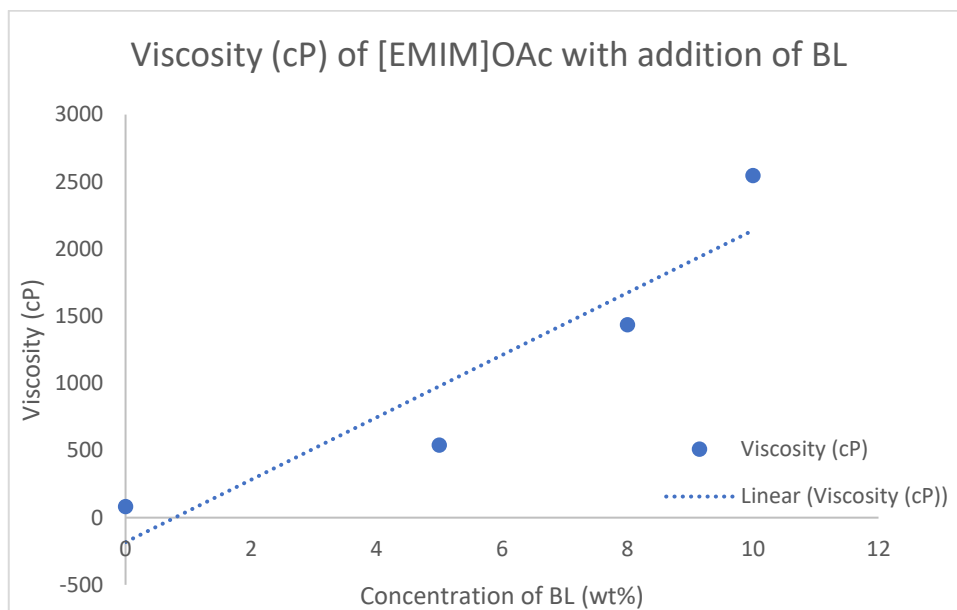

Figure 7.22. Graph of viscosity vs concentration of BL/[EMIM]OAc solutions

7.3.1 Oscillatory rheology

As Entanglement is one of the key features for electrospinning and so oscillatory rheological and FTIR data were collected to estimate the interactions between ILs and biopolymers. In this section, ionic liquids solutions of chitin and lignin are also included along with BL. The oscillatory rheometer is a useful tool to characterise the entanglements between the polymers and ILs.[444] By applying the oscillatory rheometer, the viscoelastic properties of the polymer solutions can be obtained which can then be used to estimate their molecular weight between entanglements (M_e). This quantity can represent the spacing between two neighbouring entanglements in a polymer solution or the entanglements present in a system.[445] On the other hand, fourier transform infrared spectroscopy (FTIR) was also used to analyse the polymer/IL mixtures which is one of the fastest and most convenient method to determine the inter- and intramolecular interactions.[446] The aim of this study is to indicate whether the rheological properties can be explained or whether different biomaterial – ionic liquid system exhibit different inter- and intra-molecular interactions by analysing the relative FTIR data.

The G' (storage modulus/elastic component) and G'' (loss modulus/viscous component) curves obtained using the oscillatory rheometer which can then be used to plot the curve for loss tangent ($\tan \delta = \frac{G'}{G''}$). Using all these curves, the plateau modulus (G_N^0) can be

obtained which defined as the G' value where $\tan \delta$ is at minimum.[447] The molecular weight between entanglements (M_e) can be calculate using equation, $M_e = \frac{10^3 cRT}{G_N^0}$ where c = mass concentration/density of polymer solution, R = gas constant (8.314 $JK^{-1}mol^{-1}$)[448] and T = temperature in kelvin (298.15 K).[449]

All values of M_e of different biopolymer/IL solutions are listed in Table 7.9 below. Full details with regards to the relevant measurements are discussed later in this chapter. Overall, it is noticed that 2 wt% chitin/[EMIM]OAc and 5 wt% BL/[EMIM]OAc consist of the two highest values of M_e of 4.63 x 10^{10} and 7.30 x 10^7 respectively as highlighted in Table 9. The former biopolymer/IL solution led to formation of gel during electrospinning but the latter exhibited the possibility of producing biopolymer fibres using electrospinning. These results have implied that a certain value of M_e is required for electrospinning but when the value is too high, this could bring negative outcome such as formation of gel as displayed by the 2 wt% chitin/[EMIM]/OAc.

Table 7.9. Values of M_e for a selection of biopolymer/IL solutions

Polymer solution	Value of M_e
2 wt% chitin/[AMIM]/Cl	2.54 x 10^6
2 wt% chitin/[BMIM]/Cl	2.58 x 10^6
2 wt% chitin/[EMIM]/OAc	4.63 x 10^{10}
5 wt% lignin/[AMIM]/Cl	2.33 x 10^6
5 wt% lignin/[BMIM]/Cl	7.70 x 10^5
5 wt% lignin/[EMIM]/OAc	1.36x 10^6
5 wt% BL/[AMIM]/Cl	2.47 x 10^6
5 wt% BL/[BMIM]/Cl	5.79 x 10^5
5 wt% BL/[EMIM]/OAc	7.30 x 10^7

7.3.1.1 Oscillatory rheological data for chitin/IL solutions

The results for chitin/IL solution are tabulated in Table 7.10 and the relevant graphs are shown below. Although both electrospinning of 2 wt% chitin/[AMIM]Cl and chitin/[EMIM]OAc induced formation of gel when voltage was applied, the latter has a much higher value of M_e. Although 2 wt% chitin/[BMIM]Cl has a very high viscosity of 12250 cP, its value of M_e is very similar to that of 2 wt% chitin/[AMIM]Cl. Hence, these results can

imply that the molecular weight between entanglements (M_e) are independent from their values of viscosity.

Table 7.10. Values of M_e for chitin/ionic liquid solutions

Polymer solution	2 wt% chitin/[AMIM]Cl	2 wt% chitin/[BMIM]Cl	2 wt% chitin/[EMIM]OAc
M_e	2.54 x 10^6	2.58 x 10^6	4.63 x 10^{10}

According curves in Figure 7.23, most G'' values are higher than that of G' which indicate the polymer solution has a stronger viscous character. With the aid of $\tan\delta$ curve, G_N^0 was determined to be 1291.55 Pa and so, M_e of 2 wt% chitin/[AMIM]Cl is 2.54 x 10^6
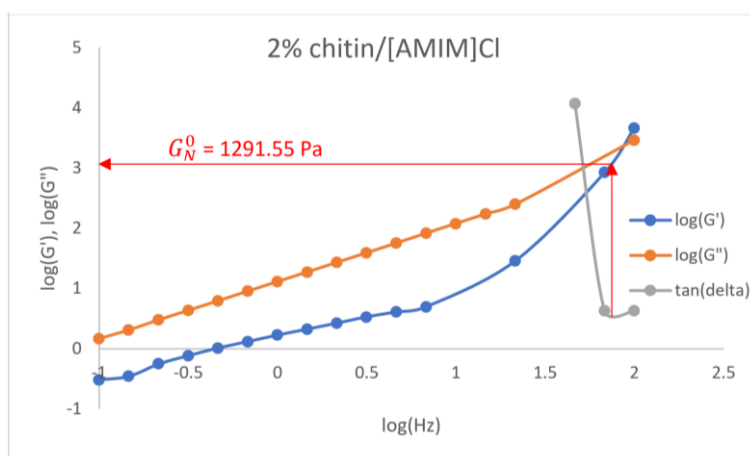
Figure 7.23. $\log(G')$ $\log(G'')$ and $\tan\delta$ curves for 2 wt% chitin/[AMIM]Cl

The curves obtained for 2 wt% chitin/[BMIM]Cl (Figure 7.24) have similar pattern compared to that of 2 wt% chitin/[AMIM]Cl since the solution also displayed a stronger viscous character. With G_N^0 determined to be 1199.35 Pa, M_e of 2 wt% chitin/[BMIM]Cl is 2.58 x 10^6.
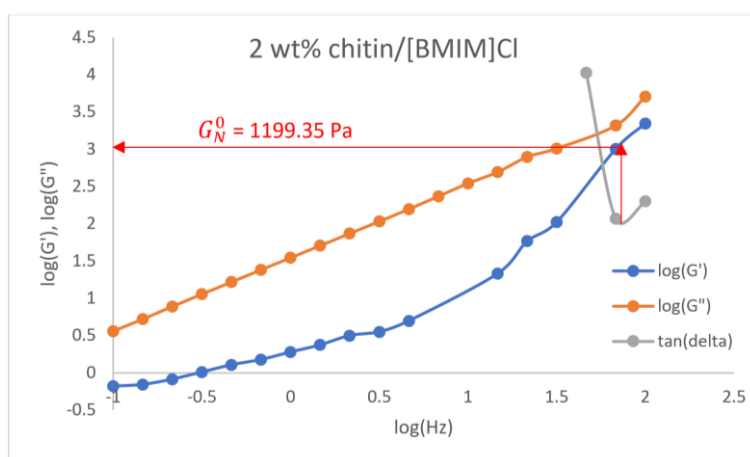
Figure 7.24. $\log(G')$, $\log(G")$ and $\tan\delta$ curves for 2 wt% chitin/[BMIM]Cl

In contrast, 2 wt% chitin/[EMIM]OAc exhibited totally different pattern (Figure 7.25). This material has a stronger elastic character in general. With a lower number of G_N^0 determined to be 645.80 Pa, 2 wt% chitin/[EMIM]OAc has a much higher M_e value of 4.63×10^{10}.
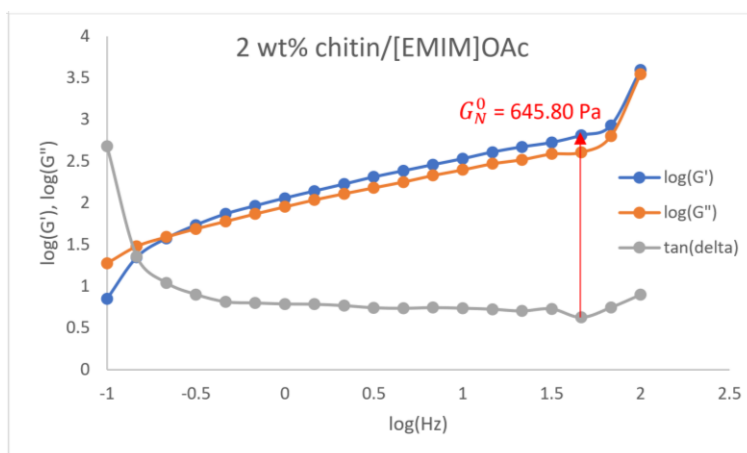
Figure 7.25. $\log(G')$, $\log(G")$ and $\tan\delta$ curves for 2 wt% chitin/[EMIM]OAc

7.3.1.2 Oscillatory rheological data for lignin/IL solutions

The results for lignin/IL solution are tabulated in Table 7.11 and the relevant graphs are shown below. 5 wt% lignin/IL solutions were measured as slippage often occurred between the parallel plates when measuring the lignin/IL solutions consisted of lower lignin content, especially for lignin/[EMIM]OAc which consist of viscosity below 300cP.

Table 7.11. Values of M_e for lignin/ionic liquid solutions

Polymer solution	5 wt% lignin/[AMIM]Cl	5 wt% lignin/[BMIM]Cl	5 wt% lignin/[EMIM]OAc
M_e	2.33×10^6	7.70×10^5	1.36×10^6

5 wt% lignin/[AMIM]Cl (Figure 7.26) showed overall stronger viscous character. G_N^0 was determined to be 1291.55 Pa and its value of M_e is 2.33×10^6.
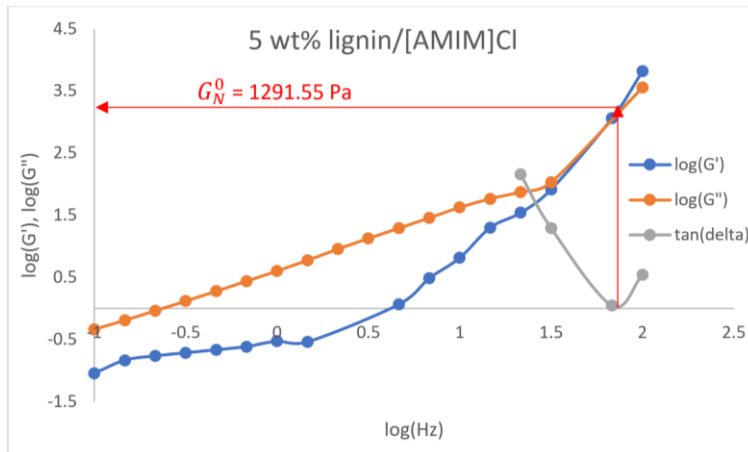
Figure 7.26. $\log(G')$, $\log(G'')$ and $\tan\delta$ curves for 5 wt% lignin/[AMIM]Cl

5 wt% lignin/[BMIM]Cl (Figure 7.27) also showed overall stronger viscous character. G_N^0 was determined to be 4197.98 Pa and has a slightly lower value of M_e, 7.70 x 10^5.
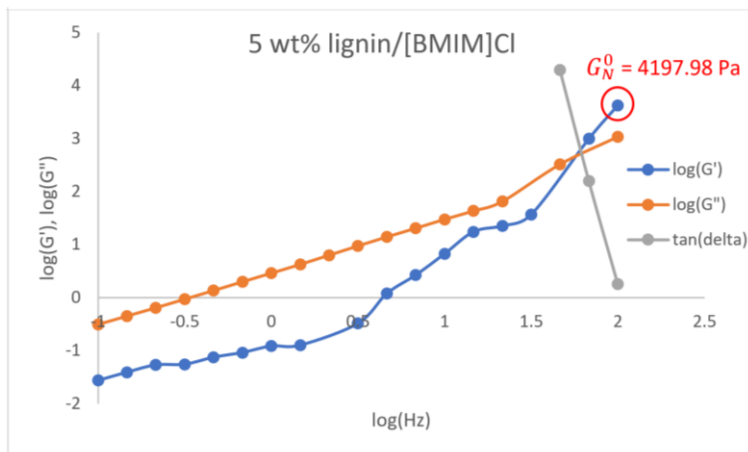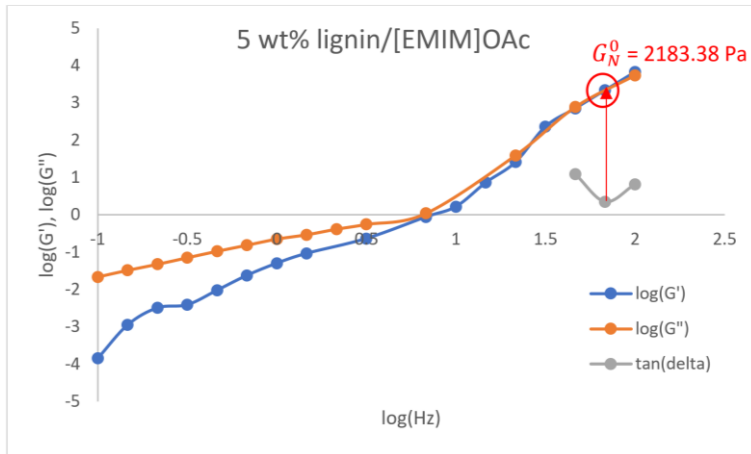

Figure 7.27. $\log(G')$, $\log(G'')$ and $\tan\delta$ curves for 5 wt% lignin/[BMIM]Cl

In figure 7.28, it can be seen that 5 wt% lignin/[EMIM]OAc had a stronger viscous character at lower frequency. When frequency increased, the viscous and elastic characters became also identical. G_N^0 was determined to be 2183.38 Pa that led to M_e of 1.36 x 10^6.

Figure 7.28. $\log(G')$, $\log(G'')$ and $\tan\delta$ curves for 5 wt% lignin/[EMIM]OAc

7.3.1.3 Oscillatory rheological data for BL/IL solutions

Finally, the results for BL/IL solution are tabulated in Table 7.12 and the relevant graphs are shown below. 5 wt% BL/[EMIM]OAc consists of higher M_e value of 7.30 x 10^7 compared to the other BL/IL solutions. This could imply that the higher molecular weight between entanglements can favour the electrospinning process. Hence, electrospinning of 5 wt% BL/[EMIM]OAc had proven to be possible.

Table 7.12. Values of M_e for lignin/ionic liquid solutions

Polymer solution	5 wt% BL/[AMIM]Cl	5 wt% BL/[BMIM]Cl	5 wt% BL/[EMIM]OAc
M_e	2.47 x 10^6	5.79 x 10^5	7.30 x 10^7

5 wt% BL/[AMIM]Cl exhibited a viscous character at lower frequency until the intersection of two curves (Figure 7.29). With G_N^0 determined to be 1232.85 Pa, value of M_e is 2.47 x 10^6
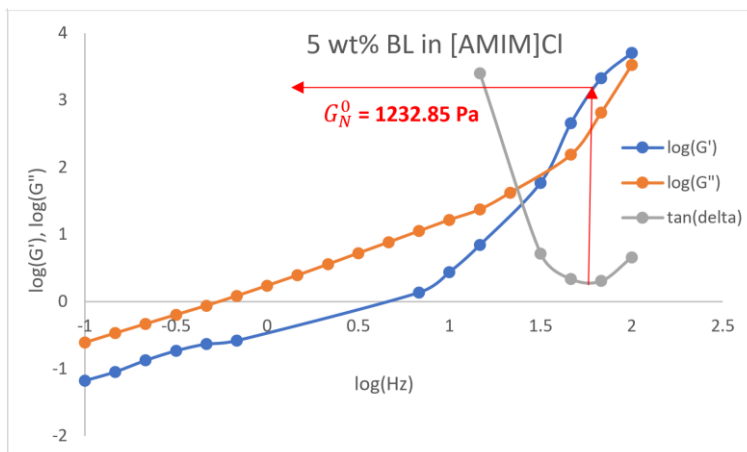
Figure 7.29. $\log(G')$, $\log(G'')$ and $\tan\delta$ curves for 5 wt% BL/[AMIM]Cl

5 wt% BL/[BMIM]Cl (Figure 7.30) showed a distinctive viscous character at lower frequency. Its G_N^0 was determined as 4936.29 Pa and thus, it has M_e value of 5.79 x 10^5
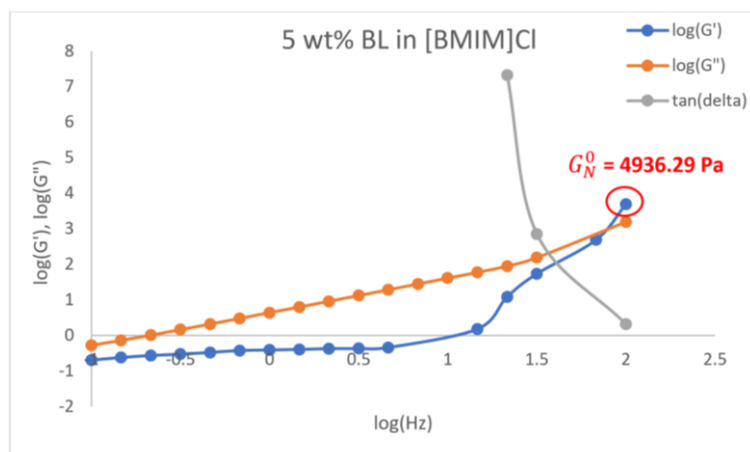

Figure 7.30. $\log(G')$, $\log(G^{"})$ and $\tan\delta$ curves for 5 wt% BL/[BMIM]Cl

Similarly, 5 wt% BL/[EMIM]OAc (Figure 7.31) displayed a higher viscous character at lower frequency. A low G_N^0 value was determined as 39.81 Pa and therefore, it has M_e value of 7.30 x 10^7
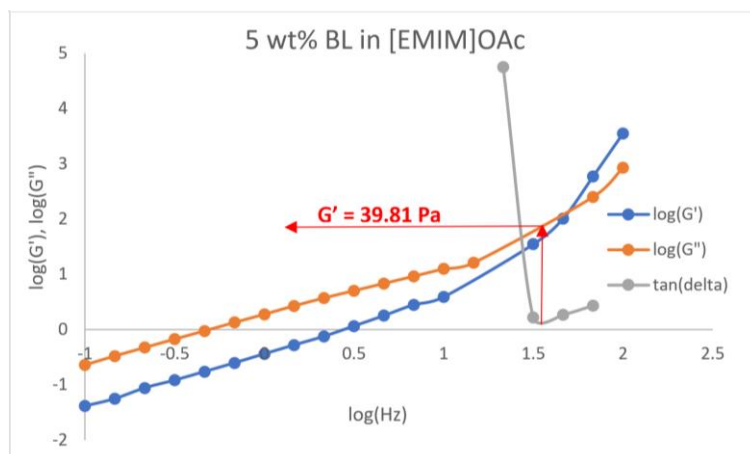

Figure 7.31. $\log(G')$, $\log(G^{"})$ and $\tan\delta$ curves for 5 wt% BL/[EMIM]OAc

7.3.2 FTIR of biopolymer/IL solutions

After oscillatory rheology data collected, FTIR spectra were then collected in order to understand the hydrogen bonding between the biopolymer and ILs. The polymer entanglement in the ILs can be influenced by intermolecular hydrogen bonding between the polymer network and ILs.[450] The aim is to see whether it is possible to observe a trend or see whether the molecular weight between entanglements (M_e) are influence by the hydrogen bonding present in the biopolymer/IL solutions.

7.3.2.1. FTIR of chitin/IL solutions

In the FTIR spectrum of chitin, there are ranges that are attributed to the hydrogen bonding which should be considered. For instances, peaks appeared in the range of *ca.* 1000 – 1200 cm^{-1} corresponded to C-O-C/C-O stretching and in particular, the peak at 1154 cm^{-1} was related to the C-O stretching of C-OH group in the polysaccharide unit is often influenced by hydrogen bonding.[451,452] The amide band in the range of *ca.* 1620 – 1660 cm^{-1} that split into two components at 1621 and 1652 cm^{-1} due to hydrogen bonding.[414] In the range of 3000-3600 cm^{-1}, board absorption peak ascribed by the stretching vibration mode of hydrogen bonded groups. In the case of chitin that was studied in this research, peaks appear at 3103, 3260 and 3426 cm^{-1} corresponded to two –NH stretching modes and –OH stretching mode respectively.[414]

By comparing the FTIR spectra of 2 wt% chitin/[AMIM]Cl, pure [AMIM]Cl and pure chitin, it can be seen that the FTIR spectra of 2 wt% chitin/[AMIM]Cl, pure [AMIM]Cl are very similar. However, it was noted that some new peaks appeared in the FTIR of 2 wt% chitin/[AMIM]Cl that should be influenced by the hydrogen bonding between the IL and chitin. The two amide bands at 1621 and 1652 cm^{-1} in the FTIR of chitin had shifted to 1626 and 1645 cm^{-1} which were located closer together (Figure 7.32a). Peak at 3260 cm^{-1} of chitin shifted to 3263 cm^{-1} (Figure 7.32b) in the spectrum of 2 wt% chitin/[AMIM]Cl could imply a weaker intermolecular hydrogen bonding between chitin with the presence of [AMIM]Cl.
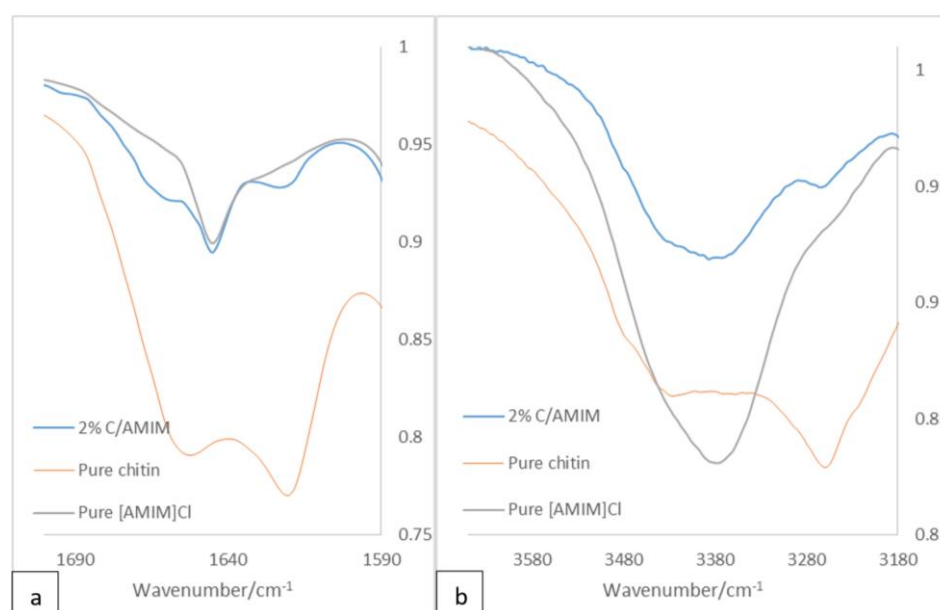

Figure 7.32. Partial FTIR for 2 wt% chitin/[AMIM]Cl, chitin and [AMIM]Cl at (a) 1590 – 1700 cm^{-1}; (b) 3180 – 3650 cm^{-1}

In the case when [BMIM]Cl was used to prepare 2 wt% chitin/IL. The spectrum of 2 wt% chitin/[BMIM]Cl also appeared to be very similar to that of pure [BMIM]Cl. Some similar changes were seen in the comparisons of spectra for 2 wt% chitin/[BMIM]Cl, pure [BMIM]Cl and pure chitin. Peaks at 1621 and 1652 cm^{-1} in the FTIR of chitin had shifted and appeared to be a lower wavenumber at 1648 cm^{-1} (Figure 7.33). However, the peaks corresponded to the intermolecular hydrogen bonding of chitin in the range of 3000 – 3600 cm^{-1} region were not seen.
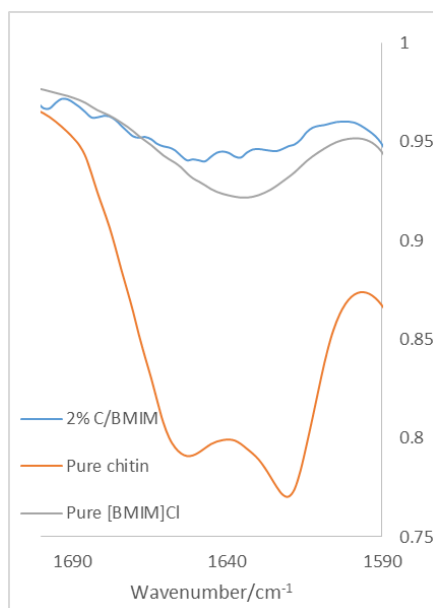
Figure 7.33. Partial FTIR for 2 wt% chitin/[BMIM]Cl, chitin and [BMIM]Cl at 1590–1700 cm^{-1}

In contrast, slightly more changes appeared between the spectra of 2 wt% chitin/[EMIM]OAc, pure [EMIM]OAc. Some peaks in the region of 1000 – 1200 cm^{-1} in the chitin's FTIR appeared in the 2 wt% chitin/[EMIM]OAc's spectrum. For instances, peaks at 1010, 1068, 1112 and 1154 cm^{-1} had shifted to 1004, 1042, 1090 and 1119 cm^{-1} respectively (Figure 7.34a). Since the peaks had shifted to lower wavenumbers, this could imply stronger interactions induced with the presence of [EMIM]OAc. Peaks at 1621 and 1652 cm^{-1} had shifted to 1635 and 1668 cm^{-1} (Figure 7.34b). Since the splitting of this amide band was slightly increased to 3 cm^{-1}, this could imply a further influence of hydrogen bonding with the presence of [EMIM]OAc. More changes can be seen in the region of 3000 – 3600 cm^{-1} as the peaks in this range do not resemble any peaks in neither the spectrum of pure [EMIM]OAc nor chitin (Figure 7.34c). It is suggested that the intermolecular hydrogen bonds of chitin were disrupted by [EMIM]OAc or new interactions induced between chitin and [EMIM]OAc. Compared to chitin/[AMIM]Cl and chitin/[BMIM]Cl solutions, the changes appear in the FTIR spectrum are more

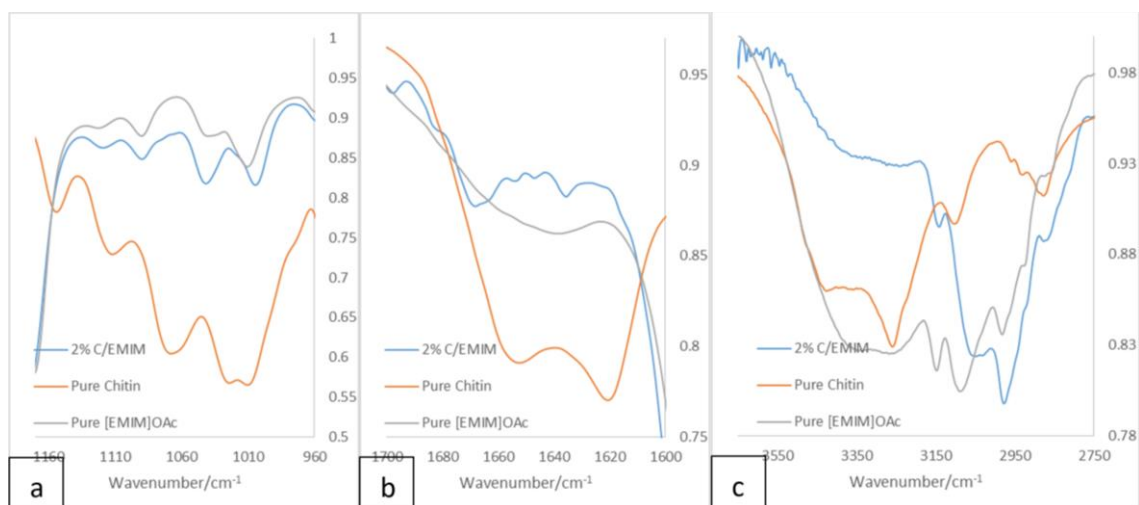significant. This can perhaps, explain the highest M_e value that was recorded for chitin/[EMIM]OAc solution.

Figure 7.34. Partial FTIR for 2 wt% chitin/[EMIM]OAc, chitin and [EMIM]OAc at (a) 960 – 1170 cm^{-1}; (b) 1600 – 1700 cm^{-1}; (c) 2750 – 3650 cm^{-1}

7.3.2.2. FTIR of lignin/IL solutions

The characteristic peaks appear in the lignin's FTIR include 1080 cm^{-1} and 1213 cm^{-1} for the aliphatic ether and secondary aliphatic hydroxyl groups respectively; guaiacyl ring's C-O-C/C-O stretching at 1265 cm^{-1}; phenolic hydroxyl groups at 1371 cm^{-1}; C-H vibrations at 1424 (methoxyl groups and aromatic rings) 1451 (methoxyl) and 1512 cm^{-1} (aromatic rings); aromatic C-H vibration along with C=O stretching at 1593 cm^{-1}; methoxyl groups C-H stretching at 2844 and 2937 cm^{-1};[453] a broad peak for methoxyl groups O-H stretching at 3224 cm^{-1} which could assigned for intermolecular hydrogen bonding.[454,455]

In the comparison of FTIR for 5 wt% lignin/[AMIM]Cl, pure [AMIM]Cl and pure lignin, it could be seen that spectra for 5 wt% lignin/[AMIM]Cl and pure [AMIM]Cl very similar. In the spectrum of 5 wt% lignin/[AMIM]Cl, a new peak appeared at 1513 cm^{-1} (Figure 35a) which should be originated from the aromatic C-H vibration in lignin.[453] In addition, peaks in the range of 2800 – 3500 cm^{-1} had slightly shifted to lower wavenumbers compared to the original [AMIM]Cl spectrum. For instances, peaks at 2856, 3065, 3140 (C-H vibrations) and 3378 cm^{-1} (O-H vibration) from the pure [AMIM]Cl FTIR had shifted to 2855, 3056, 3139 and 3377 cm^{-1} in the 5 wt% lignin/[AMIM]Cl's spectrum respectively (Figure 7.35b) which could indicate a slightly stronger hydrogen bonding induced in the mixture.[455]
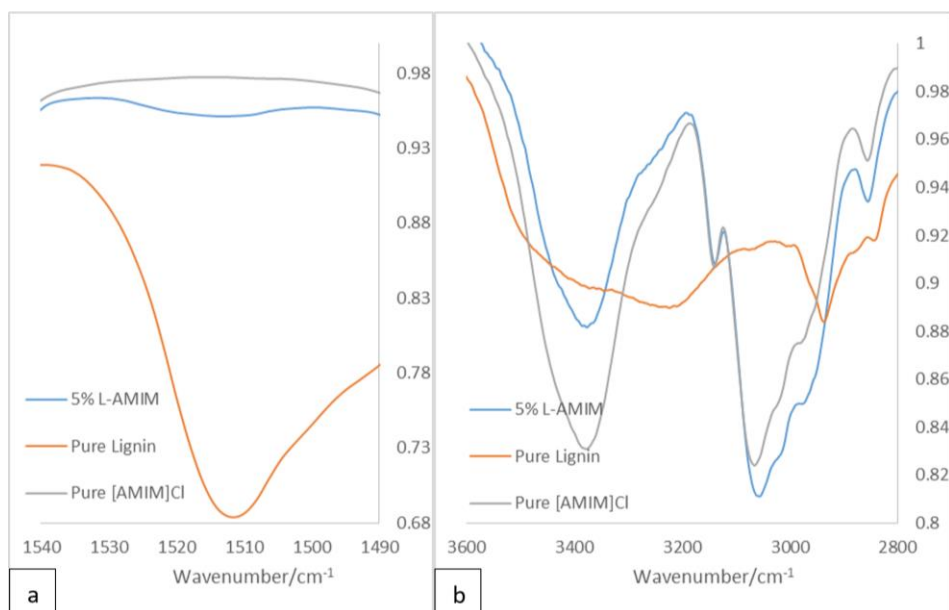
Figure 7.35. Partial FTIR for 5 wt% lignin/[AMIM]Cl, lignin and [AMIM]Cl at (a) 1490 – 1540 cm^{-1}; (b) 2800 – 3600 cm^{-1}

Similar observations were noted when comparing the spectra for 5 wt% lignin/[BMIM]Cl, pure [BMIM]Cl and pure lignin. A new peak at 1514 cm^{-1} that originated from the aromatic C-H vibration in lignin (Figure 7.36a).[453] Peaks in the region of 2800 – 3500 cm^{-1} had also shifted compared to the original pure [BMIM]Cl spectrum. Unlike the case of using [AMIM]Cl as the solvent, the peaks shifted to higher wavenumbers. Peaks at 2873, 2935, 2959, 3065, 3142 (C-H vibrations) and 3390 cm^{-1} (O-H vibrations) had shifted to 2874, 2936, 2961, 3079, 3145 and 3391 cm^{-1} (Figure 7.36b). As shifting occurred at higher wavenumbers, it is likely that weaker hydrogen bonding induced.[455]
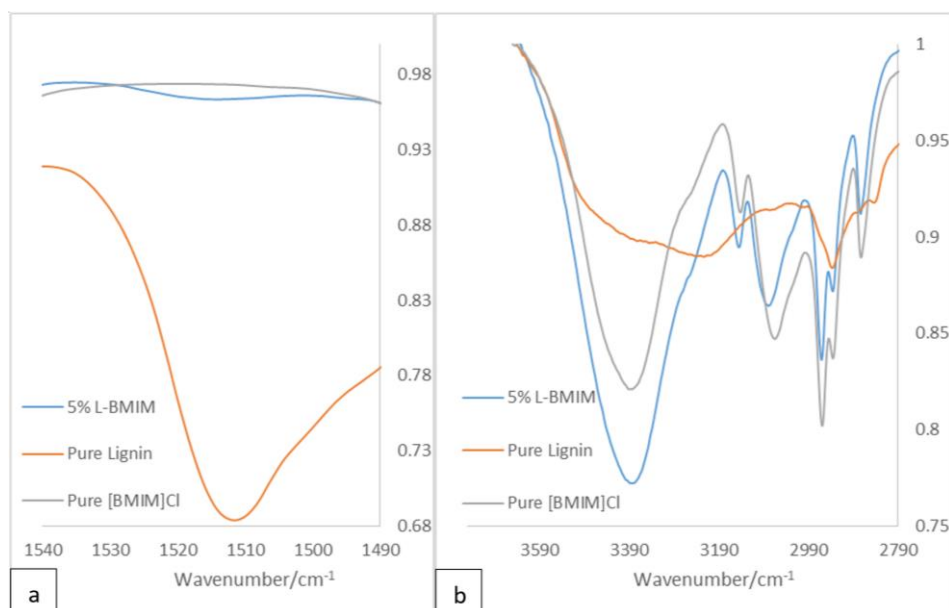

Figure 7.36. Partial FTIR for 5 wt% lignin/[BMIM]Cl, lignin and [BMIM]Cl at (a) 1490 – 1540 cm^{-1}; (b) 2790 – 3750 cm^{-1}

Slightly observations were noted when comparing the spectra for 5 wt% lignin/[EMIM]OAc, pure [EMIM]OAc and pure lignin. Intensity of the peak at 1040 cm^{-1} ([EMIM]OAc) increased and shifted to 1041 cm^{-1} (5 wt% lignin/[EMIM]OAc) which should be influenced by the peak at 1029 cm^{-1} (pure lignin) ascribed to the aromatic C-H in-plane deformation (Figure 7.37a).[453] In the region of 2800 – 3500 cm^{-1}, peaks were shifted more distinctively compared to the spectrum for [EMIM]OAc. For instances, peaks at 2982, 3089, 3148 (C-H vibrations) and 3346 cm^{-1} (O-H vibration) from the [EMIM]OAc FTIR had shifted to 2977, 3070, 3143 and 3340 cm^{-1} in the spectrum of 5 wt% lignin/[EMIM]OAc (Figure 7.37b). Since the peaks shifted more compared to BL/[AMIM]Cl and BL/[BMIM]Cl , this should indicate that stronger hydrogen bonds[455] present in the polymer solution. Perhaps, this could also explain a higher M_e value recorded for BL/[EMIM]OAc.
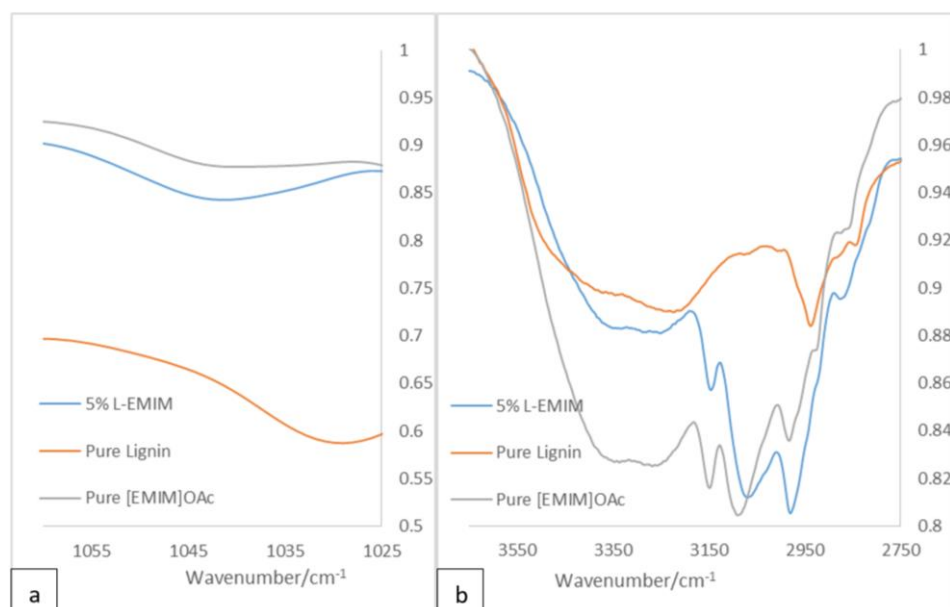

Figure 7.37. Partial FTIR for 5 wt% lignin/[EMIM]OAc, lignin and [EMIM]OAc at (a) 1025 – 1060 cm^{-1}; (b) 2750 – 3650 cm^{-1}

7.3.2.3. FTIR of BL/IL solutions

The banana leaves used in this study composed of leaf blades including midribs. Although their chemical compositions can be varied due to numerous types of banana plants as well as their growing conditions, the most common banana plant is known as Cavendish and the chemical compositions in the plant can be used as reference.[456] In the leaf blades and midribs, major components are holocellulose, cellulose, lignin as well as minor components include ash, various extractives, pentosanes, proteins and starch.[457] Hence, FTIR of plant leaves are often complex. Apart from the biopolymers and organic

constituents mentioned, some of peaks arise due to the waxy layer, water content and lead to multiple overlaps in the spectrum.[458] In the case of banana leaf, their distinctive peaks include 1265 and 1371 cm^{-1} assigned for aromatic-OCH_3 stretching for guaiacyl rings and syringyl rings respectively; 1735 cm^{-1} for C=O bond (ester groups, non-conjugated fatty acids); 2850 and 2914 cm^{-1} for C-H stretching (aliphatic compounds) and broad peak at 3353 cm^{-1} to indicate the intermolecular hydrogen bonding.[457,292]

In the comparison of FTIR for 5 wt% BL/[AMIM]Cl, pure [AMIM]Cl and pure banana leaf, it could be seen that spectra for 5 wt% BL/[AMIM]Cl and pure [AMIM]Cl very similar. New peaks were not seen and the only difference was the shifting in the region of 2800 – 3200 cm^{-1}. Peaks at 2856, 3065, 3140 cm^{-1} (C-H stretching for pure [AMIM]Cl) had slightly shifted to 2854, 3064, 3139 cm^{-1} in the spectrum for 5 wt% BL/[AMIM]Cl (Figure 7.38).
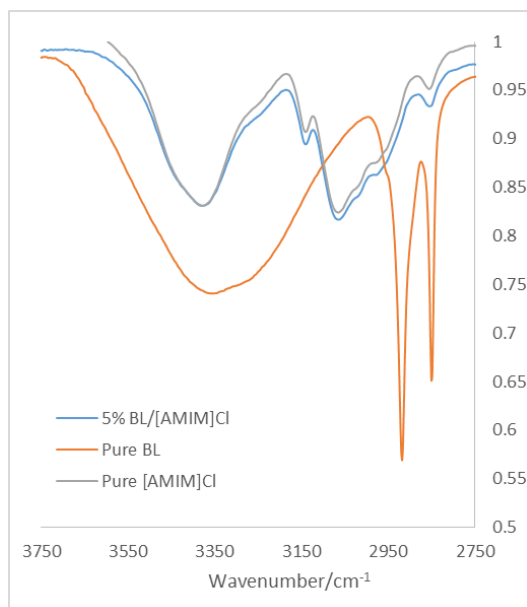

Figure 7.38. Partial FTIR for 5 wt% BL/[AMIM]Cl, BL and [AMIM]Cl at 2750 – 3750 cm^{-1}

Similarly, FTIR for 5 wt% BL/[BMIM]Cl, pure [BMIM]Cl and pure banana leaf were compared. Peak at 1250 cm^{-1} of pure [BMIM]Cl had shift to 1260 cm^{-1} in the spectrum of 5 wt% BL/[BMIM]Cl and it was very likely to be influenced by the BL peak at 1265 cm^{-1} which ascribed for guaiacyl aromatic-OCH_3 stretching. In the region of 2800 – 3500 cm^{-1}, peaks at 2873, 2935, 2959, 3065, 3142 cm^{-1} (C-H stretching) and 3390 cm^{-1} (O-H vibration/intermolecular hydrogen bonding) for pure [BMIM]Cl had shifted to 2872, 2934, 2958, 3059, 3140 and 3385 cm^{-1} which indicate a stronger intermolecular hydrogen bonding induced in solution of 5 wt% BL/[BMIM]Cl (Figure 7.39).
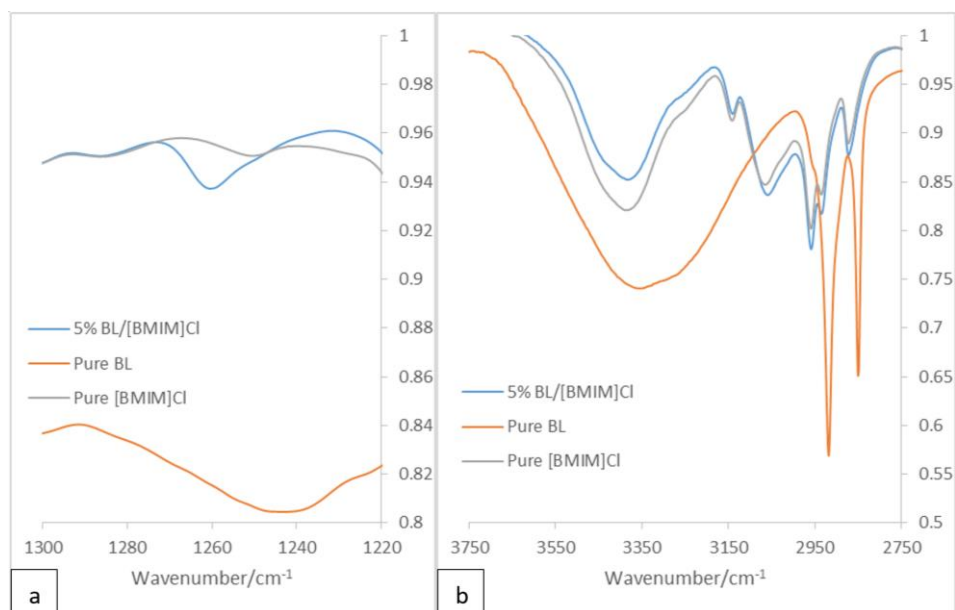
Figure 7.39. Partial FTIR for 5 wt% BL/[BMIM]Cl, BL and [BMIM]Cl at (a) 1220 – 1300 cm^{-1}; (b) 2750 – 3750 cm^{-1}

Finally, FTIR spectra of 5 wt% BL/[EMIM]OAc, pure [EMIM]OAc and pure banana leaf were compared. In the FTIR of BL/[EMIM]OAc, a new shoulder peak at 1633 cm^{-1} appeared which should be influenced by the stretching of conjugated C=C bonds to aromatic ring in the banana leaf.[457] In the region of 2800 – 3500 cm^{-1}, peaks also shifted to lower wavenumbers. The C-H stretching modes at 2982, 3089, 3148 cm^{-1} and O-H vibrations/hydrogen bonds at 3346 cm^{-1} had shifted to 2979, 3064, 3145 and 3273 cm^{-1} (Figure 7.40). Compared to the shifting occurred when using [AMIM]Cl and [BMIM]Cl, the differences were more distinctively when [EMIM]OAc were used which showed the strongest intermolecular hydrogen bonding induced.[455]
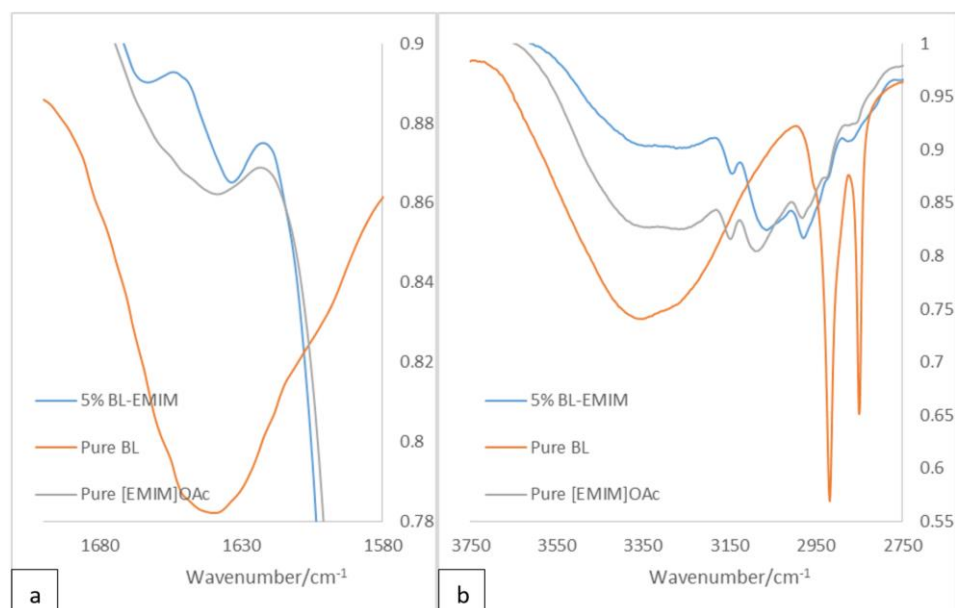

Figure 7.40. Partial FTIR for 5 wt% BL/[EMIM]OAc, BL and [EMIM]OAc at (a) 1580 – 1700 cm^{-1}; (b) 2750 – 3750 cm^{-1}

7.4 Bioassay (Bacterial Studies of Casted BL Membrane)

In order to produce BL-membrane that can be used on bioassay, film-casting was applied using [EMIM]OAc as it is the most effective solvent to dissolve BL easily. After stirring the BL pieces in [EMIM]OAc at 120 °C for overnight, precipitate that remained in the BL/[EMIM]OAc can be suspended using centrifuge and removed. The BL/[EMIM]OAc solution can then be subjected into a water bath (Figure 7.41a) to remove the excess IL. This method can be used to produce BL film, beads and fibres (Figure 7.41b). The water in the coagulation bath was exchanged with fresh water every hour to give BL film consisted of brownish green colour (Figure 7.41c).
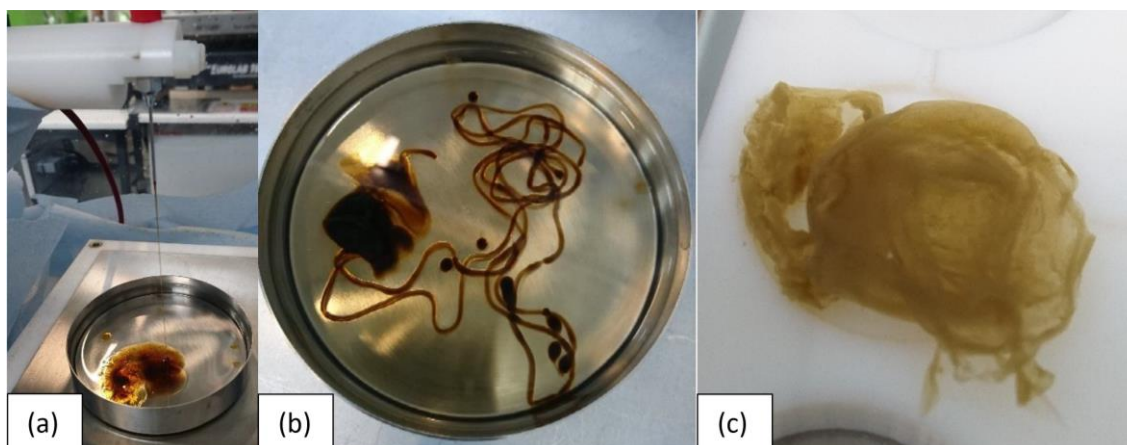

Figure 7.41. (a) Wet-spinning of BL/[EMIM]OAc into water, (b) BL film, beads and fibres coagulated in the water bath, dissolved in (a) [EMIM]OAc, (b) BL film after processed with IL

Upon drying, shelf-life of the BL product was extended to at least 1 year. Its FTIR spectrum was recorded and compared to that of fresh BL (Figure 7.42). Key FTIR absorption band of fresh BL include a very strong and broad peak at 1035 cm^{-1} (C-O-C symmetric stretching and C-O stretching vibration of carbohydrates and lignin), broad medium peak at 1167 cm^{-1} (CO, C-O-C bonds of carbohydrates), a broad peak at 1640 cm^{-1} (overlapping of C-C, C=C, OH, CO, C-O-C, CH aromatic, CH$_n$ bands), sharp peak at 1735 (C=O bond of carbohydrates and lignin), sharp peaks at 2850, 2918 cm^{-1} (CH$_n$, aliphatic and aromatic of carbohydrates and lignin) and a broad peak at 3353 cm^{-1} (hydroxyl group and bonded O-H stretching of carbohydrates and lignin).[459] After film casting, some of the peaks were shifted as the C-O-C symmetric stretching and C-O stretching vibration of carbohydrates and lignin shifted to higher wavenumber 1045 cm^{-1}, CO, C-O-C bonds of carbohydrates peak shifted to lower wavenumber at 1158 cm^{-1}, the overlapping of C-C, C=C, OH, CO, C-O-C, CH aromatic, CH$_n$ bands shifted to higher wavenumber at 1647 cm^{-1}. The C=O bond of carbohydrates and lignin at 1735 cm^{-1} was

not shifted but became very weak. The three remaining peaks at higher wavenumbers were also unshifted but the intensities reduce. They are the sharp peaks at 2850, 2919 cm^{-1} (CH$_n$, aliphatic and aromatic of carbohydrates and lignin) and a broad peak at 3284 cm^{-1} (hydroxyl group and bonded O-H stretching of carbohydrates and lignin).
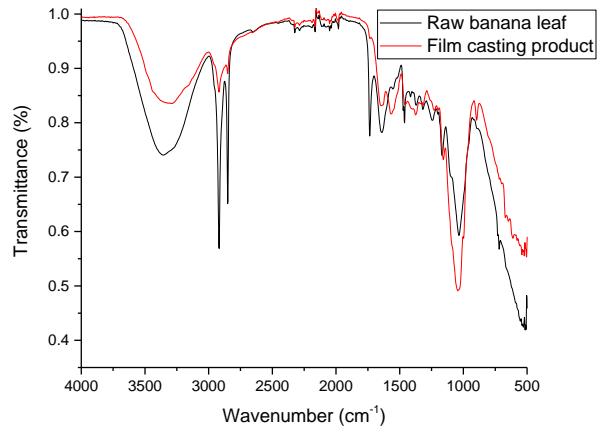

Figure 7.42. FTIR spectra of fresh BL and BL film obtained using film casting

The BL film was then tested with microbes include two *Escherichia coli* (*E. coli*) strains, two *Staphylococcus aureus* (*S. aureus*) strains, one *Candida* strain and three *Pseudomonas* strains using Kirby-Bauer disk diffusion method. Unfortunately, clear inhibition zones cannot be seen surrounding the BL pieces. Although it was observed that the agar plates containing *MSSA Newman* and *Pseudomonas PA14*, colonies around the BL pieces seemed to be reduced (Figure 7.43) but the effects were not significant and conclusions cannot be determined regarding to the antimicrobial property of this BL product.
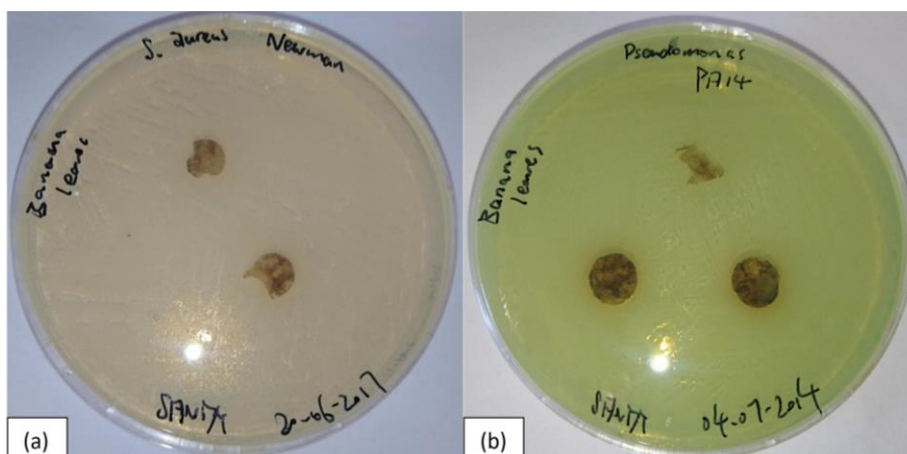

Figure 7.43. Pure BL discs on incubated (a) *MRSA JE2* and (b) *MSSA Newman*

Chapter 8.

Conclusion

8. Conclusions

In this project, a selection of biopolymer constructs were investigated with the specific aim of translating the intrinsic antimicrobial properties of naturally occurring materials (e.g. chitin, lignin, banana leaf) to a biodegradable polymer (PLA) for possible biomedical applications (e.g. would healing). The majority of the materials prepared were based on a composite of PLA with different naturally occurring additives and a plasticizer, the latter added to alter the physical properties of the PLA.

The first half of the project focused on using chitin, lignin and banana leaves as the biomaterial of interest and on using ionic liquids as the powerful solvents to prepare constructs via either electrospinning or film casting these solutions.

In the second half of the project, the biopolymer PLA was filled with naturally occurring materials that have intrinsic antimicrobial properties (i.e. chitin and lignin) and a synthetic nanoparticle, WS_2 which is known to be non-toxic. The effectiveness of triacetin as a plasticizer for the composites of PLA with chitin and lignin was also investigated. Melt-extrusion and injection moulding were the main techniques used to produce a selection of non-plasticized and plasticized PLLA-based composites for chitin and lignin content of 10 wt% and, for WS_2 loading up to 5 wt%.

The physical properties of all composites were measured as a function of chitin/lignin/WS_2 loading. The antimicrobial efficacy of these materials was tested using a range of bioassays. Composites of plasticized PLLA and lignin can reduce biofilm formation of two S. aureus strains

8.1 Plasticized and Non-plasticized Composites of PLA and lignin

PLA-based composites with 0, 0.5, 1, 2, 3, 5 and 10 wt% lignin via melt-extrusion. Another set of composites with the same compositions of PLA and lignin that contained 20 wt% triacetin as a plasticizer was also produced.

One of the most profound feature shown from this chapter is the fact that the intrinsic antimicrobial properties of lignin could be translated to PLA. When the Kirby-Bauer disk diffusion tests were applied, it was proven that lignin can inhibit the growth of *MRSA JE2* as well as *MSSA Newman*. This is indeed consistent with other studies which reported the antimicrobial properties shown by phenolic compounds[70,76,78] Although PLA-based composites incorporated with lignin does not exhibit antimicrobial properties, the triacetin-plasticized PLA-based composites incorporated with lignin were able to reduce

the formation of biofilm. This is indeed, a great example to inspire the design of an antimicrobial material as this indicates the importance of choosing a material with intrinsic antimicrobial properties as well as having an additional material which is a plasticizer in this case to deliver or enhance their functions in the polymer matrix.

With the aid of plasticizer, lignin can translate its intrinsic antimicrobial properties to PLA. In the comparison of the physical properties of the both un-plasticized and plasticized PLA/lignin composites, incorporation of lignin did not dramatically alter the T_g of the composites. In terms of mechanical strengths, values of UTS and elongation at breaks are inversely proportional to the content (wt%) of lignin. In contrast, values of YM slightly increased with increasing lignin content (wt%). Same trends for UTS and elongation were observed for the plasticized PLA/lignin-composites but ANOVA statistical test reveals that the plasticized samples have the same variance in terms of the values of YM.

Apart from delivering the antimicrobial properties of lignin, triacetin as a plasticizer can also reduce the values of T_g of the composites according to both DSC and DMTA results. On the other hand, incorporation of plasticizer resulted in the reduction of YM and UTS but the elongation at breaks were extended by more than 100 times.

Overall, further studies are required to explore the antimicrobial properties of plasticized PLA/lignin composites. These plasticized samples can be further tested on more bacteria to deeply understand the antimicrobial activities. In addition, the optimum content of lignin (wt%) and plasticizer (wt%) can be investigated for further enhancing the antimicrobial efficacy of the PLA-based composites.

8.2 Plasticized and Non-plasticized Composites of PLA and Chitin

PLA-based composites with 0, 0.5, 1, 2, 3, 5 and 10 wt% chitin via melt-extrusion. Another set of composites with the same compositions of PLA and chitin that contained 20 wt% triacetin as a plasticizer was also produced.

Chitin is a bacteriostatic[237] material and did not antimicrobial properties during the Kirby-Bauer diffusion tests. Growth curves of E. coli. (strains *K12* and *Sakai*), *MRSA JE2* and *MSSA Newman* were obtained in the presence of non-plasticized and plasticized composites with the lowest and highest chitin concentration, growths of both *E. coli. K12* and *Sakai* were suppressed by plasticized PLA composite with 10 wt% chitin. However, the overall results were inconsistent when compared with two other repeats. Unfortunately, the antimicrobial properties of PLA/chitin are yet to be confirmed.

In the comparison of the physical properties, T_g values of the composites are not depend upon the chitin content (wt%). According to the mechanical test, both values of UTS and elongation at breaks decreased slightly with increasing chitin content (wt%) whereas, YM increased slightly with increasing chitin content (wt%). After plasticization with triacetin, values of UTS and YM increased with increasing chitin content (wt%) whereas the elongation at breaks decreased with increasing chitin content (wt%).

Generally, plasticizer reduced the values of T_g of the composites according to both DSC and DMTA results. On the other hand, incorporation of plasticizer resulted in the reduction of YM and UTS but the elongation at breaks were extended by more than 100 times. These effects were also consistent with the PLA/lignin composites after plasticization. Moreover, plasticizer in this set of composites can indeed act as a dispersing aid for chitin as well as fill the void volume between PLA and chitin to improve chitin dispersion and aggregation. This was supported by the SEM images which can be seen that plasticized composites consist of smoother fracture surfaces and smaller chitin particles.

Overall, there was small evidence that plasticized PLA composite with 10 wt% chitin can suppress the growth of *E. coli. K12* and hence, further experiments should be conducted to confirm such antimicrobial activity.

8.3 Composites of PLA and WS$_2$

PLA-based composites with 0, 0.5, 1, 2, 3 and 5 wt% WS$_2$ via melt-extrusion. This is by far the first study that produce PLA/based composites with up to 5 wt% of WS$_2$. The major interest lies upon on the potential in biomedical application and hence, bioassays were conducted using some bacteria as well as HUVEC cells. During the bioassays, the composites were firstly tested with *E. coli K12* and *Sakai*. However, the growths of both strains were not affected by the composites at all. When bioassays were further conducted using HUVEC cells, the results indicated that the composites did not inhibit the growth of the HUVEC cells, they had influenced the cell attachment on the composites' surfaces. Finally, contact angles of the composites were measured which confirmed that incorporation of WS$_2$ can alter biomaterial surfaces enhanced influenced the cellular attachment and proliferation of tissue culture and engineering.

In the comparison of the physical properties of the composites, some features of the composites are independent on the WS$_2$ content (wt%). For instance, all PLA/WS$_2$ composites have the same T_g values according to the DMTA and DSC data. GPC data

revealed that all samples detected at the same retention time and consisted of M$_w$ within the range of 120 – 136 kg/mol. During the mechanical tests, the elongation at breaks (%) were not influenced by the WS$_2$ content (wt%). However, there are some features of the composites that can be influenced by the incorporation of WS$_2$. For instance, a small descending trend was seen with increasing WS$_2$ content (wt%) but a small ascending trend was seen with increasing WS$_2$ content (wt%). TGA analysis revealed that all PLA/WS$_2$ composites degraded at a lower temperature compared to the neat PLA in the ambient atmosphere. When the composites were examined using PLM, it was observed that WS$_2$ can promote formation of spherulites when the composites annealed which showed that WS$_2$ can act as nucleation sites in the composites.

In this chapter, a selection of PLA/WS$_2$ composites were produced and their physical properties were analysed in details to understand the features of these composites. The bioassays can show the potential of these composites to be developed for biomedicine and further tests such as cytotoxicity should be conducted to explore these potentials.

8.4 Electrospinning of Chitin, Lignin and BL and the Entanglement Studies

[EMIM]OAc is the best candidate over and above [AMIM]Cl and [BMIM]Cl to dissolve BL and it was possible to electrospin BL/[EMIM]OAc to give BL fibres. Previously, electrospinning of lignin/IL and chitin/IL solution was attempted. However, the continuous stream cannot be observed using lignin/IL solutions and although a Taylor cone with a continuous stream was observed using a 2 wt% chitin/[EMIM]OAc solution, a gel formed during the process. Based upon the nature of the biopolymer/IL solutions such as viscosities, ease of handling for the oscillatory rheometer, solutions of 2 wt% chitin/IL, 5 wt% lignin/IL and 5 wt% BL/IL were analysed using oscillatory rheology as well as FTIR. From the oscillatory rheological data, 2 wt% chitin/[EMIM]OAc and 5 wt% BL/[EMIM]OAc have the highest molecular weight between entanglements, (M_e) of 4.63 x 10^{10} and 7.30 x 10^7 respectively. In contrast, the rest of biopolymer/IL solutions consist of values of M_e in the range of 5.79 x 10^5 – 2.58 x 10^6. This can imply the polymer solution with higher M_e tends to favour the electrospinning process. 5 wt% BL/[EMIM]OAc with M_e of 7.30 x 10^7 can indeed produce Taylor cones with continuous stream during electrospinning. On the other hand, 2 wt% chitin/[EMIM]OAc with M_e of 4.63 x 10^{10} can also give Taylor cone but a gel if formed making the electrospinning process fail. Hence, having a certain degree of entanglement is vital but when the value

of M_e is too high, this can also cause negative effective such as gel formation to the electrospinning process. According to the FTIR spectra, biopolymer/IL solution with higher values of M_e exhibited stronger intermolecular hydrogen bonding. For instance, the shifting in the FTIR spectra revealed that the 5 wt% chitin/[EMIM]OAc exhibited the strongest intermolecular hydrogen bonding compared to that of chitin/[AMIM]Cl and chitin/[BMIM]Cl solutions. Hence, hydrogen bonding seems crucial for the polymer solutions to have the required molecular weight between entanglements for electrospinning.

Finally, film casting was used to produce BL membranes that were used for bioassays. 5 wt% BL/[EMIM]OAc was prepared and water was used in a coagulation bath to prepare BL membranes. This method has indeed extended the shelflife of BL and as BL contains lignin components it was proven that BL is able to inhibit the growth of two *S. aureus* strains. Unfortunately, clear inhibition zones could not be seen surrounding the BL pieces in the Kirby-Bauer disk diffusion method. Although, it was observed on the agar plates containing MSSA Newman and Pseudomonas PA14, colonies around the BL pieces seemed to be reduced but the effects were not distinctive and conclusions cannot be determined until conducting further experiments.

Chapter 9. Recommendations for Future Work

9. Recommendations for Future Work

Major proposal:

1. Extension of bioassays on both PLLA/lignin, PLLA/chitin composites and BL membranes with bacteria

As pure lignin was proved to be able to inhibit the growth of an MRSA strain and an MSSA strain, most of the bioassays such as anti-biofilm experiments were then focused on the PLLA/lignin composites. Anti-biofilm experiments should also be conducted with PLLA/chitin composites as well as BL membranes. In addition, it is also proposed to use SEM imaging to check whether the bacteria membrane can be disrupted which leads to growth inhibition or even death in the presence the samples.[460] In the Kirby-Bauer disk diffusion tests conducted, inhibition zones were clearly seen around MRSA JE2 and MSSA Newman in the presence of pure lignin discs. However, in the case with samples that can exhibit a bacteriostatic effect such as chitin or samples with very slow diffusion rates in the agar, the inhibition zones can be very small and difficult to be seen which can lead to inconclusive results. Therefore, SEM imaging could be used to provide a clear understanding in terms of how the bacteria react when introduced to the composite materials.

2. Bioassays with additional types of microbes especially Gram-(+) bacteria

In this project, microbes that were tested include *E. coli*., *S. aureus*, *P. aeruginosa* and *C. albicans*. It would be ideal to test more and different microbes to confirm whether any of the composite samples can have an antimicrobial effect to other microbes. Additionally, among the microbes that were tested, it is apparent that pure lignin can inhibit two *S. aureus* strains which are categorised as Gram-(+) strains. The current suggestion is to test the antimicrobial property of lignin with more Gram-(+) bacteria such as *Bacillus*,[461] *Enterococcus faecalis*[462]*s* and *Streptococcus pneumoniae*[463] to investigate whether lignin could be more effective towards Gram-(+) strains.

3. Production of more composites with various ratios of plasticizer and study how the plasticizer can enhance any antimicrobial effect

According to the bioassay results, the plasticizer played a key role in enhancing the antimicrobial property of the composites. Our hypothesis is that leaching of the plasticizer occurred within the PLA matrix which brought additive such as lignin to the surface of

the polymer matrix and hence the formation of biofilm could be prevented. Alternatively, the plasticizer can alter the hydrophobicity of the composites which can also influence biofilm formation on the surface of the composites.[464] Hence, it is pertinent to produce more plasticized composites with different ratios of plasticizer such as 5, 10 and 15 wt% to find the optimum w/w of plasticizer that can optimise the antimicrobial effectiveness of the composite materials. On the other hand, it is also important to investigate whether plasticization can influence the hydrophobicity of the composites. For instance, the contact angles (wettability) of the composites can be measured using a tensiometer to determine whether the antimicrobial property of the plasticized composites is related to the hydrophobicity of the composite surface.

4. Further study on the antimicrobial effect of lignin

Lignin is an aromatic phenol polymer which can be composed of three types of monolignol building blocks, coniferyl (G), sinapyl (S) and *p*-coumaryl alcohol (H).[193] The ratio of G/S/H lignin units can vary in different parts of the plant or across plant species.[194] It would be interesting to investigate whether the antimicrobial effect of lignin is dependant upon the ratio of G:S:H units. Further bioassays should be conducted with lignin that was extracted from different parts of plants and alternatively, experiments could be conducted with lignin that was extracted with plants that are known to be composed of specific G/S/H unit. For instance, gymnosperms are mainly composed of G lignin and angiosperm dicots are composed of G and S lignin.[194] Perhaps, this set of experiments can provide a further understanding with regards to the reason why lignin exhibits am antimicrobial effect.

5. Discover and application of additional natural phenolic compounds to develop further antimicrobial agents

As discussed in the introduction, there are natural phenolic compounds that can be found in plants[67] that exhibit antimicrobial properties and promising therapeutic properties.[68] In this project, it was also confirmed that lignin can inhibit the growth of two S. aureus strains and its application in plasticized PLA composites can reduce the formation of biofilm. Therefore, further experiments should be conducted to identify the antimicrobial properties of these phenolic compounds. Compounds such as curcumin can be consumed daily which is non-toxic to the human body[79] and makes this kind of material even more

attractive as an antimicrobial agent. Hence, phenolic compounds have the potential to play a very key role to tackle the issue of antimicrobial resistance.

6. Further investigation of the composite materials

Firstly, PLA-based materials were produced and wt% of the additives were up to 10 only. Additional composite materials can be produced with higher wt% of additives to see whether the antimicrobial properties of the materials can be improved. Second, further work could be done to explore different plasticizers that can be used in PLA. For instance, S. Choi *et. al.* synthesized 2 ILs that can exhibit antimicrobial properties[59] which are also available to be used as plasticizers. They are indeed great candidates that should be tested to see whether they can be used to plasticize PLA. Besides, more sophisticated processing methods could be explored. For examples, surface medication[465] can be considered to improve the antimicrobial effect of the composites' surfaces. Finally, the antimicrobial properties of BLs should be more deeply understood by conducting further experiments to identify the active ingredients that correspond to the wound healing effect. These active ingredients should provide further inspiration and ideas to design more antimicrobial materials

Appendix

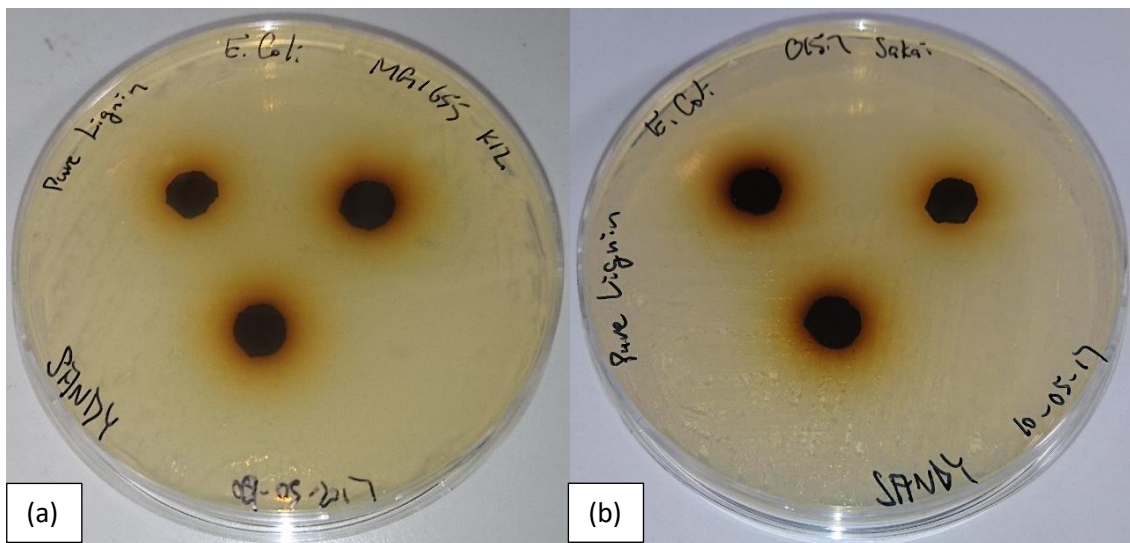1. Images of Kirby-Bauer disk diffusion test results with lignin and PLA/lignin composites discs

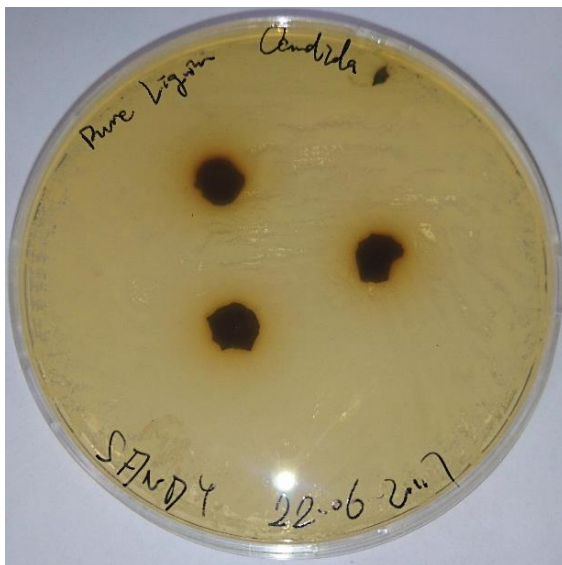*Figure 1*. Pure lignin discs on incubated (a) *E. coli. K12* and (b) *E. coli. Sakai*
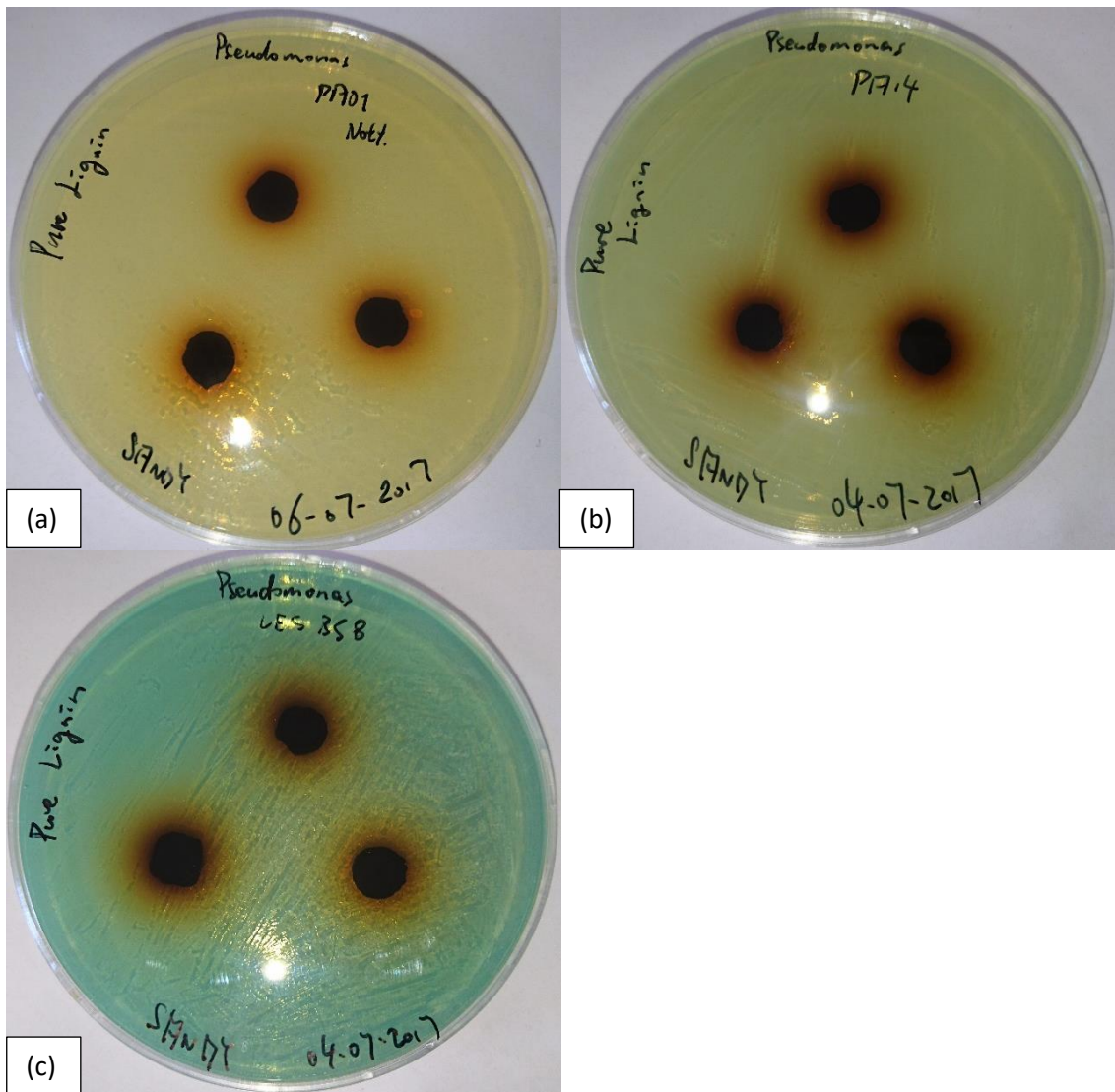

Figure 2. Pure lignin discs on incubated *Candida SC5314*

Figure 3. Pure lignin discs on incubated (a) *P. aeruginosa PAO1*, (b) *P. aeruginosa PA14* and (c) *P. aeruginosa LESB58*
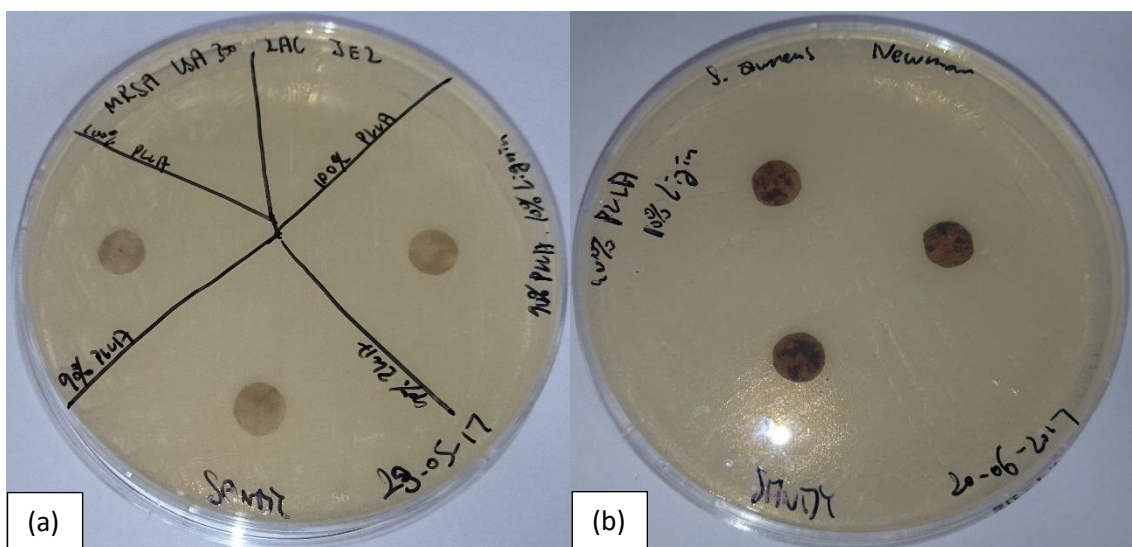

Figure 4. 90 wt% PLA/10 wt% lignin discs on incubated (a) *MRSA JE2* and (b) *MSSA Newman*

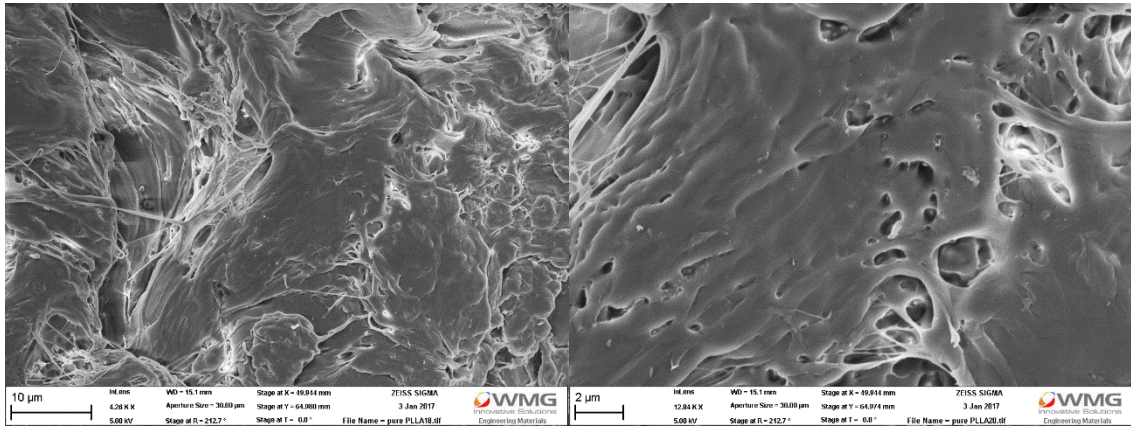2. SEM images of fractured PLA and PLA/chitin composites surfaces

Figure 5. SEM images of fractured neat PLA surface

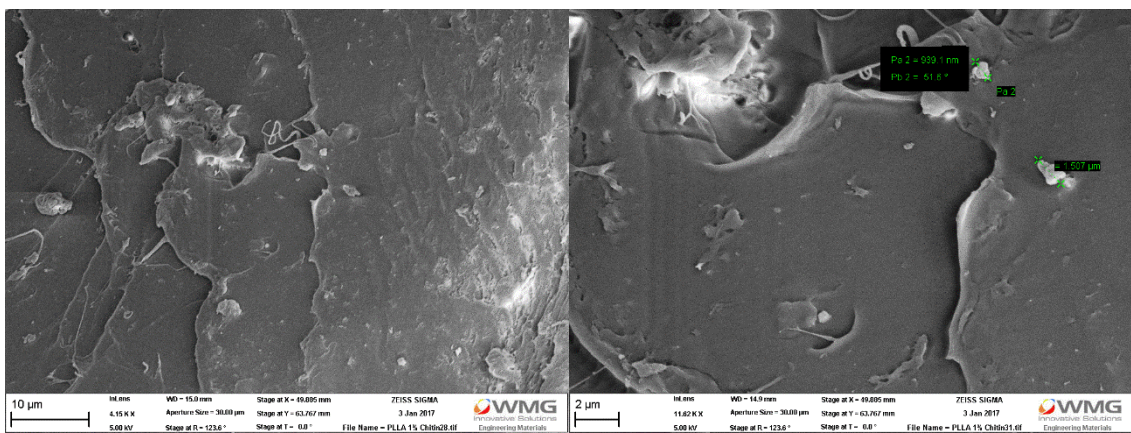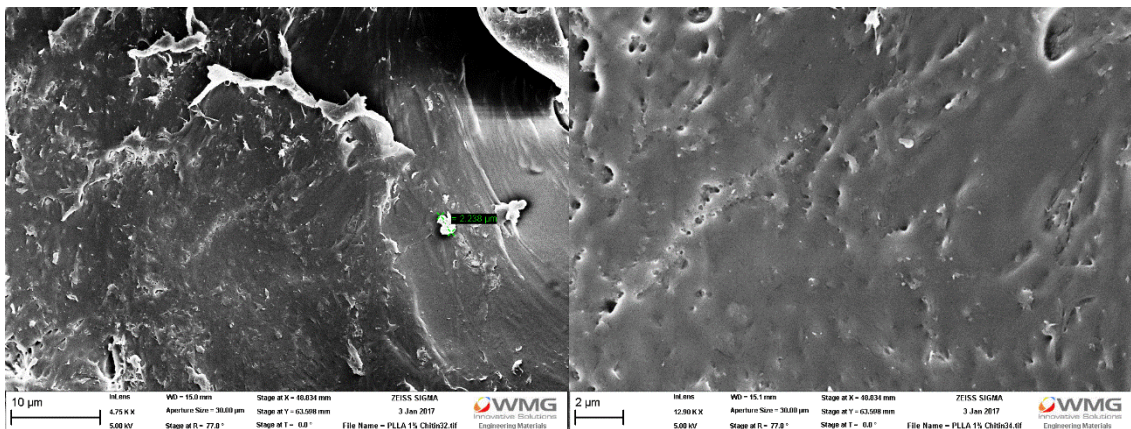*Figure 6.* SEM images of fractured 99 wt% PLA/ 1 wt% chitin surface

Figure 7. SEM images of fractured 98 wt% PLA/ 2 wt% chitin surface
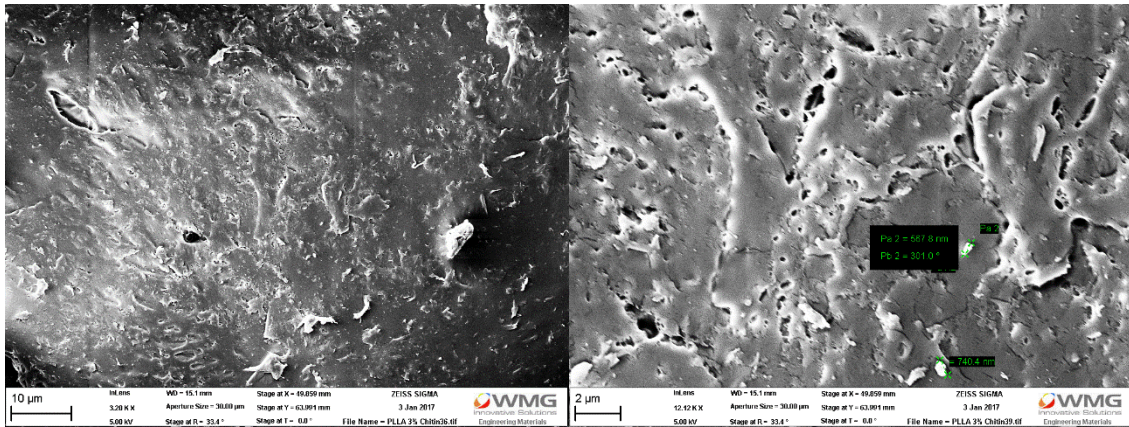
Figure 8. SEM images of fractured 97 wt% PLA/ 3 wt% chitin surface
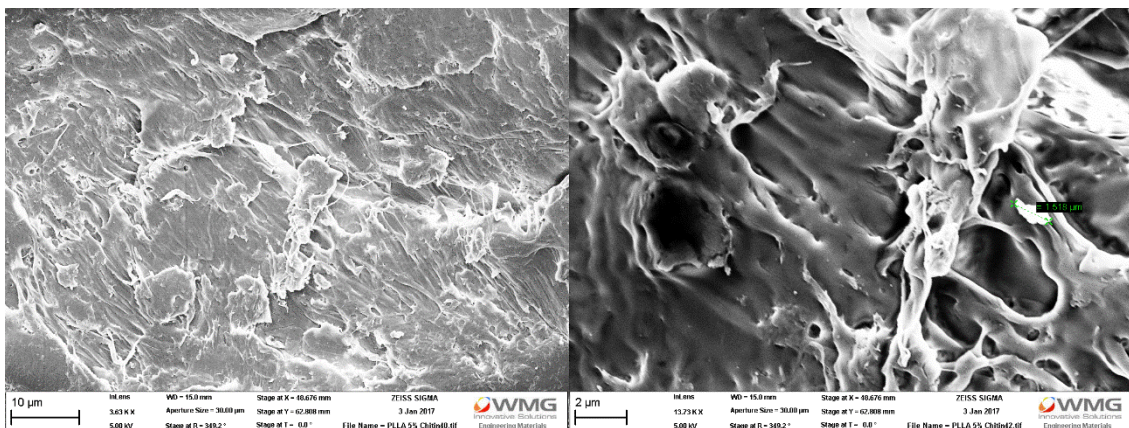
Figure 9. SEM images of fractured 95 wt% PLA/ 5 wt% chitin surface

3. SEM images of fractured plasticized PLA and PLA/chitin composites surfaces
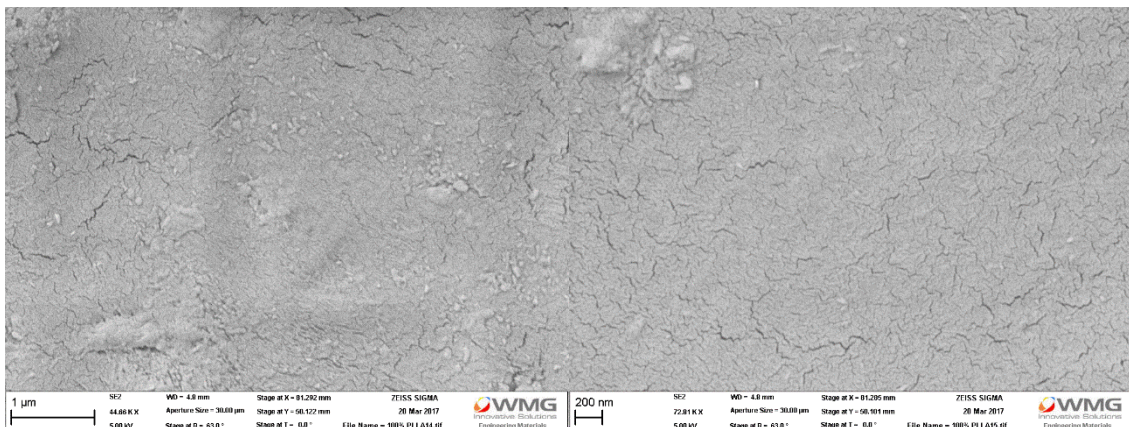
Figure 10. SEM images of fractured plasticized neat PLA surface
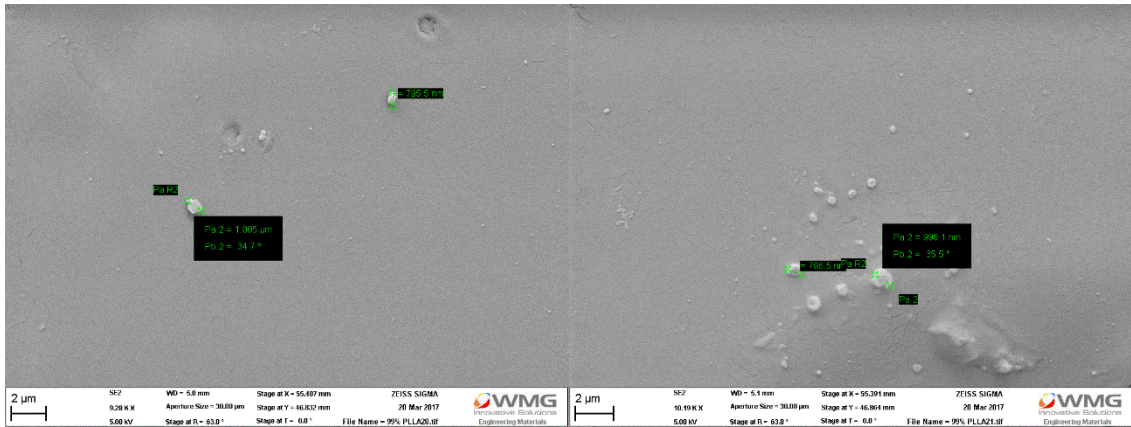
Figure 11. SEM images of fractured plasticized 99 wt% PLA/ 1 wt% chitin surface
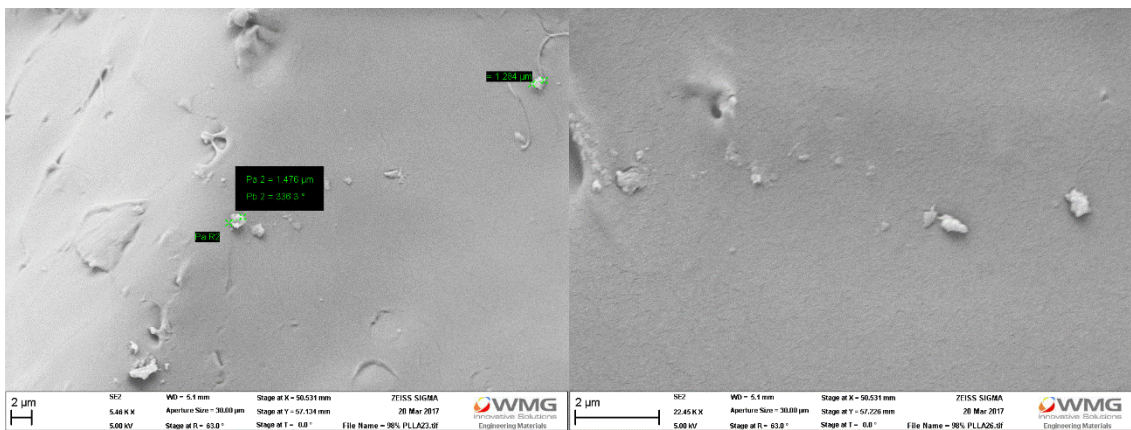
Figure 12. SEM images of fractured plasticized 98 wt% PLA/ 2 wt% chitin surface
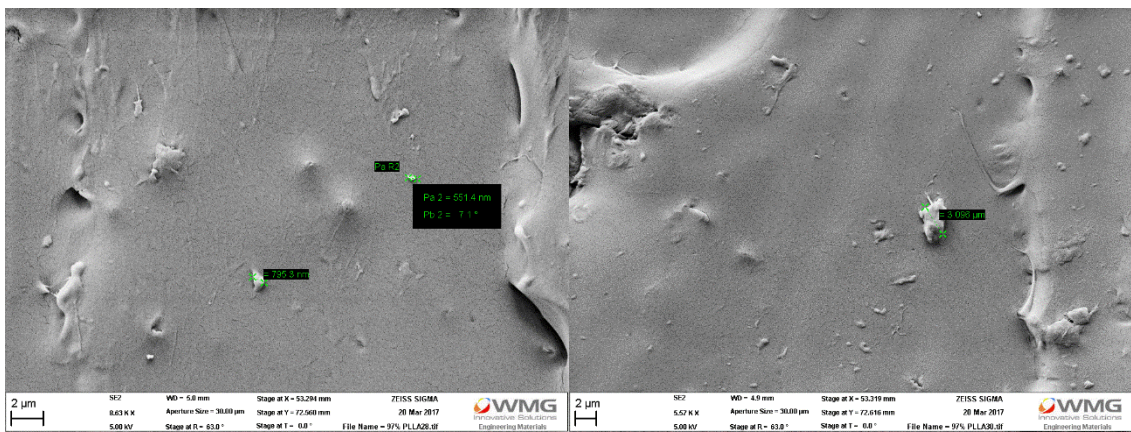
Figure 13. SEM images of fractured plasticized 97 wt% PLA/ 3 wt% chitin surface
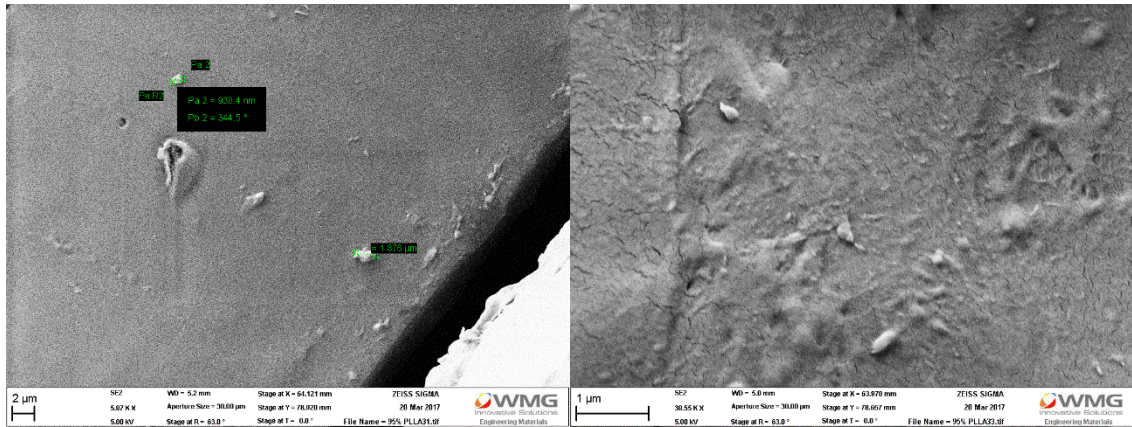
Figure 14. SEM images of fractured plasticized 95 wt% PLA/ 5 wt% chitin surface

4. SEM images of PLA and PLA/WS$_2$ composites surfaces
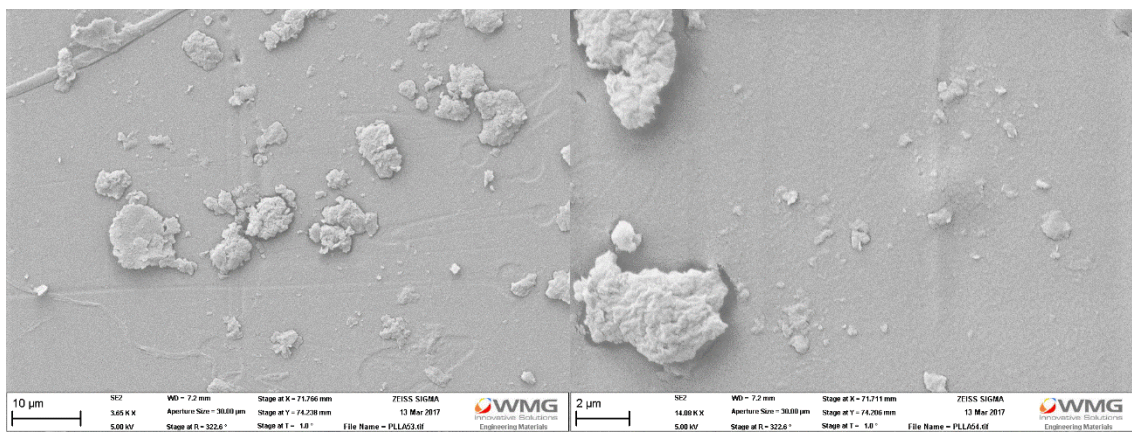
Figure 15. SEM images of neat PLA surface
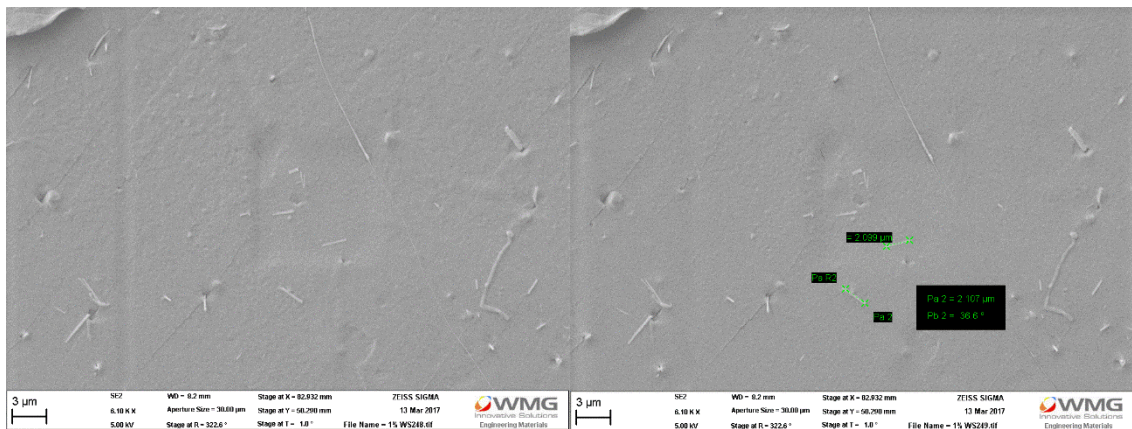
Figure 16. SEM images of 99% PLA/ 1% WS$_2$ surface
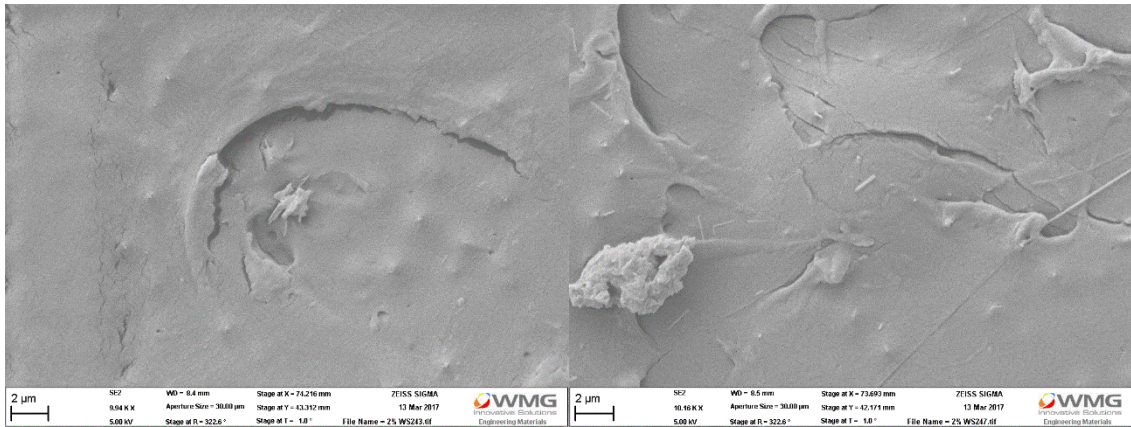
Figure 17. SEM images of 98% PLA/ 2% WS$_2$ surface
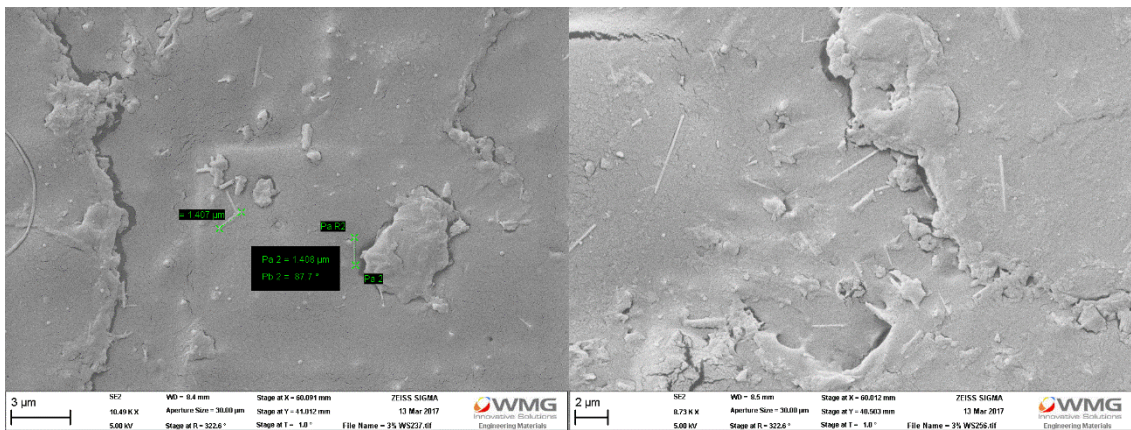
Figure 18. SEM images of 97% PLA/ 3% WS$_2$ surface

5. Images of Kirby-Bauer disk diffusion test results with chitin and PLA/chitin composites discs
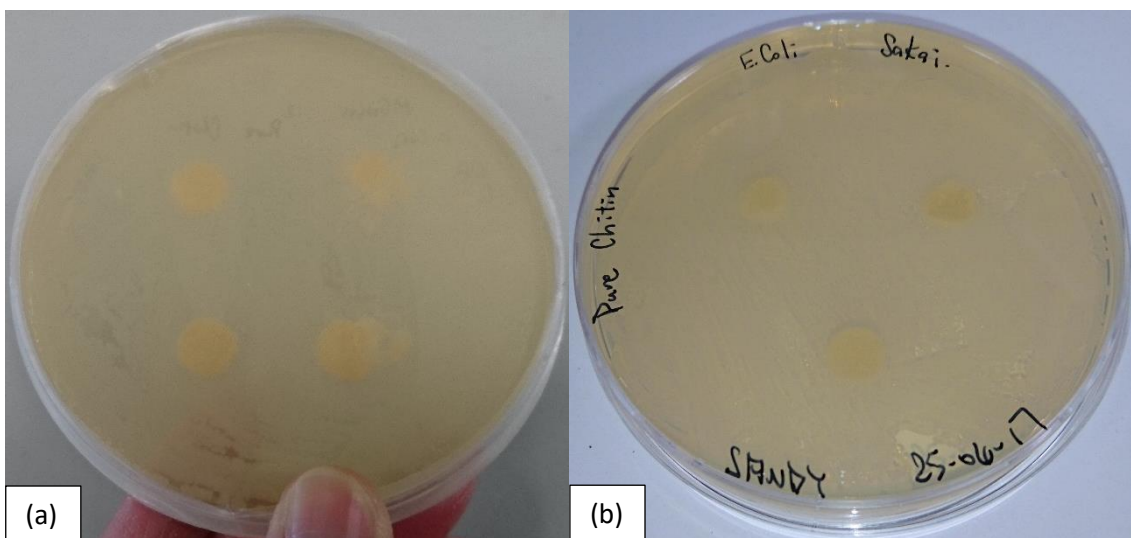
Figure 19. Pure chitin discs on incubated (a) *E. coli. K12* and (b) *E. coli. Sakai*
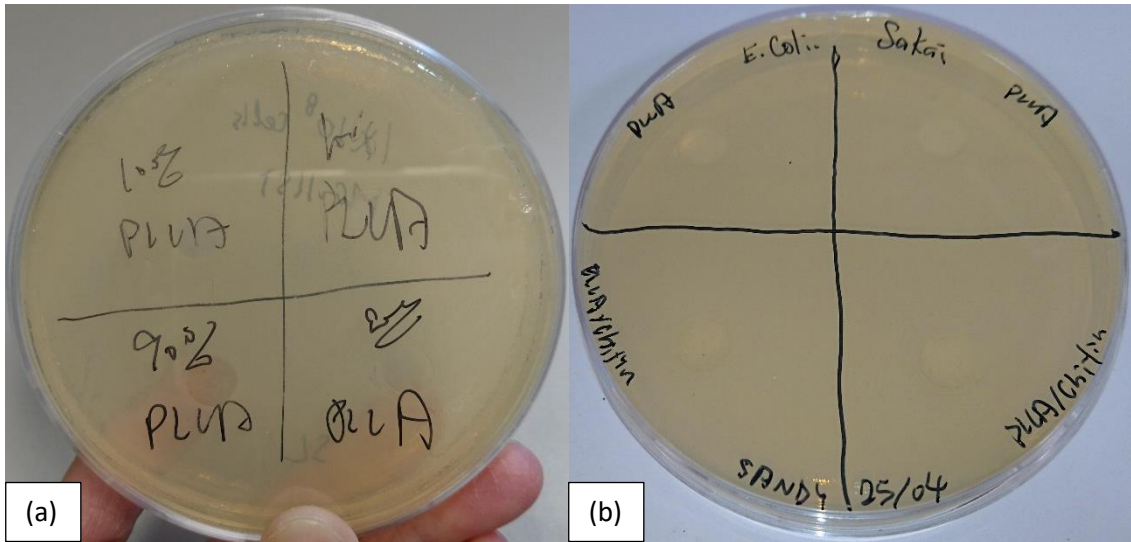
Figure 20. Neat PLA discs and 90 wt% PLA/ 10 wt% chitin discs on incubated (a) *E. coli. K12* and (b) *E. coli. Sakai*
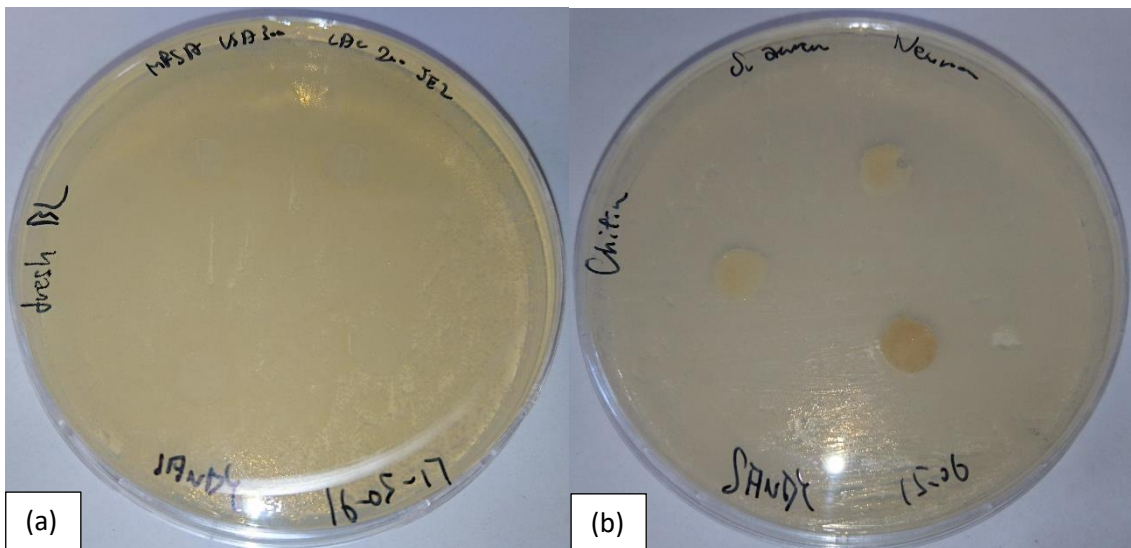
Figure 21. Pure chitin discs on incubated (a) *MRSA JE2* and (b) *MSSA Newman*
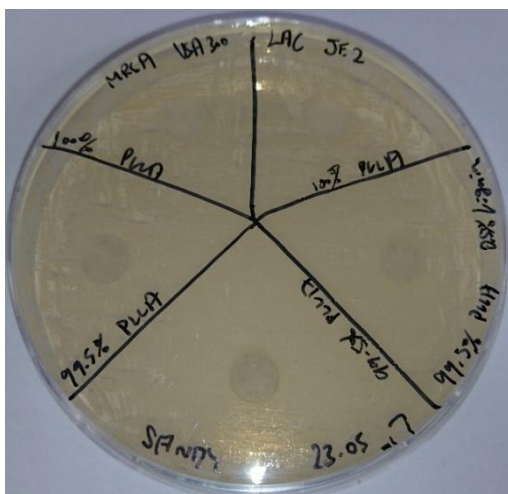
Figure 22. Neat PLA and PLA/lignin composites discs on incubated (a) *MRSA JE2*
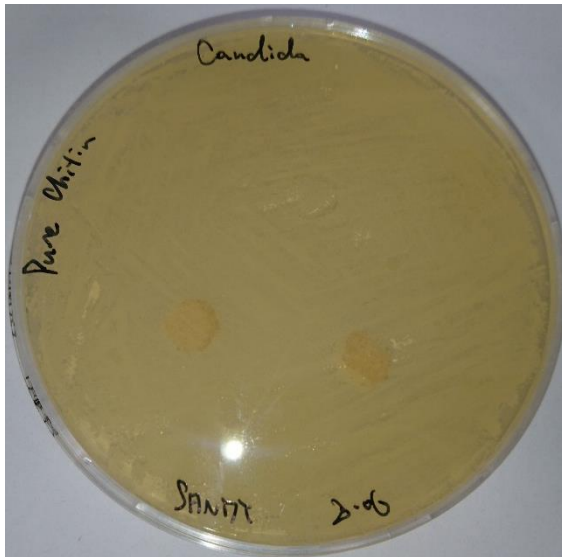
Figure 23. Pure chitin discs on incubated *Candida SC5314*
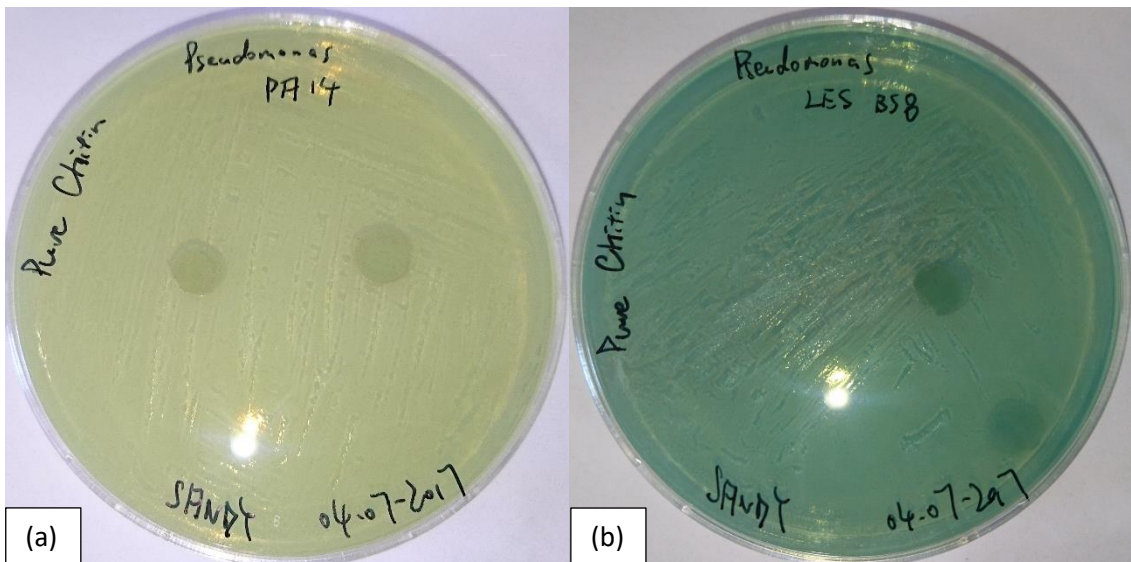
Figure 24. Pure chitin discs on incubated (a) *P. aeruginosa PA14* and (b) *P. aeruginosa LESB58*

6. Images of Kirby-Bauer disk diffusion test results with PLA/WS$_2$ composites discs
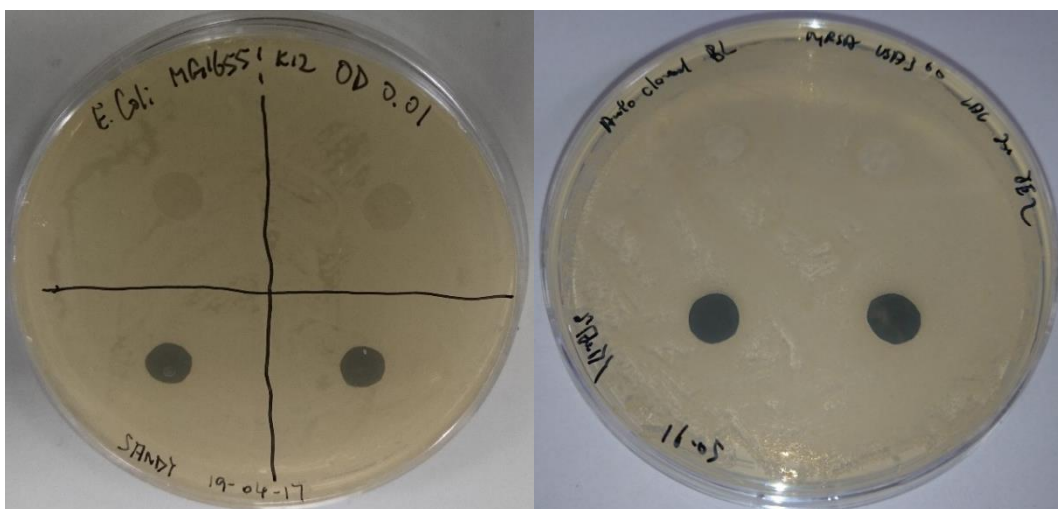
Figure 25. Neat PLA and 90 wt% PLA/ 10 wt% WS$_2$ discs on incubated (a) *E. coli. K12* and (b) *E. coli. Sakai*

7. PLM images for PLLA/WS$_2$ composites
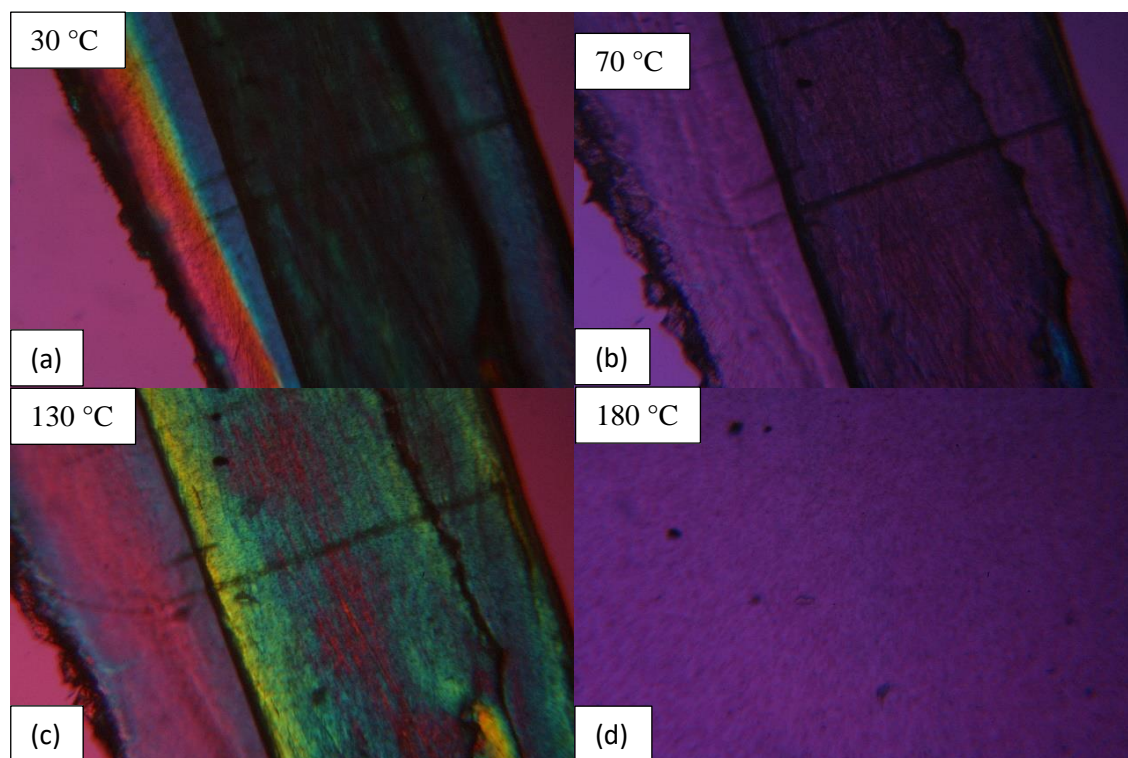
Figure 26. Birefringent crystals of PLA/WS$_2$ (99.5/0.5) at (a) 30 °C, (b) 80 °C, (c) 130 °C and (d) 180°C
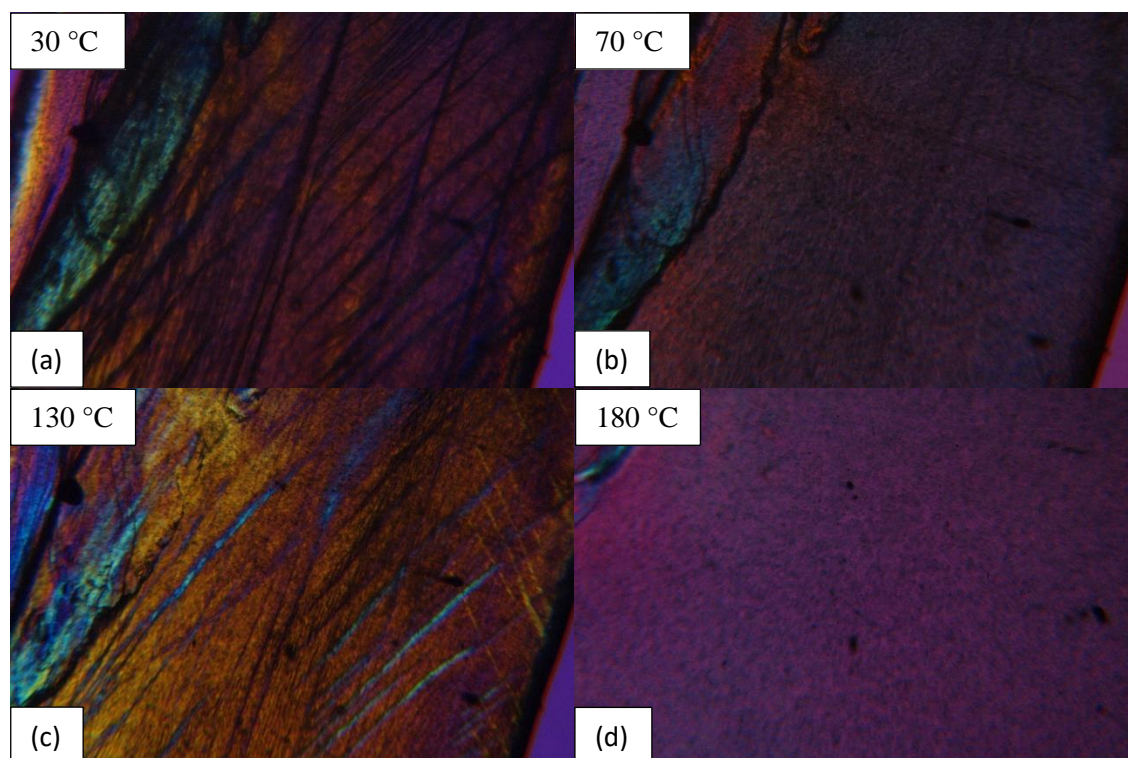
Figure 27. Birefringent crystals of PLA/WS$_2$ (99/1) at (a) 30 °C, (b) 80 °C, (c) 130 °C and (d) 180°C
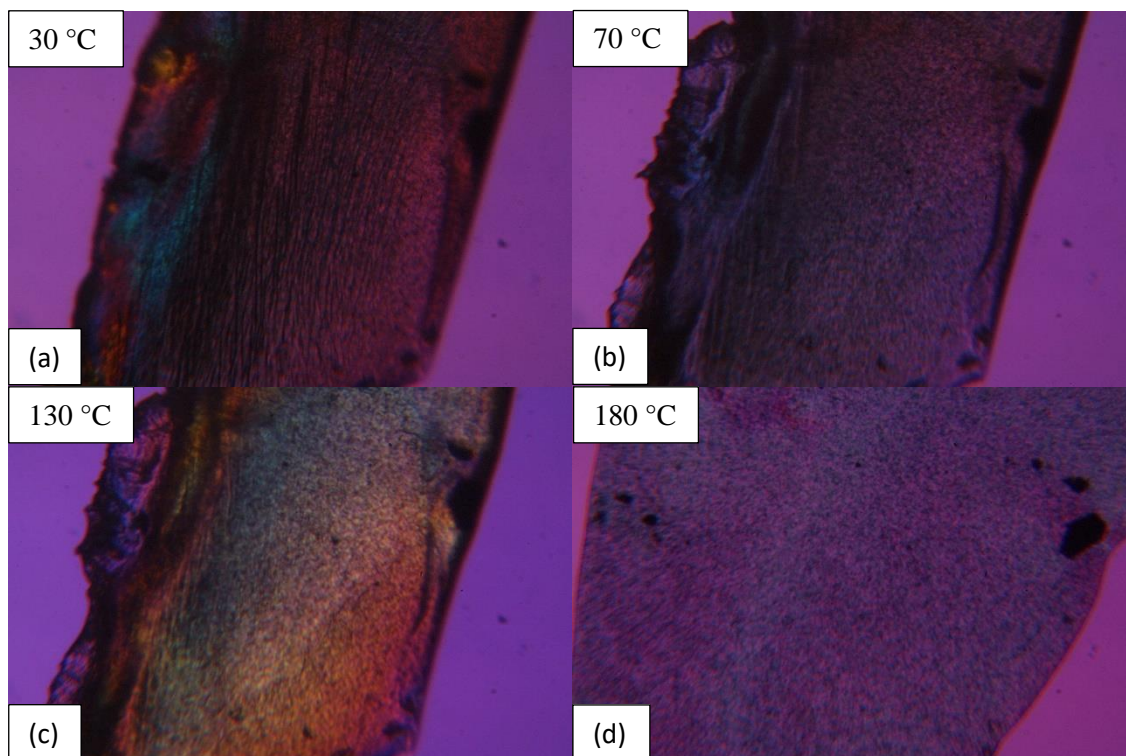
Figure 28. Birefringent crystals of PLA/WS$_2$ (98/2) at (a) 30 °C, (b) 80 °C, (c) 130 °C and (d) 180°C
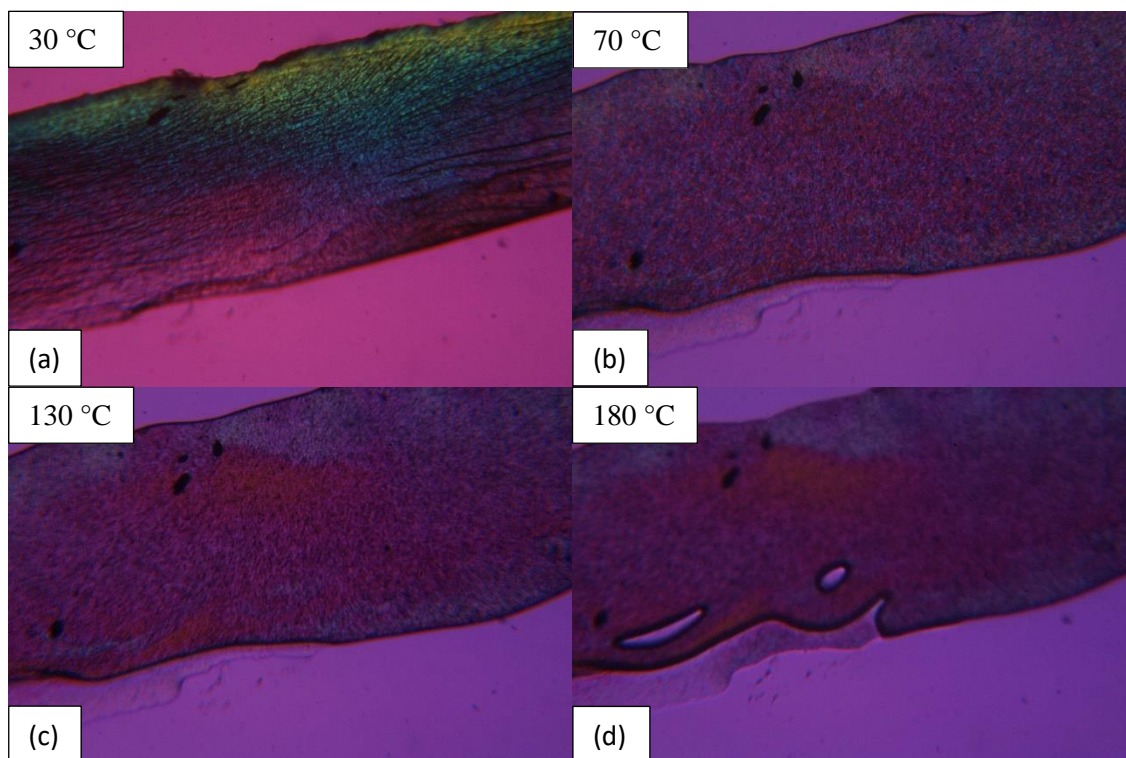
Figure 29. Birefringent crystals of PLA/WS$_2$ (97/3) at (a) 30 °C, (b) 80 °C, (c) 130 °C and (d) 180°C
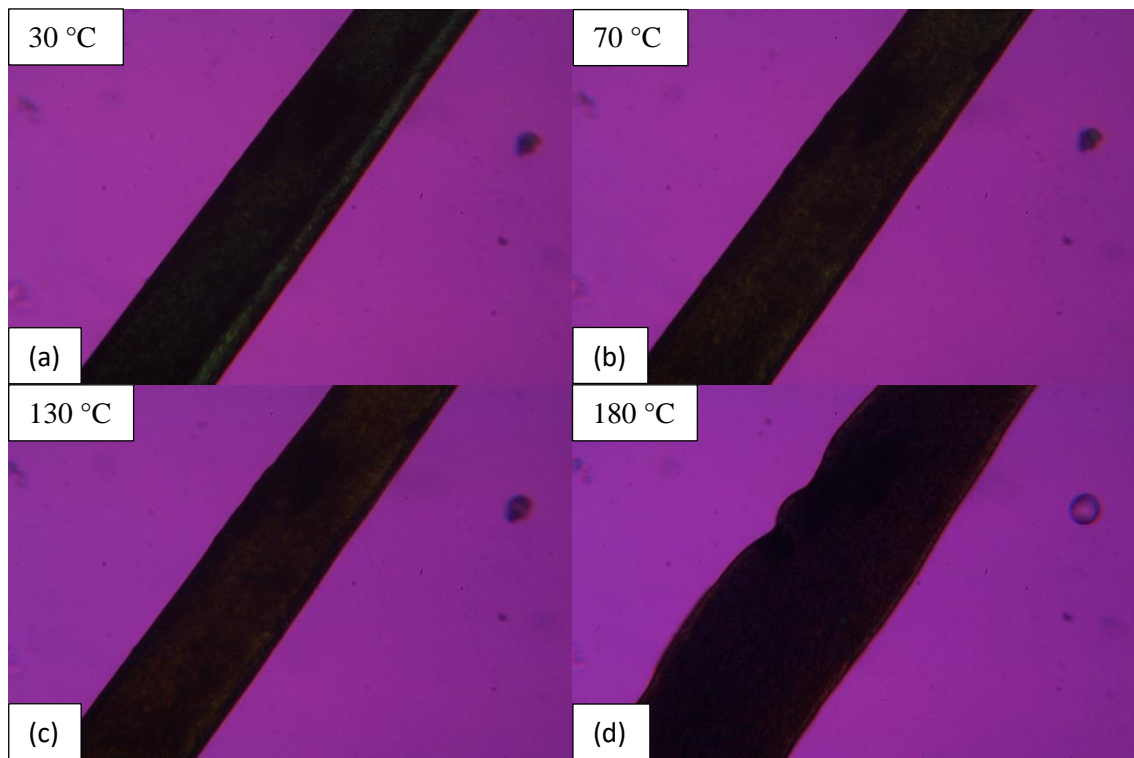
Figure 30. Birefringent crystals of PLA/WS$_2$ (95/5) at (a) 30 °C, (b) 80 °C, (c) 130 °C and (d) 180°C

References

1. Sipos, P., Gyõry, H., Hagymási, K., Ondrejka, P. & Blázovics, A. Special wound healing methods used in ancient egypt and the mythological background. *World J. Surg.* **28,** 211–6 (2004).

2. Natarajan, S., Williamson, D., Grey, J., Harding, K. G. & Cooper, R. a. Healing of an MRSA-colonized, hydroxyurea-induced leg ulcer with honey. *J. Dermatolog. Treat.* **12,** 33–6 (2001).

3. Budzyńska, A. Antibiofilm Activity of Selected Plant Essential Oils and their Major Components. *Polish J. Microbiol.* **60,** 35–41 (2011).

4. Zhou, T. *et al.* Development of biomimetic tilapia collagen nanofibers for skin regeneration through inducing keratinocytes differentiation and collagen synthesis of dermal fibroblasts. *ACS Appl. Mater. Interfaces* **7,** 3253–62 (2015).

5. Peel, E. *et al.* Cathelicidins in the Tasmanian devil (Sarcophilus harrisii). *Sci. Rep.* **6,** 35019 (2016).

6. Ackerman, D. L. *et al.* Human Milk Oligosaccharides Exhibit Antimicrobial and Antibiofilm Properties against Group B Streptococcus. *ACS Infect. Dis.* **3,** 595–605 (2017).

7. O'Neill, J. Antimicrobial resistance: tackling a crisis for the health and wealth of nations. *Rev. Antimicrob. Resist. London, UK* 1–16 (2014).

8. Aminov, R. I. A brief history of the antibiotic era: lessons learned and challenges for the future. *Front. Microbiol.* **1,** 134 (2010).

9. Aldridge, S. & Sturichio, J. *The Discovery and Development of Penicillin: 1928-1945*. (Royal Society of Chemistry, 1999).

10. Landsberg, H. Prelude to the discovery of penicillin. *Hist. Sci. Soc.* **40,** 225–227 (1949).

11. Duckett, S. Ernest Duchesne and the concept of fungal antibiotic therapy. *Lancet (London, England)* **354,** 2068–71 (1999).

12. Bucci, R. & Gallì, P. Vincenzo Tiberio : a misunderstood researcher. *Ital. J. Public Health* **8,** 404–406 (2011).

13. Duchesne, E., Pouillard, J. & Sauvy, A. Une découverte oubliée : la thèse de médecine du docteur. *Hist. Sci. Med.* 11–20 (2002).

14. Chain, E., Florey, H. W. & Jennings, M. A. An Antibacterial Substance Produced by Penicillium claviforme. *Br. J. Exp. Pathol.* **23,** 202–205 (1942).

15. Green, M. W. Microbial antagonisms and antibiotic substances, by Selman A.

Waksman. *J. Am. Pharm. Assoc.* **34,** 248 (1945).

16. Fleming, A. On the antibacterial action of cultures of a penicillium, with special reference to their use in the isolation of B. influenzae. *Br. J. Exp. Pathol.* **10,** 226–236 (1929).

17. Bosch, F. & Rosich, L. The contributions of Paul Ehrlich to pharmacology: a tribute on the occasion of the centenary of his Nobel Prize. *Pharmacology* **82,** 171–9 (2008).

18. Van Epps, H. L. Rene Dubos: unearthing antibiotics. *J. Exp. Med.* **203,** 259–259 (2006).

19. Abraham, E. Howard Walter Florey. Baron Florey of Adelaide and Marston. 1898-1968. *Biogr. Mem. Fellows R. Soc.* **17,** 255–302 (1971).

20. Dougherty, P. J., Carter, P. R., Seligson, D., Benson, D. R. & Purvis, J. M. Orthopaedic surgery advances resulting from World War II. *J. Bone Joint Surg. Am.* **86–A,** 176–81 (2004).

21. Florey, H. The use of micro-organisms for therapeutic purposes. *Yale J. Biol. Med.* **2,** 635–642 (1945).

22. Plata, G., Henry, C. S. & Vitkup, D. Long-term phenotypic evolution of bacteria. *Nature* **517,** 369–372 (2015).

23. Abraham, E. Ernst Boris Chain. 19 June 1906-12 August 1979. *Biogr. Mem. Fellows R. Soc.* **29,** 42–91 (1983).

24. Fleming, A. Nobel Lecture, December 11, 1945. in *Nobel Lecture* 83–93 (1945).

25. WHO | What is antimicrobial resistance? *World Health Organisation* Available at: http://www.who.int/features/qa/75/en/. (Accessed: 20th November 2015)

26. Lindsay, J. a & Holden, M. T. G. Staphylococcus aureus: superbug, super genome? *Trends Microbiol.* **12,** 378–85 (2004).

27. Chang, S. & Sievert, D. Infection with vancomycin-resistant Staphylococcus aureus containing the vanA resistance gene. *N. Engl. J. Med.* **348,** 1342–1347 (2003).

28. Edwards, E., Epton, R. & Marr, G. The synthesis and reactions of homonuclear ferrocene acid anhydrides and their use in the preparation of ferrocenylpenicillins and-cephalosporins. *J. Organomet. Chem.* **168,** 259–272 (1979).

29. Jones, D. S. The Health Care Experiments at Many Farms: The Navajo, Tuberculosis, and the Limits of Modern Medicine, 1952-1962. *Bull. Hist. Med.* **76,** 749–790 (2002).

30.   Nicolaou, K. C., Chen, J. S., Edmonds, D. J. & Estrada, A. a. Recent advances in the chemistry and biology of naturally occurring antibiotics. *Angew. Chem. Int. Ed. Engl.* **48,** 660–719 (2009).

31.   Peláez, F. The historical delivery of antibiotics from microbial natural products--can history repeat? *Biochem. Pharmacol.* **71,** 981–90 (2006).

32.   Fernandes, P. Antibacterial discovery and development—the failure of success. *Nat. Biotechnol.* **24,** 1497–503 (2006).

33.   Clardy, J. & Walsh, C. Lessons from natural molecules. *Nature* **432,** 829–837 (2004).

34.   Lounkine, E. *et al.* Large-scale prediction and testing of drug activity on side-effect targets. *Nature* **486,** 361–7 (2012).

35.   Bérdy, J. Thoughts and facts about antibiotics: Where we are now and where we are heading. *J. Antibiot. (Tokyo).* **65,** 385–395 (2012).

36.   Jassim, S. a a & Limoges, R. G. Natural solution to antibiotic resistance: bacteriophages 'The Living Drugs'. *World J. Microbiol. Biotechnol.* **30,** 2153–70 (2014).

37.   Heine, H. *Innate Immunity of Plants, Animals, and Humans*. **21,** (Springer Berlin Heidelberg, 2008).

38.   World Health Organization. *World Health Organization. World health statistics 2012*. (2012).

39.   Casanova, J. Bacteria and their Dyes: Hans Christian Joachim Gram. *Hist. La Immunol.* **11,** 140–150 (1992).

40.   Franklin, T. J. & Snow, G. A. *Biochemistry and Molecular Biology of Antimicrobial Drug Action*. (Springer US, 2006).

41.   Moyer, C. Some effects of 0.5 per cent silver nitrate and high humidity upon the illness associated with large burns. *J. Natl. Med. Assoc.* **57,** 95–100 (1965).

42.   Edwards-Jones, V. The benefits of silver in hygiene, personal care and healthcare. *Lett. Appl. Microbiol.* **49,** 147–52 (2009).

43.   Silver, S., Phung, L. T. & Silver, G. Silver as biocides in burn and wound dressings and bacterial resistance to silver compounds. *J. Ind. Microbiol. Biotechnol.* **33,** 627–34 (2006).

44.   Kostenko, V., Lyczak, J., Turner, K. & Martinuzzi, R. J. Impact of silver-containing wound dressings on bacterial biofilm viability and susceptibility to antibiotics during prolonged treatment. *Antimicrob. Agents Chemother.* **54,** 5120–

31 (2010).

45. Russell, A. D. & Hugo, W. B. 7 Antimicrobial Activity and Action of Silver. *Prog. Med. Chem.* **31,** 351–370 (1994).

46. Russell, A. D., Path, F. R. C., Sl, F. R. P. & Hugo, W. B. *Antimicrobial Activity and Action of. Progress in medicinal chemistry* **31,** (Elsevier, 1994).

47. Maillard, J.-Y. & Hartemann, P. Silver as an antimicrobial: facts and gaps in knowledge. *Crit. Rev. Microbiol.* **39,** 373–83 (2013).

48. Alluri, H., Ronda, S. & Settalluri, V. Biosorption: An eco-friendly alternative for heavy metal removal. *African J. Biotechnol.* **6,** 2924–2931 (2007).

49. Berra, L. *et al.* Antimicrobial-coated endotracheal tubes: an experimental study. *Intensive Care Med.* **34,** 1020–9 (2008).

50. Olson, M., Harmon, B. & MH, K. Silver-coated endotracheal tubes associated with reduced bacterial burden in the lungs of mechanically ventilated dogs. *CHEST J.* **121,** 863–870 (2002).

51. Li, X., Nikaido, H. & Williams, K. Silver-resistant mutants of Escherichia coli display active efflux of Ag+ and are deficient in porins. *J. Bacteriol.* **179,** 6127–6132 (1997).

52. Wasserscheid, P. & Welton, T. *Ionic liquids in synthesis*. **7,** (Wiley-VCH, 2008).

53. Pernak, J., Sobaszkiewicz, K. & Mirska, I. Anti-microbial activities of ionic liquids. *Green Chem.* **5,** 52–56 (2003).

54. Cole, M. R. *et al.* Design, synthesis, and biological evaluation of β-lactam antibiotic-based imidazolium- and pyridinium-type ionic liquids. *Chem. Biol. Drug Des.* **78,** 33–41 (2011).

55. Hough, W. L. *et al.* The third evolution of ionic liquids: active pharmaceutical ingredients. *New J. Chem.* **31,** 1429 (2007).

56. Andrews, J. M. Determination of minimum inhibitory concentrations. *J. Antimicrob. Chemother.* **48,** 5–16 (2001).

57. McRorie, J., Daggy, B. & Morel, J. Psyllium is superior to docusate sodium for treatment of chronic constipation. *Aliment. Pharmacol. Ther.* **12,** 491–497 (1998).

58. Choi, S. Y. *et al.* Dual functional ionic liquids as plasticisers and antimicrobial agents for medical polymers. *Green Chem.* **13,** 1527–1535 (2011).

59. Choi, S. Y. *et al.* Dual functional ionic liquids as antimicrobials and plasticisers for medical grade PVCs. *RSC Adv.* **4,** 8567–8581 (2014).

60. Anderl, J. N., Franklin, M. J. & Stewart, P. S. Role of Antibiotic Penetration

Limitation in Klebsiella pneumoniae Biofilm Resistance to Ampicillin and Ciprofloxacin. *Antimicrob. Agents Chemother.* **44,** 1818–1824 (2000).

61. Mathieu-Denoncourt, J., Wallace, S. J., de Solla, S. R. & Langlois, V. S. Plasticizer endocrine disruption: Highlighting developmental and reproductive effects in mammals and non-mammalian aquatic species. *Gen. Comp. Endocrinol.* **219,** 74–88 (2015).

62. Moyer, B. & Hixon, M. L. Reproductive effects in F1 adult females exposed in utero to moderate to high doses of mono-2-ethylhexylphthalate (MEHP). *Reprod. Toxicol.* **34,** 43–50 (2012).

63. Ernot, R. A. J. B., Rueseke, M. I. A. B., Hite, M. I. A. E. V. & Amberti, G. A. R. Y. A. L. Acute and chronic toxicity of imidazolium-based ionic liquids on Daphnia magna. *Environ. Toxicol. Chem.* **24,** 87–92 (2005).

64. Stepnowski, P., Skladanowski, A. C., Ludwiczak, A. & Laczyńska, E. Evaluating the cytotoxicity of ionic liquids using human cell line HeLaEvaluating the cytotoxicity of ionic liquids using human cell line HeLa. *Hum. Exp. Toxicol.* **23,** 513–517 (2004).

65. Stock, F. *et al.* Effects of ionic liquids on the acetylcholinesterase – a structure–activity relationship consideration. *Green Chem.* **6,** 286–209 (2004).

66. Cowan, M. M. Plant products as antimicrobial agents. *Clin. Microbiol. Rev.* **12,** 564–82 (1999).

67. Geissman, T. A. Flavonoid Compounds, Tannins, Lignins and, Related Compounds. *Compr. Biochem.* **9,** 213–250 (1963).

68. Huang, W. Y., Cai, Y. Z. & Zhang, Y. Natural phenolic compounds from medicinal herbs and dietary plants: Potential use for cancer prevention. *Nutrition and Cancer* **62,** 1–20 (2010).

69. Eckardt, N. A. Probing the mysteries of lignin biosynthesis: the crystal structure of caffeic acid/5-hydroxyferulic acid 3/5-O-methyltransferase provides new insights. *Plant Cell* **14,** 1185–9 (2002).

70. Wang, H., Provan, G. J. & Helliwell, K. Determination of rosmarinic acid and caffeic acid in aromatic herbs by HPLC. *Food Chem.* **87,** 307–311 (2004).

71. Harel, K., Mayer, A. M. & Shain, Y. Catechol Oxidases from Apples, their Properties, Subcellular Location and Inhibition. *Physiol. Plant.* **17,** 921–930 (1964).

72. Lana, E. J. L., Carazza, F. & Takahashi, J. A. Antibacterial evaluation of 1,4-

benzoquinone derivatives. *J. Agric. Food Chem.* **54,** 2053–2056 (2006).

73.   Hopkins, T. L. *et al.* Catechols involved in sclerotization of cuticle and egg pods of the grasshopper, Melanoplus sanguinipes, and their interactions with cuticular proteins. *Arch. Insect Biochem. Physiol.* **40,** 119–128 (1999).

74.   Mohammad Nazrul Islam Bhuiyan. Constituents of the essential oil from leaves and buds of clove (Syzigium caryophyllatum (L.) Alston). *African J. Pharm. Pharmacol.* **6,** 1260–1263 (2012).

75.   Mallavarapu, G. R. *et al.* Investigation of the essential oil of cinnamon leaf grown at Bangalore and Hyderabad. *Flavour Fragr. J.* **10,** 239–242 (1995).

76.   Gill, A. O. & Holley, R. A. Mechanisms of bactericidal action of cinnamaldehyde against Listeria monocytogenes and of eugenol against L. monocytogenes and Lactobacillus sakei. *Appl. Environ. Microbiol.* **70,** 5750–5755 (2004).

77.   Maddox, C. E., Laur, L. M. & Tian, L. Antibacterial activity of phenolic compounds against the phytopathogen Xylella fastidiosa. *Curr. Microbiol.* **60,** 53–58 (2010).

78.   Wu, Y. *et al.* Antibacterial activity and membrane-disruptive mechanism of 3-p-trans-coumaroyl-2-hydroxyquinic acid, a novel phenolic compound from pine needles of Cedrus deodara, against Staphylococcus aureus. *Molecules* **21,** (2016).

79.   Turmeric | Cancer in general | Cancer Research UK. *Cancer Research UK* Available at: http://www.cancerresearchuk.org/about-cancer/cancer-in-general/treatment/complementary-alternative-therapies/individual-therapies/turmeric. (Accessed: 22nd March 2018)

80.   Nelson, K. M. *et al.* The Essential Medicinal Chemistry of Curcumin. *J. Med. Chem.* **60,** 1620–1637 (2017).

81.   Ackerman, T. M.D. Anderson professor under fraud probe - Houston Chronicle. *Chron* Available at: https://www.chron.com/news/houston-texas/article/M-D-Anderson-professor-under-fraud-probe-3360037.php. (Accessed: 23rd March 2018)

82.   Zaidi, A., Lai, M. & Cavenagh, J. Long-term stabilisation of myeloma with curcumin. *BMJ Case Rep.* **2017,** (2017).

83.   Tønnesen, H. H. Chemistry of Curcumin and Curcuminoids. in *Phenolic Compounds in Food and their Effects on Health I* **1,** 143–153 (1992).

84.   Sharma, O. P. Antioxidant activity of curcumin and related compounds. *Biochem. Pharmacol.* **25,** 1811–1812 (1976).

85.   Tyagi, P., Singh, M., Kumari, H., Kumari, A. & Mukhopadhyay, K. Bactericidal activity of curcumin I is associated with damaging of bacterial membrane. *PLoS One* **10,** e0121313 (2015).

86.   Dogra, N. *et al.* Polydiacetylene nanovesicles as carriers of natural phenylpropanoids for creating antimicrobial food-contact surfaces. *J. Agric. Food Chem.* **63,** 2557–65 (2015).

87.   Coleman, M. M. & Painter, P. C. *Fundamentals of Polymer Science*. (Taylor & Francis, 1996).

88.   IUPAC. *Compendium of Chemical Terminology Gold Book*. (2014).

89.   Mülhaupt, R. Hermann staudinger and the origin of macromolecular chemistry. *Angew. Chemie - Int. Ed.* **43,** 1054–1063 (2004).

90.   Hermann Staudinger Foundation of Polymer Science - Landmark - American Chemical Society. Available at: https://www.acs.org/content/acs/en/education/whatischemistry/landmarks/staudingerpolymerscience.html. (Accessed: 27th September 2017)

91.   PlasticsEurope. *PlasticsEurope, The Compelling Facts About Plastics: An Analysis of Plastic Production, Demand and Recovery for 2006 in Europe*. (2016).

92.   Hanle, J. E., Merz, E. H. & Mesrobian, R. B. Polymers in packaging. *J. Polym. Sci. Part C Polym. Symp.* **12,** 185–195 (1966).

93.   Correia Diogo, A. Polymers in building and construction. in *Materials for Construction and Civil Engineering: Science, Processing, and Design* 447–499 (Springer International Publishing, 2015).

94.   Fuchs, E. R. H., Field, F. R., Roth, R. & Kirchain, R. E. Strategic materials selection in the automobile body: Economic opportunities for polymer composite design. *Compos. Sci. Technol.* **68,** 1989–2002 (2008).

95.   Aminabhavi, T. M., Cassidy, P. E. & Biradar, N. S. Versatile Lightweight Polymer Composites. *J. Macromol. Sci. Part C Polym. Rev.* **27,** 459–503 (1987).

96.   Geyer, R., Jambeck, J. R. & Law, K. L. Production, use, and fate of all plastics ever made. *Sci. Adv.* **3,** 1–5 (2017).

97.   Barnes, D. K. A., Galgani, F., Thompson, R. C. & Barlaz, M. Accumulation and fragmentation of plastic debris in global environments. *Philos. Trans. R. Soc. Lond. B. Biol. Sci.* **364,** 1985–98 (2009).

98.   Wagner, M. *et al.* Microplastics in freshwater ecosystems: what we know and what we need to know. *Environ. Sci. Eur.* **26,** 12 (2014).

99.   IMMERGUT, E. H. & MARK, H. F. Principles of Plasticization. in *Plasticization and Plasticizer Processes* 1 (1965).

100.   Lithner, D., Larsson, A. & Dave, G. Environmental and health hazard ranking and assessment of plastic polymers based on chemical composition. *Sci. Total Environ.* **409,** 3309–3324 (2011).

101.   Sung, M.-H. *et al.* Natural and edible biopolymer poly-gamma-glutamic acid: synthesis, production, and applications. *Chem. Rec.* **5,** 352–66 (2005).

102.   S. Slater, D. Glassner, E. Vink, T. G. Evaluating the Environmental Impact of Biopolymers. *Biopolym. Online* **10,** 473–480 (2003).

103.   Keoke, E. D. & Porterfield, K. M. *Encyclopedia of American Indian contributions to the world : 15,000 years of inventions and innovations*. (2002).

104.   Yamanaka, S. *et al.* The structure and mechanical properties of sheets prepared from bacterial cellulose. *J. Mater. Sci.* **24,** 3141–3145 (1989).

105.   Ach, A. Biodegradable plastics based on cellulose acetate. *J. Macromol. Sci. Part A* **30,** 733–740 (1993).

106.   Gomes, M. E., Ribeiro, A. S., Malafaya, P. B., Reis, R. L. & Cunha, A. M. A new approach based on injection moulding to produce biodegradable starch-based polymeric scaffolds: Morphology, mechanical and degradation behaviour. *Biomaterials* **22,** 883–889 (2001).

107.   Leach, J. B. & Schmidt, C. E. Characterization of protein release from photocrosslinkable hyaluronic acid-polyethylene glycol hydrogel tissue engineering scaffolds. *Biomaterials* **26,** 125–35 (2005).

108.   Albuquerque, M. G. E., Eiroa, M., Torres, C., Nunes, B. R. & Reis, M. A. M. Strategies for the development of a side stream process for polyhydroxyalkanoate (PHA) production from sugar cane molasses. *J. Biotechnol.* **130,** 411–421 (2007).

109.   Jacquel, N., Lo, C. W., Wei, Y. H., Wu, H. S. & Wang, S. S. Isolation and purification of bacterial poly(3-hydroxyalkanoates). *Biochemical Engineering Journal* **39,** 15–27 (2008).

110.   Chee, J.-Y. *et al.* Bacterially Produced Polyhydroxyalkanoate (PHA): Converting Renewable Resources into Bioplastics. *Curr. Res. Technol. Educ. Top. Appl. Microbiol. Microb. Biotechnol.* 1395–1404 (2010).

111.   Auras, R., Auras & Rafael. Poly(lactic acid). in *Encyclopedia of Polymer Science and Technology* 1 (John Wiley & Sons, Inc., 2010).

112.   Wang, Y. *et al.* Accelerated hydrolytic degradation of poly(lactic acid) achieved

by adding poly(butylene succinate). *Polym. Bull.* **73,** 1067–1083 (2016).

113. Lee, S. H., Kim, I. Y. & Song, W. S. Biodegradation of polylactic acid (PLA) fibers using different enzymes. *Macromol. Res.* **22,** 657–663 (2014).

114. Auras, R., Harte, B. & Selke, S. An overview of polylactides as packaging materials. *Macromol. Biosci.* **4,** 835–64 (2004).

115. Garcia, M., Martino, M. & Zaritzky, N. lasticized starch-based coatings to improve strawberry (Fragaria× ananassa) quality and stability. *J. Agric. Food Chem.* **8561,** 3758–3767 (1998).

116. Cha, D. S. & Chinnan, M. S. Biopolymer-based antimicrobial packaging: a review. *Crit. Rev. Food Sci. Nutr.* **44,** 223–37 (2004).

117. Rancan, F. *et al.* Investigation of Polylactic Acid (PLA) Nanoparticles as Drug Delivery Systems for Local Dermatotherapy. *Pharm. Res.* **26,** 2027–2036 (2009).

118. Savioli Lopes, M., Jardini, A. L. & Maciel Filho, R. Poly (lactic acid) production for tissue engineering applications. in *Procedia Engineering* **42,** 1402–1413 (2012).

119. Kaplan, D. L. High Molecular Weight Polylactic Acid Polymers. in *Biopolymers from Renewable Resources* 367–411 (Springer Berlin Heidelberg, 1998).

120. Benninga, H. (Harm). A Chapter in the History of Biotechnology. in *A History of Lactic Acid Making* 16 (Kluwer Academic Publishers, 1990).

121. Carothers, W. H., Borough, G. L. & Natta, F. J. Studies of polymerization and ring formation. X. The reversible polymerization of six-membered cyclic esters. *J. Am. Chem. Soc.* **54,** 761–772 (1932).

122. Auras, R., Lim, L. T., Selke, S. E. M. & Tsuji, H. Frontmatter. in *Poly(Lactic Acid): Synthesis, Structures, Properties, Processing, and Applications* i–xxiii (John Wiley & Sons, Inc., 2010).

123. Henshaw, J. M., Han, W. & Owens, A. D. An Overview of Recycling Issues for Composite Materials. *J. Thermoplast. Compos. Mater.* **9,** 4–20 (1996).

124. Sheavly, S. B. & Register, K. M. Marine debris & plastics: Environmental concerns, sources, impacts and solutions. *J. Polym. Environ.* **15,** 301–305 (2007).

125. Gruber, P., O'Brien, M., Gruber, P. & O'Brien, M. Polylactides "NatureWorks® PLA". in *Biopolymers Online* 238–239 (Wiley-VCH Verlag GmbH & Co. KGaA, 2005).

126. Benninga, H. (Harm). *A history of lactic acid making : a chapter in the history of biotechnology.* (Kluwer Academic Publishers, 1990).

127. Jem, K. J., van der Pol, J. F. & de Vos, S. Microbial Lactic Acid, Its Polymer Poly(lactic acid), and Their Industrial Applications. in *Plastics from Bacteria: Natural Functions and Applications* **14,** 323–346 (Springer, Berlin, Heidelberg, 2010).

128. Hartmann, M. H. High Molecular Weight Polylactic Acid Polymers. in *Biopolymers from Renewable Resources* 367–411 (Springer Berlin Heidelberg, 1998).

129. Katz, A. & Sahlin, K. Regulation of lactic acid production during exercise. *J. Appl. Physiol.* **65,** 509–18 (1988).

130. Erwin, A. L. & Gotschlich, E. C. Cloning of a Neisseria meningitidis Gene for L-Lactate Dehydrogenase (L-LDH): Evidence for a Second Meningococcal L-LDH with Different Regulation. *J. Bacteriol.* **178,** 4807–4813 (1996).

131. Chang, D. E., Jung, H. C., Rhee, J. S. & Pan, J. G. Homofermentative production of D- or L-lactate in metabolically engineered Escherichia coli RR1. *Appl. Environ. Microbiol.* **65,** 1384–1389 (1999).

132. Inkinen, S., Hakkarainen, M., Albertsson, A. C. & Södergård, A. From lactic acid to poly(lactic acid) (PLA): Characterization and analysis of PLA and Its precursors. *Biomacromolecules* **12,** 523–532 (2011).

133. Ren, J. Lactic Acid. in *Biodegradable Poly(Lactic Acid): Synthesis, Modification, Processing and Applications* 5 (Springer Berlin Heidelberg, 2010).

134. Jiménez, A., Peltzer, M. A. & Ruseckaite, R. A. *Poly(lactic acid) Science and Technology: Processing, Properties, Additives and Applications*. *RSC Polymer Chemistry Series* (2015). doi:10.1007/s13398-014-0173-7.2

135. Alavi, S. *et al.* Polymers for packaging applications. 134 (2014).

136. Hess, J., Muller, K. R. & Muller, M. Process for preparing D,L-Lactide US5149833 A. (1991).

137. Marshall, E. L., Tutu, J. J. A. O. & Smith, S. A. C. Separation Process US20140141475 A1. (2012).

138. Ovitt, T. M. & Coates, G. W. Stereoselective ring-opening polymerization of meso-lactide: Synthesis of syndiotactic poly(lactic acid). *Am. Chem. Soc. Polym. Prepr. Div. Polym. Chem.* **41,** 385 (2000).

139. Radano, C. P., Baker, G. L. & Smith, M. R. Stereoselective polymerization of a racemic monomer with a racemic catalyst: Direct preparation of the polylactic acid stereocomplex from racemic lactide [7]. *Journal of the American Chemical Society*

122, 1552–1553 (2000).

140. Li, T., Strunz, S., Radke, W., Klein, R. & Hofe, T. Chromatographic separation of polylactides by stereochemical composition. *Polymer (Guildf).* **52,** 40–45 (2011).

141. Kashima, T., Kameoka, T., Higuchi, C., Ajioka, M. & Yamaguchi, A. Aliphatic polyester and preparation process thereof US5428126 A. (1995).

142. Ajioka, M., Enomoto, K., Suzuki, K. & Yamaguchi, A. Basic Properties of Polylactic Acid Produced by the Direct Condensation Polymerization of Lactic Acid. *Bull. Chem. Soc. Jpn.* **68,** 2125–2131 (1995).

143. Ajioka, M., Enomoto, K. & K., S. The basic properties of poly lactic acid produced by the direct condensation polymerisation of lactic acid. *J. Environ. Polym. Degrad.* **3,** 225–234 (1995).

144. Ren, J. Synthesis and Manufacture of PLA. in *Biodegradable Poly(Lactic Acid): Synthesis, Modification, Processing and Applications* 21–23 (Springer Berlin Heidelberg, 2010). doi:10.1007/978-3-642-17596-1_3

145. Auras, R. A., Harte, B., Selke, S. & Hernandez, R. Mechanical, Physical, and Barrier Properties of Poly(Lactide) Films. *J. Plast. Film Sheeting* **19,** 123–135 (2003).

146. Murariu, M., Da Silva Ferreira, A., Alexandre, M. & Dubois, P. Polylactide (PLA) designed with desired end-use properties: 1. PLA compositions with low molecular weight ester-like plasticizers and related performances. *Polym. Adv. Technol.* **19,** 636–646 (2008).

147. Gilding, D. K. & Reed, A. M. Biodegradable polymers for use in surgery-polyglycolic/poly(actic acid) homo- and copolymers: 1. *Polymer (Guildf).* **20,** 1459–1464 (1979).

148. Karst, D. & Yang, Y. Molecular modeling study of the resistance of PLA to hydrolysis based on the blending of PLLA and PDLA. *Polymer (Guildf).* **47,** 4845–4850 (2006).

149. Zhang, J., Tashiro, K., Tsuji, H. & Domb, A. J. Investigation of phase transitional behavior of poly(L-lactide)/ poly(D-lactide) blend used to prepare the highly-oriented stereocomplex. *Macromolecules* **40,** 1049–1054 (2007).

150. Xu, H., Teng, C. & Yu, M. Improvements of thermal property and crystallization behavior of PLLA based multiblock copolymer by forming stereocomplex with PDLA oligomer. *Polymer (Guildf).* **47,** 3922–3928 (2006).

151. Kang, N. *et al.* Stereocomplex block copolymer micelles: Core-shell

nanostructures with enhanced stability. *Nano Lett.* **5,** 315–319 (2005).

152. Tsuji, H. & Ikada, Y. Stereocomplex formation between enantiomeric poly(lactic acid)s. XI. Mechanical properties and morphology of solution-cast films. *Polymer (Guildf).* **40,** 6699–6708 (1999).

153. Södergård, A. & Stolt, M. Properties of lactic acid based polymers and their correlation with composition. *Progress in Polymer Science (Oxford)* **27,** 1123–1163 (2002).

154. Khodabakhshi, K. Poly (Lactic Acid) Thermoplastic Composites from Renewable Materials. in *Handbook of Composites from Renewable Materials* 69–102 (John Wiley & Sons, Inc., 2017).

155. Sinclair, R. G. The Case for Polylactic Acid as a Commodity Packaging Plastic. *J. Macromol. Sci. Part A* **33,** 585–597 (1996).

156. Inamuddin. High-Performance Polylactide and Its Composites. in *Green Polymer Composites Technology: Properties and Applications* **29,** 69–75 (2001).

157. Grizzi, I., Garreau, H., Li, S. & Vert, M. Hydrolytic degradation of devices based on poly(dl-lactic acid) size-dependence. *Biomaterials* **16,** 305–311 (1995).

158. Mattiasson, B., Kumar, A. & Galaev, I. Introduction to Polylactide. in *Macroporous polymers : production properties and biotechnological/biomedical applications* 120 (CRC Press/Taylor & Francis, 2010).

159. Bergsma, J. E. *et al.* Biocompatibility study of as-polymerized poly(L-lactide) in rats using a cage implant system. *J. Biomed. Mater. Res.* **29,** 173–179 (1995).

160. Xavier, M. V. *et al.* PLLA Synthesis and Nanofibers Production: Viability by Human Mesenchymal Stem Cell from Adipose Tissue. in *Procedia CIRP* **49,** 213–221 (Elsevier, 2016).

161. Barber, F. A. & Dockery, W. D. Long-term Absorption of β-Tricalcium Phosphate Poly-L-Lactic Acid Interference Screws. *Arthrosc. - J. Arthrosc. Relat. Surg.* **24,** 441–447 (2008).

162. Fakirov, S. Biodegradable Polyester: Synthesis, Properties, Applications. in *Biodegradable polyesters* 370

163. Tokiwa, Y., Calabia, B. P., Ugwu, C. U. & Aiba, S. Biodegradability of plastics. *International Journal of Molecular Sciences* **10,** 3722–3742 (2009).

164. Fundador, N. G. V., Takemura, A. & Iwata, T. Structural Properties and Enzymatic Degradation Behavior of PLLA and Stereocomplexed PLA Nanofibers. *Macromol. Mater. Eng.* **295,** 865–871 (2010).

165. Andersson, S. R., Hakkarainen, M., Inkinen, S., Södergård, A. & Albertsson, A. C. Customizing the hydrolytic degradation rate of stereocomplex PLA through different PDLA architectures. *Biomacromolecules* **13,** 1212–1222 (2012).

166. Ishii, D. *et al.* In vivo tissue response and degradation behavior of PLLA and stereocomplexed PLA nanofibers. *Biomacromolecules* **10,** 237–242 (2009).

167. Auras, R., Lim, L.-T., Selke, S. E. M. & Tsuji, H. Modification of PLA Properties by Process Aids and Other Additives. in *Poly(lactic acid), synthesis, structures, properties, processing, and applications* 499 (Wiley, 2010).

168. Giles, H. F., Wagner, J. R. & Mount, E. M. Single Screw Extruder: Equipment. in *Extrusion: The Definitive Processing Guide and Handbook Library of Congress Cataloging-in-Publication Data* 13–32 (2005).

169. Lee, J. K. & Han, C. D. Evolution of polymer blend morphology during compounding in a twin-screw extruder. *Polymer (Guildf).* **41,** 1799–1815 (2000).

170. Taubner, V. & Shishoo, R. Influence of processing parameters on the degradation of poly(L-lactide) during extrusion. *J. Appl. Polym. Sci.* **79,** 2128–2135 (2001).

171. Rosato, D. V & Rosato, M. G. Injection Molding Machines. in *Injection molding handbook* 172 (Kluwer Academic Publishers, 2000).

172. Dimla, D. E., Camilotto, M. & Miani, F. Design and optimisation of conformal cooling channels in injection moulding tools. *J. Mater. Process. Technol.* **164–165,** 1294–1300 (2005).

173. von Oepen, R. & Michaeli, W. Injection moulding of biodegradable implants. *Clin. Mater.* **10,** 21–28 (1992).

174. Sadeghi-Avalshahr, A. R., Khorsand-Ghayeni, M., Nokhasteh, S., Molavi, A. M. & Sadeghi-Avalshahr, M. Physical and mechanical characterization of PLLA interference screws produced by two stage injection molding method. *Prog. Biomater.* **5,** 183–191 (2016).

175. Ghosh, S., Viana, J. C., Reis, R. L. & Mano, J. F. Effect of processing conditions on morphology and mechanical properties of injection-molded poly(L-lactic acid). *Polym. Eng. Sci.* **47,** 1141–1147 (2007).

176. REN, J. Shear Controlled Orientation in Injection Molding of PLLA. in *Biodegradable Poly(Lactic Acid). Synthesis, modification, processing and applications* 150–151 (Spriner, 2010).

177. Reis, R. L., Cunha, A. M., Allan, P. S. & Bevis, M. J. Mechanical Behavior of Injection-molded Starch-based Polymers. *Polym. Adv. Technol.* **7,** 784–790

(1996).

178. Ghosh, S., Viana, J. C., Reis, R. L. & Mano, J. F. Oriented morphology and enhanced mechanical properties of poly(l-lactic acid) from shear controlled orientation in injection molding. *Mater. Sci. Eng. A* **490,** 81–89 (2008).

179. Griffiths, C. A. *et al.* Investigation of polymer inserts as prototyping tooling for micro injection moulding. *Int. J. Adv. Manuf. Technol.* **47,** 111–123 (2010).

180. Park, J. H. *et al.* Polymer particle-based micromolding to fabricate novel microstructures. *Biomed. Microdevices* **9,** 223–234 (2007).

181. Liu, S. J., Chiang, F. J., Hsiao, C. Y., Kau, Y. C. & Liu, K. S. Fabrication of balloon-expandable self-lock drug-eluting polycaprolactone stents using micro-injection molding and spray coating techniques. *Ann. Biomed. Eng.* **38,** 3185–3194 (2010).

182. Zhang, J., Duan, Y., Domb, A. J. & Ozaki, Y. PLLA mesophase and its phase transition behavior in the PLLA-PEG-PLLA copolymer as revealed by infrared spectroscopy. *Macromolecules* **43,** 4240–4246 (2010).

183. Uu, H.-J., Hsieh, C.-T. & Hu, D. S. Solute diffusion through degradable semicrystalline. *Polym. Bull.* **470,** 463–470 (1994).

184. Lee, J. H., Go, A. K., Oh, S. H., Lee, K. E. & Yuk, S. H. Tissue anti-adhesion potential of ibuprofen-loaded PLLA-PEG diblock copolymer films. *Biomaterials* **26,** 671–678 (2005).

185. Maglio, G., Migliozzi, A., Palumbo, R., Immirzi, B. & Volpe, M. G. Compatibilized poly (ϵ-caprolactone)/poly (l-lactide) blends for biomedical uses. *Macromol. Rapid Commun.* **238,** 236–238 (1999).

186. Zeng, J.-B., Li, Y.-D., He, Y.-S., Li, S.-L. & Wang, Y.-Z. Improving Flexibility of Poly(l -lactide) by Blending with Poly(l -lactic acid) Based Poly(ester-urethane): Morphology, Mechanical Properties, and Crystallization Behaviors. *Ind. Eng. Chem. Res.* **50,** 6124–6131 (2011).

187. Todo, M., Park, S. D., Takayama, T. & Arakawa, K. Fracture micromechanisms of bioabsorbable PLLA/PCL polymer blends. *Eng. Fract. Mech.* **74,** 1872–1883 (2007).

188. Paul, M. A. *et al.* New nanocomposite materials based on plasticized poly(L-lactide) and organo-modified montmorillonites: Thermal and morphological study. *Polymer (Guildf).* **44,** 443–450 (2002).

189. Ghosh, S., Viana, J. C., Reis, R. L. & Mano, J. F. Development of porous lamellar

poly(l-lactic acid) scaffolds by conventional injection molding process. *Acta Biomater.* **4,** 887–896 (2008).

190. Jiang, X. *et al.* Bacterial adhesion on honeycomb-structured poly(L-lactic acid) surface with Ag nanoparticles. *J. Biomed. Nanotechnol.* **8,** 791–799 (2012).

191. de Candolle, M. A. P. *Theorie Elementaire de la Botanique ou Exposition des Principes de la Classification Naturelle et de l'Art de Decrire et d'Etudier les Vegetaux. Paris, Déterville* (Paris, Déterville, 2014). doi:10.1007/s13398-014-0173-7.2

192. Cano-delgado, A., Penfield, S., Smith, C., Catley, M. & Ã, M. B. Reduced cellulose synthesis invokes lignification and defense responses in Arabidopsis thaliana. *Plant J.* **34,** 351–362 (2003).

193. Vanholme, R., Demedts, B., Morreel, K., Ralph, J. & Boerjan, W. Lignin Biosynthesis and Structure. *Plant Physiol.* **153,** 895–905 (2010).

194. Boerjan, W., Ralph, J. & Baucher, M. LIGNIN BIOSYNTHESIS. *Annu. Rev. Plant Biol.* **54,** 519–546 (2003).

195. Vanholme, R., Demedts, B., Morreel, K., Ralph, J. & Boerjan, W. Lignin Biosynthesis and Structure. *Plant Physiol.* **153,** 895–905 (2010).

196. Chakar, F. S. & Ragauskas, A. J. Biobleaching chemistry of laccase-mediator systems on high-lignin-content kraft pulps. *Can. J. Chem.* **82,** 344–352 (2004).

197. Ralph, J. *et al.* Lignins: Natural polymers from oxidative coupling of 4-hydroxyphenyl- propanoids. *Phytochem. Rev.* **3,** 29–60 (2004).

198. Adler, E. Lignin chemistry-past, present and future. *Wood Sci. Technol.* **11,** 169–218 (1977).

199. Stewart, J. J., Akiyama, T., Chapple, C., Ralph, J. & Mansfield, S. D. The effects on lignin structure of overexpression of ferulate 5-hydroxylase in hybrid poplar. *Plant Physiol.* **150,** 621–635 (2009).

200. Du, X., Gellerstedt, G. & Li, J. Universal fractionation of lignin–carbohydrate complexes (LCCs) from lignocellulosic biomass an example using spruce wood. *Plant J.* **74,** 328–338 (2013).

201. Hubbe, M. a. & Lucia, L. a. The 'love-hate' relationship present in lignocellulosic materials. *BioResources* **2,** 534–535 (2007).

202. Sarkanen, K. & Ludwig, C. Lignins: Occurrence, formation, structure and reactions. *J. Polym. Sci. Part B Polym. Lett.* **10,** 228–230 (1971).

203. Cinelli, P., Anguillesi, I. & Lazzeri, A. Green synthesis of flexible polyurethane

foams from liquefied lignin. *Eur. Polym. J.* **49,** 1174–1184 (2013).

204. Mainka, H. *et al.* Lignin – an alternative precursor for sustainable and cost-effective automotive carbon fiber. *J. Mater. Res. Technol.* **4,** 283–296 (2015).

205. Zemek, J., Košíková, B., Augustin, J. & Joniak, D. Antibiotic properties of lignin components. *Folia Microbiol. (Praha).* **24,** 483–486 (1979).

206. Ito, Y. *et al.* Lig-8, a highly bioactive lignophenol derivative from bamboo lignin, exhibits multifaceted neuroprotective activity. *CNS Drug Rev.* **13,** 296–307 (2007).

207. Afrin, T., Tsuzuki, T., Kanwar, R. K. & Wang, X. The origin of the antibacterial property of bamboo. *J. Text. Inst.* **103,** 844–849 (2012).

208. Dong, X. *et al.* Antimicrobial and antioxidant activities of lignin from residue of corn stover to ethanol production. *Ind. Crops Prod.* **34,** 1629–1634 (2011).

209. Pu, Y., Jiang, N. & Ragauskas, A. J. Ionic Liquid as a Green Solvent for Lignin. *J. Wood Chem. Technol.* **27,** 23–33 (2007).

210. Kubo, S. & Kadla, J. F. The formation of strong intermolecular interactions in immiscible blends of poly(vinyl alcohol) (PVA) and lignin. *Biomacromolecules* **4,** 561–567 (2003).

211. Kadla, J. F. & Kubo, S. Lignin-based polymer blends: Analysis of intermolecular interactions in lignin-synthetic polymer blends. in *Composites Part A: Applied Science and Manufacturing* **35,** 395–400 (Elsevier, 2004).

212. Li, J., He, Y. & Inoue, Y. Thermal and mechanical properties of biodegradable blends of poly(L-lactic acid) and lignin. *Polym. Int.* **52,** 949–955 (2003).

213. Rahman, M. A. *et al.* Biocomposites based on lignin and plasticized poly(L -lactic acid). *J. Appl. Polym. Sci.* **129,** 202–214 (2013).

214. Yang, W. *et al.* Antioxidant and antibacterial lignin nanoparticles in polyvinyl alcohol/chitosan films for active packaging. *Ind. Crops Prod.* **94,** 800–811 (2016).

215. Yang, W. *et al.* Synergic effect of cellulose and lignin nanostructures in PLA based systems for food antibacterial packaging. *Eur. Polym. J.* **79,** 1–12 (2016).

216. Yang, W. *et al.* Effect of cellulose and lignin on disintegration, antimicrobial and antioxidant properties of PLA active films. *Int. J. Biol. Macromol.* **89,** 360–368 (2016).

217. Kai, D. *et al.* Engineering Poly(lactide)-Lignin Nanofibers with Antioxidant Activity for Biomedical Application. *ACS Sustain. Chem. Eng.* **4,** 5268–5276 (2016).

218. Rhoades, J. & Roller, S. Antimicrobial Actions of Degraded and Native Chitosan

against Spoilage Organisms in Laboratory Media and Foods. *Appl. Environ. Microbiol.* **66,** 80–86 (2000).

219. Crini, G. Recent developments in polysaccharide-based materials used as adsorbents in wastewater treatment. *Prog. Polym. Sci.* **30,** 38–70 (2005).

220. Joule, J. P. *Mémoire sur la composition chimique des parties cornées des insectes. The London, Edinburgh, and Dublin Philosophical Magazine and Journal of Science* **1,** (1823).

221. Shavandi, A., Bekhit, A. E.-D. A., Ali, M. A. & Sun, Z. Bio-mimetic composite scaffold from mussel shells, squid pen and crab chitosan for bone tissue engineering. *Int. J. Biol. Macromol.* **80,** 445–54 (2015).

222. Finney, N. S. & Siegel, J. S. In Memoriam: Albert Hofmann (1906–2008). *Chim. Int. J. Chem.* **62,** 444–447 (2008).

223. Pal, J. *et al.* Biological Method of Chitin Extraction from Shrimp Waste an Eco-friendly low Cost Technology and its. *Int. J. Fish. Aquat. Stud.* **1,** 104–107 (2014).

224. Giri, T. K. *et al.* Modified chitosan hydrogels as drug delivery and tissue engineering systems: present status and applications. *Acta Pharm. Sin. B* **2,** 439–449 (2012).

225. Hirano, S., Nakahira, T., Nakagawa, M. & Kim, S. K. The preparation and applications of functional fibres from crab shell chitin. *J. Biotechnol.* **70,** 373–377 (1999).

226. Szosland, L. & East, G. C. The dry spinning of dibutyrylchitin fibers. *J. Appl. Polym. Sci.* **58,** 2459–2466 (1995).

227. Kameda, T., Miyazawa, M., Ono, H. & Yoshida, M. Hydrogen bonding structure and stability of alpha-chitin studied by 13C solid-state NMR. *Macromol. Biosci.* **5,** 103–106 (2005).

228. Min, B.-M. *et al.* Chitin and chitosan nanofibers: electrospinning of chitin and deacetylation of chitin nanofibers. *Polymer (Guildf).* **45,** 7137–7142 (2004).

229. Ghazali, A. R. & Inayat-Hussain, S. H. *Encyclopedia of Toxicology. Encyclopedia of Toxicology* (Elsevier, 2014). doi:10.1016/B978-0-12-386454-3.01223-9

230. Poirier, M. & Charlet, G. Chitin fractionation and characterization in N,N-dimethylacetamide/lithium chloride solvent system. *Carbohydr. Polym.* **50,** 363–370 (2002).

231. Jung, W. J. *et al.* Production of chitin from red crab shell waste by successive fermentation with Lactobacillus paracasei KCTC-3074 and Serratia marcescens

FS-3. *Carbohydr. Polym.* **68,** 746–750 (2007).

232. Loke, W. K., Lau, S. K., Yong, L. L., Khor, E. & Sum, C. K. Wound dressing with sustained anti-microbial capability. *J. Biomed. Mater. Res.* **53,** 8–17 (2000).

233. Prudden, J. F., Migel, P., Hanson, P., Friedrich, L. & Balassa, L. The discovery of a potent pure chemical wound-healing accelerator. *Am. J. Surg.* **119,** 560–564 (1970).

234. Vázquez, J. A., Fraguas, I. R.-A. M. I. M. J., González, M. del P. & Murado, M. A. Chondroitin Sulfate , Hyaluronic Acid and Chitin / Chitosan Production Using Marine Waste Sources : Characteristics , Applications and Eco-Friendly Processes : A Review. *Mar. Drugs* **11,** 747–774 (2013).

235. Muzzarelli, R. A. A. *et al.* Current views on fungal chitin/chitosan, human chitinases, food preservation, glucans, pectins and inulin: A tribute to Henri Braconnot, precursor of the carbohydrate polymers science, on the chitin bicentennial. *Carbohydr. Polym.* **87,** 995–1012 (2012).

236. Lu, Y., Ohshima, T., Ushio, H., Hamada, Y. & Shiomi, K. Immunological characteristics of monoclonal antibodies against shellfish major allergen tropomyosin. *Food Chem.* **100,** 1093–1099 (2007).

237. Pankey, G. a & Sabath, L. D. Clinical relevance of bacteriostatic versus bactericidal mechanisms of action in the treatment of Gram-positive bacterial infections. *Clin. Infect. Dis.* **38,** 864–870 (2004).

238. Benhabiles, M. S. *et al.* Antibacterial activity of chitin, chitosan and its oligomers prepared from shrimp shell waste. *Food Hydrocoll.* **29,** 48–56 (2012).

239. Dweltz, N. E. The structure of chitin. *Biochim. Biophys. Acta* **44,** 416–435 (1960).

240. Lucca, G. V. De, Kezar, H. S. I. & O'Brien, J. P. High strength fibers from chitin derivatives US4857403 A. (1986).

241. Xie, H., Zhang, S. & Li, S. Chitin and chitosan dissolved in ionic liquids as reversible sorbents of CO2. *Green Chem.* **8,** 630 (2006).

242. Prasad, K. *et al.* Weak gel of chitin with ionic liquid, 1-allyl-3-methylimidazolium bromide. *Int. J. Biol. Macromol.* **45,** 221–225 (2009).

243. Mi, F. L., Lin, Y. M., Wu, Y. B., Shyu, S. S. & Tsai, Y. H. Chitin/PLGA blend microspheres as a biodegradable drug-delivery system: Phase-separation, degradation and release behavior. *Biomaterials* **23,** 3257–3267 (2002).

244. Mi, F. L. *et al.* Chitin/PLGA blend microspheres as a biodegradable drug delivery system: A new delivery system for protein. *Biomaterials* **24,** 5023–5036 (2003).

245. Park, K. E., Jung, S. Y., Lee, S. J., Min, B.-M. & Park, W. H. Biomimetic nanofibrous scaffolds: preparation and characterization of chitin/silk fibroin blend nanofibers. *Int. J. Biol. Macromol.* **38,** 165–73 (2006).

246. Peesan, M., Rujiravanit, R. & Supaphol, P. Characterisation of beta-chitin/poly(vinyl alcohol) blend films. *Polym. Test.* **22,** 381–387 (2003).

247. Niño, K. A., Imam, S. H., Gordon, S. H. & Wong, L. J. G. Extruded Plastics Containing Starch and Chitin: Physical Properties and Evaluation of Biodegradability. in *Biopolymers Utilizing Nature's Advanced Materials* 195–203 (1999). doi:10.1021/bk-1999-0723.ch012

248. Yang, A., Wu, R. & Zhu, P. Thermal analysis and miscibility of chitin/polycaprolactone blends. *J. Appl. Polym. Sci.* **81,** 3117–3123 (2001).

249. Rizvi, R., Cochrane, B., Naguib, H. & Lee, P. C. Fabrication and characterisation of melt-blended PLA-chitin composites and their foams. *J. Cell. Plast.* **47,** 283 (2011).

250. Ogawa T, Moriwaki N, Fujii R, Tanaka K, Mori E, Saitou M, Yoshizawa H, S. H. Triacetin as food additive in gummy candy and other foodstuffs on the market. *Kitasato Arch Exp Med.* **65,** 33–44 (1992).

251. Herrera, N. *et al.* Functionalized blown films of plasticized polylactic acid/chitin nanocomposite: Preparation and characterization. *Mater. Des.* **92,** 846–852 (2016).

252. Mou, S. S., Ma, A. D., Tu, M., Li, L. H. & Zhou, C. R. Preparation of polylactic acid/chitin composite material and its safety evaluation by animal experiments. *Acad. J. First Med. Coll. PLA* **23,** 245–247 (2003).

253. Arunraj, T. R., Sanoj Rejinold, N., Ashwin Kumar, N. & Jayakumar, R. Bio-responsive chitin-poly(l-lactic acid) composite nanogels for liver cancer. *Colloids Surfaces B Biointerfaces* **113,** 394–402 (2014).

254. Li, X. & Feng, Q. Porous poly-L-lactic acid scaffold reinforced by chitin fibers. *Polym. Bull.* **54,** 47–55 (2005).

255. Li, X. *et al.* In vitro evaluation of porous poly(L-lactic acid) scaffold reinforced by chitin fibers. *J. Biomed. Mater. Res. - Part B Appl. Biomater.* **90 B,** 503–509 (2009).

256. Kim, J. Y., Ha, C. S. & Jo, N. J. Synthesis and properties of biodegradable chitin-graft-poly(L-lactide) copolymers. *Polym. Int.* **51,** 1123–1128 (2002).

257. Štengl, V., Tolasz, J. & Popelková, D. Ultrasonic preparation of tungsten disulfide single-layers and quantum dots. *RSC Adv.* **5,** 89612–89620 (2015).

258.   Ohkage, M. Tungsten disulfide lubricant US3725276A. (1971).

259.   French, L. G. Machinery. in 4, 101 (Machinery Publications Corporation, 1967).

260.   Rosentsveig, R., Margolin, A., Feldman, Y., Popovitz-Biro, R. & Tenne, R. WS2 nanotube bundles and foils. *Chem. Mater.* **14,** 471–473 (2002).

261.   Nath, M., Govindaraj, A. & Rao, C. N. R. Simple synthesis of MoS2 and WS2 nanotubes. *Adv. Mater.* **13,** 283–286 (2001).

262.   Goldman, E. B. *et al.* Biocompatibility of tungsten disulfide inorganic nanotubes and fullerene-like nanoparticles with salivary gland cells. *Tissue Eng. Part A* **21,** 1013–23 (2015).

263.   Tenne, R. Inorganic nanotubes and fullerene-like materials. *Chem. - A Eur. J.* **8,** 5296–5304 (2002).

264.   Seifert, G., Köhler, T. & Tenne, R. Stability of metal chalcogenide nanotubes. *J. Phys. Chem. B* **106,** 2497–2501 (2002).

265.   Kaplan-Ashiri, I. & Tenne, R. Mechanical properties of WS2 nanotubes. *J. Clust. Sci.* **18,** 549–563 (2007).

266.   Rapoport, L. *et al.* Hollow nanoparticles of WS2 as potential solid-state lubricants. *Nature* **387,** 791–793 (1997).

267.   Zheng, N., Bu, X. & Feng, P. Synthetic design of crystalline inorganic chalcogenides exhibiting fast-ion conductivity. *Nature* **426,** 428–432 (2003).

268.   Wang, G. X., Bewlay, S., Yao, J., Liu, H. K. & Dou, S. X. Tungsten Disulfide Nanotubes for Lithium Storage. *Electrochem. Solid-State Lett.* **7,** A321 (2004).

269.   Liu, H., Su, D., Wang, G. & Qiao, S. Z. An ordered mesoporous WS2 anode material with superior electrochemical performance for lithium ion batteries. *J. Mater. Chem.* **22,** 17437 (2012).

270.   Bhandavat, R., David, L. & Singh, G. Synthesis of surface-functionalized WS 2 nanosheets and performance as li-ion battery anodes. *J. Phys. Chem. Lett.* **3,** 1523– 1530 (2012).

271.   Prasad, S. V, McDevitt, N. T. & Zabinski, J. S. Tribology of tungsten disulfide-nanocrystalline zinc oxide adaptive lubricant films from ambient to 500°C. *Wear* **237,** 186–196 (2000).

272.   Lalwani, G. *et al.* Two-dimensional nanostructure-reinforced biodegradable polymeric nanocomposites for bone tissue engineering. *Biomacromolecules* **14,** 900–9 (2013).

273.   Zohar, E. *et al.* The Effect of WS2 Nanotubes on the Properties of Epoxy-Based

Nanocomposites. *J. Adhes. Sci. Technol.* **25,** 1603–1617 (2011).

274. Reddy, C. S., Zak, A. & Zussman, E. WS2 nanotubes embedded in PMMA nanofibers as energy absorptive material. *J. Mater. Chem.* **21,** 16086 (2011).

275. Howard, D. L. & Kjaergaard, H. G. Hydrogen Bonding to Divalent Sulfur. *Phys. Chem. Chem. Phys.* **10,** 4113–4118 (2008).

276. Sonker, A. K., Wagner, H. D., Bajpai, R., Tenne, R. & Sui, X. M. Effects of tungsten disulphide nanotubes and glutaric acid on the thermal and mechanical properties of polyvinyl alcohol. *Compos. Sci. Technol.* **127,** 47–53 (2016).

277. Naffakh, M. *et al.* Influence of inorganic fullerene-like WS2 nanoparticles on the thermal behavior of isotactic polypropylene. *J. Polym. Sci. Part B Polym. Phys.* **45,** 2309–2321 (2007).

278. Mojtabaei, A. *et al.* Influence of fullerene-like tungsten disulfide (IF-WS2) nanoparticles on thermal and dynamic mechanical properties of PP/EVA blends: Correlation with microstructure. *Compos. Part B Eng.* **111,** 74–82 (2017).

279. Appel, J. H. *et al.* Low Cytotoxicity and Genotoxicity of Two-Dimensional MoS2 and WS2. *ACS Biomater. Sci. Eng.* **2,** 361–367 (2016).

280. Wu, H. *et al.* Biocompatible inorganic fullerene-like molybdenum disulfide nanoparticles produced by pulsed laser ablation in water. *ACS Nano* **5,** 1276–1281 (2011).

281. Lalwani, G. *et al.* Tungsten disulfide nanotubes reinforced biodegradable polymers for bone tissue engineering. *Acta Biomater.* **9,** 8365–8373 (2013).

282. Naffakh, M., Marco, C. & Ellis, G. Inorganic WS2 nanotubes that improve the crystallization behavior of poly(3-hydroxybutyrate). *CrystEngComm* 1126–1135 (2014).

283. Naffakh, M. & Marco, C. Isothermal crystallization kinetics and melting behavior of poly(l-lactic acid)/WS2 inorganic nanotube nanocomposites. *J. Mater. Sci.* **50,** 6066–6074 (2015).

284. Naffakh, M., Marco, C. & Ellis, G. Non-Isothermal cold-crystallization behavior and kinetics of poly(L-lactic acid)/WS2 inorganic nanotube nanocomposites. *Polymers (Basel).* **7,** 2175–2189 (2015).

285. Naffakh, M. & Díez-Pascual, A. M. WS2 inorganic nanotubes reinforced poly(l - lactic acid)/hydroxyapatite hybrid composite biomaterials. *RSC Adv.* **5,** 65514–65525 (2015).

286. Naffakh, M., Díez-Pascual, A. M. & Marco, C. Polymer blend nanocomposites

based on poly(L-lactic acid), polypropylene and WS2 inorganic nanotubes. *RSC Adv.* **6,** 40033–40044 (2016).

287. Chongchet, V. The use of sterile, steamed banana leaves in the local treatment of burns. *Burns* **6,** 264–265 (1980).

288. Navaneethakrishnan, K. S., Gill, M. I. S. & Kumar, S. R. Effect of different levels of N and P on ratoon banana (Musa spp . AAA). *J. Hortic. For.* **5,** 81–91 (2013).

289. Chongchet, V. The use of sterile, steamed banana leaves in the local treatment of burns. *Burns* **6,** 264–265 (1980).

290. Gore, M. a & Akolekar, D. Banana leaf dressing for skin graft donor areas. *Burns* **29,** 483–486 (2003).

291. Gore, M. a & Akolekar, D. Evaluation of banana leaf dressing for partial thickness burn wounds. *Burns* **29,** 487–492 (2003).

292. Oliveira, L. *et al.* Chemical Composition and Lignin Structural Features of Banana Plant Leaf Sheath and Rachis.pdf. in *Characterization of Lignocellulosic Materials* 171–188 (2008).

293. QuÍlez, J. Potential uses and benefits of phytosterols in diet: present situation and future directions. *Clin. Nutr.* **22,** 343–351 (2003).

294. Banskota, A. H. *et al.* Hepatoprotective effect of Combretum quadrangulare and its constituents. *Biol. Pharm. Bull.* **23,** 456–460 (2000).

295. Delporte, C. & Backhouse, N. Antipyretic, hypothermic and antiinflammatory activities and metabolites from Solanum ligustrinum Lood. *Phyther. Res.* **12,** 118–122 (1998).

296. KIRIAKIDIS, S., STATHI, S., JHA, H. C., HARTMANN, R. & EGGE, H. Fatty Acid Esters of Sitosterol 3.BETA.-Glucoside from Soybeans and Tempe(Fermented Soybeans) as Antiproliferative Substances. *J. Clin. Biochem. Nutr.* **22,** 139–147 (1997).

297. Tock, J. Y., Lai, C. L., Lee, K. T., Tan, K. T. & Bhatia, S. Banana biomass as potential renewable energy resource: A Malaysian case study. *Renewable and Sustainable Energy Reviews* **14,** 798–805 (2010).

298. Fernandes, E. R. K., Marangoni, C., Souza, O. & Sellin, N. Thermochemical characterization of banana leaves as a potential energy source. *Energy Convers. Manag.* **75,** 603–608 (2013).

299. Tan, S. S. Y. & MacFarlane, D. R. Ionic liquids in biomass processing. *Top. Curr. Chem.* **290,** 311–339 (2009).

300. Graenacher, C. Cellulose solution (US1943176 A). (1931).

301. Turner, M. B., Spear, S. K., Holbrey, J. D. & Rogers, R. D. Production of bioactive cellulose films reconstituted from ionic liquids. *Biomacromolecules* **5,** 1379–1384 (2004).

302. Phillips, D. M. *et al.* Regenerated silk fiber wet spinning from an ionic liquid solution. *J. Mater. Chem.* **15,** 4206 (2005).

303. Gupta, M. K. *et al.* Patterned silk films cast from ionic liquid solubilized fibroin as scaffolds for cell growth. *Langmuir* **23,** 1315–1319 (2007).

304. Swatloski, R. P., Spear, S. K., Holbrey, J. D. & Rogers, R. D. Dissolution of Cellose with Ionic Liquids. *J. Am. Chem. Soc.* **124,** 4974–4975 (2002).

305. Seddon, K. R. K. Ionic liquids for clean technology. *J. Chem. Technol. …* **68,** 351–356 (1997).

306. Freemantle, M. *An Introduction to Ionic Liquids*. (The Royal Society of Chemistry, 2009). doi:10.1039/9781849737050

307. Freemantle, M. *An Introduction to Ionic Liquids*. (The Royal Society of Chemistry, 2009).

308. Gabriel, S. & Weiner, J. Ueber einige Abkömmlinge des Propylamins. *Berichte der Dtsch. Chem. Gesellschaft* **21,** 2669–2679 (1888).

309. Walden, P. Molecular Weights and Electrical Conductivity of Several Fused Salts. *Bull. Russ. Acad. Sci.* 405–422 (1914).

310. Hurley, F. H. & Wier, T. P. The electrodeposition of aluminum from nonaqueous solutions at room temperature. *J. Electrochem. Soc.* **98,** 207–212 (1951).

311. Wilkes, J. S., Levisky, J. A., Wilson, R. A. & Hussey, C. L. Dialkylimidazolium chloroaluminate melts: a new class of room-temperature ionic liquids for electrochemistry, spectroscopy and synthesis. *Inorg. Chem.* **21,** 1263–1264 (1982).

312. Wilkes, J. S. & Zaworotko, M. J. Air and water stable 1-ethyl-3-methylimidazolium based ionic liquids. *J. Chem. Soc. Chem. Commun.* 965–967 (1992). doi:10.1039/C39920000965

313. Yuan, J., Giordano, C. & Antonietti, M. Ionic Liquid Monomers and Polymers as Precursors of Highly Conductive, Mesoporous, Graphitic Carbon Nanostructures. *Chem. Mater.* **22,** 5003–5012 (2010).

314. Dyson, P. J. *et al.* Organometallic synthesis in ambient temperature chloroaluminate. *J. Chem. Soc., Dalt. Trans.* 3465–3469 (1997).

315. Dyson, P. J. & Geldbach, T. J. Applications of Ionic Liquids in Synthesis and

Catalysis. *Electrochem. Soc. Interface* **16,** 50–53 (2007).

316. Bonhôte, P. *et al.* Hydrophobic, Highly Conductive Ambient-Temperature Molten Salts. *Inorg. Chem.* **35,** 1168--1178 (1996).

317. Carmichael, A. J., Haddleton, D. M., Bon, S. a. F. & Seddon, K. R. Copper(I) mediated living radical polymerisation in an ionic liquid. *Chem. Commun.* 1237–1238 (2000). doi:10.1039/b003335i

318. Silva, S. S. *et al.* The use of ionic liquids in the processing of chitosan/silk hydrogels for biomedical applications. *Green Chem.* **14,** 1463 (2012).

319. Min, B.-M. *et al.* Chitin and chitosan nanofibers: electrospinning of chitin and deacetylation of chitin nanofibers. *Polymer (Guildf).* **45,** 7137–7142 (2004).

320. Wang, W.-T., Zhu, J., Wang, X.-L., Huang, Y. & Wang, Y.-Z. Dissolution Behavior of Chitin in Ionic Liquids. *J. Macromol. Sci. Part B* **49,** 528–541 (2010).

321. Xie, H., Zhang, S. & Li, S. Chitin and chitosan dissolved in ionic liquids as reversible sorbents of CO2. *Green Chem.* **8,** 630–633 (2006).

322. Wu, Y., Sasaki, T., Irie, S. & Sakurai, K. A novel biomass-ionic liquid platform for the utilization of native chitin. *Polymer (Guildf).* **49,** 2321–2327 (2008).

323. Fukaya, Y., Sugimoto, A. & Ohno, H. Superior Solubility of Polysaccharides in Low Viscosity, Polar, and Halogen-Free 1,3-Dialkylimidazolium Formates. *Biomacromolecules* **7,** 3295–3297 (2006).

324. Qin, Y., Lu, X., Sun, N. & Rogers, R. D. Dissolution or extraction of crustacean shells using ionic liquids to obtain high molecular weight purified chitin and direct production of chitin films and fibers. *Green Chem.* **12,** 968–971 (2010).

325. Barber, P. S., Kelley, S. P., Griggs, C. S., Wallace, S. & Rogers, R. D. Surface modification of ionic liquid-spun chitin fibers for the extraction of uranium from seawater: seeking the strength of chitin and the chemical functionality of chitosan. *Green Chem.* **16,** 1828–1836 (2014).

326. Barber, P. S., Griggs, C. S., Bonner, J. R. & Rogers, R. D. Electrospinning of chitin nanofibers directly from an ionic liquid extract of shrimp shells. *Green Chem.* **15,** 601–607 (2013).

327. Shamshina, J. L. *et al.* Chitin–calcium alginate composite fibers for wound care dressings spun from ionic liquid solution. *J. Mater. Chem. B* **2,** 3924–3936 (2014).

328. Kilpeläinen, I. *et al.* Dissolution of wood in ionic liquids. *J. Agric. Food Chem.* **55,** 9142–8 (2007).

329. Sun, N. *et al.* Complete dissolution and partial delignification of wood in the ionic

liquid 1-ethyl-3-methylimidazolium acetate. *Green Chem.* **11,** 646–655 (2009).

330. Wu, R.-L., Wang, X.-L., Li, F., Li, H.-Z. & Wang, Y.-Z. Green composite films prepared from cellulose, starch and lignin in room-temperature ionic liquid. *Bioresour. Technol.* **100,** 2569–74 (2009).

331. Tucker, N. & Stanger, J. The History of the Science and Technology of Electrospinning from 1600 to 1995. *J. Eng. Fiber. Fabr.* 63–73 (2012).

332. Boys, C. V. On the Production, Properties, and some suggested Uses of the Finest Threads. *Proc. Phys. Soc. London* **9,** 8–19 (2002).

333. Tucker, N. & Stanger, J. The History of the Science and Technology of Electrospinning from 1600 to 1995. *J. Eng. Fiber. Fabr.* 63–73 (2012).

334. Petryanov-Sokolov, I. V. On the 100th anniversary of the birth of I.V. Petryanov-Sokolov. *Izv. Atmos. Ocean. Phys.* **43,** 395 (2007).

335. Taylor, G. Electrically Driven Jets. *Proc. R. Soc. London A Math. Phys. Eng. Sci.* **313,** 453–475 (1969).

336. Doshi, J. & Reneker, D. H. Electrospinning process and applications of electrospun fibers. *J. Electrostat.* **35,** 151–160 (1995).

337. Demir, M. ., Yilgor, I., Yilgor, E. & Erman, B. Electrospinning of polyurethane fibers. *Polymer (Guildf).* **43,** 3303–3309 (2002).

338. Fang, X. & Reneker, D. H. DNA fibers by electrospinning. *J. Macromol. Sci. Part B Phys.* **36,** 169–173 (2006).

339. Yarin, A. L., Koombhongse, S. & Reneker, D. H. Bending instability in electrospinning of nanofibers. *J. Appl. Phys.* **89,** 3018 (2001).

340. Demir, M. ., Yilgor, I., Yilgor, E. & Erman, B. Electrospinning of polyurethane fibers. *Polymer (Guildf).* **43,** 3303–3309 (2002).

341. Bhardwaj, N. & Kundu, S. C. Electrospinning: a fascinating fiber fabrication technique. *Biotechnol. Adv.* **28,** 325–47 (2010).

342. Supaphol, P. & Chuangchote, S. On the electrospinning of poly(vinyl alcohol) nanofiber mats: A revisit. *J. Appl. Polym. Sci.* **108,** 969–978 (2008).

343. Deitzel, J. ., Kleinmeyer, J., Harris, D. & Beck Tan, N. . The effect of processing variables on the morphology of electrospun nanofibers and textiles. *Polymer (Guildf).* **42,** 261–272 (2001).

344. Tan, S.-H., Inai, R., Kotaki, M. & Ramakrishna, S. Systematic parameter study for ultra-fine fiber fabrication via electrospinning process. *Polymer (Guildf).* **46,** 6128–6134 (2005).

345. Doshi, J. & Reneker, D. H. Electrospinning process and applications of electrospun fibers. *J. Electrostat.* **35,** 151–160 (1995).

346. Haghi, a. K. & Akbari, M. Trends in electrospinning of natural nanofibers. *Phys. Status Solidi Appl. Mater. Sci.* **204,** 1830–1834 (2007).

347. Hayati, I., Bailey, A. & Tadros, T. . Investigations into the mechanism of electrohydrodynamic spraying of liquids. *J. Colloid Interface Sci.* **117,** 222–230 (1987).

348. Zong, X. *et al.* Structure and process relationship of electrospun bioabsorbable nanofiber membranes. *Polymer (Guildf).* **43,** 4403–4412 (2002).

349. Reneker, D. H. & Chun, I. Nanometre diameter fibres of polymer, produced by electrospinning. *Nanotechnology* **7,** 216–223 (1999).

350. Yördem, O. S., Papila, M. & Menceloğlu, Y. Z. Effects of electrospinning parameters on polyacrylonitrile nanofiber diameter: An investigation by response surface methodology. *Mater. Des.* **29,** 34–44 (2008).

351. Zuo, W. *et al.* Experimental study on relationship between jet instability and formation of beaded fibers during electrospinning. *Polym. Eng. Sci.* **45,** 704–709 (2005).

352. Wang, X. *et al.* Formation of water-resistant hyaluronic acid nanofibers by blowing-assisted electro-spinning and non-toxic post treatments. *Polymer (Guildf).* **46,** 4853–4867 (2005).

353. Yarin, A. L., Koombhongse, S. & Reneker, D. H. Bending instability in electrospinning of nanofibers. *J. Appl. Phys.* **89,** 3018–3026 (2001).

354. Wang, X. *et al.* Formation of water-resistant hyaluronic acid nanofibers by blowing-assisted electro-spinning and non-toxic post treatments. *Polymer (Guildf).* **46,** 4853–4867 (2005).

355. Xu, S. *et al.* Electrospinning of native cellulose from nonvolatile solvent system. *Polymer (Guildf).* **49,** 2911–2917 (2008).

356. Yang, F., Murugan, R., Wang, S. & Ramakrishna, S. Electrospinning of nano/micro scale poly(L-lactic acid) aligned fibers and their potential in neural tissue engineering. *Biomaterials* **26,** 2603–10 (2005).

357. Ki, C. S. *et al.* Electrospun three-dimensional silk fibroin nanofibrous scaffold. *J. Appl. Polym. Sci.* **106,** 3922–3928 (2007).

358. Geng, X., Kwon, O.-H. & Jang, J. Electrospinning of chitosan dissolved in concentrated acetic acid solution. *Biomaterials* **26,** 5427–32 (2005).

359. Pham, Q. P., Sharma, U. & Mikos, A. G. Electrospun Poly(ε-caprolactone) Microfiber and Multilayer Nanofiber/Microfiber Scaffolds: Characterization of Scaffolds and Measurement of Cellular Infiltration. *Biomacromolecules* **7,** 2796–2805 (2006).

360. Buchko, C. J., Chen, L. C., Shen, Y. & Martin, D. C. Processing and microstructural characterization of porous biocompatible protein polymer thin films. *Polymer (Guildf).* **40,** 7397–7407 (1999).

361. Jalili, R., Hosseini, S. A. & Morshed, M. The Effects of Operating Parameters on the Morphology of Electrospun Polyacrilonitrile Nanofibres. *Iran. Polym. J.* **14,** 1074–1081 (2005).

362. Geng, X., Kwon, O.-H. & Jang, J. Electrospinning of chitosan dissolved in concentrated acetic acid solution. *Biomaterials* **26,** 5427–32 (2005).

363. Zhang, Y. *et al.* Viscometric study of poly(vinyl chloride)/poly(vinyl acetate) blends in various solvents. *Eur. Polym. J.* **38,** 333–337 (2002).

364. Ohkawa, K., Kim, H., Lee, K. & Yamamoto, H. Electrospun non-woven fabrics of poly(??-caprolactone) and their biodegradation by pure cultures of soil filamentous fungi. *Macromol. Symp.* **216,** 301–306 (2004).

365. Mit-uppatham, C., Nithitanakul, M. & Supaphol, P. Ultrafine Electrospun Polyamide-6 Fibers: Effect of Solution Conditions on Morphology and Average Fiber Diameter. *Macromol. Chem. Phys.* **205,** 2327–2338 (2004).

366. Baumgarten, P. K. Electrostatic spinning of acrylic microfibers. *J. Colloid Interface Sci.* **36,** 71–79 (1971).

367. Casper, C. L., Stephens, J. S., Tassi, N. G., Chase, D. B. & Rabolt, J. F. Controlling Surface Morphology of Electrospun Polystyrene Fibers: Effect of Humidity and Molecular Weight in the Electrospinning Process. *Macromolecules* **37,** 573–578 (2004).

368. ISO 527-1:2012(en), Plastics — Determination of tensile properties — Part 1: General principles. Available at: https://www.iso.org/obp/ui/#iso:std:iso:527:-1:ed-2:v1:en. (Accessed: 8th May 2018)

369. Blattner, F. . R. *et al.* The Complete Genome Sequence of Escherichia coli K-12. *Science (80-.).* **277,** 1453–1462 (1997).

370. Hayashi, T. Complete Genome Sequence of Enterohemorrhagic Eschelichia coli O157:H7 and Genomic Comparison with a Laboratory Strain K-12. *DNA Res.* **8,** 11–22 (2001).

371. Fey, P. D. *et al.* A genetic resource for rapid and comprehensive phenotype screening of nonessential Staphylococcus aureus genes. *MBio* **4,** 1–8 (2013).

372. Grundmeier, M. *et al.* Truncation of Fibronectin-Binding Proteins in Staphylococcus aureus Strain Newman Leads to Deficient Adherence and Host Cell Invasion Due to Loss of the Cell Wall Anchor Function. *Infect. Immun.* **72,** 7155–7163 (2004).

373. Abraham, N. M. & Jefferson, K. K. Staphylococcus aureus clumping factor B mediates biofilm formation in the absence of calcium. *Microbiol. (United Kingdom)* **158,** 1504–1512 (2012).

374. Odds, F. C., Brown, A. J. P. & Gow, N. A. R. Candida albicans genome sequence: A platform for genomics in the absence of genetics. *Genome Biol.* **5,** 230 (2004).

375. Snyder, L. A. *et al.* Epidemiological investigation of Pseudomonas aeruginosa isolates from a six-year-long hospital outbreak using high-throughput whole genome sequencing. *Euro Surveill* **18,** 1–9 (2013).

376. Hudzicki, J. Kirby-Bauer disk diffusion susceptibility test protocol. *American Society for Microbiology* 1–14 (2009).

377. Chen, P., Abercrombie, J. J., Jeffrey, N. R. & Leung, K. P. An improved medium for growing Staphylococcus aureus biofilm. *J. Microbiol. Methods* **90,** 115–118 (2012).

378. Beenken, K. E., Blevins, J. S. & Smeltzer, M. S. Mutation of sarA in Staphylococcus aureus limits biofilm formation. *Infect. Immun.* **71,** 4206–4211 (2003).

379. Kueng, W., Silber, E. & Eppenberger, U. Quantification of cells cultured on 96-well plates. *Anal. Biochem.* **182,** 16–19 (1989).

380. Berridge, M. V. & Tan, A. S. Characterization of the Cellular Reduction of 3-(4,5-dimethylthiazol-2-yl)-2,5-diphenyltetrazolium bromide (MTT): Subcellular Localization, Substrate Dependence, and Involvement of Mitochondrial Electron Transport in MTT Reduction. *Arch. Biochem. Biophys.* **303,** 474–482 (1993).

381. Berridge, M., Tan, A., McCoy, K. & Wang, R. The biochemical and cellular basis of cell proliferation assays that use tetrazolium salts. *Biochemica* **4,** 14–19 (1996).

382. Martins, A. *et al.* Surface modification of electrospun polycaprolactone nanofiber meshes by plasma treatment to enhance biological performance. *Small* **5,** 1195–1206 (2009).

383. Yuan, Y. & Lee, T. R. Contact angle and wetting properties. *Springer Ser. Surf.*

Sci. **51,** 3–34 (2013).

384. Scipioni, L., Huynh, C. & Smith, I. Imaging of Bioengineering Surfaces with the Helium Ion Microscope. *Mater. Sci.* **3,** 345–346 (2009).

385. Fakirov, S. Chapter 3. Amorphous State of Polymers. in *Fundamentals of polymer science for engineers* 82 (2017).

386. Esposito, A. *et al.* From a Three-Phase Model to a Continuous Description of Molecular Mobility in Semicrystalline Poly(hydroxybutyrate-co-hydroxyvalerate). doi:10.1021/acs.macromol.6b00384

387. Yasuniwa, M., Tsubakihara, S., Sugimoto, Y. & Nakafuku, C. Thermal analysis of the double-melting behavior of poly(L-lactic acid). *J. Polym. Sci. Part B Polym. Phys.* **42,** 25–32 (2004).

388. Cai, Y. H. Crystallization and melting behavior of biodegradable Poly(L-lactic acid)/talc composites. *E-Journal Chem.* **9,** 1569–1574 (2012).

389. Krikorian, V. & Pochan, D. Crystallization behavior of poly(lactic acid) nanocomposites: nucleation and growth probed by infrared spectroscopy. *Macromolecules* **38,** 6520–6527 (2005).

390. Sengupta, R. *et al.* A Short Review on Rubber / Clay Nanocomposites With Emphasis on Mechanical Properties. *Engineering* **47,** 21–25 (2007).

391. Zhang, R.-C. *et al.* Equilibrium Melting Temperature of Polymorphic Poly(l-lactide) and Its Supercooling Dependence on Growth Kinetics. *Polymers (Basel).* **9,** 625 (2017).

392. Fischer, E. W., Sterzel, H. J. & Wegner, G. Investigation of the structure of solution grown crystals of lactide copolymers by means of chemical reactions. *Kolloid-Zeitschrift und Zeitschrift für Polym.* **251,** 980–990 (1973).

393. Wang, Y. *et al.* Unusual structural evolution of poly(lactic acid) upon annealing in the presence of an initially oriented mesophase. *Soft Matter* **10,** 1512 (2014).

394. Sanchez, M. S., Mathot, V. B. F., Poel, G. Vanden & Ribelles, J. L. G. Effect of the cooling rate on the nucleation kinetics of poly(L-lactic acid) and its influence on morphology. *Macromolecules* **40,** 7989–7997 (2007).

395. Pradhan, D. K. *et al.* Effect of plasticizer on structural and electrical properties of nanocomposite solid polymer electrolytes. *Ionics (Kiel).* **17,** 127–134 (2011).

396. Steinmann, W., Walter, S., Beckers, M., Seide, G. & Gries, T. Thermal Analysis of Phase Transitions and Crystallization in Polymeric Fibers. in *Applications of Calorimetry in a Wide Context - Differential Scanning Calorimetry, Isothermal*

Titration Calorimetry and Microcalorimetry 277–306 (2013).

397. Bouapao, L., Tsuji, H., Tashiro, K., Zhang, J. & Hanesaka, M. Crystallization, spherulite growth, and structure of blends of crystalline and amorphous poly(lactide)s. *Polymer (Guildf).* **50,** 4007–4017 (2009).

398. Rahman, M. S. State diagram of foods: Its potential use in food processing and product stability. *Trends Food Sci. Technol.* **17,** 129–141 (2006).

399. Rahman, M. S., Al-Marhubi, I. M. & Al-Mahrouqi, A. Measurement of glass transition temperature by mechanical (DMTA), thermal (DSC and MDSC), water diffusion and density methods: A comparison study. *Chem. Phys. Lett.* **440,** 372–377 (2007).

400. Shakoor, A., Muhammad, R., Thomas, N. L. & Silberschmidt, V. V. Mechanical and thermal characterisation of poly (l- lactide) composites reinforced with hemp fibres Related content Mechanical and thermal properties of polylactic acid composites reinforced with cellulose nanoparticles extracted from kenaf fibre. *J. Phys. Conf. Ser.* **451,** 4 (2013).

401. Gordobil, O., Egüés, I., Llano-Ponte, R. & Labidi, J. Physicochemical properties of PLA lignin blends. *Polym. Degrad. Stab.* **108,** 330–338 (2014).

402. Anwer, M. A. S. & Naguib, H. Evaluation of the Mechanical and Morphological Characteristics of PLA-Lignin, PLA- Tannin and PLA-CNF Composites. *Compos. Part B* **91,** 631–639 (2016).

403. Help Online - Tutorials - One Way ANOVA. Available at: https://www.originlab.com/doc/Tutorials/1WayANOVA. (Accessed: 28th May 2018)

404. Harijati, N., Azrianingsih, R. & Prawaningtyas, E. A. The Study of Anatomy and Fiber Banana Leaf as a Potensial Wrapping. **2013,** 1461–1465 (2013).

405. Jorgensen, J. H. & Ferraro, M. J. Antimicrobial Susceptibility Testing: A Review of General Principles and Contemporary Practices. *Clin. Infect. Dis.* **49,** 1749–1755 (2009).

406. Awerbuch, T. E., Lustman, L. & Piret, J. M. A numerical method to determine minimal inhibitory concentrations (MICs) of antibiotics directly from disc-diffusion susceptibility tests. *J. Microbiol. Methods* **9,** 1–7 (1989).

407. Nijs, A. *et al.* Comparison and evaluation of Osiris and Sirscan 2000 antimicrobial susceptibility systems in the clinical microbiology laboratory. *J. Clin. Microbiol.* **41,** 3627–3630 (2003).

408. Herrera, N. *et al.* Triethyl citrate (TEC) as a dispersing aid in polylactic acid/chitin nanocomposites prepared via liquid-assisted extrusion. *Polymers (Basel).* **9,** 406 (2017).

409. Zia, K. M., Zuber, M., Barikani, M., Bhatti, I. A. & Khan, M. B. Surface characteristics of chitin-based shape memory polyurethane elastomers. *Colloids Surfaces B Biointerfaces* **72,** 248–252 (2009).

410. Alvarez, F. J. The Effect of chitin size, shape, source and purification method on immune recognition. *Molecules* **19,** 4433–4451 (2014).

411. Kittur, F. S., Harish Prashanth, K. V., Udaya Sankar, K. & Tharanathan, R. N. Characterization of chitin, chitosan and their carboxymethyl derivatives by differential scanning calorimetry. *Carbohydr. Polym.* **49,** 185–193 (2002).

412. Chawla, K. K. Melting point and glass transition temperature. in *Fibrous materials* 45 (2016).

413. Di Gioia, L., Cuq, B. & Guilbert, S. Thermal properties of corn gluten meal and its proteic components. *Int. J. Biol. Macromol.* **24,** 341–350 (1999).

414. E, B. *et al.* Chitin-based scaffolds are an integral part of the skeleton of the marine demosponge Ianthella basta. *J. Struct. Biol.* **168,** 539–547 (2010).

415. Tenne, R., Margulis, L., Genut, M. & Hodes, G. Polyhedral and cylindrical structures of tungsten disulphide. *Nature* **360,** 444–446 (1992).

416. Chow, P. K. *et al.* Wetting of Mono and Few-Layered WS 2 and MoS 2 Films Supported on Si/SiO 2 Substrates. *ACS Nano* **9,** 3023–3031 (2015).

417. Committee, E. D. R. 4. Elemental Analysis. in *Microelectronics Failure Analysis: Desk Reference* **3,** 518 (ASM International, 2011).

418. Kim, S. W. & Ahn, J.-P. Polycrystalline nanowires of gadolinium-doped ceria via random alignment mediated by supercritical carbon dioxide. *Sci. Rep.* **3,** 1606 (2013).

419. Thermo Scientific XPS: Knowledge Base. Available at: http://xpssimplified.com/elements/tungsten.php. (Accessed: 14th September 2017)

420. XPS Interpretation of Sulfur. Available at: http://xpssimplified.com/elements/sulfur.php. (Accessed: 14th September 2017)

421. XPS Interpretation of Carbon. Available at: https://xpssimplified.com/elements/carbon.php#adventitious. (Accessed: 31st October 2017)

422. Evans, S. Correction for the effects of adventitious carbon overlayers in quantitative XPS analysis. *Surf. Interface Anal.* **25,** 924–930 (1997).

423. Berkdemir, A. *et al.* Identification of individual and few layers of WS2 using Raman spectroscopy. *Sci. Rep.* **3,** 1755 (2013).

424. Garcia-Sanchez, R. F., Ahmido, T., Casimir, D., Baliga, S. & Misra, P. Thermal Effects Associated with the Raman Spectroscopy of WO $_3$ Gas-Sensor Materials. *J. Phys. Chem. A* **117,** 13825–13831 (2013).

425. He, Y., Fan, Z., Wei, J. & Li, S. Morphology and melt crystallization of poly(L-lactide) obtained by ring opening polymerization of L-lactide with zinc catalyst. *Polym. Eng. Sci.* **46,** 1583–1589 (2006).

426. Beaufort, L., Barbarin, N. & Gally, Y. Optical measurements to determine the thickness of calcite crystals and the mass of thin carbonate particles such as coccoliths. *Nat. Protoc.* **9,** 633–642 (2014).

427. Woo, E. M., Ni'Mah, H. & Wang, Y. H. Anisotropic nucleation and Janus-faced crystals of poly(l -lactic acid) interacting with an amorphous diluent. *Ind. Eng. Chem. Res.* **53,** 9772–9780 (2014).

428. Sun, J., Yu, H., Zhuang, X., Chen, X. & Jing, X. Crystallization Behavior of Asymmetric PLLA/PDLA Blends. *J. Phys. Chem. B* **115,** 2864–2869 (2011).

429. Hoogsteen, W., Postema, A. R., Pennings, A. J., Ten Brinke, G. & Zugenmaier, P. Crystal structure, conformation and morphology of solution-spun poly(L-lactide) fibers. *Macromolecules* **23,** 634–642 (1990).

430. Zhu, Y. Q. *et al.* Morphology, structure and growth of WS2 nanotubes. *J. Mater. Chem.* **10,** 2570–2577 (2000).

431. Iijima, S. Helical microtubules of graphitic carbon. *Nature* **354,** 56–58 (1991).

432. Residual stress characterization of diamond-like carbon coatings by an X-ray diffraction method. *Surf. Coatings Technol.* **122,** 219–224 (1999).

433. Ahmed, J., Varshney, S. K. & Janvier, F. Rheological and thermal properties of stereocomplexed polylactide films. *J. Therm. Anal. Calorim.* **115,** 2053–2061 (2014).

434. Chin, S. J. *et al.* Electrical conduction and rheological behaviour of composites of poly(ε-caprolactone) and MWCNTs. *Polym. (United Kingdom)* **58,** 209–221 (2015).

435. Ashbee, K. H. G. *Fundamental principles of fiber reinforced composites.* (Technomic Pub. Co, 1993).

436. Colthup, N. B., Daly, L. H. & Wiberley, S. E. *Introduction to infrared and Raman spectroscopy*. (Academic Press, 1990).

437. Maldonado-Codina, C. & Efron, N. Dynamic wettability of pHEMA-based hydrogel contact lenses. *Ophthalmic Physiol. Opt.* **26,** 408–418 (2006).

438. Han, D. K. *et al.* Plasma protein adsorption to sulfonated poly(ethylene oxide)-grafted polyurethane surface. *J. Biomed. Mater. Res.* **30,** 23–30 (1996).

439. Menzies, K. L. & Jones, L. The Impact of Contact Angle on the Biocompatibility of Biomaterials. *Optom. Vis. Sci.* **87,** 387–399 (2010).

440. ZISMAN, W. A. Relation of the Equilibrium Contact Angle to Liquid and Solid Constitution. in *Contact Angle, Wettability, and Adhesion* 1–51 (American Chemical Society, 1964).

441. Förch, R., Schönherr, H. & Jenkins, T. A. Appendix C: Contact Angle Goniometry. in *Surface Design: Applications in Bioscience and Nanotechnology* 471–473 (Wiley-VCH Verlag GmbH & Co. KGaA, 2009).

442. Mateyawa, S. *et al.* Effect of the ionic liquid 1-ethyl-3-methylimidazolium acetate on the phase transition of starch: dissolution or gelatinization? *Carbohydr. Polym.* **94,** 520–30 (2013).

443. Ahn, Y. *et al.* Electrospinning of lignocellulosic biomass using ionic liquid. *Carbohydr. Polym.* **88,** 395–398 (2012).

444. Eckstein, A. *et al.* Determination of Plateau Moduli and Entanglement Molecular Weights of Isotactic, Syndiotactic, and Atactic Polypropylenes Synthesized with Metallocene Catalysts. *Macromolecules* **31,** 1335–1340 (1998).

445. Horinaka, J., Urabayashi, Y., Takigawa, T. & Ohmae, M. Entanglement network of chitin and chitosan in ionic liquid solutions. *J. Appl. Polym. Sci.* **130,** 2439–2443 (2013).

446. Rajakumar, K., Sarasvathy, V., Thamarai Chelvan, A., Chitra, R. & Vijayakumar, C. T. Natural Weathering Studies of Polypropylene. *J. Polym. Environ.* **17,** 191–202 (2009).

447. Horinaka, J., Honda, S. & Takigawa, T. Rheological properties of concentrated solutions of gellan in an ionic liquid. *Carbohydr. Polym.* **78,** 576–580 (2009).

448. Podesta, M. De *et al.* A low-uncertainty measurement of the Boltzmann constant. *Metrologia* **50,** 354–376 (2013).

449. Fischer, J. *et al. Report to the CIPM on the implications of changing the definition of the base unit kelvin.* **1,** (2007).

450. Lv, Y. *et al.* Chain entanglement and molecular dynamics of solution-cast PMMA/SMA blend films affected by hydrogen bonding between casting solvents and polymer chains. *RSC Adv.* **5,** 44800–44811 (2015).

451. Sankri, A. *et al.* Thermoplastic starch plasticized by an ionic liquid. *Carbohydr. Polym.* **82,** 256–263 (2010).

452. Ning, W., Xingxiang, Z., Haihui, L. & Benqiao, H. 1-Allyl-3-methylimidazolium chloride plasticized-corn starch as solid biopolymer electrolytes. *Carbohydr. Polym.* **76,** 482–484 (2009).

453. El Mansouri, N.-E., Yuan, Q. & Huang, F. Synthesis and Characterisation of Kraft Lignin-based Epoxy Resins. *BioResources* **6,** 2492–2503 (2011).

454. Kubo, S. & Kadla, J. F. Hydrogen bonding in lignin: a Fourier transform infrared model compound study. *Biomacromolecules* **6,** 2815–21 (2005).

455. Huang, H., Liu, Q., Sun, T., Chen, J. & Guo, W. Viscoelastic Behavior and Submolecular Level Dynamic Heterogeneity of Hydrogen-Bonded Polymer Blends Probed by Dynamic FTIR Spectroscopy. *J. Appl. Polym. Sci.* **113,** 662–666 (2009).

456. Oliveira, L. *et al.* Lipophilic extractives from different morphological parts of banana plant "Dwarf Cavendish". *Ind. Crops Prod.* **23,** 201–211 (2006).

457. Oliveira, L., Cordeiro, N., Evtuguin, D. V., Torres, I. C. & Silvestre, a. J. D. Chemical composition of different morphological parts from 'Dwarf Cavendish' banana plant and their potential as a non-wood renewable source of natural products. *Ind. Crops Prod.* **26,** 163–172 (2007).

458. Ribeiro da Luz, B. Attenuated total reflectance spectroscopy of plant leaves: a tool for ecological and botanical studies. *New Phytol.* **172,** 305–318 (2006).

459. Bilba, K., Arsene, M. A. & Ouensanga, A. Study of banana and coconut fibers. Botanical composition, thermal degradation and textural observations. *Bioresour. Technol.* **98,** 58–68 (2007).

460. Hartmann, M. *et al.* Damage of the bacterial cell envelope by antimicrobial peptides gramicidin S and PGLa as revealed by transmission and scanning electron microscopy. *Antimicrob. Agents Chemother.* **54,** 3132–3142 (2010).

461. Thwaite, J. E. & Atkins, H. S. Bacillus: Anthrax; food poisoning. in *Medical Microbiology: Eighteenth Edition* 237–244 (Elsevier, 2012). doi:10.1016/B978-0-7020-4089-4.00036-6

462. Van Tyne, D., Martin, M. J. & Gilmore, M. S. Structure, function, and biology of

the Enterococcus faecalis cytolysin. *Toxins* **5,** 895–911 (2013).

463. Ampofo, K. & Byington, C. L. Streptococcus pneumoniae. in *Principles and Practice of Pediatric Infectious Diseases: Fourth Edition* 721–728.e6 (2012). doi:10.1016/B978-1-4377-2702-9.00125-2

464. Donlan, R. M. Biofilms: Microbial life on surfaces. *Emerging Infectious Diseases* **8,** 881–890 (2002).

465. Hatton, B. D. Antimicrobial coatings for metallic biomaterials. in *Surface Coating and Modification of Metallic Biomaterials* 379–391 (Elsevier, 2015). doi:10.1016/B978-1-78242-303-4.00013-2